Chemical Tools to Interrogate Protein Sulfenylation by Fluorescence Microscopy and NMR

by

Christopher Tom

A dissertation submitted in partial fulfillment
of the requirements for the degree of
Doctor of Philosophy
(Chemical Biology)
in the University of Michigan
2016

Doctoral Committee:

Assistant Professor Brent R. Martin, Chair
Professor Anna K. Mapp
Professor John Montgomery
Professor David H. Sherman

Dedication

leete latu polito ulos a'riolos baru n'tori

Acknowledgments

I can't believe this time is drawing to a close. I started my quest for a PhD in 2003, thirteen years ago at UC Berkeley. Because I wasn't sure at the time whether it was truly the right choice, I left the redwoods and eucalyptus grove, choosing the wandering path of a life scientist. For five years I tested this theory. Five years I questioned. Satisfied with my data, and sure of my controls, I found that I indeed wanted to be a scientist, and I returned to graduate school at the University of Michigan.

Before anyone else, I have to thank my friend, mentor, and professor Prof. Brent Martin. Despite not being around during my recruitment, he reached out to me while I was still on my bike ride out to Michigan, and we started our positions at Michigan at the same time. I had the great fortune to immediately know that I wanted to work for him, and this feeling has only proven to be increasingly true in time. As far as the field of chemical biology is concerned, I define it as 'finding chemical solutions to biological problems.' As an excellent biochemist, Dr. Martin has always provided me with the best problems, and allowed me the freedom to find those chemical answers. I am immensely grateful for this opportunity to find the way for my strengths to shine, which at the same time challenging me to develop those that were not as strong.

Beyond this, my time in graduate school has been enormously difficult, with many unexpected challenges through personal discovery, and I hope anyone reading this knows: I could not have asked for a more supportive professor. Graduate school is a difficult experience, and mine, for many reasons, was nearly heart-breaking. I have gone through divorce after a 10-year relationship collapsed, and been diagnosed with not insubstantial mental health issues. Had I been under the guidance of someone who was not sympathetic to the difficulties I was going through, who continued to bear down on me while I was trying to regain my footing, I would not have made it. I will always be thankful for him being the person that he is. Without his support, and his understanding, and his empathy to stand by me when things were at their worst, there is a good chance I would not have made it through graduate school a second time, and this would be a sad defeat indeed.

I would also like to thank my former advisor, Prof. Matt Francis, Associate Professor at UC Berkeley. The chemistry that I learned there set me on a path to join together the biomacromolecule and the small organic, the natural and the synthetic, to learn how to use bioconjugation chemistry to create wonderful materials and to literally fuse the biological and chemical. This information has proved to be invaluable throughout all stages of my education and research, and it is experience imagine it will continue to draw on for the rest of my life.

I would like to graciously acknowledge the Program in Chemical Biology both admitting me to the program and for initial funding during my first year; the Department of Education GAANN training program for funding me for a semester and for permitting to work on such a large range of spastic problems (including an Zombie Survival Guide,

American Sign Language organic chemistry vocabulary, 3d models; the Department of Chemistry for providing funding when I was a GSI; and the National Institute of Health Graduate Research Fellowship Program (F31 #14-PAF03279) that funded my work my last two years. Without these fellowships I would have put a much greater burden on our lab. This funding has allowed me to walk more lightly upon our resources and travel further with more intellectual freedom. I am grateful to Erim Zynep, the program coordinator at the NIH for supporting my research.

I would like to thank my committee, Prof. Anna Mapp, Prof. David Sherman, and Prof. John Montgomery for providing excellent guidance over my tenure at the University. I would also particularly like to thank Prof. Mapp and Prof. Sherman for the initial conversations during the PCB recruitment weekend that convinced me that the University of Michigan was very much the right place to be, and for the first time in applying for a job or school since exiting Berkeley, didn't look down upon my decision to leave with derision. It meant the world to me. To all of you, thank you for generously writing letters of support that helped me secure external funding.

Dr. Jaimeen Majmudar, you were a wonderful addition to the lab, and I was overjoyed to have such a strong synthetic chemist to reflect ideas off of and provide guidance. I'm not sure I could have done half the things that I did without your expertise, wisdom, and patience, and I wish you much luck at your next position.

Dr. Matt Stone, thank you for providing the expertise and patience to bear with me as we worked out the kinks of the DiNaps. I remember the excitement when we got those first images, and that's what the science is all about. Thanks for being a part of it.

The sisters Rodriguez were great people and wonderful additions to lab. Laura, you've become one of my best friends, and I've enjoyed our walks and talks and I wish you both the best in becoming that kind of doctor and one of you consents to give me kangaroo bouncy legs when the time is right.

Matt Waugh, you were there with me through thick and thin and more thick. You were a strong advocate for me doing the right thing even when I felt trapped. I've enjoyed the adventures we've gone on and I very much look forward to the adventures we will go on. I realize I've picked up as many hobbies as you. Here's to the beard.

If it is the people inside of lab that have made the academic experience so valuable, it is the people that I have found outside of lab that will make leaving Ann Arbor so difficult. Syncytium, and the remnants of the Fancy few, you're a creative force that constantly leaves me in awe of your drive to create and build. From fire art to wooden sculpture to crafting community to relationship building, I am honored to be a part of it all. Matt and Kim and Nadia, Madga and Marcus, Rick and Ricki, Little Tree and Valdez, Cho Cho and Amanda, Tumbleweed, Highwire, Thor, the Bunnies. David Yates, Thad and Kyrie Micelli, it's been a pleasure making two Effigies with you. Yanna, Alison, Theresa, Evelyn, Amy, Dana, all the interactions large and small have made life rich and fulfilling. Nora, that you have come back into my life at this exact moment, like the roaring fire you always are. You are a star. You are the fire.

Amy, in the last two and a half weeks I've gotten to know you, you've been an inspiration in my life. I'm excited to see where this goes, and I'm glad we both swiped right. Even though I'm about to embark on this upcoming journey, it does not feel like anything is coming to a close.

Mom, Dad, you have provided me all the tools to be the person I am today. From supporting my education at all levels. Dad, I have not often acknowledged how you have taught me so much about life. From cycling, to playing ‘the Game’ (oh how I hated you for that at the time, but now realize the realism of it), I am your son. So much of what I do, what I have become is because of how you raised me. I will also be forever indebted for the knowledge of the use of powertools. Mom, you taught me compassion, creativity, origami. You cautioned me when something was a bad idea and encouraged me in all the right ways. Thank you both, I literally would not be without you.

Finally, I would like to thank Rachel. During my most difficult times I did not rise to the challenge of being the best person I could be, and you bore the brunt of it. Thank you for staying with me and believing in me as long as you did; I am truly sorry for everything that happened, and dismayed to learn of all the latent things that were uncovered during this period. I owe it to you to continue to overcome these challenges with all of my strength. I owe it to you to be the best I can be, for all the times that I was not. You were a great partner and my best friend. I hope to stay that way in the end.

I do not know where the future will be, or where it will take me. I do not know how best to go forward, I do not know the secrets. But I will do as I have always done: I will be a life scientist. I will experiment and test and change and shift and arrange my theories in life to be consistent with the living data of my days. I will, without a doubt, mess it up bit time, but that is life science. I think we, humanity as a whole, has a very interesting time ahead of us, and I urge us to move forward with eyes open.

Thank you everyone. I am deeply indebted to you for your guidance, your support, your ideas, and your friendship.

It’s because of you that there will always be more questions.

Table of Contents

List of Figures

List of Tables

List of Schemes

List of NMR spectra

List of HPLC traces

List of Mass Spectra

List of Appendices

List of Abbreviations, Acronyms, and Symbols

[Ox]: oxidant or oxidizing
[Red]: reductant or reducing
% v/v: Percent volume
% w/v: Percent weight per volume
16:0: Palmitic acid
^{1}H: hydrogen proton
17-ODYA: 17-octadecynoic acid
^{18}F: isotope of fluorine that undergoes rapid β^{+} decay
^{19}F: stable isotope of fluorine that is NMR active
20:4: Arachidonic acid
20:5: Eicosapentenoic acid
^{2}H: deuterium
2IA: Iodoacetamide (also IAA)
^{3}H: Tritium
4-HNE: 4-hydroxynonenal
Å: Ångstrom
Ab: Antibody
ABHD: Alpha, beta hydrolase
Ac: Acetyl
AcOH: acetic acid
ADH: Alcohol dehydrogenase
AhpC: Alkyl hydroperoxide reductase subunit C
Alk: Alkynyl
AMC: active methylene compound
Apaf1: apoptotic protease-activating factor 1
APT: Acyl-protein thioesterase
β^{+}: positron, or anti-electron
Bn: benzyl
BOC: tert-butyloxycarbonyl
BODIPY: 4,4-difluoro-4-bora-3a,4a-diaza-s-indacene, an organic fluorophore
BPM: Biotin polyethylene glycol maleimide
BSA: Bovine serum albumin
BSB: (*E,E*)-1-bromo-2,5-bis(3-hydroxycarbonyl-4-hydroxy)styryl-benzene

Bt: benzotriazole
CβS, cystathionine β-synthase
Cbz: carbonyl benzyl
Cbz-Cl: benzyl chloroformate
CγL, cystathionine γ-lysase
$CN/^{-}CN$: cyanide anion
CO: carbon monoxide
CO_2: carbon dioxide
CoA: Coenzyme A
CR: Congo Red
$CuSO_4$: Copper II sulfate
CT: Computed tomography / computer-aided tomography
d or D: deuterium
Da: Daltons, in g/mol
DCF: dichlorofluorescein
$DCFH_2$: reduced dichlorofluorescein
DCM: dichloromethane
EDC: N-(3-Dimethylaminopropyl)-N'-ethylcarbodiimide hydrochloride
DHHC: Aspartate-histidine-histidine-cysteine containing motif or enzyme
DiNap: molecules based on the 1*H*-phenalene-1,3(2*H*)-dione dimedone-naphthalene scaffold, fused DImedone and NAPhthalene rings
DIPEA: diisopropylethylamine
DMAP: 4-(dimethylamino)pyridine
DMF: dimethylformamide
DMSO: dimethylsulfoxide
$DMSO\text{-}d_6$:perduterated dimethylsulfoxide
DNA: deoxyribonucleic acid
DOTA: 1,4,7,10- tetraazacyclododecane-1,4,7,10-tetraacetate
DTNB: 5,5'-dithiobis-(2-nitrobenzoic acid)
DTT: dithiothreatol
Dyn-2: 4-(pent-4-yn-1-yl)cyclohexane-1,3-dione
E.coli: Escherichia coli
EC_{50}: Half maximal stimulatory concentration
ECAD: Epithelial cadherin
EDC: N-Ethyl-N′-(3-dimethylaminopropyl)carbodiimide hydrochloride
EGF: Epidermial growth factor
EGFR: Epidermal growth factor receptor
EIC: extracted ion chromatogram
Em: emission spectrum or wavelength
eq: equivalents of chemical in relation to limiting reagent
ER: endoplasmic reticulum
Ero1: ER oxidase 1
ESI: electrospray ionization
Ether: diethyl ether
EtOAc: ethyl acetate
Ex: excitation spectrum or wavelength

FDG: Fluordeoxyglucose (often ^{18}F)
FL: fluorescein, fluorescein-like, or fluorescein-conjugated
FRET: fluorescence resonance energy transfer
FP: fluorescent protein
FSB: (*E,E*)-1-fluoro-2,5-bis(3-hydroxycarbonyl-4-hydroxy)styryl-benzene
FWHM: full-width at half-max
g: Grams
ΔG: free energy change
$\Delta G^{\ddagger}$: free energy change of the transition state
GAPDH: Glyceraldehyde-3-phosphate dehydrogenase
GFP: green fluorescent protein
Grx: glutathione reductase
GSH: glutathione, reduced
GSSG: glutathione, oxidized
GSNO: nitroso glutathione
H_2O_2: hydrogen peroxide, an important endogenous oxidant
HCl: hydrochloric acid
HEPES: 4-(2-hydroxyethyl)-1-piperazineethanesulfonic acid
HOMO: highest occupied molecular orbital
HPLC: High-performance liquid chromatography
HRMS: high-resolution mass spectrometry
HSA: human serum albumin
HSF: heat shock factor
Hsp: heat shock protein
IB: Immunoblot
IC_{50}: Half maximal inhibitory concentration
J: NMR coupling constant, in Hz
kDa: Daltons, in g/mol
K_i: Equilibrium inhibitory constant
K_m: Substrate concentration at half maximal enzyme velocity
KO_2: potassium superoxide
k_{obs}: the observed rate constant associated with the apparent order and molecularity of a given reaction
k_{off}: the dissociation rate constant of a first-order unimolecular reaction
λ_{max}: maximum wavelength
L: Liters
LCFA: Long-chain fatty acid
LPA: Lysophosphatidic acid
LPC Lysophosphatidyl choline μ
LPE: Lysophosphatidyl ethanolamine
LPI: Lysophosphatidyl inositol
LUMO: lowest unoccupied molecular orbital
LYPLA: Lysophospholipase
M: Molarity
MeCN: acetonitrile
Me: methyl

MeOH: methanol
MeOVal-CysSA-Cbz: methyl (*S*)-2-((*S*)-4-(((benzyloxy)carbonyl)amino)-3-oxoisothiazolidin-2-yl)-3-methylbutanoate
MeOVal-CysSA-Cbz: methyl *N*-((benzyloxy)carbonyl)-*S*-hydroxy-*L*-cysteinyl-*L*-valinate
Methanol-d_4: perduterated methanol
MHz: megahertz
min: Minutes
MMTS: methyl methane thiosulfonate
mol: Moles
MPO: myeloperoxidase
MRI: magnetic resonance imaging
MRS: magnetic resonance spectroscopy
MWC: molecular weight cutoff
NaCl - Sodium chloride
NAD^+: nicotinamide adenine dinucleotide, oxidized
NADH: nicotinamide adenine dinucleotide, reduced
$NADP^+$: nicotinamide adenine dinucleotide phosphate, oxidized
NADPH: nicotinamide adenine dinucleotide phosphate, reduced
NaN_3/N_3^-: sodium azide, azide anion
NaOH: sodium hydroxide
NaSH: sodium hydrosulfide
NBD-Cl: 4-chloro-7-nitrobenzo- 2-oxa-1,3-diazole
NBO: Natural bond orbital
NEM: N-ethylmaleimide
NH_2OH: Hydroxylamine
nm: nanometers
NMR: nuclear magnetic resonance, a method to probe the chemical environment of active nuclei.
NOS: Nitric oxide synthase, including iNOS, eNOS, and nNOS
NOX: NADPH Oxidase
O_2^-: superoxide radical, a very short lived reactive species
OD_{600}: optical density at 600 nm
Palm: Palmitic acid
PAT: Protein acyltransferase
PBS: Phosphate buffered saline (pH 7.4)
PDA: photodiode array
PDI: protein disulfide isomerase
PET: positron emission tomography
PET: photoelectron transfer / photoinduced electron transfer
Ph: Phenyl
pK_a: acidic dissociation constant
pO_2: partial pressure of oxygen
PPA: polyphosphoric acid
ppm: parts per million
Prx: peroxyredoxin
PTM: post translational modifications
PTP: protein tyrosine phosphatase

PUFA: polyunsaturated fatty acid
PVDF: Polyvinylidene fluoride
RARE: rapid acquisition with relaxation enhancement
Ras: Ras sarcoma virus oncogene
RCF: Relative centrifugal force
RCS: reactive carbon species
Res-O-Ac: Resorufin O-Acetate
rhEGF- Recombinant human epidermal growth factor
RNA: ribonucleic acid
RNS: reactive nitrogen species
ROS: reactive oxygen species
RSOH: sulfenic acid
RSO_2^-: sulfinic acid
RSO_3^-: sulfonic acid
RSS: reactive sulfur species
RxS: small reactive species
s: Seconds
Scrib: Scribble planar cell polarity protein
SOD: Superoxide dismutase
SDS - Sodium dodecyl sulfate, a.k.a. Sodium lauryl sulfate
SDS-PAGE - Sodium dodecyl sulfate polyacrylamide gel electrophoresis
S/N: signal to noise
Srx: sulfiredoxin
T: Tesla, unit of magnetic field strength
T1: nuclear spin-lattice relaxation time
T2: nuclear spin-spin relaxation tim
TB: Terrific broth
TCA: trichloroacetic acid
TCEP: Tris(2-carboxyethyl)phosphine
Tris: tris(hydroxymethyl)aminomethane
TEA: triethylamine
TFA: trifluoroacetic acid
THF: tetrahydrofuran
TIC: total ion chromatogram
TIRF: total internal reflectance microscopy
Trx: thioredoxib
TUBA: Tubulin alpha subunit
Tween20: Polysorbate 20
TX100: Triton X-100
UPR: unfolded protein response
UV: ultraviolet
WT: Wild-type
X-CT: X-ray computed tomography

Abstract

The cellular redox environment is a complex milieu of reactive oxygen, nitrogen, sulfur, carbon, and lipid species (ROS, RNS, RSS, RCS, RLS respective; collectively, RxS) that all have functional group interplay. Nowhere is this more apparent than on cysteine, which is readily oxidized to a wide range of functional groups. One group, the sulfenic acid, is the first oxidative step forward into this web. It has been studied extensively with biochemical and proteomic tools based upon the active methylene compound dimedone, but study of the localization of sulfenic acids has been limited to fixed cells due to the use of constitutively active dyes and antibodies to image. Herein we propose a design for a chemical 'switch' that would change the photoelectronics of an attached dye upon conjugation to a sulfenic acid, which he have developed in **Chapter 2**. This is based upon the observation that only one of the two α-protons is necessary for the reaction. We have successfully synthesized an aminonaphthalene-based dye with a fluorodimedone, F-DiNap, that allows for ratiometric imaging of live cells on TIRF and confocal microscopy. We have demonstrated F-DiNaps utility as a live-cell probe by collecting images before and after stimulation, as well as distinguishing established models of cancer malignancy with the cell lines that have been transfected with the transcription factor Snail. Critically, we have shown that our probe both increases

selectivity over aldehydes, which are post-translational modifications that are formed from the same oxidative stimuli as sulfenic acids; and that the rate of these probes is dramatically enhanced by over a thousand-fold by the addition of the fluorine. Serendipitously, ^{19}F is a minimalist reporter group for nuclear-spin instrumentation such as NMR and MRI. In **Chapter 3** we have leveraged this capacity to study sulfenic acids in NMR, synthesizing several probes based on minimalist fluorobarbituic acids, or F-Barbs. We have made preliminary studies into profiling these probes rates of conjugation, selectivity over other functional groups, and reactivity with biological samples, including purified proteins and lysates. The probes will be a large step towards imaging and interrogating the biological role of sulfenic acids *in vivo*.

Chapter 1: An Introduction to Protein Cysteine Oxidation and their Sensors and Probes

1.01. General Introduction

For all aerobic organisms, cellular respiration via molecular oxygen plays a critical role in metabolism. However, O_2 specifically, and oxidation in general, is a two-edged sword: too little, and cells become hypoxic and die; too much, and it not only fuels the intended metabolic fire, but it lays waste to genetic information, all the surrounding protein machinery, and lipid structure. This is one reason why relatively strong oxidants such as bleach and peroxides make effective disinfectants. Thus, a prime challenge of all aerobic organisms is to develop cellular infrastructure to modulate and moderate cellular reduction-oxidation (redox) and balance the high degree of oxygen's constructive reactivity with its high degree of destructive reactivity into a tightly controlled, well-regulated system.

The extracellular region of the cell is typically an oxidizing environment, as it is in constant contact with either atmospheric oxygen itself, or delivered through the body via oxygen-rich arterial blood in the vascular system. In contrast, the interior of the cell tends to be a reducing environment, possessing high concentrations of free thiols and redox sponges that protect the cell from oxidative damage.

Many of these regulatory, antioxidant proteins are highly conserved[1], and likely harken back to the time of the Great Oxygenation Event when anaerobic species had to adapt to deal with the drastic atmospheric change.

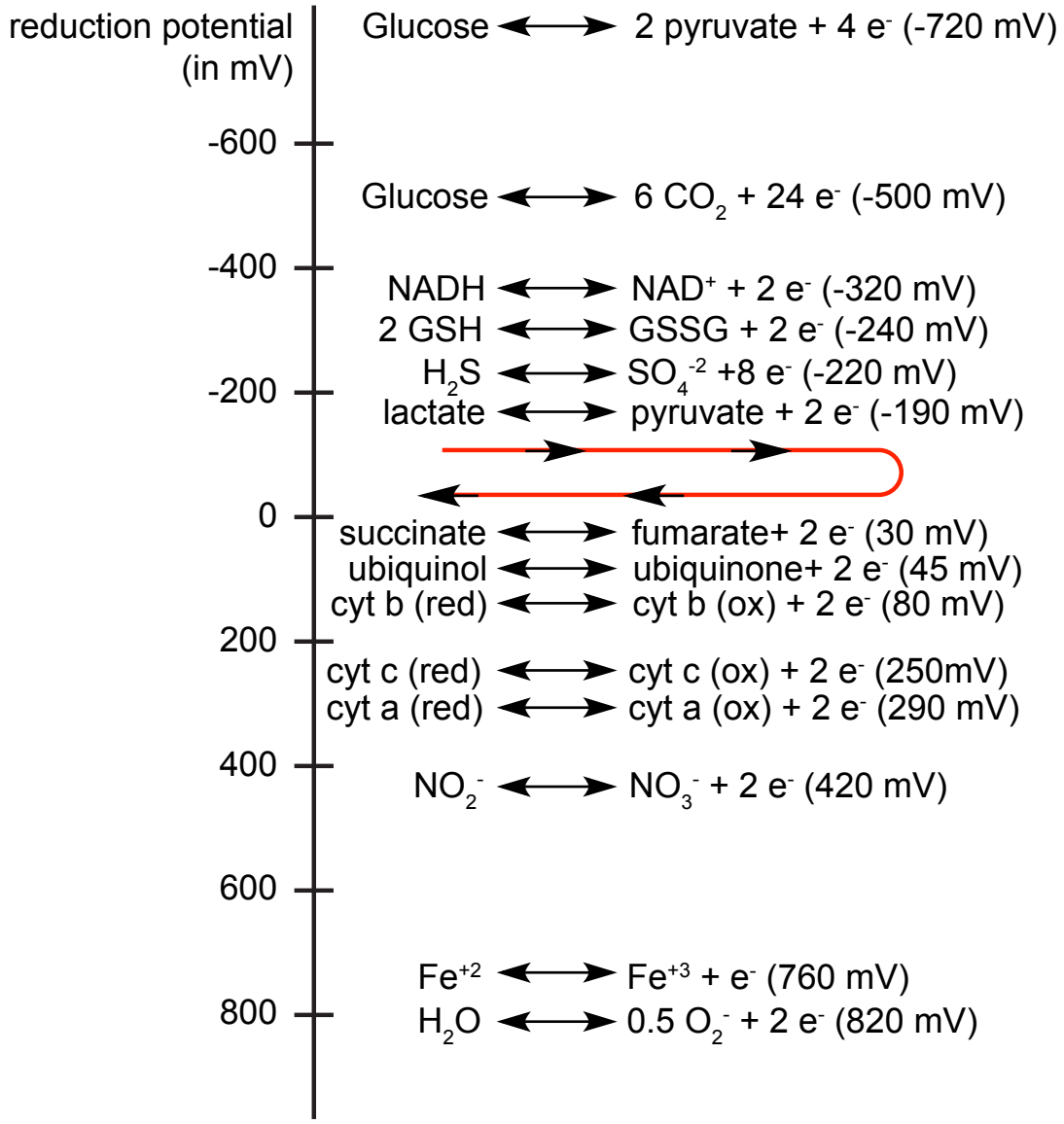

Figure 1-01. Select redox species inside the cell, sorted by their redox potential[2].
The red line indicates energetically favorable electron flow i.e. the conversion of lactate into pyruvate is sufficient to turn fumarate into succinate.

In addition to these macroscopic, environmental redox sources, there are a large number of redox active small molecules and molecules that act as either oxidizing or reducing equivalents (**Figure 1-1**). The cell produces other specific, extremely small-molecule inorganic reactive redox species endogenously. These enzymatically-produced molecules are typically highly reactive, and lead to localized, non-enzymatic changes to protein function and structure. Because of their high reactivity, their diffusion distances are limited before redox machinery degrades them. Before that point, gaseous or low-molecular weight molecules can react with metabolites and proteins, altering their function and structure in reversible or irreversible ways.

1.02 Reactive species and gasotransmitters

Though many of the pathways in the cell are modulated by protein-protein, protein-metabolite, and protein-organelle interactions, extremely small molecules of two or less heavy atoms are also prevalent means of transmitting cellular information via modification of key residues. These molecules, being small, often rapidly diffuse across membranes and cells and many of them possess high enough vapor pressures to be considered gaseous, thus earning the name gasotransmitters. These are typically enzymatically produced or produced through side-reactions, though their reactivity with biomolecules tends to be dependent to the individual reactivity of a residue, or binding ability of the protein, metabolite, or cofactor.

To this end, the cell produces a number of extremely small molecule reactive oxygen species (ROS), reactive nitrogen species (RNS), reactive sulfur species (RSS) and reactive carbon species (RCS), collectively referred to herein as RxS. Collectively they

make up some of the smallest molecules possible. We will review some of the most prominent species herein.

Reactive Oxygen Species

ROS exist in the cell both as metabolic byproducts, and specifically through enzyme-mediated processes. The vast majority of aerobic organisms derive the primary oxidation source from molecular oxygen, which makes up roughly 20.8% v/v of the atmosphere currently, up to the geological historical maximum of approximately of 35%[3]. At concentrations as low as 28%, O_2 can cause hyperoxia[4]. It is produced historically first by cyanobacteria and then by photosynthesis by plants as a way to fix gaseous carbon dioxide from the atmosphere[5]. Diatomic molecular oxygen has a standard reduction potential of:

$$O_{2(g)} + 4H^+ + 4e^- \rightarrow 2H_2O_{(l)} \qquad \xi^{0'} = +0.815\ V^6$$

$$O_{2(g)} + 2H^+ + 2e^- \rightarrow H_2O_{2(aq)} \qquad \xi^{0'} = +0.281\ V^6$$

This makes it a strong common oxidant, the one that is highest in concentration, and thus the primary electron sink in respiration. It has a high atmospheric partial pressure, and it is pervasive throughout the physiology of higher-order species due to it's efficient distribution by the vascular system. After travelling through the blood stream by hemoglobin, it is readily able to cross cellular membranes at 96% of the rate if would diffuse through pure water[7]. It is sometimes transferred to myoglobin, which has a higher affinity for and acts like a cellular oxygen store[8]. Therefore, when dealing with

biological samples, molecular oxygen always has to be considered in oxidative biochemical reactions.

Several secondary oxidants are also produced. A metabolic side product, the superoxide radical, $O_2^{\circ -}$, is produced when the electrons from the mitochondrial electron transport chain in eukaryotes (and from the electron transport chain in the chloroplasts of plants) do not complete the journey along the pathway from complex I to IV and instead find other side reactions[9]. Such 'leaky electrons' combine with molecular oxygen, forming the highly reactive superoxide[9].

$$O_{2(g)} + e^- \rightarrow O_2^{\circ -} \qquad \xi^{0'} = -0.33\ V^{6}$$

$$O_2^{\circ -} + e^- + 2H^+ \rightarrow H_2O_2 \qquad \xi^{0'} = +0.89\ V^{6}$$

Superoxide is also enzymatically generated by NADPH oxidase (NOx)[10].

$$2O_{2(g)} + NADPH + [2e^-] \rightarrow NADP^+ H^+ + 2O_2^{\circ -} + [2e^-]$$

$O_2^{\circ -}$ can react in a number of ways, both as a nucleophile, and in radical reactions. Superoxide $O_2^{\circ -}$, rapidly dismutates into H_2O_2, by the following pH-dependent process[11]:

$$2HO_2^{\circ} \rightarrow H_2O_2 + O_2 \qquad k_1 = 7.61 \times 10^5\ M^{-1}\ s^{-1}$$

$$HO_2^{\circ} + O_2^{\circ -}\ H_2O \rightarrow H_2O_2 + O_2 + OH^- \qquad k_2 = 8.86 \times 10^7\ M^{-1}\ s^{-1}$$

$$O_2^{\circ -}\ 2H_2O \rightarrow H_2O_2 + O_2 + 2OH^- \qquad k_3 = < 0.3\ M^{-1}\ s^{-1}$$

The hydroperoxy radical may have different roles in cellular oxidation than superoxide, but it is not yet understood. Regardless, it will exist in the mostly anionic state at physiological pH:

$$O_2^{\circ -} + H^+ \rightarrow HO_2^{\circ} \qquad \text{pKa: } 4.85^{12}$$

Due to the short lifetime of the superoxide radical, hydrogen peroxide is the more prevalent small molecule oxidant. It has the following reduction half-reaction:

$$H_2O_{2(aq)} + 2H^+ + 2e^- \rightarrow 2H_2O_{(aq)} \qquad \xi^{0\prime} = +1.34\ V^6$$

$$H_2O_{2(aq)} + H^+ + e^- \rightarrow H_2O_{(aq)} + OH^{\circ} \qquad \xi^{0\prime} = +0.38\ V^6$$

Outside the cell, strong solutions of hydrogen peroxide (30-40% v/v) can be stored indefinitely in aqueous solutions in cool, dark locations.

Hydroxyl radicals are among the most reactive species present in a cell. They are produced from a process akin to the Fenton Reaction shown in **Figure 1-02**[13], which involves the use of a Cu^{I}/Cu^{II} or Fe^{II}/Fe^{III} pair, along with hydrogen peroxide and a reductant:

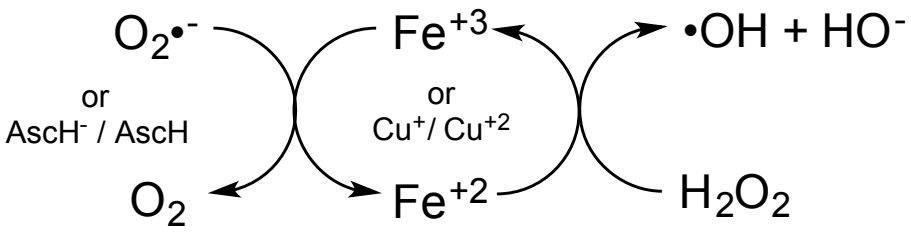

Figure 1-02. The Fenton reaction.
In an electron cascade originating with an electron from the superoxide anion or from ascorbate, reduces CuII or FeIII to CuI or FeII. This in turn, reduces hydrogen peroxide in a single-electron cleavage, producing highly reactive hydroxyl radicals and hydroxide.

The radical has the large standard reduction potential:

$$OH^{\circ} + H^{+} + e^{-} \rightarrow H_2O_{(aq)} \qquad \xi^{0\prime} = +2.32\ V^{6}$$

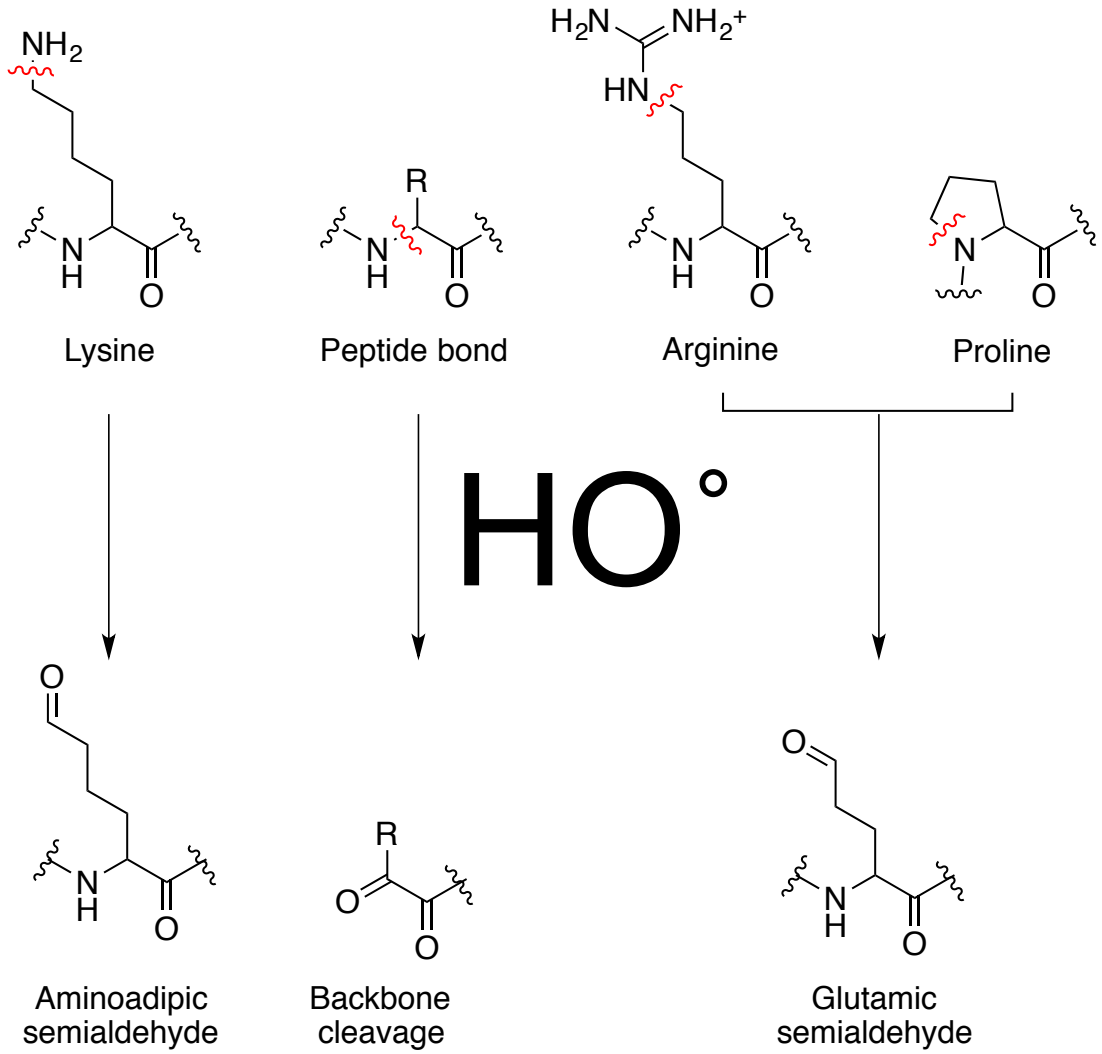

Figure 1-03. Conversion of lysine, arginine, proline, and the peptide back bond into their corresponding carbonyls by hydroxyl radical.

A particular feature of the high reactivity of hydroxyl radicals is the ability to oxidize C-H bonds proximal to amines at diffusion-limited rates, which converts it to the imine with subsequent hydrolysis to the aldehyde. Of interest is the ability to convert the sp^3-carbon attached to the nitrogen of lysine, arginine, proline, and the amide backbone into their corresponding aldehyde or ketone[14], with lysine being the most reactive[15]. This process is referred to in the literature as metal-centered oxidation (MCO), or primary carbonylation. This is of importance because aldehydes are highly reactive groups on their own, and interact with a wide number of functional groups in reversible and irreversible ways.

Myeloperoxidase (MPO) combines cellular H_2O_2 and Cl^- to make ClO^-[16]. MPO is primarily expressed in white blood cells, which breaks apart peroxide into hypochlorous acid and water. This heme-based enzyme is active during the respiratory burst of white blood cells and is responsible for some of the antimicrobial of neutrophil granulocytes[17-19].

$$HClO_{(aq)} + H^+ + 2e^- \rightarrow Cl^-_{(aq)} + H_2O_{(l)} \qquad \xi^{0,} = +1.49\ V^{20}$$

Reactive Nitrogen Species

The primary biological reactive nitrogen species is the gaseous radical nitric oxide, and it is an of itself an important biological signaling molecule. When released outside of the body, it rapidly oxidizes to nitrogen dioxide in air. Biologically, it is produced from nitric oxide synthase via the following reaction:

$$\text{L-Arginine} + 2\ O_2 + {}^{3}/_{2}\ \text{NADPH} + \tfrac{1}{2}\ H^{+} \rightarrow$$

$$\text{citrulline} + NO^{\circ} + 2\ H_2O + {}^{3}/_{2}\ NADP^{+}$$ [21]

There are several important isoforms of NOS, which are complex, multi-cofactor enzymes, including inducible iNOS[22], neuronal nNOS[23-25] and endothelial eNOS[26-28]. Like MPO, iNOS is also involved in immune response, as NO is highly reactive and as a small neutral nonpolar molecule it is able to diffuse through bacterial, fungal, and viral membranes, and at high concentrations it is toxic[29]. Interestingly, NO° is the only one of the family of small molecule & gasotransmitters that is also a radical, since superoxide dismutates too rapidly to be considered a signal transducer.

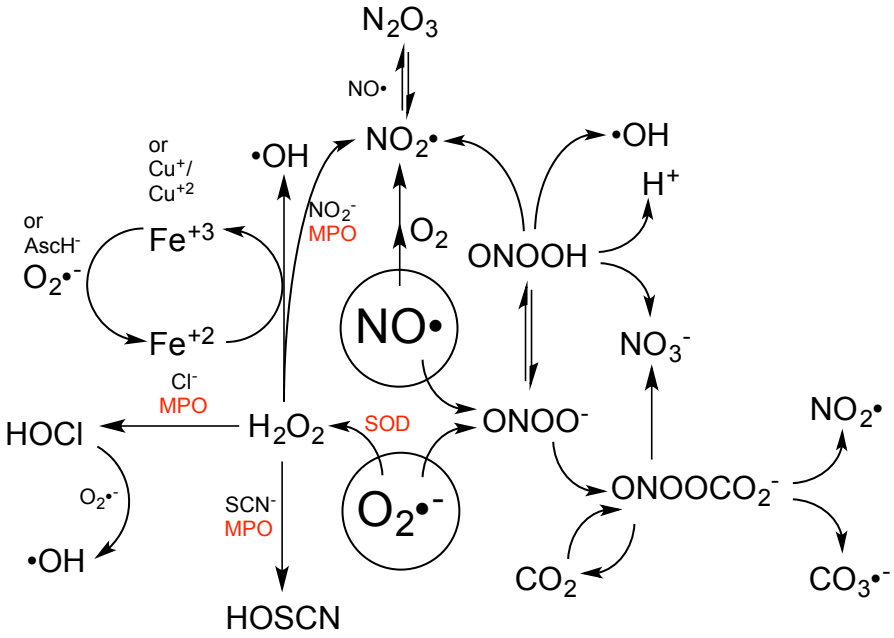

Figure 1-04. The complex interplay of primary ROS, RNS and their secondary species. RSS, RCS, and RLS are not included in this diagram.

When neutrophils sense an antigen, iNOS is activated by cytokines induced by interferon-γ[30]This produces a respiratory 'burst' of activity, which can damage or kill the intruder, and is one of the primary mechanisms for antibiolic defense. Other biological functions of nitric oxide is involved in vascular relaxation and vasodilalation by way of activating guanadyl cyclase (sGC)[28], sexual stimulation by way of activating sGC[31], and neutrotransmission[32].

However, due to the interplay between various RNS and ROS species, many additional species are possible, including peroxynitrite ($ONOO^-$) (**Figure 1-04**)[33], nitrogen dioxide (NO_2°)[34], nitrate (NO_3^-)[35], carbonate radical ($CO_3^{\circ -}$)[34] and more. Each of these species has their own individual, but at times overlapping reactivity, making their specific contributions to protein modification in the cellular context difficult to determine. Each species may potentially react in a nucleophilic, electrophilic, or radical fashion. It is well beyond the scope of this document to describe the role of all of these species, except to note that all of these highly reactive molecules and ions may play their own unique role in the redox environment and signaling processes by virtue of their concentration, charge, diffusion, membrane permeability, rates, and individual reactivity and rates of reactivity with various functional groups which may also be affected by the local chemical environment.

Reactive Sulfur Species

Hydrogen sulfide (H_2S) is another gaseous transmitter. H_2S is highly toxic on its own, with doses of 320-530 ppm able to kill a human[36]. However, when produced endogenously by cystathionine γ-lysase[37] (CγL), cystathionine β-synthase[38] (CβS), and

several other enzymes, at physiological levels of ~14 nM[39], it plays a similar role to NO: it acts as an endothelium-derived relaxing factor[40], as well as relaxing the smooth muscles and acting as a vasodilator[41]. In this vein, H_2S has also been shown to play a role in sexual stimulation in males[42]. It in the central nervous system, it appears to have a extremely wide range of functions, including activating Ca^{+2}-, K^{+}-, and Cl^{-}ion channels; activating protein kinase A; and acting upon γ-amino butyric acid (GABA), glutamate, and cachetolamine receptors[43]. It is a potent neuroprotectant, helping to diminish damage during repeated seizures[44] and is produced endogenously upon hypoxia[45], where carbon monoxide produced by heme oxygenase ceases, increasing H_2S production and stimulating cerebral circulation[46]. It seems to mitigate stroke damage[47,48] though this effect may be disputed[50]. In extreme examples, H_2S has been shown to and induce suspended animation in which metabolism decreased to 10% and core body temperature decreased to 2˚C above ambient with no apparent long-term damage[49], and increasing wound and blood-loss survivability[50].

Reactive Carbon Species

Reactive carbon species include a pair of isoelectronic molecules: carbon monoxide (CO) and hydrogen cyanide (HCN or $^{-}$CN). They are each highly toxic exogenously, with death occurring at 3200 ppm after 30 min for carbon monoxide[51,52] and death occurring in 10-60 min with 320 ppm hydrogen cyanide. Their toxicity is due to their high affinity for iron-based porphyrin (heme). The lone pair of each carbon has strong Lewis-basic electron-donating properties that are supplemented by strong π backbonding into the -

CX. Both CO and $^{-}$CN competes for binding at a higher affinity than oxygen[53], preventing oxygenation of the blood, and, more critically, poisoning cellular respiration.[54]

Carbon monoxide is produced endogenously from a family of proteins known as heme oxygenase (HO-x)[54]. This is a heme degradation pathway that oxidizes heme with molecular oxygen and NADPH to release $CO_{(g)}$, iron^{+3}, biliverdin, and H_2O and $NADP^+$. Carbon monoxide is derived from one of the bridging methyne unites of heme, producing biliverdin as a linearized chain of pyrroles[54]. Heme plays a central role in cellular redox processes due to its ability to bind and transport oxygen, as well as the ability of the iron to go from Fe^{+2} to Fe^{+3} and back again. Cytochromes, oxidating enzymes that are conserved all the way down to viruses[55] also use heme as a cofactor to oxidize and metabolize drugs. Thus heme degradation plays its own role in regulating these processes. The production of CO has effects on its own, with it binding and deactivating catalase[56], cytochrome p450[57], hemoglobin[58], NADPH oxidase[59], nitric oxide synthases[60,61], and myoglobin[62]. Interestingly CO activates some enzymes too, guanylyl cyclase[63] and cyclooxygenase[64]. Exogenous CO has been shown to be a, paradoxically, vasorelaxant[65] and as a vasoconstrictant[65], as well as involved in platelet aggregation[66] by inducing the release of NO$^{\circ}$ stores, and plays roles in neurotransmission[67] and long-term memory[68], and binds hemoglobin 200-250 times higher than oxygen,[69] amongst other roles[54].

The last small-molecule transmitter that will be discussed is hydrogen cyanide, or its deprotonated anion, cyanide. Cyanide has a pKa of 9.2, so all but ~1.5% will be in the less nucleophilic, less coordinating, but more diffusible HCN form. It is a potent nucleophile an even more potent binder of heme than CO due to increased Lewis

basicity. In macrophages, cyanide is produced by an MPO-mediated N-terminal oxidation of glycine or N-terminal glycyl peptide for phagocytosis[70]. In this process, N-chloroamino product degrades to cyanide. Other routes include the oxidation of thiocyanate[71]. CN^- also decreases cellular metabolism[72] and initiates hypoxic-stress related proteins such as protein kinase C[73]. Cyanide is generated by μ-opiate receptor and evidence suggests that it modulates NMDA receptor response[74]. Likewise, stimulating muscarinic cholinergic receptors in cultured cells increases HCN production, while in vivo the same action decreases HCN production[75].

Reactive Lipid Species

Another class of RCS are reactive species that derive from the perodixation of polyunsaturated fatty acids (PUFA) such as arachidonic acid (20:4), eicosepentenoic acid (20:5), or docosahexaenoic acid (DHA) that are present in the lipid membrane. These PUFAs help maintain membrane fluidity, are precursors to prostaglandins[76] and other signaling molecules such as anadamide[77], and aid in memory[78].

Lipid peroxidation:

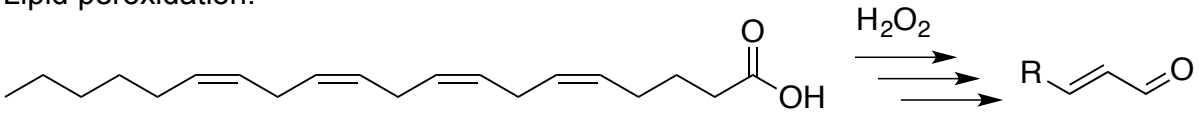

arachedonic acid (20:4)

Reactive lipid species:

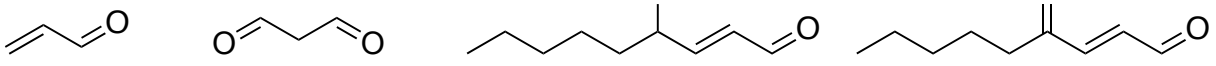

acrolein malonyl dialdehyde 4-hydroxy nonenal (HNE) 4-oxononenal (ONE)

Figure 1-05. Reactive lipid species producted from the peroxidation of PUFAs.

Due to their high degree of unsaturation, they are also prone to oxidation by peroxides, and are cleaved by the Hock reaction (**Figure 1-05**)[79]. This causes their breakdown into a wide number of products, including acrolein, 4-hydroxynonenal (HNE), and 4-oxononenal (ONE). These ene-als are bifunctional, able to undergo 1,4 (Michael) addition and aldehyde chemistry. They react in a 1,4 fashion with the following order: cysteine >> lysine > histidine. Though usually a sign of oxidative stress[80] and are implicated in neurodegeneration[81], RLS can act as signaling molecules[82], as shown by its modification of NF-κβ[83,84], and at low concentrations, inducing activation of Nrf2[85] and acting as a neuroprotective agent in response to oxidative insult.

In summary, these molecules are extremely toxic when administered at any meaningful concentration exogenously, much of which is explained by their bioactivity[86]. However, they all play biological roles at endogenously low levels produced by well-regulated enzymes and buffered by high redox concentrations of GSH.

1.03. Small-molecule antioxidant species

The highly reactive nature of all of the RxS species means that their regulation is highly necessary. Each of these plays a role in maintaining the overall redox state, though their small diffusible, but highly reactive nature shows that they have increasing roles in localized small molecule signaling, inflammation, immune response, and response to disease and redox stress. Their degradation-limited localization and ability

to affect proteins either on the short or long-distance is dependent on their reaction with GSH (**Table 1-1**)[87].

GSH + oxidant	Average diffusion distance (μm)	Rate constant (M^{-1} s^{-1})
H_2O_2	1600	0.2
$ONOO^-$	60	700
$O_2^{\bullet-}$	0.5	10^5
HOCl	0.3	$3x10^7$
NO_2	0.4	$3x10^7$
$^{\bullet}OH$	0.02	10^{10}

Table 1-01. Rate constants and average diffusion distances of ROS and RNS in the cell. Superoxide diffusion is rate-limited by its own disproportionation[87].

Glutathione (GSH) is a secondary reductive metabolite and the primary small molecule reducing cofactor for most for antioxidant proteins. Due to its high cellular concentration, we will also include glutathione (GSH) as a RSS. Though it varies tissue to tissue, most sources put intracelluar glutathione concentrations in the low single-digit mM range[88]. This high concentration allows it to act as an effective and electron source, forming oxidized glutathione, GSSG (**Figure 1-06**). Glutathione reductase (Grx) is responsible for turning over GSSG back to GSH using NADPH. It can react on its own at physiological pH; however, the pKa of GSH is high for a thiol at 9.65[89], compared to 8.2 for typical cysteine residues, likely due to the molecule's net negative charge thanks to the two carboxylates. We speculate that the fact that <1% of GSH exists as GS^- may in fact be favorable for the cell, so that there is a large cellular reservoir of neutralized and/or acid-passivated reductant that can converted to a much more reactive anionic form in the microenvironment of a protein, but oxidative and nitrosative species such as ROS and RNS can diffuse relatively freely and their products can persist for as longer. This gives the cell more opportunities for oxidative regulation and signaling, but allows

the cell regulate the production and activity of antioxidant proteins that convert GSH into the more reactive GS^- in order to deal with the oxidative stress. By tightly controlling the concentration and limiting range of the redox modulators, the cell can benefit from the signaling capabilities of these species while abrogating the potential damage and negative effects.

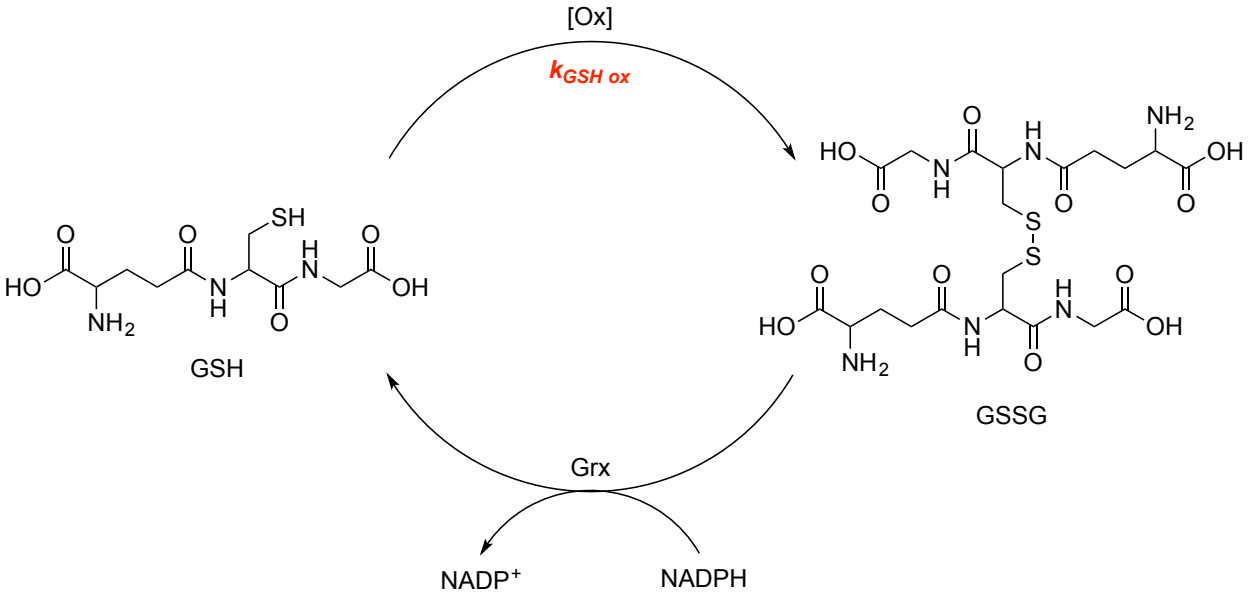

Figure 1-06. Glutathione reduction cycle.
Glutathione (GSH) is a tripeptide that has an oxidizable thiol derived from cysteine. It gets oxidized to a disulfide GSSG dimer, which subsequently gets reduced by glutathione reductase (Grx) using NADPH as a cofactor.

Other small-molecule electron sources are nicotinamide adenine dinucleotide phosphate (NADPH) and nicotinamide adenine dinucleotide (NADH). NADPH is produced from pentose phosphate pathway[90] as well as phosphorylation from NAD^+/NADH. Due to its direct production from exogenous energy sources (i.e. nutrients and food) it is the progenitor reducing species. These are cofactors in protein reactions

and rarely react with anything on their own. When GSH gets oxidized to GSSG, it provides the electron pairs to re-reduce it.

1.04. Proteins contributing to the antioxidant biology

The diversity of oxidant species and the necessity for careful regulation in maintaining a redox balance results in numerous pathways that cell can regulated the intracellular redox state. This leads to two classes of regulation: powerful antioxidant species that rapidly turn over to decrease the concentration and prevent the buildup of ROS and mitigate the ever-present threat of environmental and endogenous oxidants, and less active, regulatory proteins that chemically, structurally, and/or transrelocate and react to oxidative stress which induces downstream antioxidant response.

In the first, highly active antioxidant proteins are the front line of defense against high levels of ROS and regulate and limit the concentration of these oxidants. These include peroxyredoxin (Prx)[91], which reduces H_2O_2 into H_2O in combination with GSH via a pair of proximal thiols (**Figure 1-7a** and **1-7c**); superoxide dismutase (SOD)[92], which converts $O_2^{\cdot -}$ into either H_2O_2 or O_2; and catalase[93], which converts H_2O_2 into H_2O and O_2, which dramatically increase the rate of the degradation of these ROS. Some of these enzymes, such as catalase, are amongst the most active enzymes known, with catalytic efficiencies approaching the diffusion limits. These proteins put concentration limits on ROS under basal levels, apply stringent diffusion limits to ROS in the time of oxidative signaling and respiratory bursts, and protect the cell from high levels of primary oxidants during times of oxidative stress. AhpC C165S or C166S, in which the resolving cysteine is mutate out, lacks this catalytic ability.

Glutathione is a the primary small-molecule re-reducing agent for peroxyredoxins, when it gets oxidized, a second equivalent of GSH forms disulfide-linked dimers (GSSG), which are ultimately reduced by glutathione reductase (Grx) utilizing NADPH as an electron source (**Figure 1-7d**).

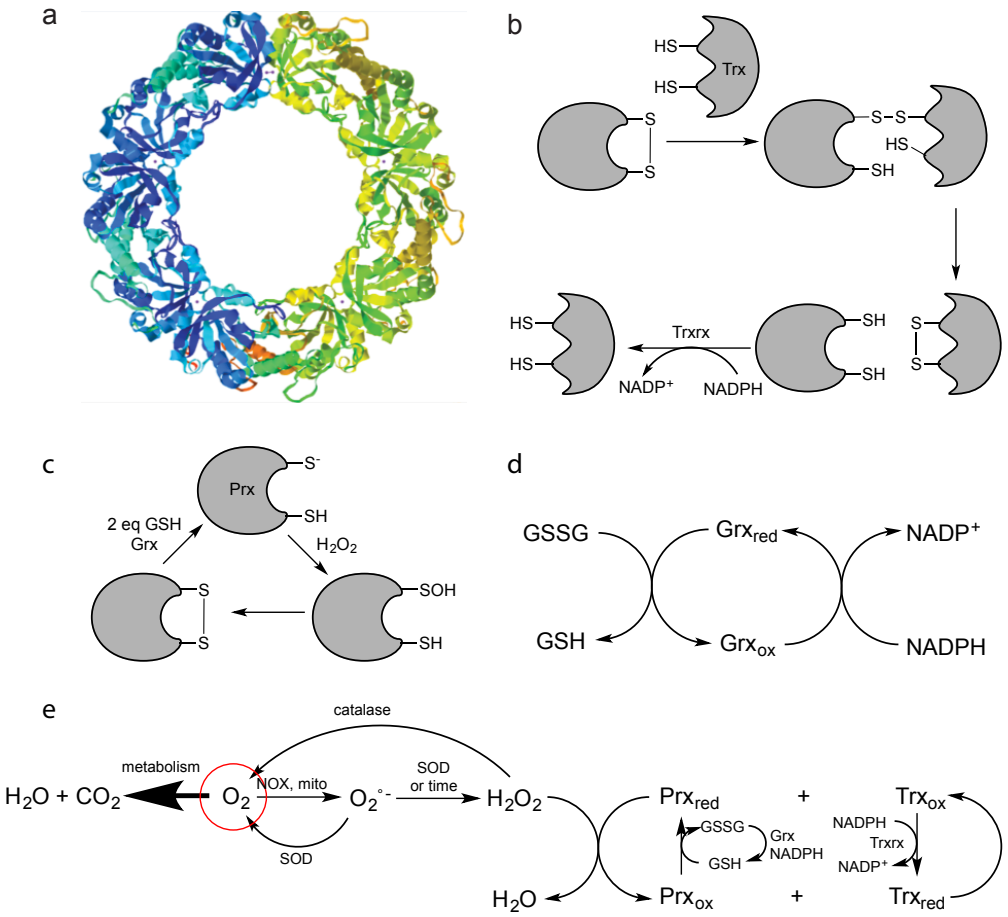

Figure 1-07. Redox management in the cell.
a) Peroxyredoxin, in this case AhpC, often has dimers and higher-ordered ring structures. b) Thioredoxin mechanism. The molecule has a two-cysteine CXXC motif. Two reduced thiols encounter an oxidized species. One thiol attacks, forming a transient disulfide, which the second cysteine resolves into a disulfide, freeing the now-reduced substrate. c) Like Trx, the structure of monomeric Prx has two proximal thiols, either intermolecularly or inter-subunit . The first is the peroxidase thiol, which is more reactive, and forms a transient sulfenic acid. The resolving thiol then attacks the sulfenic acid to form an intramolecular disulfide bond. It is regenerated by GSH/Grx. d) The mechanism of glutathione turnover. Grx_{red} reduces GSSG to GSH, forming oxidized Grx. Grx_{ox} is then reduced to active form by NADPH. e) An overview of the fate of

oxidative species in the cell. Molecular oxygen is the progenitor oxidant of the cell. The majority of it goes to metabolism, where it catabolizes carbohydrates, lipids, and proteins. However, some gets reduced to $O_2^{\circ-}$, either accidentally through the ETC of the mitochondria, or through the enzymatic production by NOX. $O_2^{\circ-}$ either gets reoxidized to O_2 by SOD, or further reduced to H_2O_2 by SOD or rapid disproportionation. From there, Prx reduces it into water, forming a disulfide. Prx can be regenerated by converting GSH into GSSG, which gets reduced by Grx and NADPH. Alternatively, Trx can reduce Prx. The oxidized Trx is converted back to the reduced Trx by Trxrx and NADPH.

Thioredoxins (Trx) are small proteins with CXXC motif. When they encounter disulfides in proteins, thioredoxin undergoes and oxidative thiol-disulfide exchange, transferring the reducing equivalent onto the substrate, and leaving the substrate protein with reduced thiols (**Figure 1-7b**)[94]. The close proximity of the Trx cysteines make this possible, much like the small-molecule biochemical reducing agent dithiothreitol (DTT). Trx is then re-reduced by thioredoxin reductase (Trxrx), a flavin protein that uses an NADPH cofactor[95].

This first class of antioxidant proteins combines stray byproducts of molecular oxygen ultimately with NADPH through a series of thiol-disulfide exchange and cofactor-enabled reactions, an overview of which can be seen in **Figure 1-7e**.

The second class of antioxidant response proteins acts as upfield sensors of oxidative stress. Such proteins often have a redox-sensitive residue or cofactor, typically a cysteine, and help to maintain the balance of a cell or compartment. These are not directly related to this research, but they are critical to maintaining the redox balance of the cell. Descriptions of some of the important species can be found in **Appendix C**.

1.05. The post-translational modifications of cysteine and sulfenic acids

Like the thiol moiety of glutathione, protein cysteine residues present a reductive sink and an electron source for these reactive species, albeit at much lower concentrations in the cell. Though other amino acids, such as tyrosine, tryptophan, lysine, and methionine are also at times oxidized, the free thiol of cysteine is in particular susceptible to these numerous changes and diverse chemistries (**Figure 1-08**). Because sulfur is the only third-row element that natively exists with multiple oxidation states within the cellular context, it adopts a diverse array of post-translational modifications (PTMs). Each of these PTMs can be reversible or irreversible, and play a different functional role for the protein.

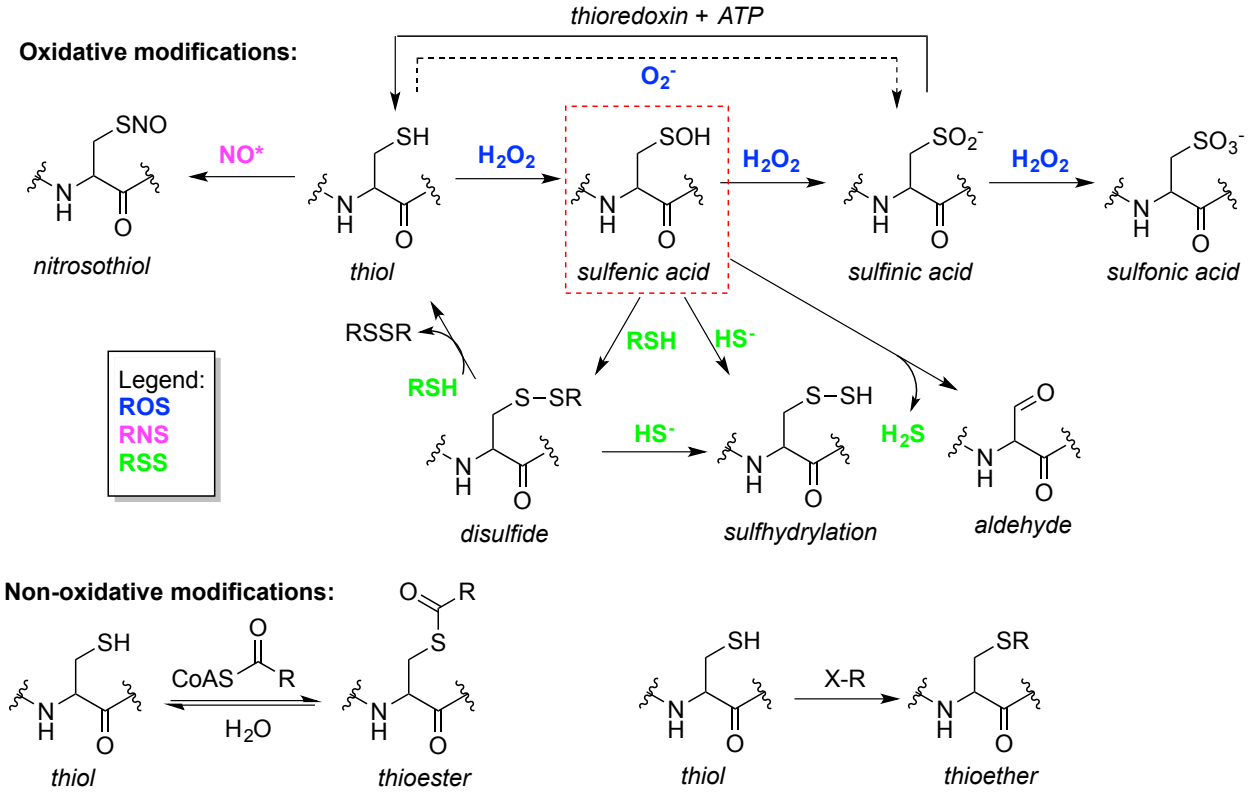

Figure 1-08. A simplified view of the post-translational modifications of cysteine. Cysteine can occupy a number of different oxidation states. Starting from its thiol form, it may be oxidized with nitric oxide to a nitrosothiol or transnitrosylated from another

nitrosothiol, or in the presence of ROS, can be oxidized to a sulfenic, sulfinic, or sulfonic acids.[96] Sulfenic acids themselves can be reduced to sulfyhydrylated polysulfides of cysteine with inorganic H_2S[97,98], or to a disulfide with an organothiol, as was seen with the redoxins. Furthermore, it has been shown that a sulfenic acid can degrade to an aldehyde. Other important modifications are lipidation through thioester formation, which includes palmitoylation, and alkylation e.g. prenylation.

Indeed, this is small list, for thiosulfinates, thiosulfonates, sulfinamides, sulfonothioic *S*-acid, disulfur trioxides, disulfone, alkylated-sulfoxides, alkylated sulfones, conversion to dehydroalanine, serine[99], and carbonylglycine[100] have been observed in HRMS (**Figure 1-09**).

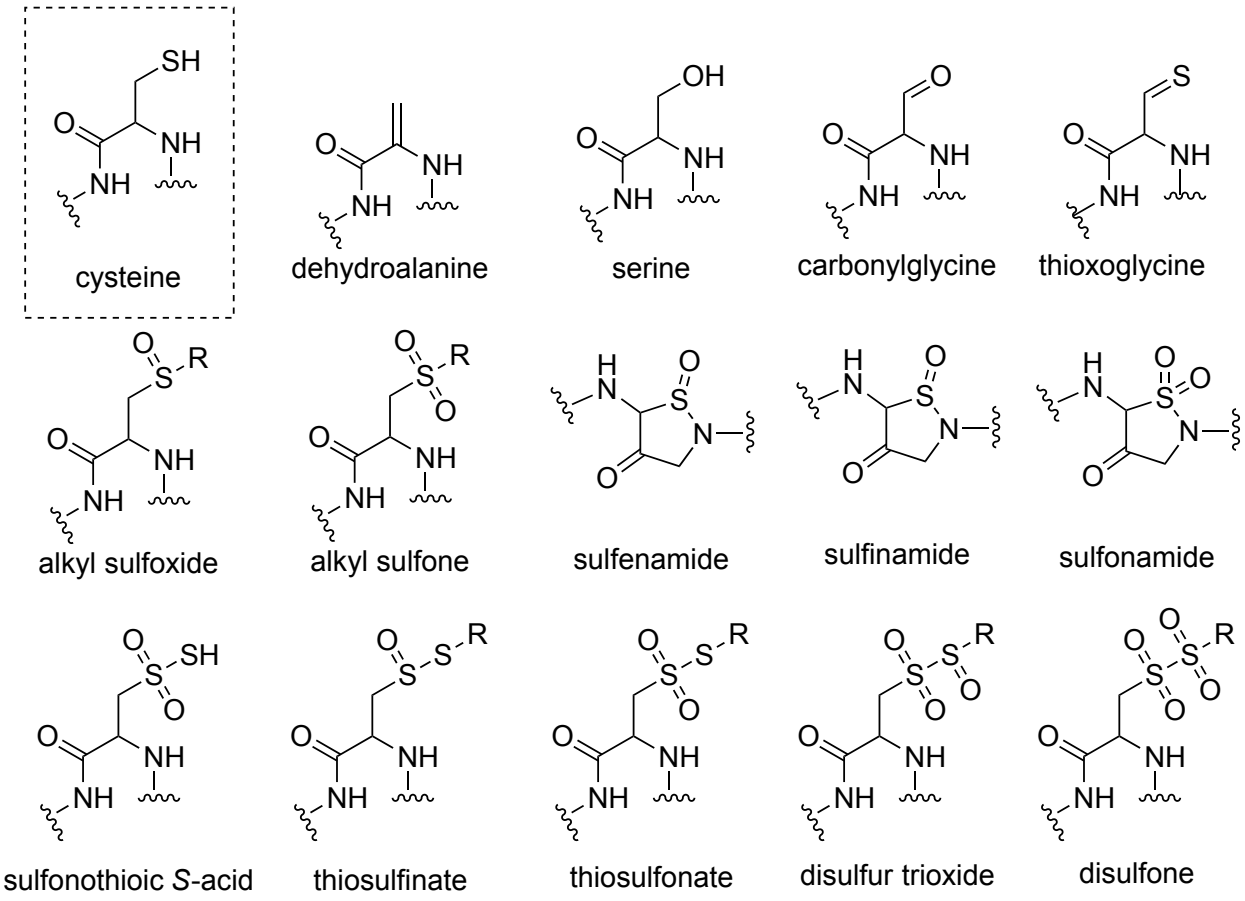

Figure 1-09. Other less common PTMs of cysteine, as detected *in vitro* with HRMS[99100].

1.06. Factors influencing the post translational modification of cysteine by RxS

The small molecule ROS, RNS, RSS, and RCS species are enzymatically produced, and ROS leads to the production of RLS from PUFAs. Then these species may be rapidly enzymatically and/or non-enzymatically degraded, and are typically non-enzymatically appended to the proteins, several factors play into this whether a certain cysteine residue will be modified:

1. The protein must be sufficiently colocalized near the point of generation of the RxS for the molecule to reach the protein.
2. The reactivity of the cysteine residue must be sufficiently high so as to compete with the intracellular redox machinery that is working to degrade the ROS, RNS, and RSS. Without competitive rates with this system, the protein will not be modified.
3. These reactions tend to either be nucleophilic or radical-driven, so catalytic cysteine residues and those with favorable microenvironments are decisively more reactive towards ROS, RNS, and RSS, because their thiols tend to be in the much more reactive and electron-rich and more easily oxidized thiolate form.
4. The most prevalent RSS, glutathione, tends to be the sink for ROS, RNS, and RLS species and modifications.

1.07. Early study of sulfenic acids

Some of the first references to sulfur in the sulfenyl oxidation state, which includes sulfenyl halides (R-SX), sulfenic acids, and sulfenamides, occurs in 1911 for a sulfenyl

chloride (R-SCl). The first evidence of a sulfenyl group forming on a protein was uncovered by Heinz Fraenkel-Conrat in 1955, then at UC Berkeley. A single thiol on the coat protein of the Tobacco Mosaic Virus was converted into a sulfenyl iodide with triiodide (I_3^-), and in studies with radioactive ^{131}I, the stoichiometry was subsequently shown to consume twice the the amount of isolated thiols, indicating no disulfide was formed[101]. and early biological research focused on the application of exogenous sulfenyl halide species to proteins, noting that they formed disulfides[102], the modification of tryptophan by sulfenyl chlorides[103]. It became clear that sulfenyl species were involved in the antioxidant properties of certain enzymes such as peroxidases[104]. By 1969, the mechanism of inactivation of GAPDH as a dehydrogenase via a sulfenic acid intermediate was elucidated by William Allison, using tetrathionate, iodosobenzoate and iodine monochloride[105]; in the same year it was determined that the activity of GAPDH could be switched to an acyl phosphatase by Ehring et al.[106]. In 1973, it was already known that cyanide, thiosulfate, bisulfite, hydrazine, and dimedone were reactive.[107] Other proteins, along with wide range of oxidants and reactants with sound mechanistic insight were found[108]. Of these initial studies on GAPDH, dimedone emerged from the pack as the scaffold of choice, both for its relatively high degree of activity against GAPDH-SOH, its selectivity against other residues and disulfides, and because it forms a stable CysS-dimedone thioether bond with the protein.

1.08. Isolated stability of sulfenic acids

Small molecule sulfenic acids can be extremely unstable. The half-life of methanesulfonic acid in the gas-phase at low pressure (0.1 torr or 0.00013 atm) is

approximately 1 min at 25˚C[109]. The rapid disproportionation of the sulfenic acid to the thiosulfinate prevents facile study of simple unhindered derivatives such as cysteine sulfenic acid (**Figure 1-10a**). When this disproportionation is prevented via steric occlusion, species such as triptycenesulfenic acid can be long-lived (**Figure 1-10b**)[110]. It is from such hindered molecules that we know that the structure of the sulfenic acid is predominantly R-SOH and not its tautomer RS(=O)H; the pKa of the oxo-acid is 12.5[110], closer to the pKa of a hydroxyl than a thiol. Like their hindered small-molecule cousins, cysteinyl sulfenyic acids on proteins may be sterically occluded from interaction with either other sulfenic acids (putatively present in a low concentration in the cell) or from the high concentrations of cellular thiols such as GSH or other proteins that would reduce the sulfenic to a disulfide (**Figure 1-10c**). Such proteinacious sulfenic acids may be stable for extended times. For instance the PTP1b sulfenic acid decays in the course of one to five minutes, while the GAPDH-SOH appears to be stable for thirty minutes or longer[111]. Our own research supports the hypothesis that the sulfenic acid in AhpC C166S, there the resolving cysteine has been mutated out, is stable essentially indefinitely as a bacterial lysate. Furthermore, their local microenvironment may prevent further oxidation to sulfinic and/or sulfonic acids.

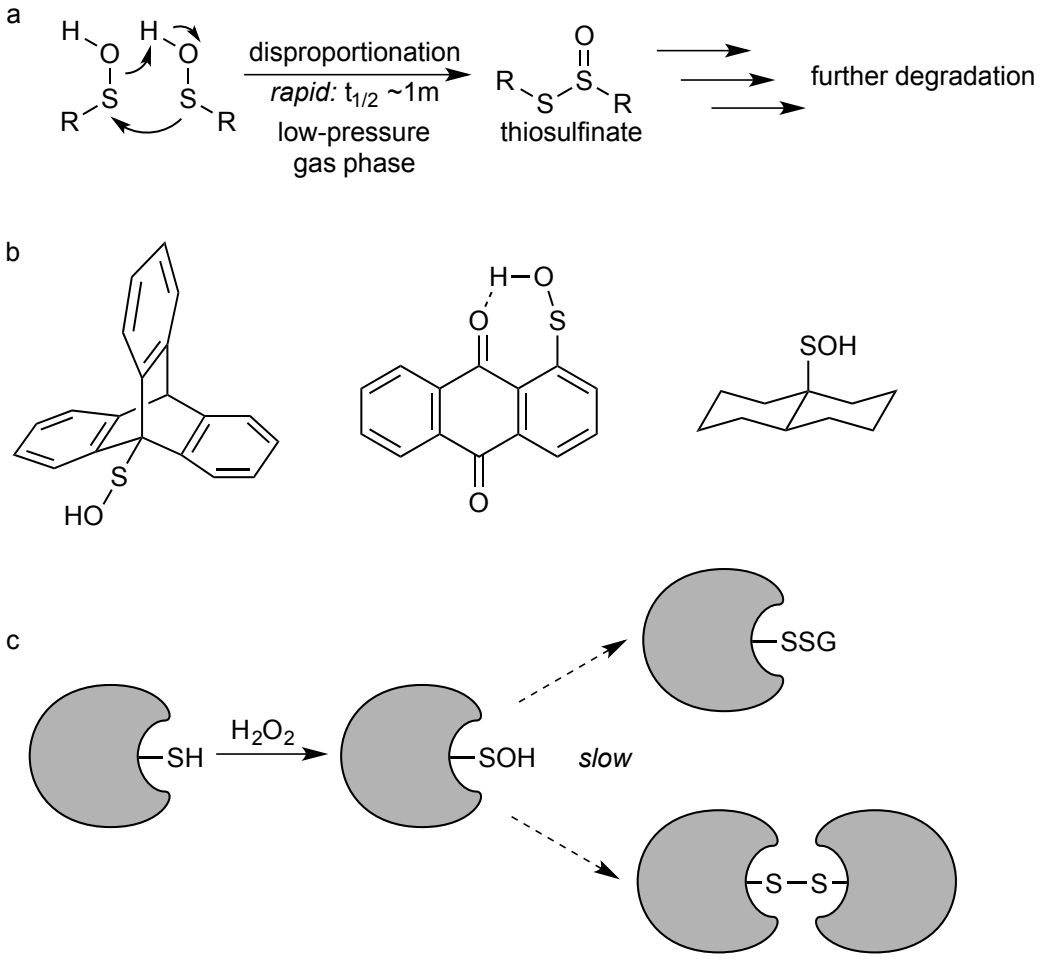

Figure 1-10. Sulfenic acid lifetime and stability.
a) Small, unhindered sulfenic acids disproportionate to thiosulfinates extremely rapidly, with lifetimes on in seconds. These undergo additional complex degradation pathways. b) Stable, sterically hindered sulfenic acids can be made, with features such as intramolecular hydrogen bonds providing additional stability. c) Proteins that have cysteine residues that are sterically occluded from either glutathione (top path) or other proteins (bottom path) can have very long-lived sulfenyl species.

1.09. Oxidant proteins and the formation of sulfenic acids

Our studies focus on the biological role of sulfenic acids within the cellular context. It is the first oxidative step a thiol may take within a cell, and it stands at the crossroads in between all other ROS-induced functional groups, including irreversible sulfinic acids, disulfide formation, sulfhydrylation, and even elimination of water and hydrolysis to form

aldehydes (**Figure 1.08** and **1.09**). As a highly reversible modification, it is capable of turning on and turning off signaling based on the redox environment, and thus may play an important regulatory role. The transition from thiol to sulfenic acid requires one equivalent of oxidant, and has the highest reduction potential, so it is fundamentally the most accessible.

Sulfenic acids are labile, reversible functional groups that are non-enzymatically appended to the sites of intracellular cysteine residues, which tend to reduced in the basal state of the cell due to the high glutathione concentration and action of efficient antioxidant enzymes. A reactive cysteine comes into contact with peroxide, liberating water and forming the sulfenic acid. There are two main sources of hydrogen peroxide in cells. The first is enzymatically produced by the inducible NADPH Oxidase (NOX)[10,112]. Upon stimulation, NOX produces extracellular sources of superoxide radical ($O_2^{\bullet -}$), which rapidly disproportionates into H_2O_2 and diffuses into the cell, either through the membrane or through aquaporin channels, where it modifies thiols proximal to the plasma membrane. A second route comes from so-called 'leaky electrons' from the mitochondrial electron transport chain, which get taken in by elemental oxygen, again forming $O_2^{\bullet -}$ leading to disproportionation to H_2O_2 (**Figure 1-11**)[9]. Once formed, the sulfenic acid has several fates. Most often it is reduced by cellular thiols, either forming protein-protein disulfide bonds or is fully reduced by two equivalents of glutathione, regenerating the original thiol in two-step process, producing GSSG as a byproduct. However, sulfenic acids are *intersectional* biological functional groups, and depending on the particular redox environment and presence of other ROS, RNS, and RSS species, can be further converted in to some of the species mentioned above.

Futhermore, with a proximal thiol, an intramolecular disulfide bond can form. And given the appropriate local microenvironment, a sulfenic acid can convert to a sulfonamide by cyclizing with the backbone amide by dehydration[113]. It can reversibly hydrolyze to the sulfenic acid.

It has been shown on small molecule peptidyl analogues that this cyclization into a sulfenamide can protect a cysteine thiol from irreversible overoxidation when it further oxidizes into the sulfinamide[114]. Its analogue, the sulfinic acid, is irreversible in by glutathione. However, the sulfinamide is fully, non-enzymatically reducible to the thiol by four equivalents of glutathione. This is also the case for thiosulfinates, though they are more labile. Because of their dynamic nature is unknown the full extent of the biological roles of either the sulfenic acid or sulfenamide in biological systems, what their relative population and reactivity is. An oxidized version of the protein tyrosine phosphatase 1b (PTP1b) was crystalized with a sulfenic acid in the active site[115].

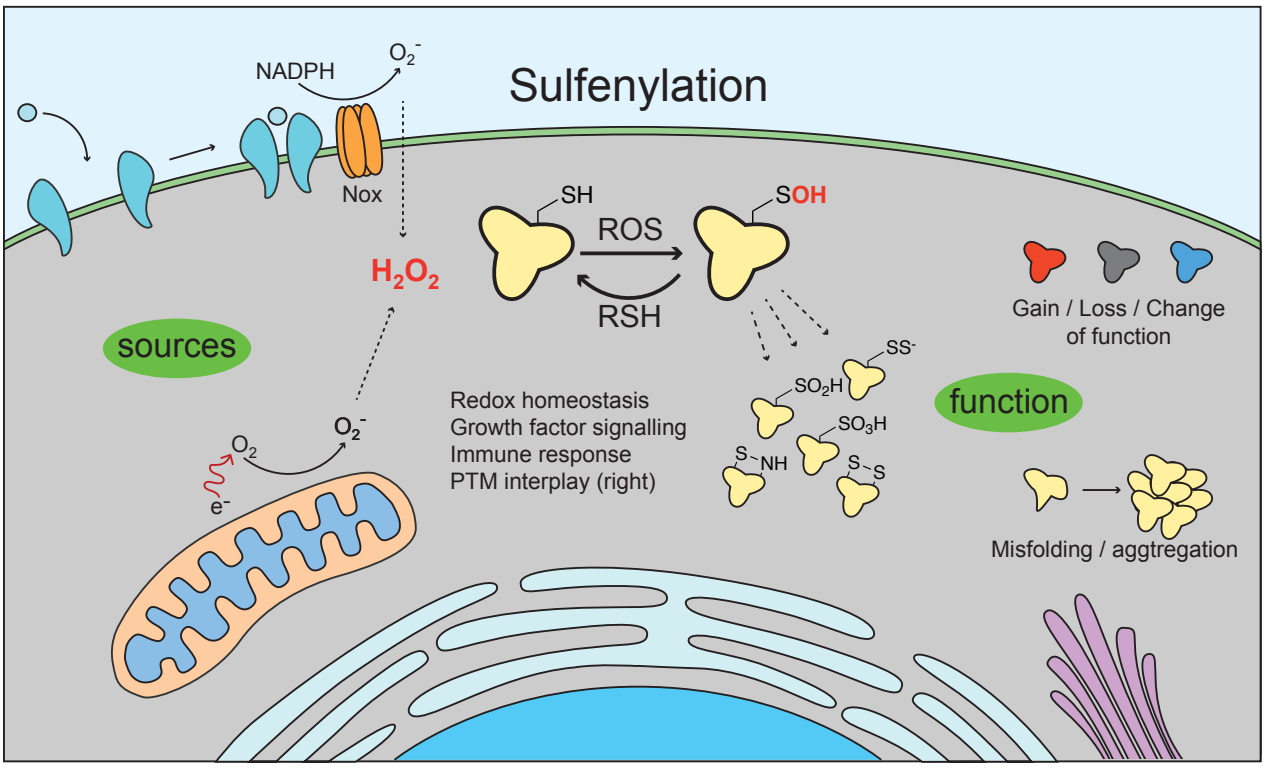

Figure 1-11. Overview of biological sulfenylation.
Hydrogen peroxide is originally derived from the rapid disproportionation of the superoxide radical, produced primarily at the mitochondria and from NADPA oxidase (NOX). These react with protein cysteine thiols, oxidizing them to sulfenic acids. Sometimes these form protein-protein disulfide bonds, but most often, sulfenic acids are reduced by the high concentration of intracellular glutathione back to the original thiol. However, depending on the protein, and the concentrations of RNS, ROS, and RSS, these can be taken on to other PTMs. Among their roles, sulfenic acids can change the function, structure, and aggregation state of proteins.

A well-studied system for peroxide regulation is the signal transduction of epidermal growth factor (EGF) by the EGF receptor (EGFR)[116]. In this model, upon binding of EGF to EGFR, EGFR colocalizes on the plasma membrane with NOX by an unknown mechanisms, which induces NOX to produce H_2O_2, which has several effects. In the first, EGFR is itself directly sulfenylated by NOX at Cys797. This is proximal to the ATP

binding site of the kinase. At low concentrations of 0.05 – 0.5 μM peroxide, kinase activity is enhanced; above 0.5 μM was inhibited[117]. In the second, the catalytic cysteine of protein tyrosine phosphatase (PTP) is sulfenylated[118]. PTP redox regulation has been extensively studied[119]. In the crystalized form of PTP1b, this emerges as a sulfenamide[115], calling into question both what the predominant sulfenyl species is, and which is most reactive, and if there are different structural and regulatory roles for a sulfenic acid vs. sulfenamide. Regardless of form, this prevents the phosphatase activity of PTP, leading to increased levels of growth factor receptor phosphorylation, which leads to downstream RAS-to-ERK signaling. In healthy cells, this leads to normal growth. In cells where the oxidative balance has been disrupted, this can lead to cell death or abnormal cell proliferation.

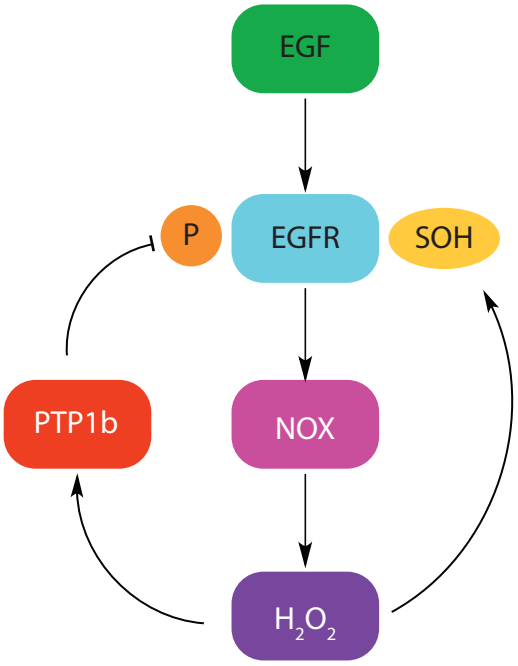

Figure 1-12. The redox regulation of EGF signaling.
Activation of EGFR by EGF, sulfenylation at Cys797, and by inhibition of dephosphorylation by PTP1b increases the growth response through the RAS pathway.

1.10. Functional group interplay between other oxidative, acylating, and alkylating modifications.

Cysteine has, arguably, the largest number of unique post-translational modifications (in possible contention with lysine) that can be induced by ROS, RNS, and RSS, in addition to acylating and alkylating modifications, such as palmotylation, prenylation, and lipidation via RLS. It is clear that no more than one PTM can exist on a particular cysteine residue at a particular time (i.e. two sulfenic acids on a cysteine make a sulfinic acid). Therefore, competition and interaction must exist on residues that are capable of multiple modifications.

Recently, it has been shown that cysteine modifications have reciprocally regulated each other. Most prominently, it was shown that palmoylated PSD-95 in complex with nNOS can be released from the membrane by Ca^{+2}-induced stimulation of the NMDA receptor[120]. This activates nNOS, which produces NO°, with then goes on to nitrosylate the same residues that were palmitoylated. This prevents palmitoyl acyl transferases (PATs), sometimes called aspartate-histidine-histidine-cysteine (DHHC), enzymes from repalmitoylating PSD-95.

Given that multiple modifications are present in a cell, it is unsurprising that they interact with each other. Recent work by Madjumar et al. has shown that nitrosocysteine and sulfinic acids can react form a thiosulfinate, a highly reactive thiosulfonate that, unlike typical disulfides, are rapidly reduced by cellular thiols[121]. It is hypothesized that the denitrosative and antioxidant properties of DJ-1 is due to its stable sulfenic acid.

Though the exact role of sulfenic acids in reciprocal modification and regulation is unclear, its intersectional role in nearly every other ROS- and RSS-governed process seems to be of great importance. Furthermore, sulfenylated cysteine residues cannot be nitrosylated, demonstrating their inhibitory effect on RNS. Sulfenylation, namely the residue-specific ease of sulfenylation by ROS and the residue-specific susceptibility of sulfenylation to conversion to other functional groups, including GSH reduction, dehydration to sulfenamides, and further oxidation to sulfinic and sulfonic acids, and the regulatory functionality of this complex interplay of oxidative, nitrosative, and acylative functional groups remains a prime question in the cellular context.

1.11 Fluorescent redox sensors

Fluorescent probes are central tools in chemical biology[122]. Since the discovery of the first fluorescent molecule, the antimalarial quinine, fluorescent dyes have have captured the attention of chemists and biologists alike. Visible-light stains were previously used to stain various organelles, and in modern biochemistry fluorescent dyes have largely taken over this role. Fluorescence in certain molecules is induced by the excitation of an electron through one frequency of light, the excitation. There is then a fast relaxation of the electron, followed by a relatively slow decay back to ground state (**Figure 1-13a**). Because of that fast intermediate relaxation, the frequency of light that is used to elevate the electron to the higher frequency (excitation frequency) is lower than the frequency of light that is released from its fall (emission frequency). This allows fluorescent to be a large step forward from visible-light stains by the increased of signal-to-noise by separating the excitation-emission frequencies and monitoring only at the

emission. Typically the λ_{max} of the excitation is separated from the λ_{max} of emission by 10-50 nm (**Figure 1-13b**). This is called the Stokes shift. Because of this shift, the excitation light can be filtered from the signal, thus resulting in a much higher S/N over conventional dyes. A brief review of these principles can be found here[123]. An estimated >80% of images published are with fluorescent probes due to their generally excellent sensitivity and resolution, with new super-resolution techniques being developed to break the theoretical resolution barrier[124]. Though the classes of dyes are fairly well-established (xanthene, coumarin, porphyrin, cyanine etc.), the properties of each dye can be tailored by the pendant groups connected directly and indirectly to the fluorophore. Sometimes, large improvements can be made to the photophysics across entire classes of dyes, as is the case of substituting an amine ($-NH_2$) for the four member nitrogen-containing heterocycle azetidine ($-N(CH_2)_2CH_2$)[125].

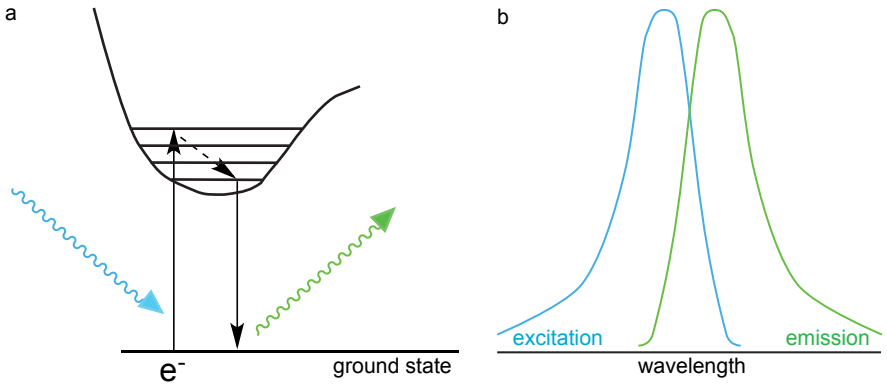

Figure 1-13. Fundamentals of fluorescence.
a) Jablonski diagram. A molecule absorbs light (blue squiggly arrow), exciting an electron to a higher energy level. The electron undergoes fast vibrational non-radiative decay (dashed arrow), resulting in a lower-energy photon emission (green squiggly arrow). b) Typical excitation/emission spectra for fluorescent dyes. The separatation between the λ_{max} of the excitation and the λ_{max} of the emission is called the Stokes shift.

Redox sensors and probes play a critical role in evaluating and comparing redox states. For the sake of this document, we will define fluorescent *sensors* as small-molecules that are either non-fluorescent, weakly fluorescent, or experience a spectral shift in either the excitation or emission or both (**Figure 1-14**). These proto-fluorophores activate upon exposure to a particular input (H_2O_2, H_2S, etc.). These sensors are chemically changed, but remain as small molecules unattached to larger biomolecules. Therefore, in the absence of targeting moieties or biological traps, they may be able to freely diffuse throughout their organelle, into different compartments, or out of the cell. In order to overcome the background of unreacted probe, sensors must *always* change their photophysical properties, either altering their excitation or emission properties, or both. The mechanisms of some such mechanisms will be discussed below. Samples visualized with sensors are not amiable to preparation by cell fixation, because the small molecule dyes are easily washed away.

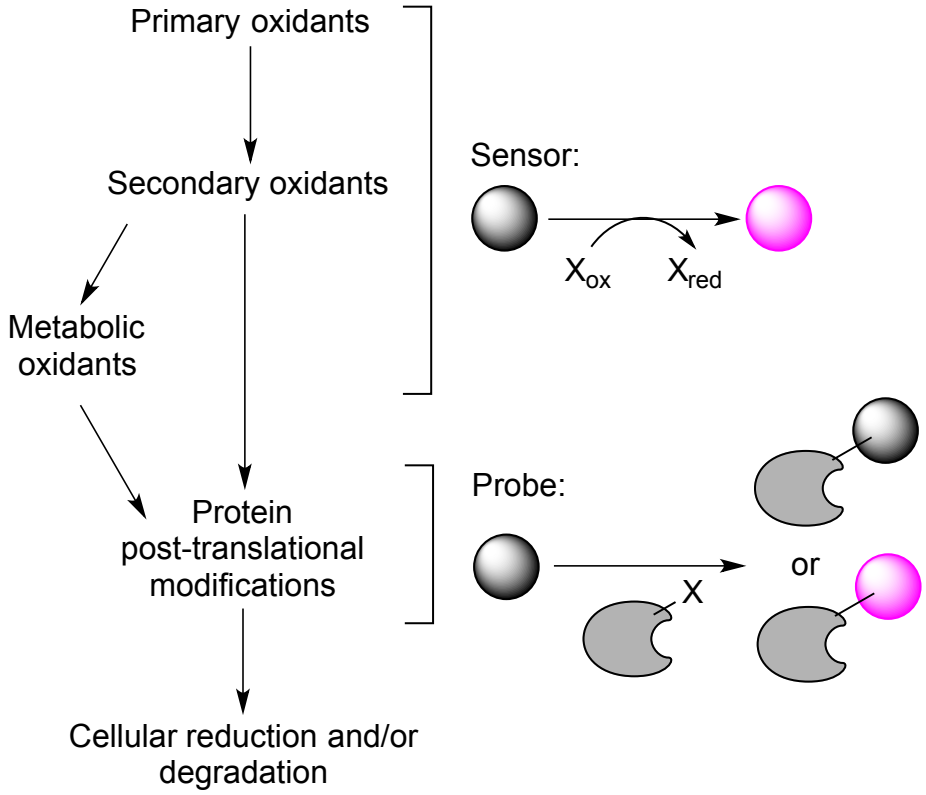

Figure 1-14. Methods to detect cellular oxidation.
Small molecule primary, secondary and tertiary oxidants can be detected with redox sensors. These molecules are modified selectively or non-selectively by the oxidant, and change their spectral properties to allow detection. However, they remain as,diffusible small molecules. Probes react at the protein level with a specific post translational modification X (PTM) and remain attached. The probe can either be used as an affinity capture (black sphere) or as a fluorescent tag (pink sphere).

Both sensors and probes can be used to evaluate the redox state of the cell, but they interrogate different aspects of the process. Sensors typically react to the small-molecule primary and secondary oxidants such as peroxide, hydrogen sulfide, and nitric oxide. As we saw in **Figure 1-04**, this interplay can be quite complex, with many similarly reacting species complicating specificity.

An example of this lack of specificity is the in the commonly used redox-activated dihydrodichlorofluorescein ($DCFH_2$)[126]. In the hydrogenated form, the probe is non-

fluorescent (**Figure 1-15a**). It is activated to dihydrofluorescein (DFC) by reactive oxygen species, and is often billed as a selective probe for peroxide. However, as one can see from **Figure 1-15b**, the activation chemistry is complex and non-specific, where nitrogen dioxide radical, carbonate radical, even glutathione radical can activate it. Critically, molecular oxygen can play a role in its activation, taking the monoradical species to the activated DCF, and generating $O_2^{\circ -}$. It is generally preferable that molecular oxygen not be involved in the activation because it is both prevalent and its concentration varied in tissues. It is generally also not preferred for a redox-sensing dye to generate redox-active species. So while $DFCH_2$ is sometimes used as a sensor for a specific ROS, it should much more correctly be applied as a general sensor for the oxidation state of a cell as a whole.

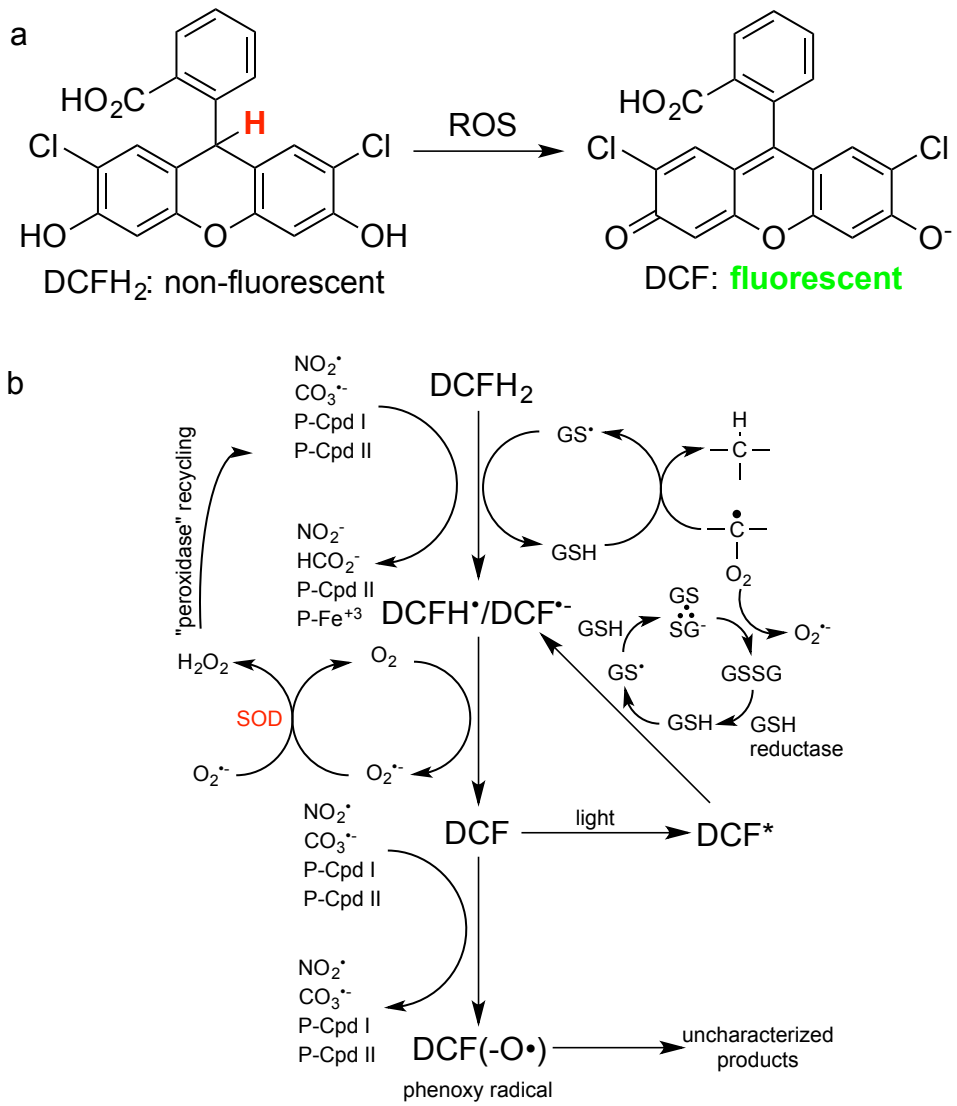

Figure 1-15. Dichlorofluorescein.
a) Reduced dichlorofluorescein (DCFH2) is a widely used sensor for the visualization of reactive oxygen species. b) However, the pathways for non-fluorescent $DCFH_2$ to fluorescent dichlorofluorescein are highly non-specific, with multiple reactive oxygen species, reactive nitrogen species, and reactive sulfur species involved in the activation, degradation, and reactivation in the complex network.

Below we shall discuss some of the mechanisms of more specific probes. These generally go by one of two mechanisms. In the first, the electronics directly attached or part of the fluorophore core is directly modified and an active form is generated from an inactive form. The $DCFH_2$-to-DFC transformation is an example of this, where the

central *meso* carbon of $DCFH_2$ is sp^3-hybridized, rendering the dye completely non-fluorescent. The esters of fluorescein, resorufin, and coumarin are popular to measure the properties of esterase, while the amides of rhodamine, aminonaphthalene and aminocoumarin can measure protease activitycaspase[127]. The acyl groups attached to the electron-donating portions of the dyes prevent the necessary electronics.

The second mechanism alters the chemical properties of pendant groups that do not directly contribute to the fluorophore core. In order to affect the fluorescence of the dye, these pendant groups quench fluorescence by a process known as photoinduced electron transfer (PET, or simply photoelectron transfer). In this, the excited electron of the fluorophore, which normally decays from the excited state to the ground state with the release of an electron, has favorable electronics to be transferred to the slightly lower energy of the LUMO of the acceptor. From there, it undergoes non-radiative decay and collapses non-productively (i.e. non-fluorescently) to the ground state (**Figure 1-16a**). Alternatively, the HOMO of the pendant group can be higher than the HOMO of the dye, and so when the electron of the dye is excited, the donor electron transfers to fill the molecular orbital. The excited electron then, like the first case, collapses non-productively (**Figure 1-16a**).

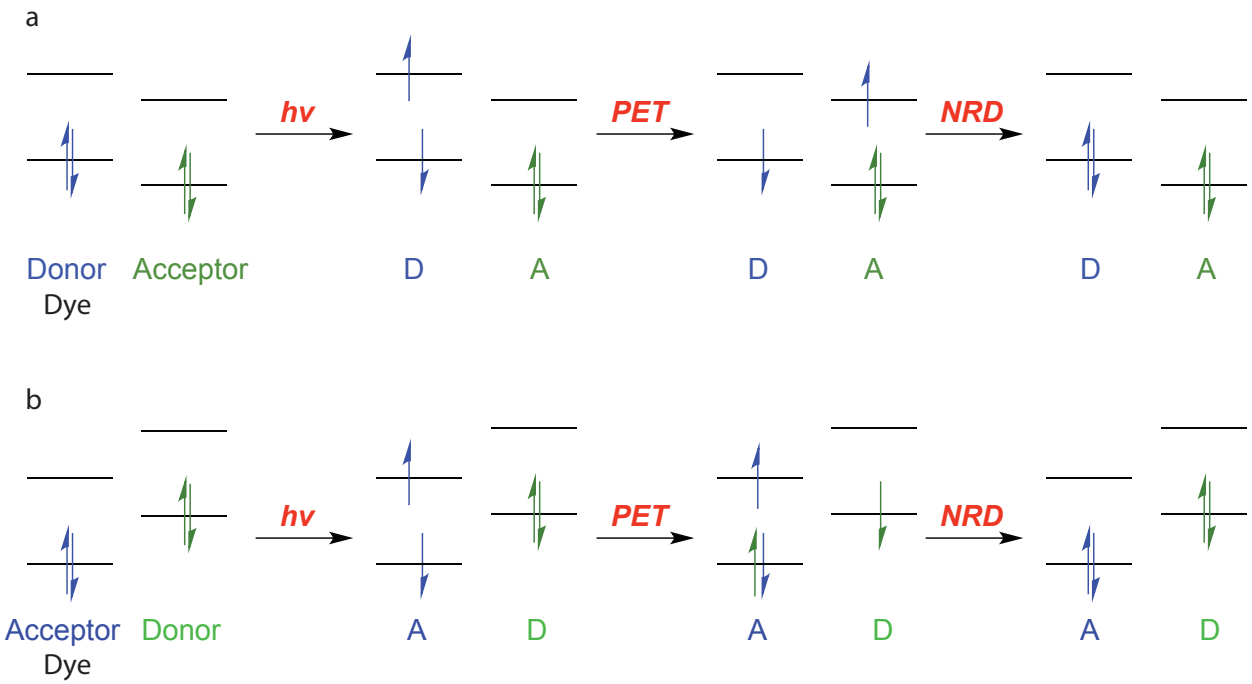

Figure 1-16. Mechanism of fluorescence quenching by photoinduced electron transfer (PET).
a) Upon exposure to an appropriate wavelength of light, an electron of donor D, typically a dye is excited. It relaxes through transfer to a lower acceptor energy level through PET, where it further relaxes to the ground state by non-radiative decay (NRD). b) Alternatively, in the case where the pendant group has a higher HOMO, the donor electron fills the hole left by the excited electron of the fluorophore, which then undergoes non-radiative decay.

To demonstrate some of the sensors that have been developed for RxS, **Figure 1-17** and **Figure 1-18** shows some examples of the mechanisms used to detect H_2S, H_2O_2, $NO^{\cdot}$, and $O_2^{\cdot -}$. Of these, H_2S has the greatest variety of mechanisms, from reductions of masked amines (-NHOH[128], $-N_3$[129], $-NO_2$[129]) or oxide (from –O-R[130]), reactions with disulfides[131], Michael acceptors[132], aryl substitutions[133], and other cleavage mechanisms. In contrast, detection of peroxide almost universally relies on direct peroxolysis of aryl boronic esters on the fluorophore core[134], installing a hydroxyl group and generating the active fluorophore. Detection of nitric oxide involves

condensation with an ortho-diaminobenzene ring to a benzotriazole[135-137]. The electron-rich diaminobenzene acts as a PET quencher, and transformation of the group into the much more electron-poor benzotriazole sensors. And the superoxide sensor relies on simple nucleophilic cleavage of the triflate group to release the fluorophore[138].

In this brief overview, is becomes clear that despite the diversity of dye scaffolds, which include aminonapthalenes, xanthene (fluorescein and rhodamine), cyanines, and BODIPY structures, there are only a small number of mechanisms by with RxS sensors work. While these sensors have each demonstrated to be sufficient to measure RxS in simple and complex mixtures, they are limited to fluorescence microscopy of small molecules. Because of their diffusion, they will only be able to tell gross locational information: cytoplasm, nucleus, Golgi. Therefore, we will now discuss chemical probes for oxidation.

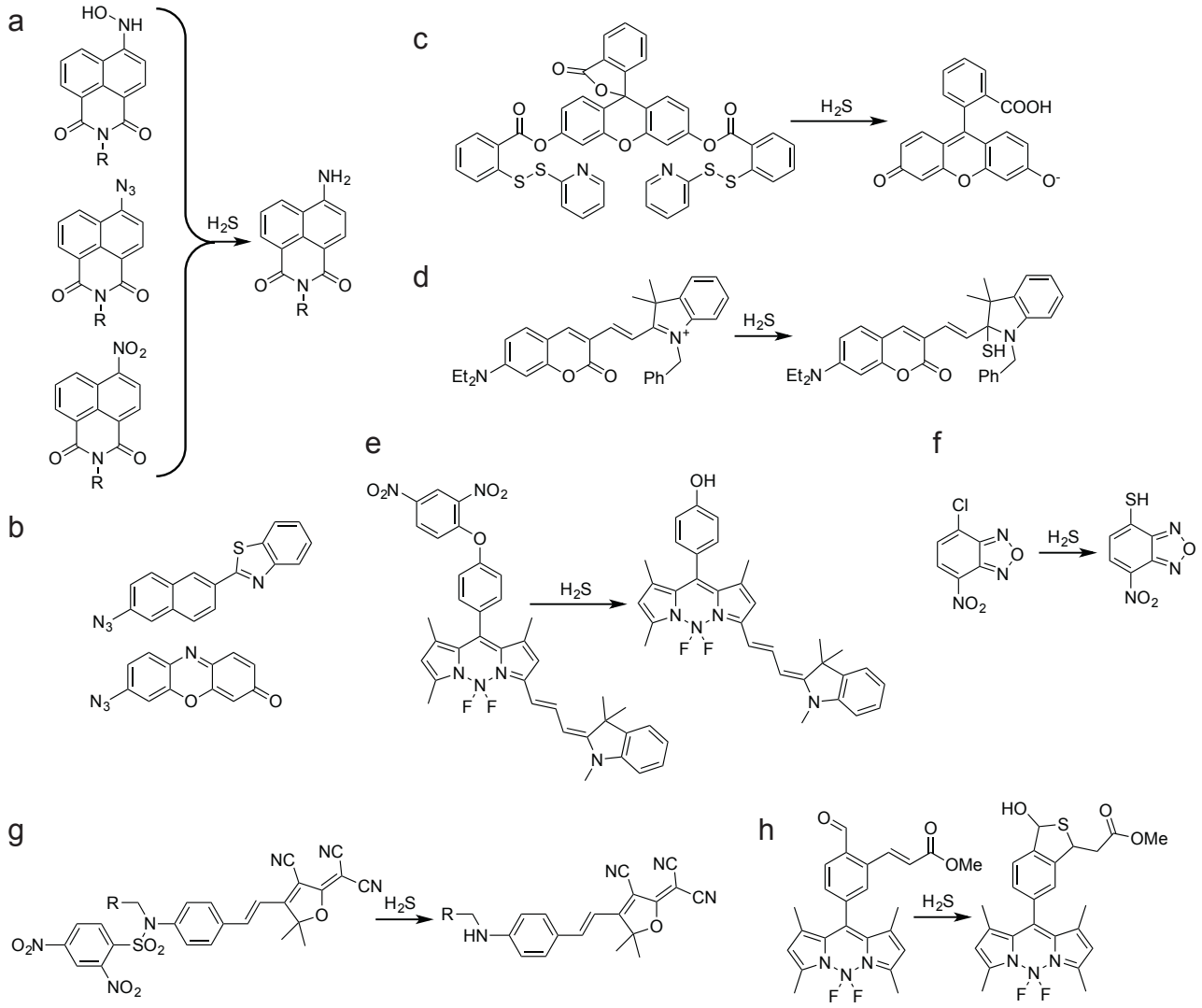

Figure 1-17. Mechanisms of H_2S sensor detection.
a) Hydrogen sulfide can easily reduce many functional groups. These turn electron-withdrawing groups into electron-donating groups, enhancing fluorescence. b) Many different scaffolds use the azide-reduction approach. c) The nucleophilic properties of H_2S can be exploited to regioselectively cleave disulfides and form a reactive thiosulfide that can cleave the ester and release the latent fluorophore[131]. d) This soft nucleophilicity of H_2S can also disrupt conjugation to quenching moieties[139]. e, f) H_2S can participate in SnAr to either remove a quenching group[133] or establish favorable electronics[140]. g) Activated sulfonamides can also be cleaved[141]. H) Other sensors utilize the bifunctional nature of H_2S for a two-step nucleophilic addition to negate a quenching group[132].

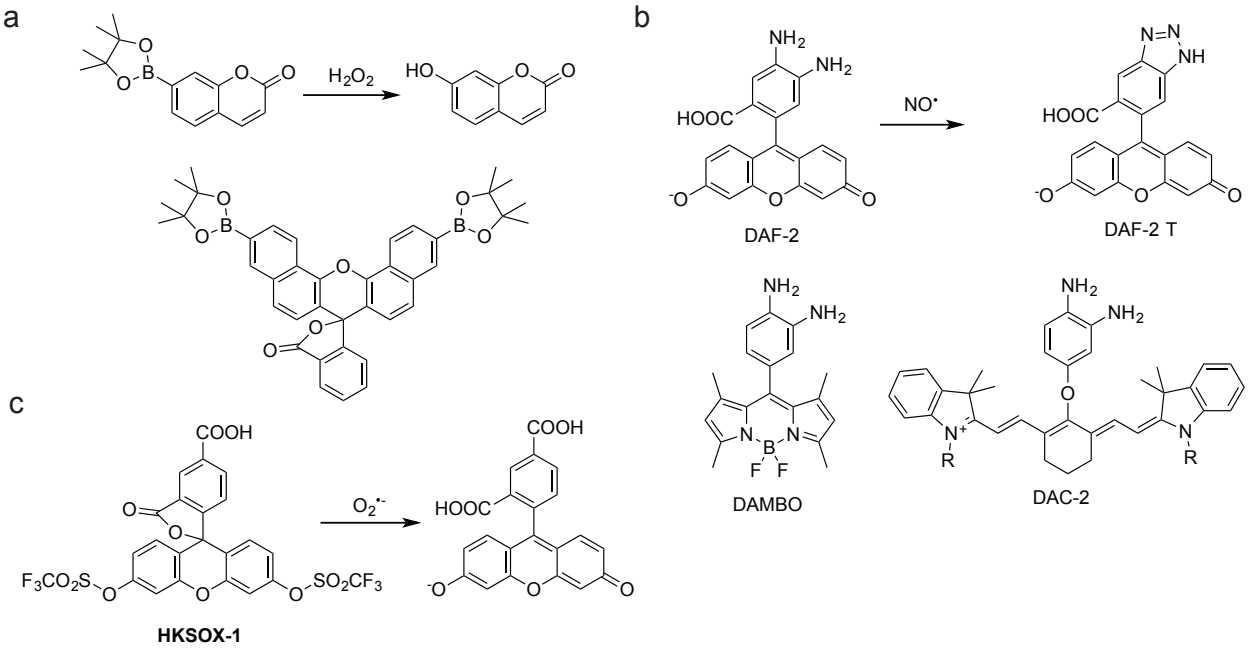

Figure 1-18. Other small-molecule redox sensors.
a) Peroxide sensors utilize boronic acid peroxolysis to release a latent fluorophore[137,142,143]. b) nitric oxide sensors use 1,2-diamino phenols as PET quenchers. Upon conjugation to NO˚ the resulting triazole no longer quenches the florophore[135-137]. c) A superoxide probe uses the nucleophilic aspect of the $O_2^{\circ-}$ to release fluorescein.

There is some controversy as to whether or not the activity of sensors that typically have been attributed to ROS are actually RSS[144].

1.12. Genetically encoded redox sensors

Since the discovery of green fluorescent protein (GFP)[145] and development of the host of fluorescent protein (FP)[146], the ability to genetically encode, and express a fluorescent dye has played a central role in biochemistry. GFP (**Figure 1-19a**) is an eleven-sheet barrel than encases an internal fluorophore composed of inward-facing

amino acids. These are routinely joined to proteins of interest to track expression and cellular localization. Many excitation-emission pairs have been developed across the visible light spectrum, and while the chromaphore for GFP is displayed below, in actuality these are built off of several colors of fluorescent protein.

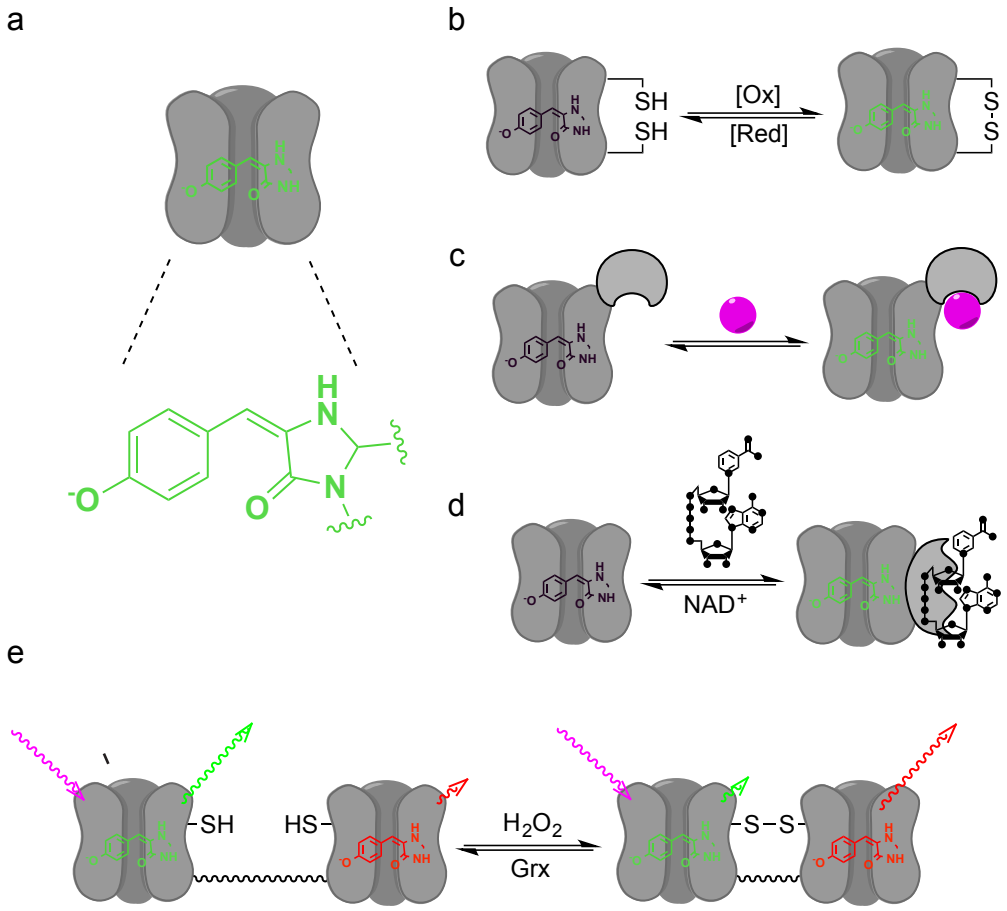

Figure 1-19. Genetically encoded redox sensors.
a) The chromaphore of GFP is tucked inside the β-sheets that are critical for fluorescence. b) Simple redox sensor in which a disulfide bond formed from two proximal cysteines increases the fluorescence of the dye. c) General model for protein co-sensor. d) NAD^+ sensor incorporates a Rossman fold to bind NAD^+. The NAD^+/NADH balance is one indication of the redox state of the cell. e) FRET-based redox sensor

The simplest of the redox-FP's is one in which two thiols are proximal on the external face (**Figure 1-19b**). Like Prx or Trx, upon exposure to an oxidant, these form

an intramolecular disulfide bond, which activates the dye[147]. In practice, this exchange happens quite slowly. Thus as a general feature of genetically encoded sensors, additional biomolecules can be express onto this to either improve the biochemical properties or fluorescent sensing (**Figure 1-19c**). The simple co-expression of some proteins, like glutathione reductase (Grx) to the media greatly increases the rate of sensing for the sensors in **Figure 1-19b**[148]. Others have fused peroxidases, such as Orp1, to the fluorescent protein with the theory that hydrogen peroxide-derived oxidation of thiols to disulfides is in fact mediated in a stepwise fashion by the much more rapid peroxidases, which appears to be the case[149]. Sensing other aspects of the redox balance of cells, Rex domains contain a Rossmann fold, a nucleotide binding domain, whose specificity can be selectively tuned to bind to NAD^+ (**Figure 1-19d**)[150]. The NAD^+/NADH balance is one indicator of redox balance. Finally, fluorescence resonance energy transfer (FRET) probes operate in a similar manner to the monomeric disulfide-forming fluorescent proteins, but with the added bonus of having lower intrinsic background due to the excitation of FP-1 being further from the excitation of FP-2 (**Figure 1-19e**)[151]. Like many of these probes, they are often ratiometric, with one conformation and spectral peak going up with another conformation and spectral peak going down. It should be noted that all genetically encoded fluorescent molecules are sensors, as no endogenous protein functional groups react with irreversible covalent bonds with oxidized cysteine species.

1.13. Covalent sulfenic acid probes

As opposed to fluorescent sensors, fluorescent *probes* remain covalently or pseudo-covalently attached to the biomolecule. They are not free to diffuse around the cell without the movement of the appended protein. Therefore the samples can be prepared by cell fixation, in which proteins are crosslinked with formaldehyde or denatured with a methanol or acetone solution and rendered insoluble while the background of remaining small molecules are washed away. Therefore, due their compatibility with cell fixation, probes do not necessitate activation, or to be 'turned on'.

Because chemical probes are covalently bound to the protein of interest, they are also amiable to other sorts of study besides fluorescence microscopy, such as SDS-PAGE analysis or proteomic analysis by LC-MS.

The diversity of chemical probes for all sorts of post-translational modifications is large, so we will focus simply on the reactive probes for sulfenic acid. The primary molecule that has been used to study sulfenic acids is dimedone (**Figure 1-20a**)[108]. Dimedone is an active methylene compound (AMC) that can readily enolize into a soft nucleophile that can then attack sulfenic acids.

However, the published reaction in **Figure 1-20a** is unlikely to be the true reaction mechanism, because the pKa of dimedone is 4.3, meaning that only 0.1% of the reacted probe is going to be in the neutral protonated form[152]. Thus the enolate is more likely to be the reactive nucleophile, which makes a great deal of chemical sense (**Figure 1-20b**). This is supported by the observation that reaction rates drop drastically when the pH is dropped, from 1.7 M^{-1} s^{-1} at 37 °C[153] and pH 7.0 to 0.008 M^{-1} s^{-1} at 25 °C pH 5.5[152]. The substrate in both cases was AhpC C166S.

Once the probe reacts and forms the stable thioether, it has a *second* remaining α-proton that likely has a pKa not substantially far from the pKa of the unreacted probe, thus we hypothesize that the probe undergoes a second deprotonation, returning to the anionic form.

Dimedone-based probes may be as simple as DYne-2[154], a 'click'able version of the AMC. The 'click' reaction is a copper-catalyzed terminal alkyne-azide cycloaddition, resulting in a highly thermo- and chemostable 1,4-triazole[155]. This allows the attachment of a wide array of probes, from fluorescent dyes to affinity probes like biotin for pull-down procedures and proteomic analysis. Alternatively, these probes can come with the reporter group pre-conjugated, such as dimedone-FL[153], and α-dimedone antibodies have been developed for enrichment of labeled samples (**Figure 1-20b**)[156]. Finally sotopically labeled d_6-dimedone/iododimedone pairs for ratiometric profiling of thiols and sulfenic acids by mass spectrometry[154].

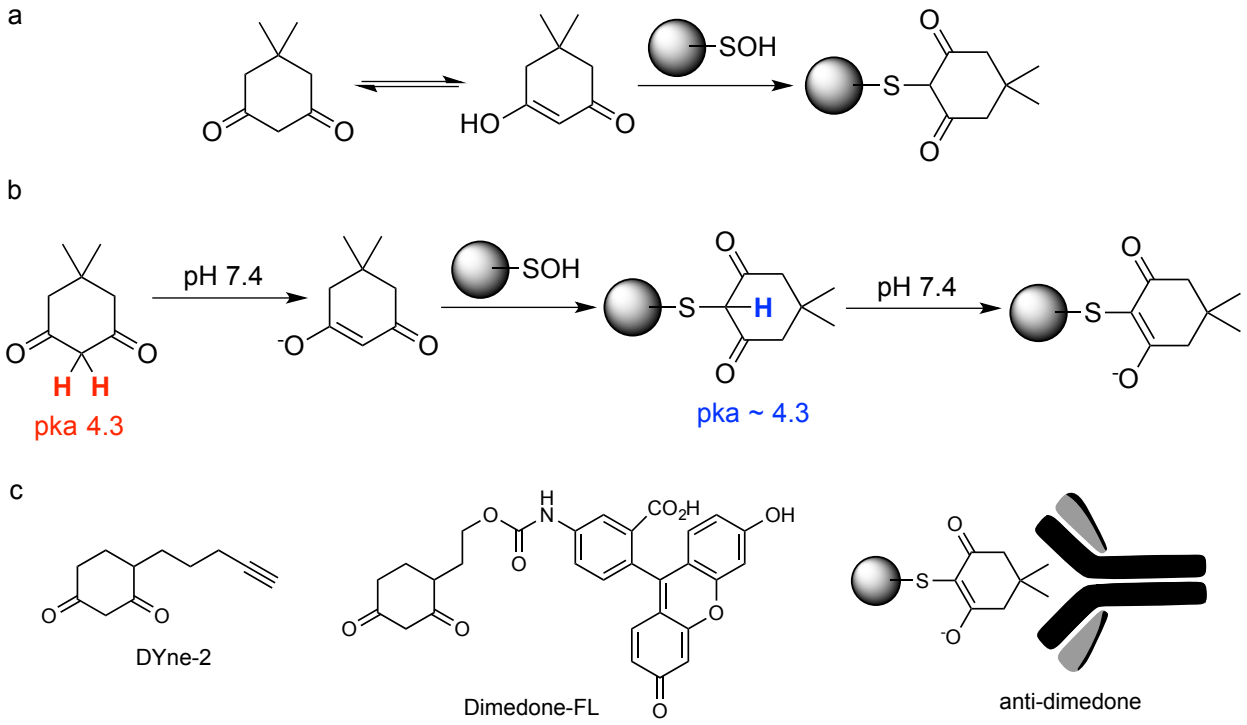

Figure 1-20. Dimedone as a sulfenic acid probe.
a) Published mechanism of sulfenic acid condensation with dimedone. The enol form of dimedone reacts with the sulfenic acid, forming a stable thioether. b) However, this is unlikely to be the correct mechanism, due to the pKa of the α-proton that is far below physiological. Furthermore, a second deprotonation is likely, leaving an anionic product. c) Several different types of probes have been developed, for either secondary conjugation (DYn-2), direct fluorescent detection (Dimedone-FL) or α-dimedone affinity.

Though sulfenic acids are not stable on their own, sulfenamides are isolable and by traditional chemistry[157]. The dipeptide sulfenamide MeOVal-CysSA-Cbz is stable in DMSO solution, but when put into water, hydrolyzes to the sulfenic acid (**Figure 1-21a**)[158]. As stated previously, it is unknown which species contributes to the reactivity more. The sulfenic acid eventually disproportionates and degrades to a complex mixture. However, MeOVal-CysSA-Cbz can be used to test the rate of addition of various probes (**Figure 1-21b**)[158].

Because the slow kinetics other biochemical properties of dimedone leave something to be desired, effort has been made to search for other reactive AMCs (**Figure 1-21c**). Leslie Poole's lab introduced linear probes based on alkyl acetoacetates[159]. These probes have the apparent advantage of low cellular toxicity and facile cleavage; once bound and enriched, the AMC can be separated from the alkyne/triazole by hydroxylamine. The Carroll Lab conducted mass-spectrometry based rate profiling of a truly astounding number of AMCs, some of which are highlighted here. Their maximum rate was 3.175 M^{-1} s^{-1}, an increase of approximately 450 times faster than dimedone[158]. This remarkable rate increase speaks to the high degree that the electronics of the electron withdrawing groups surrounding the α-carbon of the probe can influence the reaction.

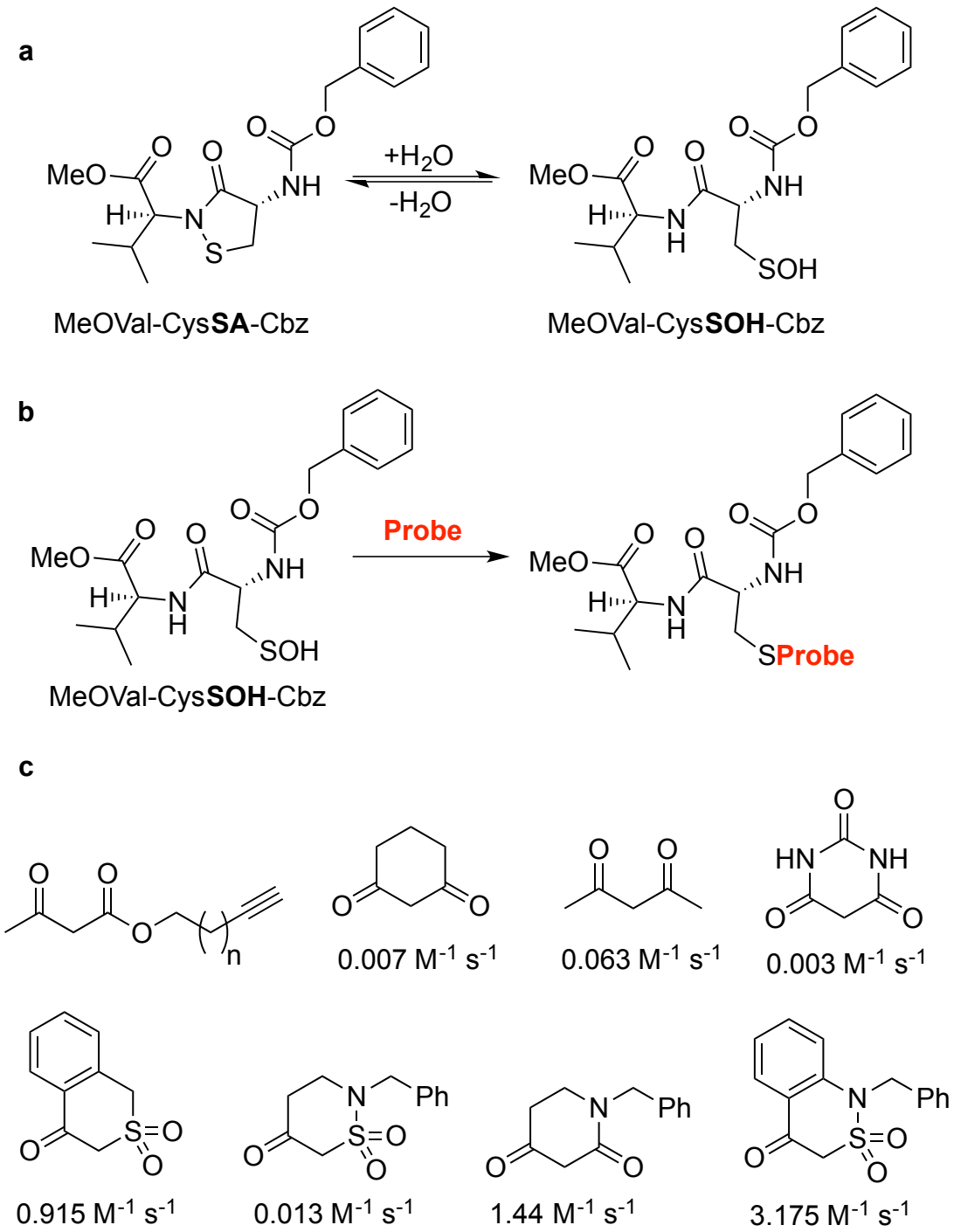

Figure 1-21. Model sulfenic acids and rates.
a) The small molecule sulfonamide MeOVal-CysSA-Cbz is a stable, isolable peptide, which b) reacts with AMC probes. c) a selection some of the probes, and their rates, that have been developed recently.

1.14. Electrophilic and electrocyclic reagents

The sulfur of the sulfenic acid is a potential nucleophile. Though the reactivity of it as a nucleophile is dampened somewhat by the electron-withdrawing effect of the oxygen, alkylating agents such as methyl iodide are sometimes used to trap the sulfenic acid as a sulfoxide. The pKa of the sulfenic acid (12.5) renders it too weakly acidic to be largely deprotonated at physiological pH, and so it will largely be in its less reactive neutral form. The nucleophilic anionic form will also be present in much smaller amounts (0.0001%) than its cysteine counterpart (~8%) at physiological pH. Furthermore, a widespread issue of electrophilic reagents is that all the native reactive residues of proteins are nucleophilic, so competition and selectivity is a general problem.

4-chloro-7-nitrobenzo-2-oxa-1,3-diazole (NBD-Cl) is an electrophilic trapping reagent that reacts via nucleophilic aromatic substation to covalently bind to sulfenic acids and change absorbtion maxima to 347 nm[160]. However, because many nucleophilic residues exist (thiols, lysines, serines) this is not selective, or considered a favorable probe for imaging or quantitation. However, it does highlight one way that photophysical changes can be induced by sulfenic acid binding to the probe.

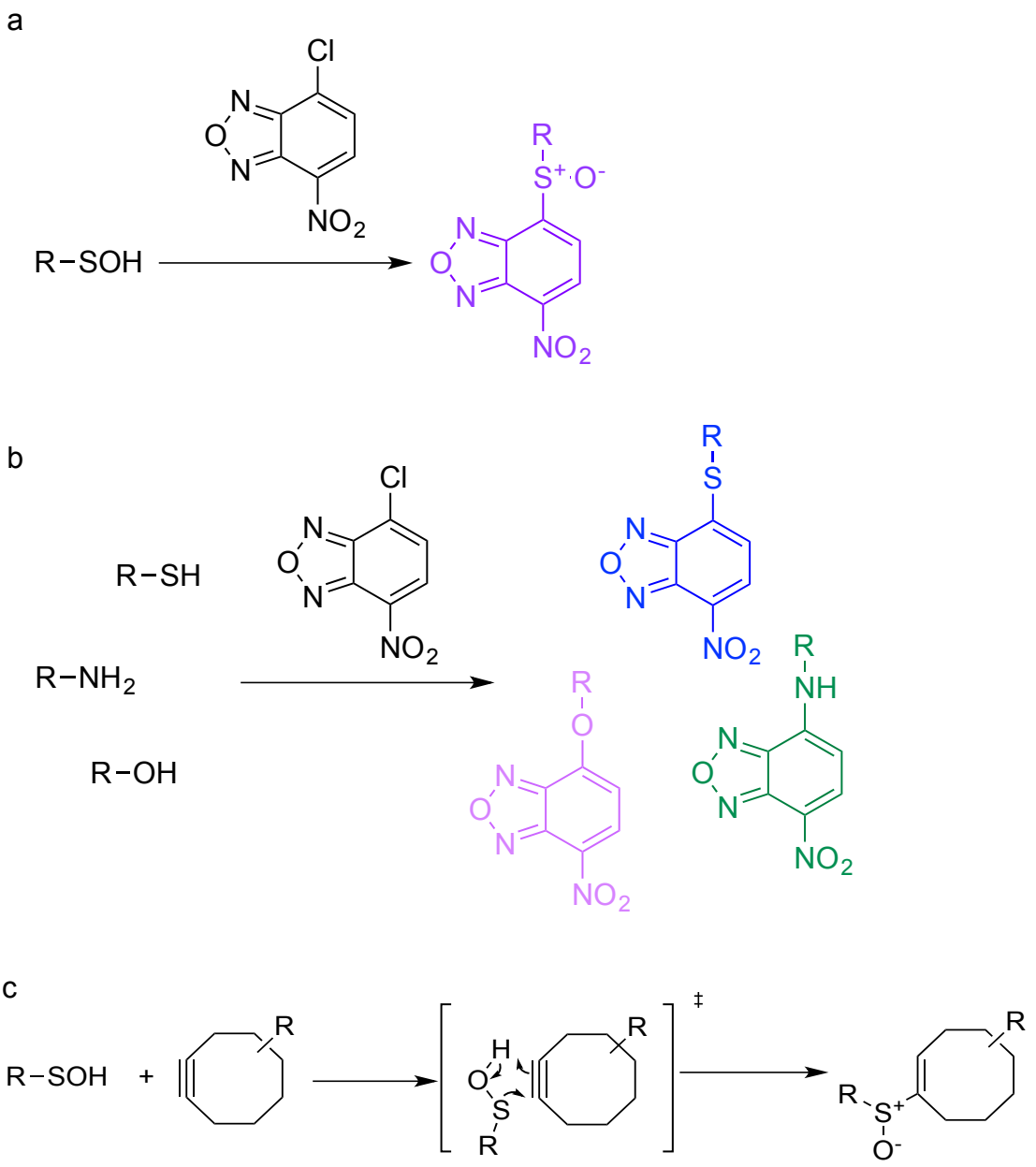

c

Figure 1-22. Electrophilic and electrocyclic reagents.
a) Sulfenic acids react with the pro-dye NBD-Cl to form a colored sulfoxide product with an absorbance maximum at 347 nm. b) However, because of the prevalence of other nucleophilic groups in the cell, other colored products are formed with thiols, alcohols, and amines. These functional groups are like present in vastly higher amounts than cysteines in the specific oxidation state of sulfenic acids. c) Cyclooctynes undergo a putative electocyclization with suldenic acides, forming ene-sulfoxides.

For the sake of completeness, some other probes should be mentioned. Cyclooctynes have achieved some level of popularity as ‘copper free’ click reagents,

allowing the reagent to form a triazole without a catalyst or the requirement of being a terminal alkyne. However, the strained nature of the bond also makes it susceptible the addition reactions. Alkynes are known to undergo the thiol-yne reaction and alkenes the thiol-ene reaction. Cyclooctynes have been shown to undergo an addition reaction with sulfenic acids; however, forming sulfoxides-enes[161]. It is highly unlikely that this is selective for sulfenic acids, and in fact has been shown to be also is attacked by thiols.

1.15. Conclusions.

Cellular redox homeostasis exists in a complex milieu of highly reactive small-molecules species that straddles the narrow divide between enough oxidative power to support respiratory metabolism but not enough to tear apart the genetic memory and protein machinery of the cell. An interconnected network of antioxidant proteins, redox-sensing proteins, transcription factors, and redox chaperones maintains the macroscopic redox homeostasis, while at a microscopic level, NOX, xNOS, and CγL and CβS, HO-x produce small-molecule ROS, RNS, RSS, and RCS respectively and lead to RLS. While the macroscopic regulation keeps the background redox environment of the cell fairly constant, these RxS protein produce bursts of redox species that are quickly consumed and diluted in the cell, but can dramatically influence the local environment. Because structure informs function and location informs function, the spacial constraint is a critical regulatory mechanism of the cell.

Sulfenylation is an intersectional modification. Dimedone, and derivatives of 1,3-cyclohexanedione remain the primary probes to study this. However, in the current state of the art, such probes have only been used with fixed cells, and are incompatible with

live-cell imaging. Live cell imaging represents a more accurate state of the cell, does not wash away small organelles or features, and allows for before-and-after measurements and stimulation.

In order to overcome the high background of unbound probe*, the challenge of developing a live-cell probe is that it must be designed to leverage its covalent attachment to induce a sensor-like spectral shift*. Therefore, some sort of chemical change must occur upon binding, rendering a measurable spectroscopic shift. Furthermore, being able to find a way to study them in live cells is a necessary step to advance to working *in vivo*. While live-cell imaging is an improvement over fixed-cells as a more representative way to examine the biology, *in vivo* analysis is an improvement over plate-grown cultured cancer cell lines.

Therefore the questions that will attempt to be answered herein are:

- How can we utilize rationale organic chemistry to develop probes to examine the biochemistry of and visualize sulfenic acid formation in live cells? Can we use these probes to visualize cellular stimulation? Can we distinguish between different cancer cell lines?
- Further questions are: how can we translate what we have learned in via rationale organic chemistry to image sulfenic acids *in vivo*, where organs and structures are as they are in living creatures, as opposed to various cancer cell lines grown in an extracorporeal setting *in vitro*?
- Ultimately, what is the role of sulfenic acids in normal biology, and in disease states?

This thesis contains work that has attempted to develop and describe tools that can interrogate these questions.

Chapter 2: Rapid bioorthogonal ratiometric live-cell imaging of protein *S*-sulfenylation

Abstract. Protein *S*-sulfenylation describes the dynamic post-translational oxidation of cysteine residues, which is integral to redox regulation and cellular signaling. Here we report an α-fluoro-substituted aminonaphthalene-dimedone (F-DiNap) probe, which displays a dramatic excitation ratio change after sulfenic acid conjugation. DiNap α-fluorine substitution accelerates sulfenic acid condensation by 10^3- to 10^5-fold and blocks nonspecific condensation with biological aldehydes. Overall, F-DiNap provides a selective ratiometric tool for live-cell imaging of protein S-sulfenylation.

Individual contributions

Christopher T.M.B. Tom designed and carried out all chemical synthesis, characterization, and biochemical analysis of the DiNap probes. Lyanne Gomez-Rodriguez performed spectroscopic measurements. Kristin J. Labby cloned, expressed, and purified recombinant proteins. Prof. Paul M. Zimmerman performed computational modelling. Jeannie L. Hernandez prepared MCF10A-Snail cells. Yu-Hsuan Kuo performed MCF10A-Snail DiNap labelling and gel-based analysis. Matthew B. Stone

and Prof. Sarah L. Veatch performed TIRF microscopy and analysis. Prof. Paul M. Jenkins performed confocal imaging and analysis. Christopher T.M.B. Tom and Prof. Brent R. Martin designed the experiments and wrote the manuscript. Prof. Brent R. Martin was gracious enough to provide funding for this over the last four years.

2.01. Introduction

The cysteine sulfhydryl group is a key target of oxidative stress and is readily modified by redox-active species to induce temporary and sometimes permanent protein damage. When exposed to hydrogen peroxide or other select redox active agents, cysteine thiols are oxidized to sulfenic acids, which are quickly resolved by a second thiol to form disulfides[162,163]. In the absence or steric occlusion of a resolving thiol, the sulfenic acid can be long-lived, establishing *S*-sulfenylation a reversible protein post-translational modification[164]. In several examples, *S*-sulfenylation has emerged as a redox regulatory switch, coordinating complex cellular cues[116,163-165] by chemically modifying proteins as part of conserved redox-dependent signaling cascades[116,163].

The active methylene compound dimedone is the primary method for detecting sulfenic acids in biological systems[159,166-170]. When added to cells, the dimedone nucleophilic enolate reacts with sulfenic acids to form a stable thioether, linking the probe to sites of *S*-sulfenylation. This covalent adduct can then be detected either by anti-dimedone antibodies[156] or by conjugation to a reporter group[159,166,167,169,171]. Strained cyclooctynes, benzoxaborazoles, and boronic acids have also been explored as sulfenic acid labeling reagents[161,171], opening new directions for improved analysis. Nonetheless, in order to monitor protein oxidation in living cells, new fluorophores are needed that change their fluorescent properties after sulfenic acid conjugation.

2.02 Results and Discussion

In order to engineer such a fluorescence probe for *S*-sulfenylation, we began by examining the reaction mechanism of dimedone. Dimedone possesses two acidic α-

hydrogens (pK_a = 4.3)[172], which promotes deprotonation and enolate formation at physiological pH. When in proximity to a sulfenic acid, the enolate reacts with the sulfenic acid to form a transient diketone, which is followed by a second deprotonation to form the product enolate (**Scheme A-01**). Based on this scheme, we hypothesize that only one α-hydrogen is required to react with a sulfenic acid, and substitution of a single α-hydrogen with a small blocking group would prevent the second deprotonation and trap the product diketone. Thus, the enolate-to-diketone transition could switch the chemical and electronic properties of a conjugated dye after reaction with a sulfenic acid, providing a direct approach for live-cell imaging of this emerging post-translational modification.

2.03. DiNap design and testing

Aminonaphthalene fluorophores, such as Lucifer Yellow, are typically attached to biomolecules at the imide nitrogen for use in biological imaging[173]. We hypothesized that replacement of the imide nitrogen with a carbon would create a sulfenic acid reactive fluorophore. Dimedone-naphthalene (DiNap) probes were synthesized at gram scale in two steps as dark red powders (**Scheme A-02 and A-03**). In the enolate form, H-DiNap (**3a**) has a single α-hydrogen, while the substituted Me-DiNap (**3b**) and F-DiNap (**3c**) have none (**Figure 2-01a**). Next, each DiNap probe was evaluated for labeling efficiency using the mutant *E.coli* peroxiredoxin AhpC (C166S), which lacks the resolving thiol and forms a stable sulfenic acid[162]. F-DiNap showed surprisingly more intense labeling of AhpC (C166S) than H-DiNap (**Figure 2-01b**), but little labeling by Me-DiNap. Importantly, F-DiNap yields a similar profile of labeled proteins as the

alkyne-linked dimedone derivative Dyn-2 (**Figure A-01**)[116], labels AhpC (C166S) in an oxidation-dependent manner (**Figure A-02**) while also being subject to overoxidation to sulfinic (RSO_2^-) and/or sulfonic (RSO_3^-) acids at higher concentrations of peroxide (**Figure A-03**). F-DiNap labeling can be removed by dimedone (**Figure A-04**) albeit at concentrations exceeding the concentration of F-DiNap itself. F-DiNap reacts to completion with a sulfenamide standard (**Figure A-05**), and furthermore, sulfenic acid conjugation yielded a >50 ppm ^{19}F-NMR shift (**Figure A-06**), potentially offering an expanded toolkit for sulfenic acid detection that will be discussed in **Chapter 3**.

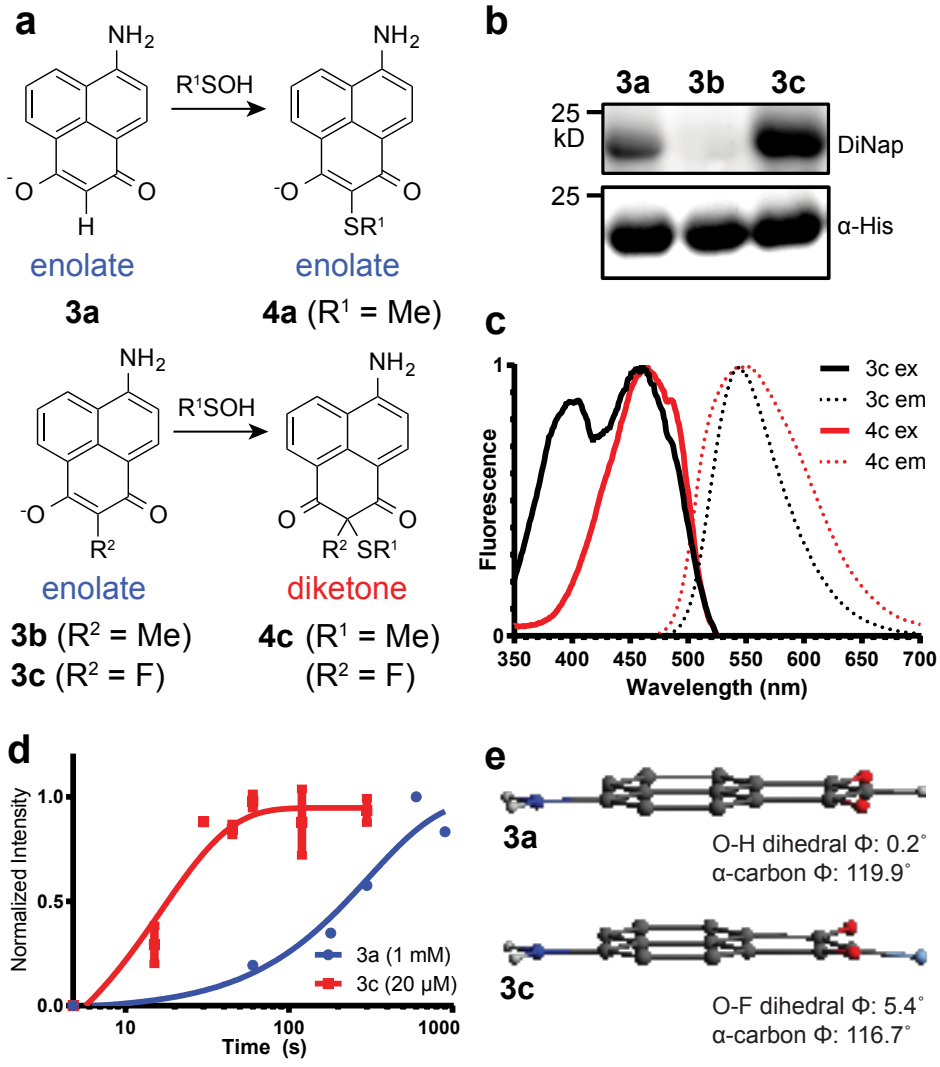

Figure 2-01. DiNap probes react with *S*-sulfenylated proteins.
a) Unsubstituted active methylenes, such as DiNap **3a**, react with sulfenic acids in their enolate form. After sulfenic acid conjugation, the probe undergoes a second deprotonation to return to the enolate form. However, α-substituted Me- and F-DiNap probes are locked as a diketone after conjugation. b) Comparison of reactivity between **3a-c** in AhpC (C166S) over-expressing bacterial lysates by in-gel fluorescence (Ex. 488 nm, Em: 555/20 nm). c) F-DiNap fluorescent excitation and emission spectra before and after conjugation. d) Comparison of the rates of reaction between H-DiNap and F-DiNap with AhpC (C166S). e) Simulated substituent geometries demonstrate that F-DiNap distorts significantly from sp^2 planarity to increase the reaction rate.

We then synthesized small-molecule standards to determine the spectral properties of the dyes-conjugate pairs for their potential in cell imaging. Since small-molecule sulfenic acids are unstable ($t_{1/2}$ <1 min)[174], we found that methylmethane thiosulfonate (MMTS) can act as simple one-step surrogate to provide a direct route to the reacted standards **4a** and **4c** (**Scheme A-04**). In aqueous buffer, MMTS reacts quickly with dimedone, but F-DiNap reacts only with MMTS in organic solvent with base (**Figure A-07**). Both H-DiNap (**3a**) and F-DiNap (**3c**) have similar spectral properties (**Table A-01**), although **3a** is nearly three times brighter than **3c**. Both DiNap probes are maximally excited at 460 nm and to a lesser degree near 400 nm. After conjugation with MMTS, the 400 nm excitation peak in is reduced in **4a** and completely absent in **4c** (**Figure 2-01c and Figure A-08**). In acidic buffers, the protonated enol tautomer lowers the violet excitation peak (**Figure A-09**), confirming the enolate as the predominant physiological species and established a spectroscopic method to measure the pK_a of each DiNap probe (**Figure A-10**). In addition, **3a** is 6.8 times brighter than **4a**, which largely cancels out any effective ratio change (**Table A-01**). Conversely, **3c** and **4c** are nearly the same effective brightness, presenting an effective ratiometric sensor for imaging protein *S*-sulfenylation.

2.04 Rate determination and quantum simulation

In an effort to understand why F-DiNap labels more efficiently, we examined the reaction rates for **3a** and **3c**. *S*-sulfenylated human serum albumin is reported to slowly react with dimedone (0.027 M^{-1} s^{-1}), but reacts with glutathione 100-fold faster (2.9 M^{-1} s^{-1})[160] to form a disulfide. Accordingly, when added to living cells dimedone must compete with cellular thiols to efficiently label *S*-sulfenylated proteins, hence new probes with faster reaction rates are highly desirable. As measured by in-gel fluorescence, H-DiNap labeled AhpC (C166S) at roughly the reported rate of dimedone (3.24 M^{-1} s^{-1} and 1.7 M^{-1} s^{-1}, respectively)[96]. Surprisingly, F-DiNap reacted with AhpC (C166S) >900-fold faster than H-DiNap (3020 M^{-1} s^{-1}) (**Figure 2-01d**), and on average 3500-fold faster across a panel of *E.coli* proteins (**Figure A-11** and **Table A-02).**

In order to shed light on the mechanism of rate enhancement, we carried out quantum chemical simulations on both H- and F-DiNap probes. H- and F-DiNap can only react with methyl sulfenic acid when the sulfenic acid hydroxyl group and an available proton leave to form water, and the calculated free energy change for the rate-determining step of F-DiNap is 5.4 kcal / mol lower than H-DiNap. The simulated transition state barrier for methyl sulfenic acid to react with H-DiNap is 28.4 kcal / mol, but only 18.3 kcal / mol when simulated with F-DiNap. This 10.1 kcal / mol difference between the H- to F-DiNap transition energies translates to a maximal 10^7-rate acceleration, supporting the 10^3- to 10^5-fold rate acceleration observed on AhpC (C166S) and other proteins. The fluorine on F-DiNap contributes a strong electron

withdrawing effect, dropping the p_z orbital energy at the α-carbon. However, as compared to the planar H-DiNap, the quantum chemical simulation also revealed the fluorine is 5.4 degrees out of plane (**Figure 2-01e**), suggesting a primed electronic configuration for subsequent sp^3 hybridization following sulfenic acid conjugation is the determining factor for this remarkable rate enhancement (**Figure A-12** and **Table A-03**).

2.05 Selectivity against *in vitro* and biologically-generated aldehydes

Active methylene compounds are known to undergo Knoevanegal condensation reactions with aldehydes in both organic and aqueous solvents (**Figure 2-02a**)[175,176]. After a brief incubation with pyridoxal or glyceraldehyde in phosphate-buffered saline (PBS), we observed complete conversion to the predicted condensation products, as well as secondary Michael addition to the resulting electrophilic unsaturated ketone (**Figure A-13** and **A-14**). We find that dimedone reacts with glyceraldehyde at a rate of 0.059 M^{-1} s^{-1} (**Figure A-15**), which is similar to the rate of reaction with *S*-sulfenylated albumin (ref)**.** In light of these studies, it is important to note that F-DiNap is mechanistically blocked from reacting with aldehydes, since the Knoevanegal condensation requires two α-hydrogens (**Figure 2-02a**).

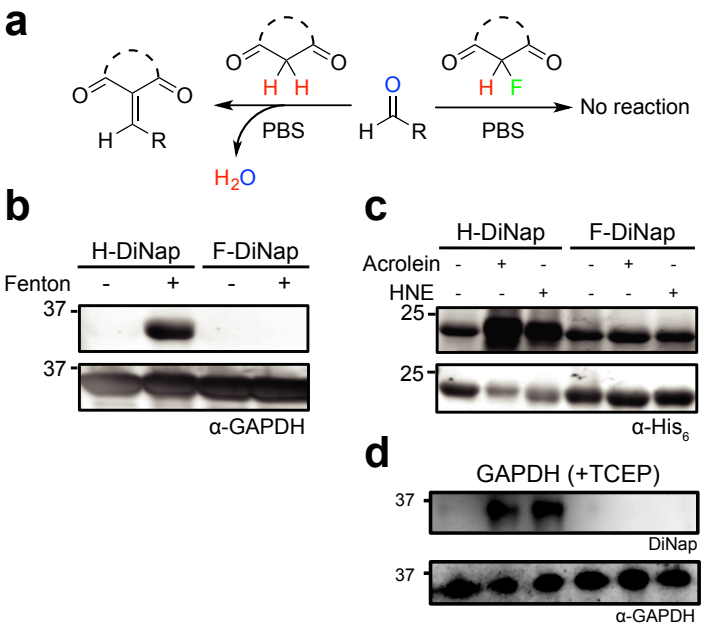

Figure 2-02. F-DiNap is bioorthogonal to aldehydes.
a) DiNap α -fluorine substitution prevents aldehyde condensation. b) Oxidized GAPDH reacts with H-DiNap, but not F-DiNap (Ex. 488 nm, Em: 555/20 nm). c) Addition of acrolein or 4-hydroxynonenal (HNE) to AhpC (C166S) increases labeling by H-DiNap, but not F-DiNap. d) Pre-treatment with TCEP reduces all sulfenic acids and removes all non-aldehyde labeling.

While proteins are proteins are generally not modified with aldehydes under basal conditions, they can be heavily modified under conditions of redox stress. In a process analogous to the Fenton reaction, Cu^{+1}/Cu^{+2} or Fe^{+2}/Fe^{+3}, ascorbate, and hydrogen peroxide react to release hydroxyl radicals, which modify nearby proteins by direct oxidation of arginine, lysine, proline, and the peptide backbone to form protein-linked aldehydes at diffusion-limited rates (**Scheme A-05a**)[177]. To examine the reactivity of DiNap derivatives under these conditions, recombinant glyceraldehyde-3-phosphate dehydrogenase (GAPDH) was incubated with $CuSO_4$, ascorbate, and peroxide. These conditions mimic the common 'click' chemistry conditions used for dimedone labeling of peroxide treated samples. Next, TCEP was added to reduce any sulfenic acids, leaving

aldehydes as the sole electrophiles. Under these Fenton conditions, GAPDH was efficiently labeled with H-DiNap, but there was no detectable labeling by F-DiNap (**Figure 2-02b**).

Protein-linked aldehydes are also formed following peroxidation of long-chain polyunsaturated fatty acids, releasing a diverse array of α,β-unsaturated aldehydes including acrolein and 4-hydroxynonenal (4-HNE). These ene-als react by 1,4-addition primarily with cysteine, tethering a reactive aldehyde to proteins (**Scheme A-05b**). To explore any cross-reactivity, dimedone, acrolein and N-acetyl cysteine were mixed together and produced a series of aldehyde condensation products. Importantly, F-DiNap is completely unreactive under these conditions (**Figure A-16** and **A-17**). Next, the biological ene-als acrolein and 4-HNE were added to AhpC (C166S) or GAPDH-overexpressing bacterial lysates. H-DiNap labeling of AhpC (C166S) was greatly enhanced by each ene-al, while F-DiNap labeling remained constant (**Figure 2-02c**). Similarly, pre-treatment with TCEP eliminated all F-DiNap labeling of ene-al conjugated GAPDH (**Figure 2-02d**), confirming that α-fluoro substitution of active methylene compounds prevents condensation with peroxide-catalyzed aldehyde byproducts on proteins. Because both sulfenylation *and* aldehyde elaboration are initiated by hydrogen peroxide input, this is a relevant level of selectivity that is offered by fluorination.

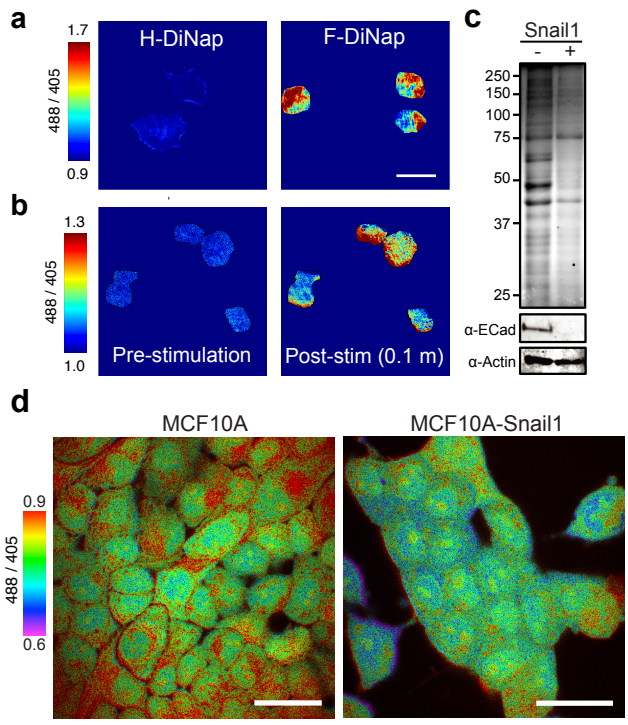

Figure 2-03. Live cell ratiometric imaging of sulfenic acids in CH27 B-cells with DiNap probes.
a) Images were acquired by TIRF microscopy 15 minutes after probe addition, showing spatially resolved ratio changes with F-DiNap. b) Hydrogen peroxide (1 mM) induces rapid F-DiNap ratio changes within a few seconds. Data is normalized to ratios measured after 9 minutes of F-DiNap labeling. Scale bar = 20 μm. c) Snail expression attenuates F-DiNap labeling in MCF10A cells. d) Confocal ratiometric imaging of F-DiNap between MCF10A and MCF10A-Snail cells. MCF10a shows clearly higher levels of sulfenylation, and this appears to be localized in the secretory pathway and along the cellular membranes, with lower levels appearing in the nucleus.

2.06 TIRF and confocal microscopy with stimulation and comparing cell lines

When added to cultured mammalian cells, F-DiNap is highly cell permeant, allowing live cell labeling and gel-based fluorescence profiling of *S*-sulfenylation in different cancer cell lines, corroborating high levels of protein S-sulfenylation in MDA-MD-231 cells (**Figure A-18**)[156]. Next, CH27 B-cells were incubated with H- or F-DiNap probes and imaged by total internal reflection microscopy, alternating excitation between 405 and 488 nm lasers. Over the time course of 15 minutes, H-DiNap labeled cells showed

no change in excitation ratio. In contrast, F-DiNap labeled cells demonstrated a robust excitation ratio change, revealing distinct hotspots at the cell membrane (**Figure 1-03a and Figure A-19**). In some F-DiNap labeled cells, the rapid F-DiNap reaction rates enabled detection of spatially restricted ratio changes within 6 seconds of hydrogen peroxide stimulation, revealing sites of rapid membrane-localized redox stress (**Figure 1-03b and Figure A-20**).

Reactive oxygen species are reported to both promote and suppress cancer, suggesting a complicated network of redox regulation[178]. The transcription factor Snail is elevated in metastatic cancers, and plays a key role in reprogramming cells to undergo epithelial-to-mesenchymal transition[179]. Upon Snail overexpression, we observed a significant reduction in F-DiNap labeling in MCF10A breast cancer cells (**Figure 1-03c**). Confocal ratiometric F-DiNap imaging in live cells confirmed reduced sulfenylation (**Figure 1-03d**), particularly outside of the nucleus. Accordingly, Snail both represses cell adhesion proteins and reprograms the cellular antioxidant response. Indeed, quantitative mass spectrometry profiling of Snail-expressing cells revealed >3-fold elevation of many antioxidant enzymes[180], including peroxiredoxins, superoxide dismutase, and thioredoxin.

2.07. Conclusion

In summary, we present a ratiometric probe for live cell imaging and gel-based profiling of *S*-sulfenylation, and import redox post-translational modification. F-DiNap improves the selectivity and rate of sulfenic acid detection, enabling live-cell ratiometric fluorescence imaging of *S*-sulfenylation at the plasma membrane, as well as revealing a

new role for the transcription factor Snail in reprogramming an antioxidant response in malignancy. By extension, this approach should be transferrable to brighter dye scaffolds and to the development of α-substituted 1,3-dicarbonyls as both fluorescent reporters, affinity probes for mass spectrometry profiling of native *S*-sulfenylation, and ^{19}F-NMR probes for multimodal analysis of protein *S*-sulfenylation.

Chapter 3: ^{19}F probes for the study of sulfenylation by NMR

Abstract

Contrary to the imaging in cultured cells, fluorescence is not in general an appropriate technique to *in vivo* work. Of the available *in vivo* imaging techniques, only nuclear spin techniques, which include nuclear magnetic resonance (NMR) and magnetic resonance imaging (MRI), allow us to probe the chemical state of a sensor or probe, and give several additional dimensions of information besides spacial location and concentration/bioaccumulation. The F-DiNap probe has a fluorine atom at the α-position, and ^{19}F is an excellent candidate for an NMR/MRI sulfenylation reporter. To this end, we be will lay the foundation for an *in vivo* MRI probe by developing a ^{19}F-based NMR probe.

Individual contributions

Christopher T.M.B. Tom designed and carried out all chemical synthesis, characterization, biochemical analysis, and ^{19}F NMR of the fluorobarbituic acid derivatives.

Jack E. Crellin carried out some of the HPLC selectivity, the mass spectrometry analysis, and kinetics experiments.

Christopher T.M.B. Tom and Prof. Brent R. Martin designed the experiments and wrote the manuscript.

z

3.01 Introduction

The study of biological systems *in vivo* by fluorescence microscopy is greatly limited by the broad absorption by tissue of light across the ultraviolet and visible spectrum, which renders most organisms, save a few like zebrafish embryo, opaque. Far-infrared dyes have been used for some limited purposes[181,182]. PEGylated polymers[183], some built with tumor-targeting oligosaccharide groups[184], some are built from quantum dots or other mesoscale particles[185]. Long cyanine dyes can be reversibly photoswitched by thiol-ene addition to one of the double bonds to turn them off[27]. However, these dyes are, by necessity and design, have high molecular weights and possess a high degree of unsaturation that endows them with a number of different chemical and biochemical properties that renders them unsuitable for general study, e.g. low cellular permeability or solubility. Though our previous work represents a significant advancement by enabling live-cell imaging from previous requirements of fixed-cell labeling, imaging sulfenylation on plate-grown cancer cell lines in an oxygenated atmospheric environment is far from the native environment of blood-fed tissues in living organisms. Therefore, we would seek to expand our detection toolkit to enable imaging of sulfenylation *in vivo* to increase our understanding of this phenomenon in physiological systems.

The prominent techniques that can image tissues *in vivo* include ultrasound, X-ray, positron emission tomography (PET), and magnetic resonance imaging, and their *in vivo* applications and factors affecting image sensitivity and resolution are described in detail in **Appendix D** and summarized in **Figure 3.01**. However, of these techniques, only nuclear magnetic resonance, (NMR), magnetic resonance imaging (MRI), and

magnetic resonance spectroscopy (MRS), which directly measure nuclear-spin, can directly measure the chemical environment of the reporter nucleus. Fortunately, one of the most powerful and sensitive nuclei for imaging includes ^{19}F, lies at the heart and is the basis of our chemical switch.

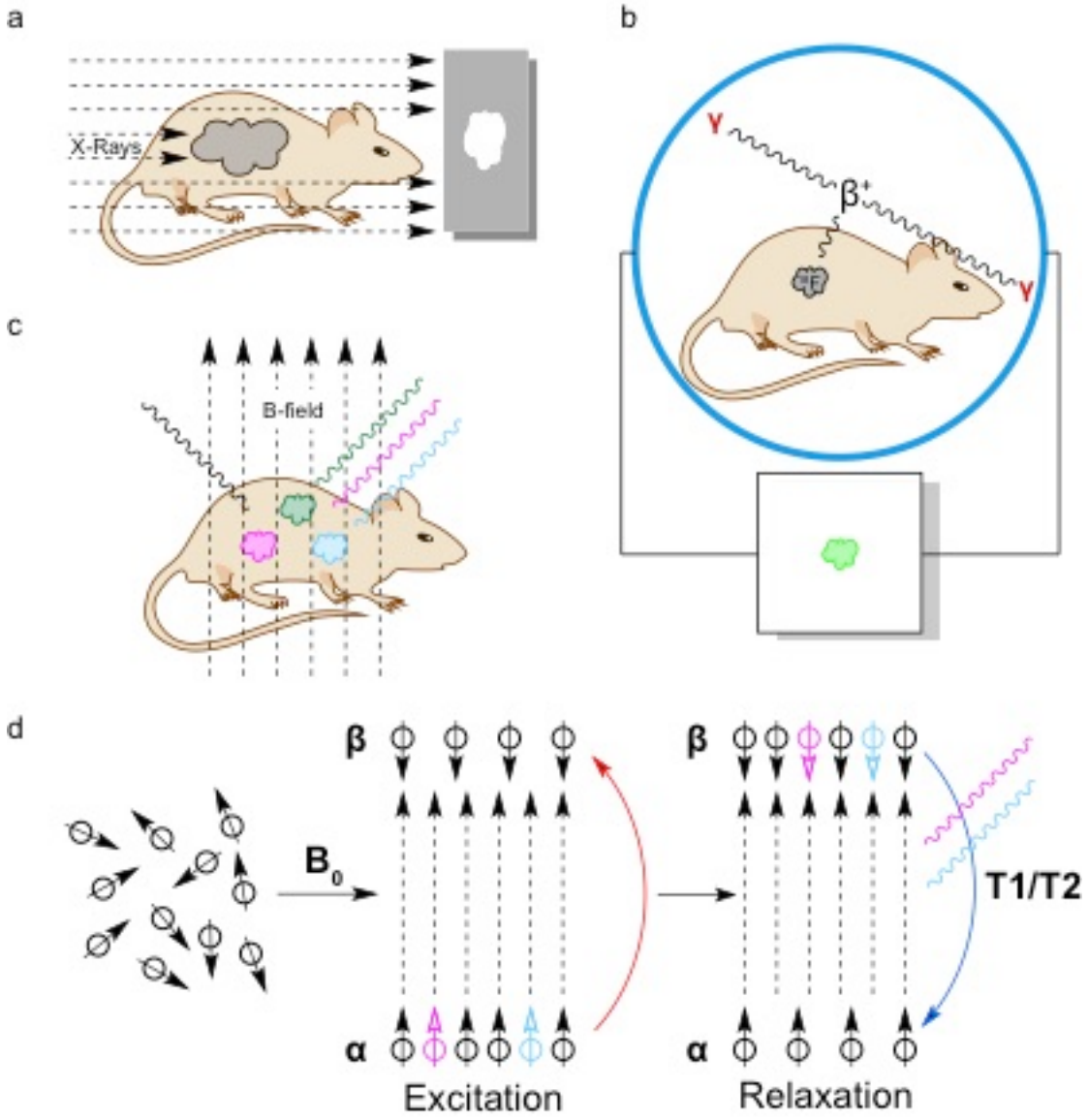

Figure 3-01. Forms of *in vivo* imaging.
a) X-rays are the oldest, and standard way to visualize hard images. Like most photography techniques, it produces a negative images where the X-rays cannot penetrate. b) PET scanners utilize short-lifetime β^+-emitting isotopes such as ^{18}F. Upon emission, the antimatter particle undergoes a collision and annihilation, resulting in a pair of gamma particles (red γ) going in antiparallel directions, which are detected by the ring. These can be reconstructed by computed tomography. This is not a direct measurement of ^{18}F, only where ^{18}F has been. c) In MRI/MRS, the specimen is placed into a strong magnetic field, where it is pulsed with a radio wave. The nature of the relaxation yields spectral information. d) Principles of NMR/MRI. Many nuclei such as ^{1}H and ^{19}F have non-zero magnetogyric moments, which upon alignment in a magnetic field results in a population of lower-energy nuclei that are aligned with the magnetic field (α) and a smaller population of higher-energy nuclei that is aligned against the magnetic field (β). Pulsing the sample with radio waves results in an excitation of the α-state to the β-state. The relaxation from β-state to α-state yields spectral information in the form of nuclear magnetic resonance response, expressed in ppm, along with T1/T2 information.

As a reporter group, ^{19}F is possesses single-atom minimalist functionality[186] and, unlike ^{18}F used in PET, is indefinitely stable. It has several convenient commercial active methylene compound starting materials (**Scheme B-09 & B-010**), as well as several powerful and commercially available sources of electrophilic ("F^+") and nucleophilic ("F^-") fluorine (**Figure B-03**), allowing for much greater synthetic reach over ^{18}F, which has no commercial products at all.

As an spin-active nuclei ^{19}F has comparable molar receptivity (83%) and isotopic abundance (100.0%) to ^{1}H NMR, but unlike hydrogen it is virtually absent in biological samples, providing a low intrinsic background[187]. Due to the similarity of the Lamor frequency to hydrogen (300.1 MHz vs 282.4 MHz for a 7 T magnet), many ^{1}H instruments and probes should be compatible and/or adaptable to detect ^{19}F, significantly broadening its practical applications for utilizing existing NMR and MRI instruments. It also has a wide chemical shift range for organic molecules (>300 ppm) but peaks are typically sharp (FWHM ~0.01 ppm) and changes in chemical shift can be

measured down to ~1 ppm[188]. It has several other physical properties than can be exploited for detection purposes, including T1 and T2 relaxation times, and these properties and probes that leverage them are described in **Appendix D**. Thus, detection by ^{19}F-NMR is highly sensitive to small chemical changes and this has been used to report biological activities or binding to cellular targets, in addition to biodistribution and pharmacokinetics.

Of particular interest to us are mechanism-based small-molecule probes that *change* their ^{19}F spectroscopic properties upon binding or reaction. In the near-term this allows us to examine the shifts of the reporter probes for biomolecules and cells in vitro inside an NMR. Our long-term goal, which is beyond the scope of this current research, is to develop *in vivo* imaging tools for In **Figure 3-2e**, this sensor was developed to measure monoamine oxidase A activity, which undergoes oxidation and β-elimination of an *ortho*-fluorophenolate to induce a 4.2 ppm ^{19}F chemical shift[189]. A β-galactosidase dual ^{19}F MRS / ^{1}H MRI was developed based on a trapped Fe^{+3} chalator that was freed after hydrolysis by β-gal[190]. It has the additional feature of being a potential therapeutic-diagnostic tool: rapidly dividing cancer cells take up more iron, so its chelation-siderophore qualities can be leveraged at the same time the spectroscopic changes take place.

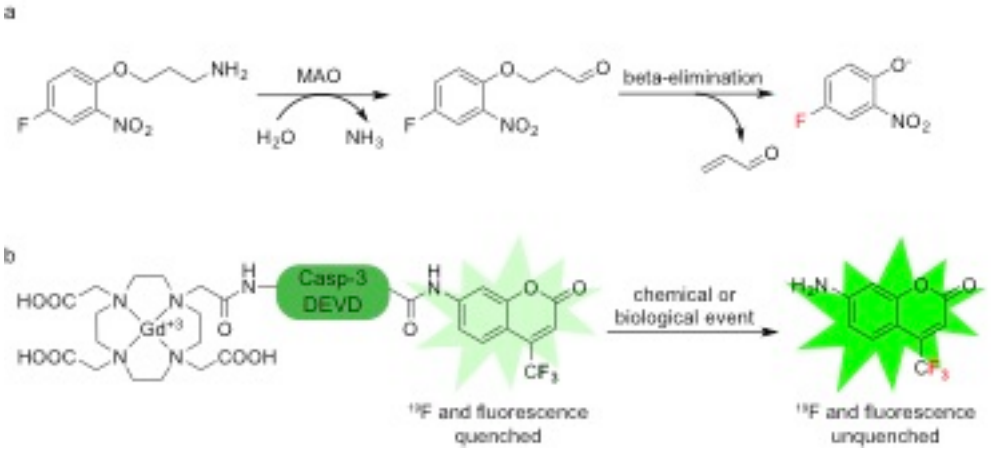

Figure 3-02. Established methods of ^{19}F MRI detection[191]: probes that utilize the difference chemical transformation.
a) In this case, the change from the phenyl ether to the phenoxide by the oxidation of monoamine oxidadase resulted in a clearly detectable -133.3 to -137.5 ppm change. b) Amide liunkage of a -CF_3 containing aminocoumarin vto a gadolinium T2-quencher via a caspase-9 recognition peptide results in a dual-functionality sensor. Upon cleavage, both the ^{19}F and coumarin become detectable.

Relevant to this, to our discussion is the development of caspase-3-activated dual-mode ^{19}F/fluorescent sensor.[192] A trifluoromethyl group is attached to an amino coumarin that is joined through that amine via an amide to the substrate peptide for caspase-3, DEVD. On the distal end is a Gd^{+3}-DOTA complex. Upon cleavage of the amide releasing the amino coumarin, and as the -CF3 separates from the Gd quencher, fluorescence and ^{19}F signal increases.

From a long-term clinical perspective of *in vivo* work, unlike the aforementioned imaging techniques of X-ray and PET, radio waves and magnetic fields are non-ionizing radiation that is easily transmitted through the body, which increases their application for clinical and diagnostic potential, particularly in pregnancies where the fetus is highly susceptible to DNA damage.

3.02. Applications to DiNap, AMCs, and sulfenylation

In our previous studies, we noticed that F-DiNap ^{19}F NMR spectrum presented a large shift from -170 ppm to -120 ppm when sulfenylated, which piqued our interest as using this nucleus in combination with this chemical switch as an orthogonal detection method (**Figure 3-03**).

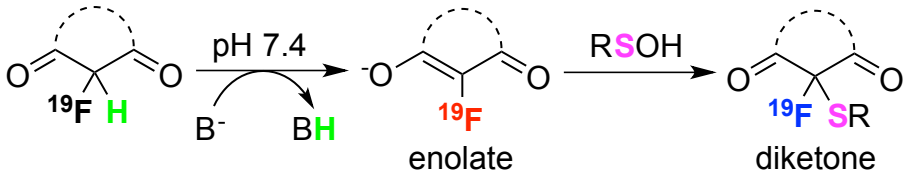

Figure 3-03. The ^{19}F chemical switch.
By leveraging the changing chemical environment of fluorine resulting from the conjugation of α-fluoro AMCs as a means to assess sulfenylation by ^{19}F nuclear-spin techniques.

Perhaps other α-fluoro-dimedone analogues might display a similarly large chemical shift between the sp^2-hybridized carbon in its anionic form and the sp^3-hybridized neutral diketone thioether. Searching the literature for similar compounds, sure enough we find that the unbound α-fluorodimedone[193] does in fact have have a different chemical shift than its sulfenylated analogue (**Figure 3-04**)[194].

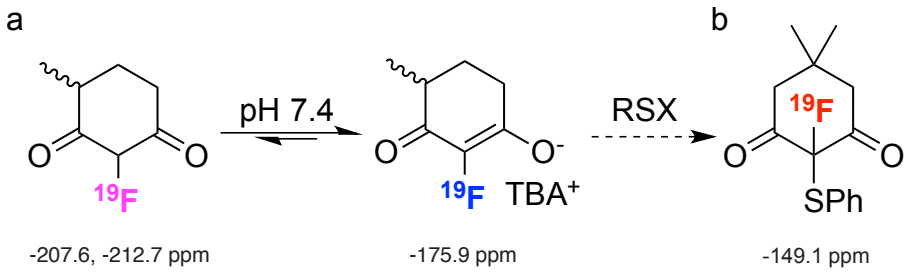

Figure 3-04. Chemical shifts of literature fluorodimedone and sulfenylated fluoro dimedone.
a) 6-Me-α-F-Dimedone has two peaks corresponding to its diastereomers. When deprotonated, it collapses into one (TBA^+ = tetrabutyl ammonium cation). Both spectra were taken in $CDCl_3$. b) Upon sulfenylation, the ^{19}F chemical shift becomes larger. All shifts relative to $CFCl_3$ (0 ppm).

And as we have already shown that the α-fluorine can increase the rate of the reaction by thousandfold or more, potentially allowing us to use a lower concentration of probe to compete with cellular reduction processes, we are interested seeing if effect extends to other AMCs. Therefore, we decided to explore ^{19}F as a reporter for NMR and MRI-based probes.

Though F-DiNap exhibits all the hallmarks of a successful *in vitro* ratiometric probe, the fluorescent aminonaphthalene scaffold is unnecessary for ^{19}F NMR and the electron-rich aniline may present unfavorable biodistribution and metabolic properties *in vivo*. Furthermore, we wanted to ensure that our probe had maximum biocompatibiliy, taking into account pharmacaphore models and other groups. As the enolate-to-diketone transition results in the loss of charge and hydrophilicity, we also wanted to ensure that the reacted probe-protein conjugate was soluble, which had presented a problem with F-DiNap at higher probe and protein loading. Intrigued, we decided to investigate the use of other ^{19}F active methylene compounds (AMC) for the study of sulfenic acids with nuclear-spin instruments. We now aim to design minimalist, optimized ^{19}F probes targeting sulfenylation. Based on our initial studies that were described in **Chapter 2**, in which we discovered that fluorination of traditional dimedone scaffolds were highly functional, we expect that other simplified ^{19}F AMCs will also effectively label sulfenic acids. Determining the reactivity and spectra probes will lay the

foundation for analysis for protein oxidation *in vivo*, and allow us to determine the role of sulfenylation in the complex web of cysteine post-translational modifications. We further believe that such probes could potentially be used as diagnostic tools to detect the early buildup of oxidative damage.

With these considerations in mind, we now propose to leverage the same chemical switch (**Figure 3-03**) that was developed to induce fluorescent spectroscopic shifts to produce NMR spectral shift in utilizing ^{19}F as a minimal reporting group, thus taking a step towards our long-term goal to quantitatively detect sulfenylation *in vivo* using nuclear spin instrumentation. We have synthesized and tested an array of ^{19}F-AMCs and use ^{19}F-NMR to profile the reactivity and distinguish between various lysates and eventually, cell types.

3.03 Results and discussion

One drawback of using F-DiNap as a ^{19}F probe is the relative insolubility of the conjugated probe. Due to the nature of the switch, the charged, soluble F-DiNap loses it and becomes much more insoluble, and protein precipitate is observed. Indeed, even with either the linear diethyl 2-fluoromalonate or ethyl fluoroacetoacetate showed significant protein precipitation in BL21 lysates overexpressing AhpC C166S at 34.5 mg/mL (data not shown). Therefore, we sought to synthesize simple water-soluble probes. Numerous attempts to leverage electrophilic fluorinating agents such as Selectfluor™, XeF_2, and AgF_2 on dimedone and dimedone derivatives were unsuccessful, so we turned to the commercially available diethyl fluoromalonate and ethyl fluoroacetoacetate as starting materials, as well as a non-commercially available

fluoroacetoacetone (**Scheme B-01**). Diethyl fluoromalonate effectively coupled with urea, guanidine, and amandine reagents to form 1,3-dicarbonyl-2-fluoro barbituic acid derivatives (**Scheme B-02**) by modified procedures[195-200]. We also synthesized one derivative from ethyl fluoro acetoacetate, which coupled less smoothly[201]. Because these are derivatives of fluorobarbituic acid, we decided to call them **F-Barb's**.

3.04 Profile F-barb derivatives against MeOVal-CysSA-Cbz

In order to test our probes, we synthesized the sulfenamide-containing peptide MeOVal-CysSA-Cbz according to a modified literature procedures (**Scheme B-03**)[157,158]. This peptide is an isolable sulfenic acid precursor. Upon exposure to water it spontaneously hydrolyzes to a sulfenic acid. It is unknown specifically which species is responsible for the reactivity with AMCs; the sulfonamide is known to react with active methylene compounds and other nucleophiles in ethanol and DCM[157], indicating that while hydrolysis may be sufficient, it may not be necessary. Regardless, this may be a complex process in which the sulfonamide, sulfenic acid, and other side products might couple to the products. We also synthesized a simplified sulfonamide Pyr-SEt in one step to provide a secondary substrate (**Scheme B-04**).

We combined compounds **5-7** with MeOVal-CysSA-Cbz in a NMR tube that contained PBS / 10% D2O with TFA as an internal standard (**Figure 3-05**, with procedure in **Scheme B-05** and products in **Scheme B-06**, and table of chemical shifts in **Table B-01**). Both **5a** and **6a** complete conversion from the starting material peak at <-150 ppm to one at about -120 ppm. **5a'** showed partial conversion while **7a** and **5b** were unreactive. Surprisingly, Pry-SEt was unreactive (**Scheme B-07**, data not shown).

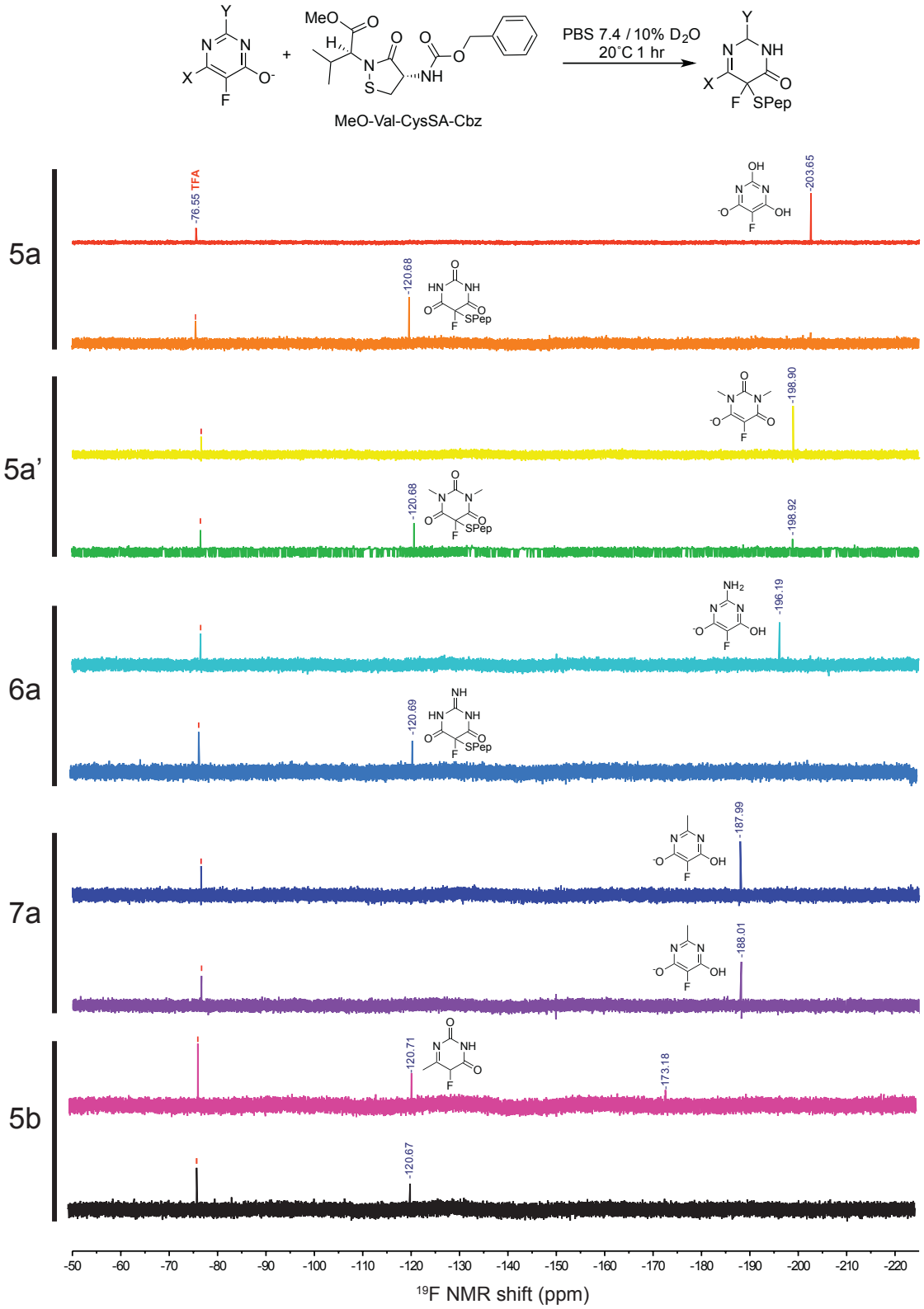
PBS 7.4 / 10% D2O
20˚C 1 hr
MeO-Val-CysSA-Cbz
5a
5a'
6a
7a
5b
-76.55 TFA
-203.65
-120.68
-198.90
-120.68
-198.92
-196.19
-120.69
-187.99
-188.01
-120.71
-173.18
-120.67
-50 -60 -70 -80 -90 -100 -110 -120 -130 -140 -150 -160 -170 -180 -190 -200 -210 -220
19F NMR shift (ppm)

Figure 3-05. Reactions of equimolar amounts of ^{19}F AMCs with MeOVal-CysSA-Cbz in PBS.
5a and **6a** showed clear full conversion to a reacted product, while **5a'** showed partial conversion. **7a** and **5b** were unreactive toward the sulfonamide.

We profiled the reactivity of these F-Barb derivatives to see if the rate enhancement on FDiNap was a general phenomenon, or specific to that that AMC. We initially found that rate of reaction of **6a** is too fast to be assayed by NMR or by the simple LCMS used by Carroll *et al*[158], as by the time sample could be mixed and put into the instrument, the maximum ion counts and/or peak conversion was already obtained. Therefore we tried to quench the reaction as quickly as possible. We initially tried to quench the reaction with 100 mM HCl, but the reaction products degraded and no product could be detected by the LCMS; instead, we used 100 mM final acetic acid to stop the reaction. This acidic environment protonates the enolate form, diminishing the reactivity and slowing and quenching the reaction. **6a** demonstrated fast rate kinetics of 214.5 M^{-1} s^{-1} (**Figure 3-06a**). However, unlike **6a-pep**, it appears as though there is rapid degradation of the product of **5a-pep** and **5a'-pep** after reaction (**Figure 3-04b** and **Figure B-01**). It is also possible that the acid rapidly degrades the sulfenic acid and/or sulfonamide. Surprisingly, Pyr-SEt was unreactive.

a

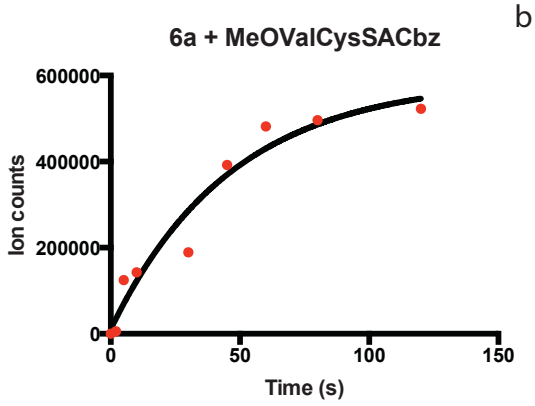

b

	k_{obs} μM^{-1} s^{-1}	k_{rxn} M^{-1} s^{-1}
5a	0.1695	1695
5a full	ambiguous	--
5a'	ambiguous	--
6a	0.02145	214.5
7a	no reaction	--

Figure 3-06. Rates of reaction of **5-7** with MeOVal-CysSA-Cbz.
a) Rate curve of 1:10 mixture of 10 μM MeOVal-CysSA-Cbz to 100 μM **6a**. b) Table of reaction rates of the ^{19}F AMC probes. The reaction for **5a** and **5a'** were unable to be fit due to their degradation. **7a** was unreactive.

3.05. Selectivity profile of F-barb 6a

Based on these rate results, we decided to use **6a** for the remainder of our studies. We incubated **6a** with a series of biologically relevant small molecule nucleophiles, electrophiles, and oxidants such as peroxide, sugars (aldehydes), and the strong Michael acceptor maleimide, as well as disulfides, sulfinic acids, nitrosocysteine, and thiosulfones (**Figure 3-07**). Promisingly, none of these functional groups led to any reaction across the ^{19}F-NMR spectra, suggesting the probe is highly selective for sulfenic acids and/or sulfenamides.

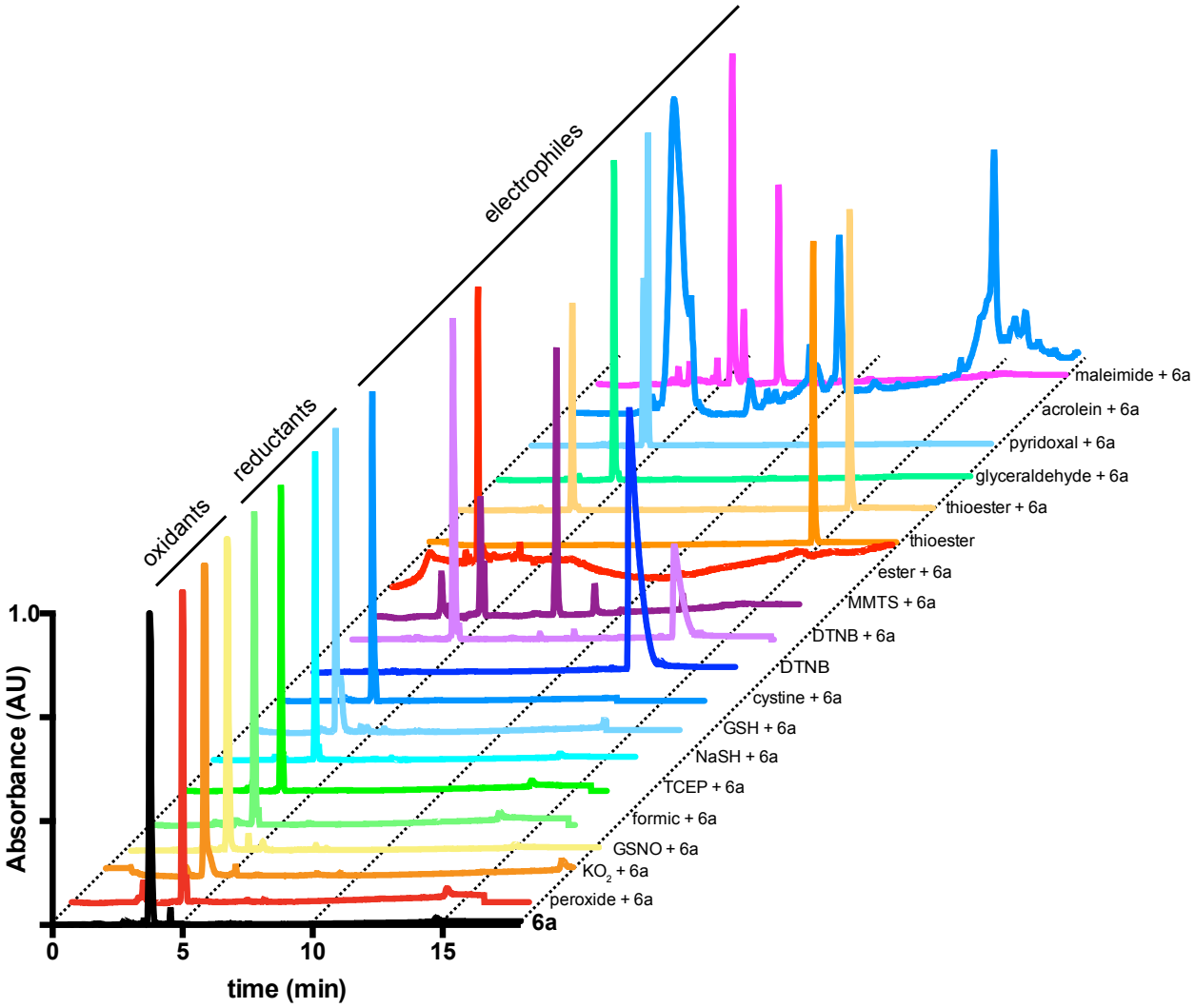

Figure 3-07. Selectivity profile of **6a** with biological and biochemical reactants.
All oxidants and reductants that were tested were unreactive. Of the electrophile disulfides, only the activated MMTS is reactive. Neither esters nor thioesters are reactive (ester: methyl acetate; thioester: S-ethyl benzylthioate). Aldehydes on their own were unreactive, but Michael acceptors such as acrolein and maleimide appeared to react.

3.06. F-barb 6a with purified protein and in cell lysates

Encouraged by these results, we then set out to ascertain if the sulfenylation of biological proteins could be determined with by ^{19}F-NMR. BSA and AhpC C166S were

evaluated for reactivity (**Figure 3-08**). BSA appeared to smoothly convert; however, AhpC showed a large atypical peak at -178 ppm in addition to the typical peak at -121 ppm. At this time it is unknown; however, considering its size it is unlikely that it could be a protein conjugate because the concentration is too high.

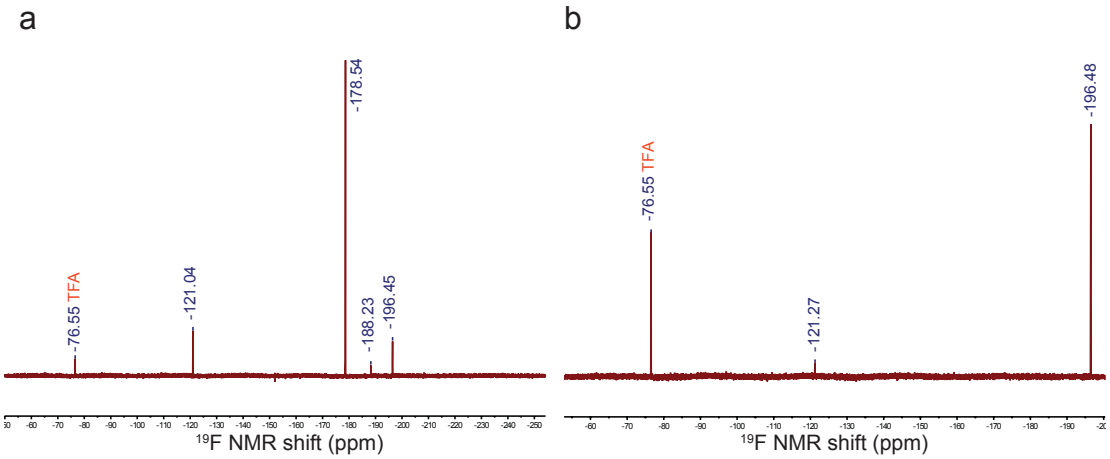

Figure 3-08. Labeling of purified proteins with **6a**
a) AhpC C166S. It is unknown what the peak at -178.54 ppm is. b) BSA shows the typical conversion peak at -121 ppm.

We were then interested in whether we could observe this conversion in complex biological mixtures, and if this was oxidation-dependent. We treated BL21 lysates overexpressing AhpC C166S with either 1 mM NaSH or vehicle for 1 hr, and then added **6a**, 10% D2O, and TFA. Conversion was observed in the –NaSH but not in the +NaSH sample (**Figure 3-09a**). Similarly, when WT and C166S mutants were pretreated with 5 mM GSH or vehicle then labeled with **6a**, only those samples that had the expected sulfenic acid were labeled.

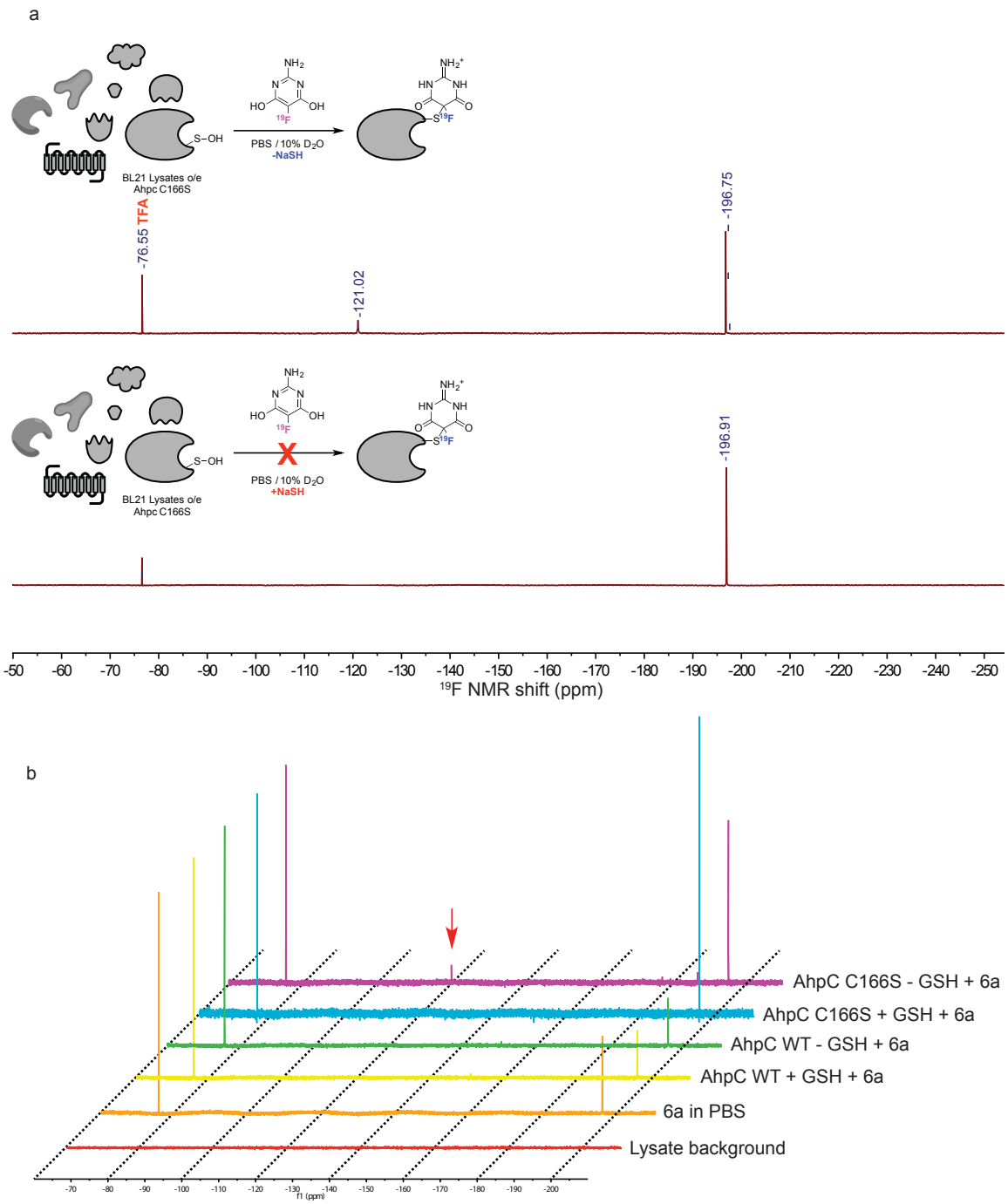

Figure 3-09. Reactions with the ^{19}F **6a** with cell lysates in PBS.
a) Concentrated lysates (34.5 mg/mL) of BL21 cells overexpressing AhpC C166S were treated with vehicle (top) or sodium sulfide (bottom) have been differentiated from each other, with the reduced samples showing no labeling putatively due to the lack of sulfenic acids. This is recapitulated in b), where the concentrations of WT and C166S lysates were matched and then pretreated with 5 mM GSH or vehicle for 15 min. Only mutant lysates without GSH were reactive.

3.07. Conclusions

We have demonstrated, first through our studies with F-DiNap, that F-AMCs may undergo a significant ^{19}F NMR shifts upon conjugation to sulfenic acids. This shift is significant, often more than 50 ppm. By trimming off the aminonaphthalene core a

nd synthesizing a number of different ^{19}F pyrimidine AMC probes based on the barbituic acid scaffold from the commercially available diethyl fluoromalonate and ethyl fluoroacetoacetates, we have synthesized simplified, specialized probes for spin-based instruments. Additional probes can be synthesized from hydroxyl-pyrimidines (**Scheme B-08**) and from diethyl fluoromalonate (**Scheme B-09**) and ethyl fluoroacetoacetates (**Scheme B-10**). Many routes to α-fluorinate dimedone and dimedone derivatives were attempted, including a range of electrophilic "F^+" reagents, nucleophilic F- sources, and attempting to modulate the reactivity of dimedone itself (**Figure B3**). In my hands, none of these appeared to work. Alkynyl versions of **6a**, **6a-yne**, can be adapted for biochemistry and proteomics (**Scheme B-11**). Each can be synthesized in gram scale in one step with simple purification. These probes have been demonstrated to work with small molecules sulfenic acids, and one of these probes, **6a**, has been taken on to analyze proteins, show different levels of oxidation in lysates, and differentiate cells. Such NMR-based nuclear-spin measurements should be transferable to MRI- and MRS-based analysis, enabling for the first time *in vivo* study of protein sulfenylation.

Chapter 4: Conclusion

As I define it (and others may differ), is that chemical biology as a field is about coming up with chemical answers to biological questions. In this document, we have described a number of the small-molecule redox transmitters, their byproducts and complex interplay. we have gone into detail on the redox regulatory mechanisms that govern this delicate balance between too much and too little oxidative fire. we have shown how those species can affect cysteine, the amino acid with the greatest number of oxidative states, and alluded to how those various states can interact, block, or augment each other. we have honed in on sulfenic acids, as they occupy as a key position as being easily reversible, modified by the prevalent ROS species (H_2O_2), and intersectional between nearly every other oxidative PTM, and we have tried to put their study in historical perspective. we have described some of the biology of these sulfenic acids, their role in growth signaling pathways and redox signaling and homeostasis. This the background to the biological problem described in **Chapter 1**, (part 1).

Our problem, where we started four years ago, that problem arises from the nature of the tools described in **Chapter 1** (part 2), which are used to image biological sulfenic acids within the cell: either the tools are fluorescent *sensors*, that change their chemistry and spectral properties, but don't give any information about protein location; or they are

constitutively active *probes* that can describe the location but only after cellular fixation to wash away the rest of the active dye. The problem then became: how can we advance the field from fixed-cell labeling, with all its inherent problems, to live-cell imaging? Live-cell imaging more closely interrogates the true state of the cell, allows us to dynamically look at the same population of cells in a way that permits reproducible stimulation, and does not wash away the small organelles, vesicles, and cytosolic proteins that fixation does, or can.

This was the basis of **Chapter 2**. And we accomplished that, in F-DiNap, a ratiometric aminonaphthalene probe that used rational chemical principles to promote an electronic change in the warhead that was in conjugation to the fluorophore. We showed reactivity, increased selectivity, and then – what was a real surprise – a massively accelerated rate.

Having come up with an answer to this problem, we then moved on to the next question: how can we apply what we have learned about this chemical transformation to image sulfenylation *in vivo*? A finite number of techniques exist to do this, which I described in **Chapter 3**, and one of them serendipitously uses fluorine as a reporter group, or rather, our molecule fortunately had a fluorine atom at the heart of its chemical switch. This class of instrumentation – NMR, MRI, MRS – are collectively a powerful set of analytical tools to measure a number of properties about nuclear spin states. A number of fluorophore-free probes were made and characterized, and shown to react with the standard small-molecule sulfenamide substrate, on proteins and in complex lysates, showing a sharp, distinct, and reproducible new peak where one was not before.

With this, we have taken a large step towards developing a tool that can help in answering the true question: what is the role of sulfenic acids in mammalian biology? Since location informs function, and we have made one step towards examining this in the context of cellular location, we ask, where do sulfenic acids occur in the body, and how much, and in response to which stimuli, or diet, or diease? These questions remain unanswered.

And even beyond this, we ask: how can we apply what we have learned here to other problems, other unanswered challenges that the tools of today cannot yet answer? How can we unravel this incredibly complex interacting networks of thousands or millions of interacting parts, working most of the time in near-perfect harmony, yet often appears to us to be just noise?

There are all the questions we already know, and all the ones we don't yet know because we don't have the right tools and knowledge to even come up with them yet. So I present **Chapter 5**, the future directions, a collection of some of the random and crazy ideas that I've picked up and put down along the way, just in case someone wants to pick them up again and start asking questions.

There will always be more questions to be answered.

Chapter 5: Future directions

5.01 Introduction

The study of protein oxidation is a rapidly evolving field. Constant need for new probes to evaluated the effects of ROS, RNS, and RSS on proteins, their visualization localization, and imaging it *in vivo*. The work described in **Chapter 2** with F-DiNap represents a significant step forward in paving the way for live-cell imaging over the fixed-cell imaging that the field was previously limited to. The work described in **Chapter 3** represents the first steps in being able to apply this technology *in vivo* using nuclear-spin instrumentation.

Though we have made significant advances there are still many ways in which our probes could be improved. Herein we describe some of those improvements, as well as other biological redox states of cysteine groups that we may be able to apply some of our chemical rationale.

5.02 Chapter 2 Variants and new mechanisms of F-DiNap fluorophores

Improved dyes incorporating the fluoro-AMC 'switch':

One of the problems of the DiNap dyes is that the aminonapthalene core is a relatively poor fluorophore, and that the ratio change is modest. Because we have identified the highly increased reactivity of fluoro-AMCs, we may be able to dispense

with the low-Φ low-ε properties of DiNap (which would be necessary if the reactivity of these probes remained at the typical 1-5 mM used for dimedone).

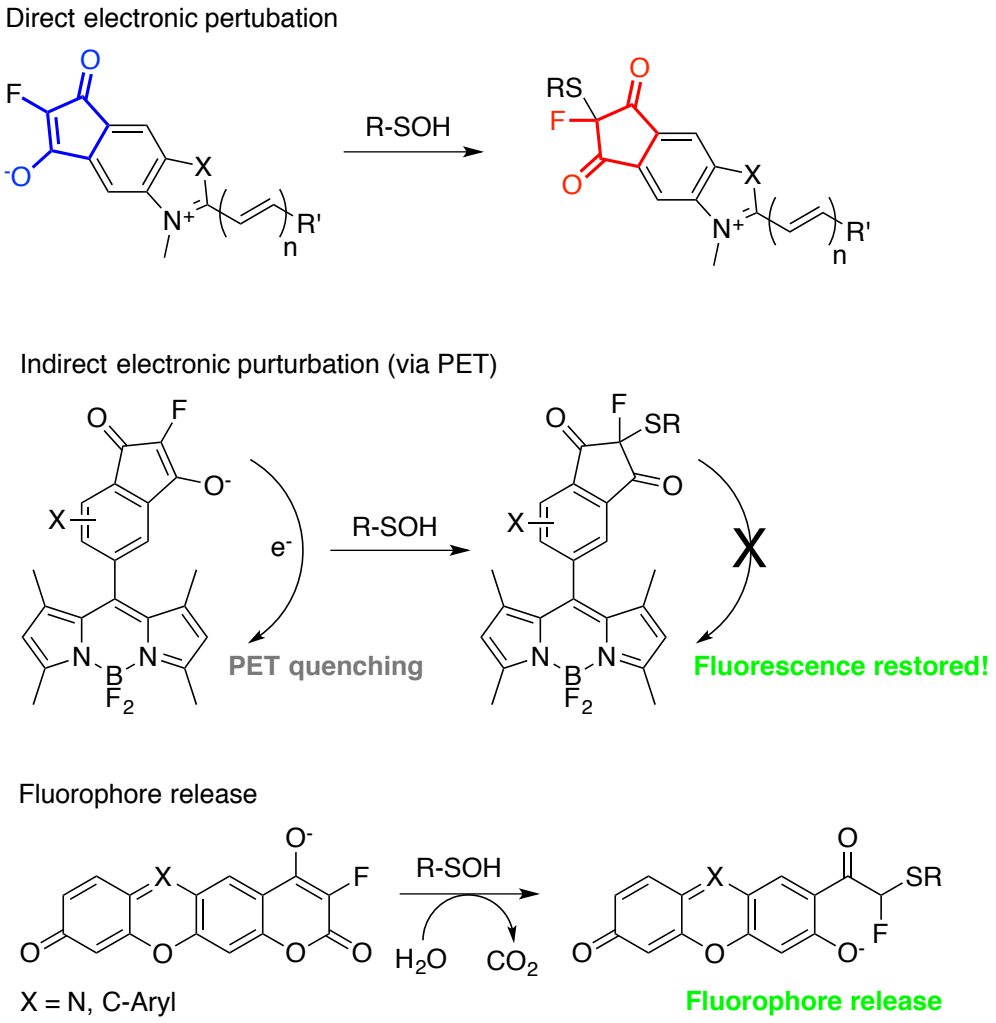

Figure 5-01. Additional scaffold diversity for fluoro-AMC probes.

Examples of probes with these different mechanism of activation:

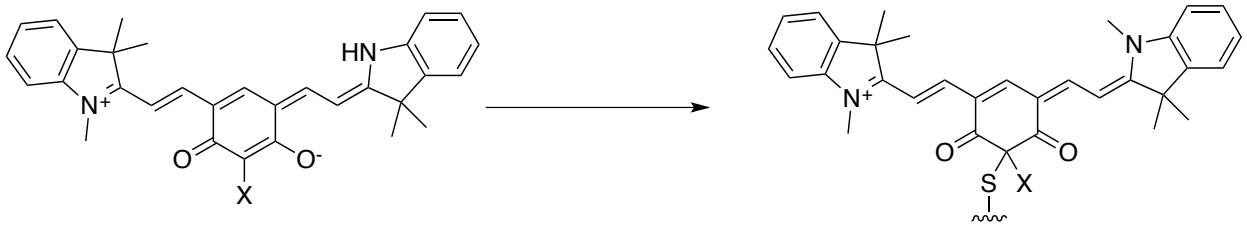

Scheme 5-01. Direct electronic perturbation with a cyanine dye.

We can also explore different mechanisms for the switch. F-DiNaps utilized direct electronic perturbation, in which fluorophore was directly electronically connected to the site of reaction. As we discussed before, there are two addition means of releasing the dye, chemical disruption of PET quenching, and fluorophore release

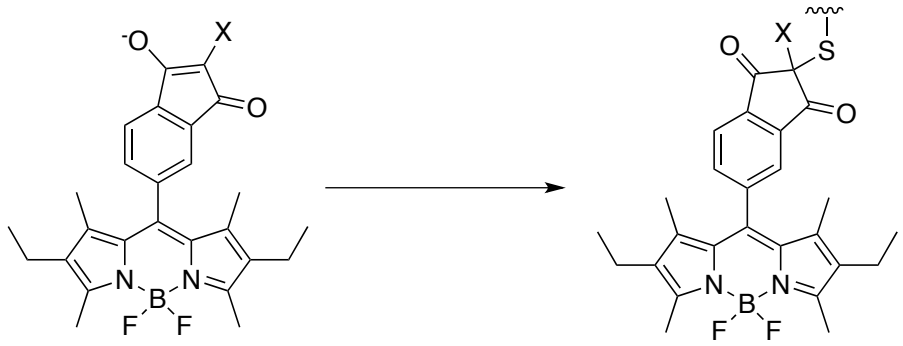

Scheme 5-02. BODIPY PET quenchers.

The second mechanism utilizes changes in the electronics to suppress PET following binding. On a hypothetical BODIPY dye, the electron-rich enolate of the pendant AMC suppresses the fluorescence of the BODIPY fluorophore by turning it into an electron-poor diketone. The electronics of this could be tuned and optimized by groups on the BODIPY system of –X off the top.

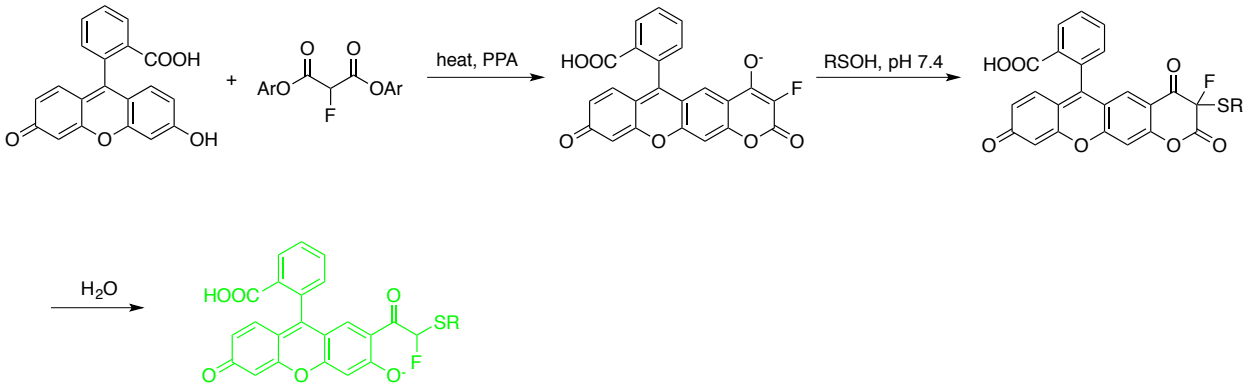

Scheme 5-03. Synthesis of a fluorescein-based chemically-induced fluorophore release.

In the third mechanism, conjugation to a sulfenic acid leads to a chemical change in the dye. This renders an ester, that was formerly stabilized by being an enolate, into a fairly activated electrophile that is subject to hydrolysis and fluorophore release. It is likely that the starting material will have fluorescence all of its own, and that diminishing the ring size it diminish both the brightness and excitation wavelength.

Figure 5-02. Further variants of the catch and release probes. All are built off of the 4-hydroxy coumarin scaffold.

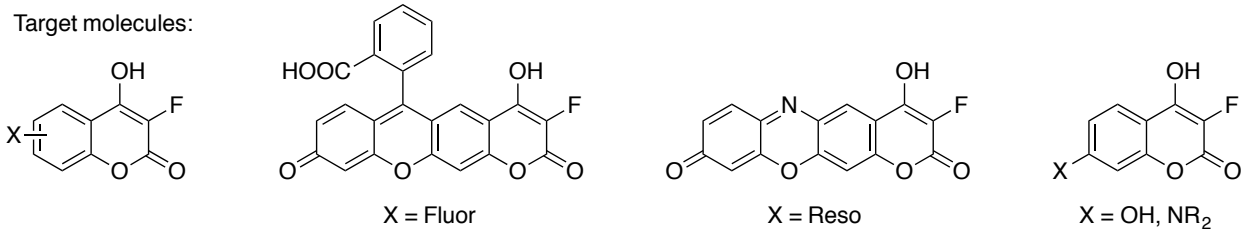

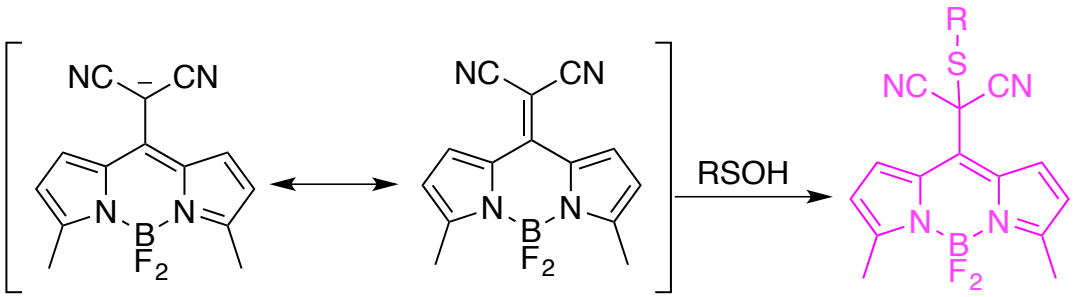

Scheme 5-04. BODIPY malonate dyes as sulfenic acid capture reagents and turn-on dyes.

The *meso* position for xanthene and BODIPY dyes seems to be critical for their activity. If there is too much double-bond character, either in a carbon-based “ene” format or with heteroatom ketone-like character, it disrupts the favorable electronics needed for fluiorescence.

5.03. Simplified F-dimedone probes for proteomics

Building off of dimedone and serendipitously experiencing a 1000+ fold increase in reaction rates, and we were also able to develop it for live-cell imaging. However, from a proteomic standpoint, the fluorescent part of the molecule is dispensable. While our efforts to electrophilically fluorinate dimedone repeatedly failed, with multiple substrates and with multiple electrophilic fluorine sources, it is still desirable to have an α-fluorodimedone alkyne. Preferably this will also bear an amine, for functionality and to help make peptides more readily ionizable in the ESI. Below are some proposed routes to this:

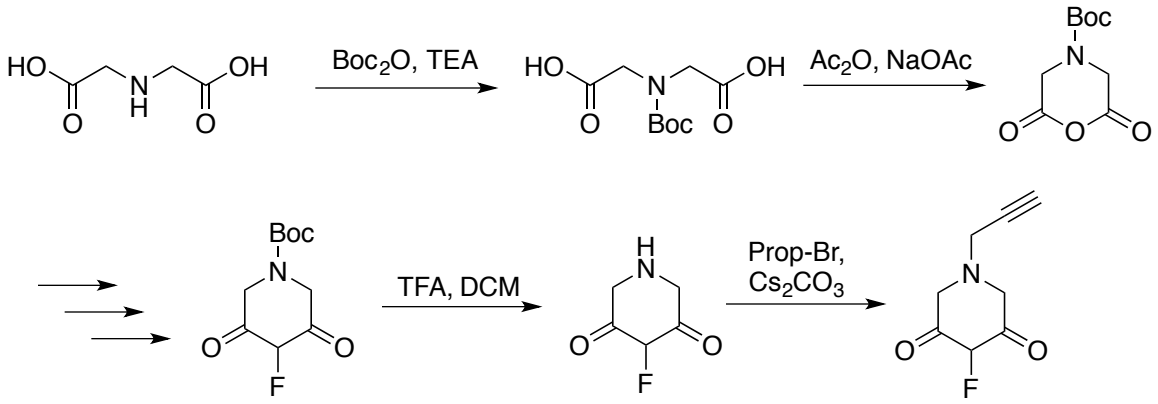

Scheme 5-05. Synthesis of an alkyne F-dimedone

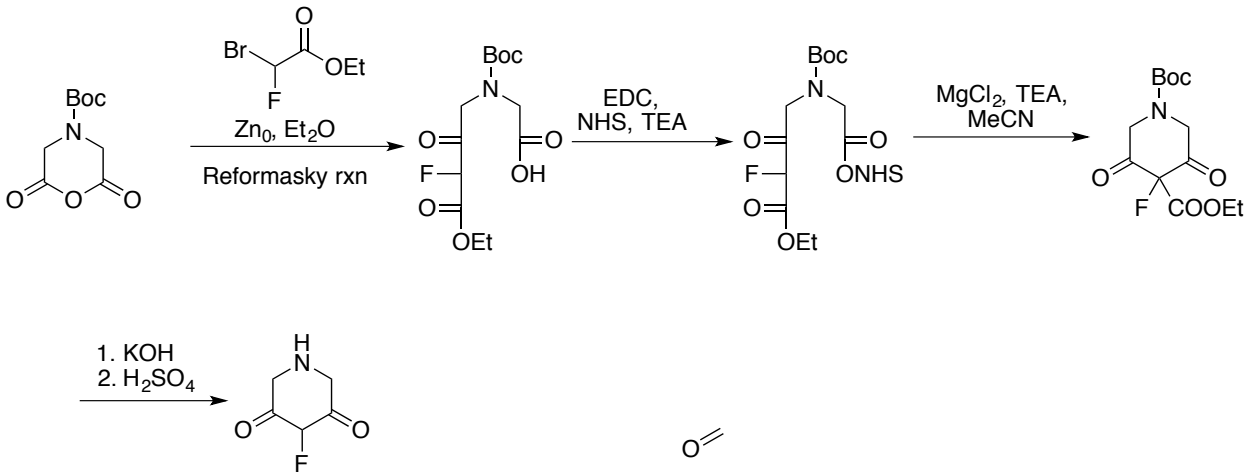

Scheme 5-06. Expanded synthesis of ring-opening and cleavage using the Reformansy reaction.

5.04. Reversible sulfenylation probes for fluorescence

The cellular redox environment is dynamic. When cellular respiration goes up, so does the amount of free radicals and superoxide formation. When cellular signaling cascades are activated, such as the B-cell receptors on B-cell plasma membranes, the clustering induces NOX, which produces a localized burst of peroxide that diffuses out into a cell; thus a 'wave of oxidation' occurs between primary oxidants (Prx), secondary

oxidants (GSH), and finally getting diluted and reduced by the cell. Though FDiNap can capture, for the first time, stimulation within a cell, it cannot also see that cell return to normal. That takes reversible probes.

Thiols and disulfises are the obvious choice to play these reversible roles. Thiols are highly reactive with sulfenic acids and disulfides are readily reduced by GSH and other reductive machinery. The principle is fairly simple: installation of a reactive thiol on an electronically important part of the fluorophore could allow the photophysical properties of the dye to change upon conjugation. The reactivity is tunable based on the pKa and electronics of the thiol itself, and the reactivity can be tuned so as to release the dye first, inactivating it again.

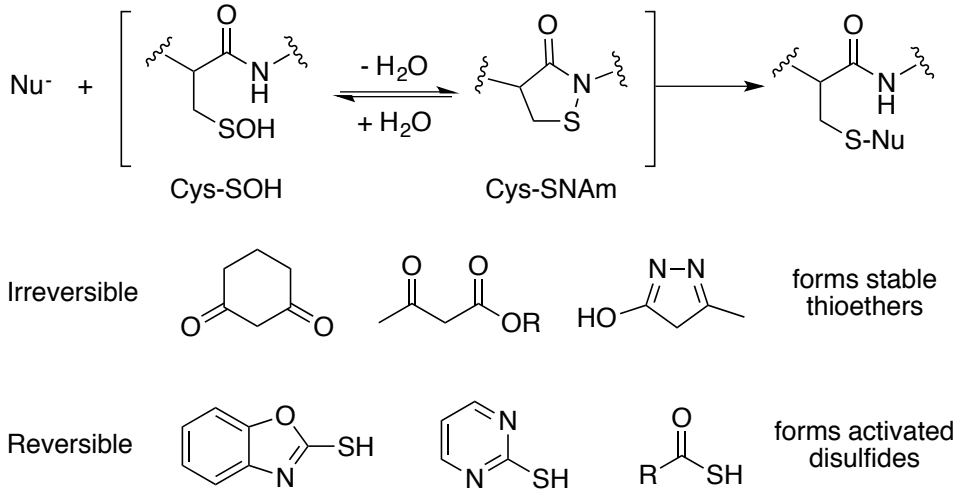

Scheme 5-07. Examples of reversible and irreversible functional groups

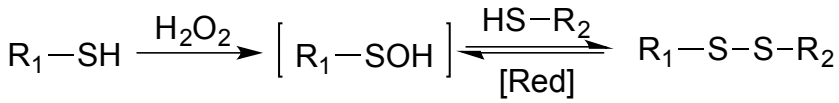

Scheme 5-08. Using thiol/disulfide based probes as platforms for reversible dyes. The cellular environment is a reducing one, so upon release of an oxidant, then and only then will the probe react. If it is designed properly, then the disulfide-linked form should be “on”

Thus far we have identified three different classes of dyes. The first two are xanthene dyes, based on fluorescein and rhodamine. The next one is on a BODIPY scaffold. Though there are many different reactive and reversible moieties, most of them are based on thiols. In each case the thiol is in the *meso* position, which in in its ‘keto’ resonance form interrupts some or all of the resonance that is important the fluorescent properties of the dye. After conjugation, the disulfide locks it in the fluorescent enol form. This persists until the wave of oxidation passes and cellular reduction properties change the local environment of the cell. As expected MMTS significantly changes the fluorescence properties of FluoSH, leading it to be more fluorescein-like, fluorescing bright green. Though this has not been fully explored, it is a promising lead for next-generation reversible sulfenic-acid fluorescent probes.

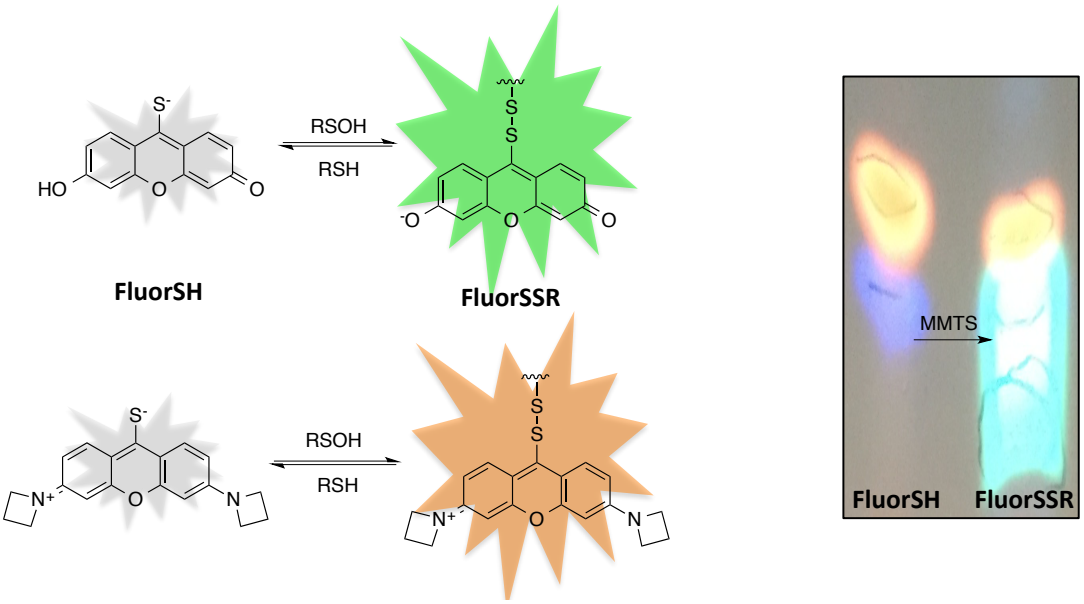

Figure 5-03. Reversible fluorescent dyes.
FluoSH was incubated with MMTS and TEA, at which point a dramatic change in fluorescent character, potentially due the proposed conversion to FluorSSR

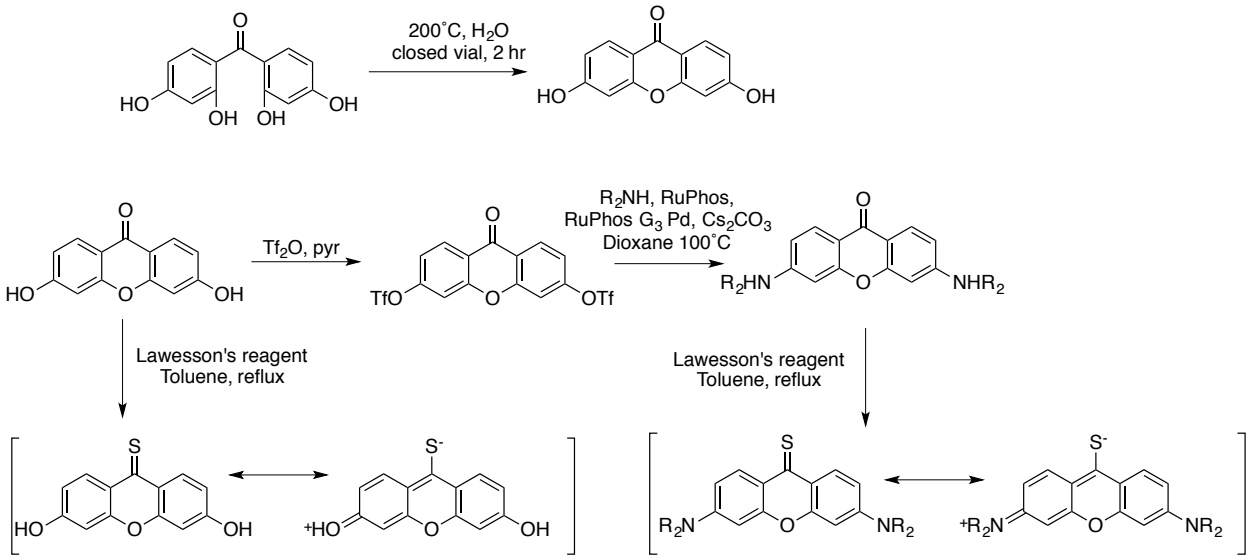

Scheme 5-09. Synthesis of FluorSH.

These come from fairly standard literature procedures. Dehydration the commercially available bis(2,4-dihydroxyphenyl)methanone (o,o',p,p'-tetrahydroxybenzophenone) in a sealed tube yields the dihydroxy xanthenone. Simple replacement of the *meso* ketone form with Lawesson's reagent results in FluorSH. Continuning on, triflation of the phenolic hydroxyl allows replacement of by any number of chemistries, followed by Lawesson's reagent leading to RhoSH

However, BODIPY one is not recommended to be prioritized because the literatures suggests that when this is in a free keto form, the -BF_2- is no longer bound tightly to the dipyrroles, and dissociates, and the dye loses its fluorescent character.

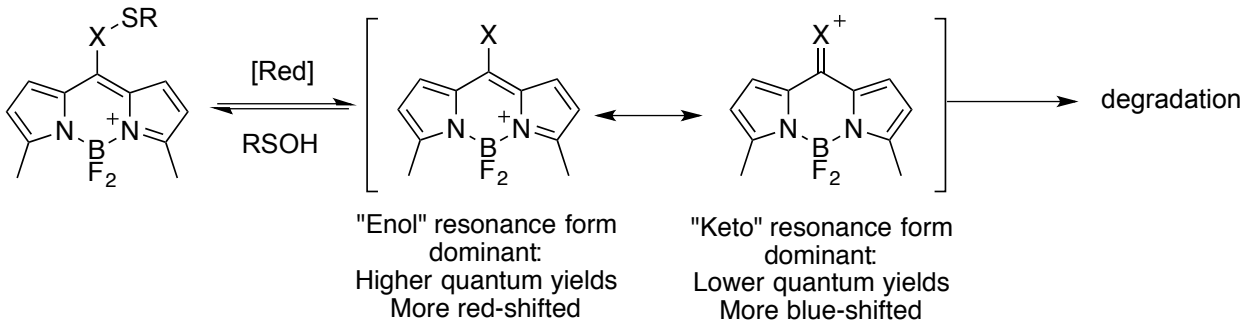

Scheme 5-10. Degradation pathway of *meso*-reactive BODIPY

5.05 Chapter 3 Reversible and irreversible NMR/MRI probes

Though ^{19}F NMR is an attractive method for the above reasons, the nuclear-spin based instrumentation can suffer from low sensitivity. To bridge the gap from imaging live cells to an *in vivo* system, appropriate instrumentation must be used. MRI is the ideal candidate for all the reasons covered extensively in **Chapter 3**. Its main problems are one of resolution and sensitivity. Specifically in the transition from NMR to MRI/MRS, resolution issues can be overcome by special pulse sequences using resonators specifically tuned to ^{19}F. This approach can be used to reach nominal resolutions of as low as 156 μm, only 2-fold higher than the reported 78 μm by ^{1}H MRI[187] and similarly only twice the size of a macrophage. Such resolution is sharper than the fundamental limits of that of ^{18}F PET, where the full-width half-max blurring effect of β^+ range prior to γ decay is 0.54 mm[202].

The equation for signal to noise ratio is as follows[203]:

$$\mathrm{SNR} \propto N\,\gamma^{5/2}\,{B_0}^{3/2}\,T^{-3/2}\,I\,(I+1)\sqrt{\frac{T_2}{T_1}}\sqrt{t_{\mathrm{meas}}}\ .$$

Where N is the % active nuclei in the sample, γ is the gyromagnetic ratio; B_0 is the magnet field strength, T is temperature in Kelvins, I is the nuclear spin state, T1/T2 are the two relaxation constants, with a long T2 and a short T1 being desirable the, and t_{meas} is the number of scans or amount of time the measurements have been taken.

. Ways to optimize the signal to noise thus derive from this equation:

Instrument side:

- Increase field strength. Using higher-strength magnets, which improve signal-to-noise ratio by the 3/2 power of the field strength[203] e.g going from a 200 MHz instrument to a 400 MHz instrument increases the S/N by a factor of 5.6.
- Lower the temperature. Cryogenic NMR probes exist.
- Increase scan times, which improves the signal-to-noise ratio at the square root of the number of scans. Generally the goal is to have the lowest number of scans produce the highest signal, and there are increasingly diminishing returns for longer times.

Probe side:

- Choose an isotope that has a high abundance of active nuclei, like ^{1}H or ^{19}F; a high gyromagnetic ratio, or a high spin state. However, these are constants for a given naturally abundant element, without enrichment.
- Decrease T1 by proximity to other spin-active nuclei. This may either quench or enhance the probe, so optimization may be necessary.
- Increase T2 removing proximity to other quenching spin-active nuclei, or removal from a large, slowly tumbling trapped state.
- Increase effective concentration by adding degenerate nuclei that increase the S/N linearly.

Since we have little control over the instrument that will be used and how long they can be used for, focus will be on probes that improve the latter set of improbements.

Typical concentrations of small molecules measured in an NMR tube are on the millimolar scale, with practical sensitivity dipping into the tens of micromolar lower ranges. On the probe side, the signal-to-noise can also be enhanced by using polyfluorinated probes to present a multiple similar or identical fluorine atoms[204]. In this approach, we anticipate the output would not be a chemical shift observed from the α-proton. Instead, as with our fluorescent probes, conjugation could act as a chemical switch to trigger an environmental change sensed by the so-called ‘antennae’ fluorine nuclei. This gain in signal (3- to 18-fold) amplifies the effect of conjugation to improve detection. In these cases, we would expect the signal change, in ppm, to be much smaller because the chemical alteration is not happening directly at the site of modification. Additionally, contrast agents utilize a paramagnetic metal proximal to the

pulsed nuclei to decrease the overall relaxation time. This can greatly increases the number of scans that can be taken, and increases the overall contrast and resolution of the image. Cell-permeable gadolinium contrast agents have been demonstrated[205], as well as less-common manganese-porphyrins[206]. Organic radicals, such as one based on a TEMPO-dimedone hybrid, may also present small, oxidation state-sensitive paramagnetic electron spin rate-enhancing probes[207]. Finally, the use of higher-reactivity ^{19}F AMCs that conjugate more effectively to sulfenic acids *in vivo* would increase the concentration of sulfenic-acid conjugated ^{19}F probe. However, to avoid increasing reactivity at the expense of selectivity, these optimized AMCs will be assayed against a similar panel of functional groups and thiol modifications by ^{19}F-NMR *in vitro*.

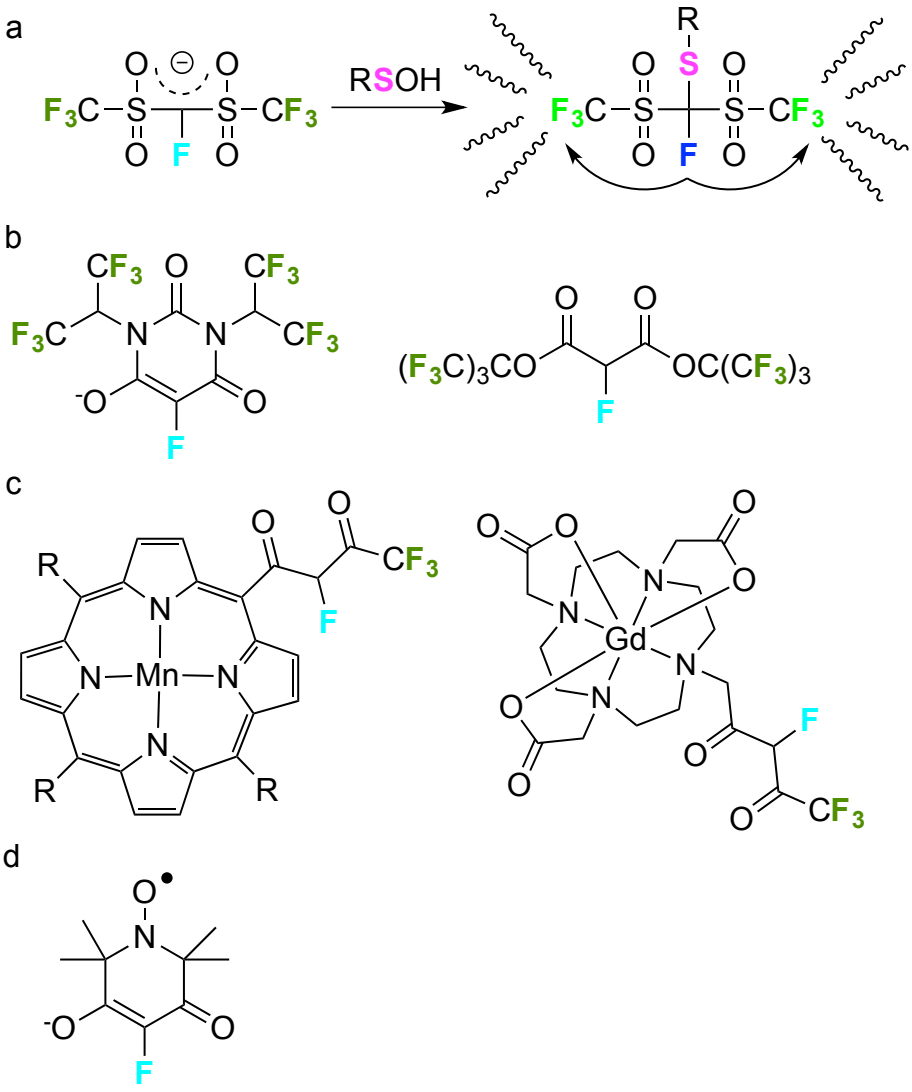

Figure 5-04. 19F sulfenylation probes.
a) The antenna effect can be used to enhance the sensitivity of NMR and MRI. The blue fluorine changes the charge state of the probe, which then changes the chemical environment of the green fluorine's. The 6-fold stoichiometric increase results in 6-fold greater signal-to-noise. b) Examples of a 12-fold and a 18-fold antenna amplification probes. c) Transition metals can enhance the spin relaxation times, which allows for more scans to achieve higher signal to noise. d) Organic radicals can also decrease nuclear relaxation times to achieve higher signal to noise.

a

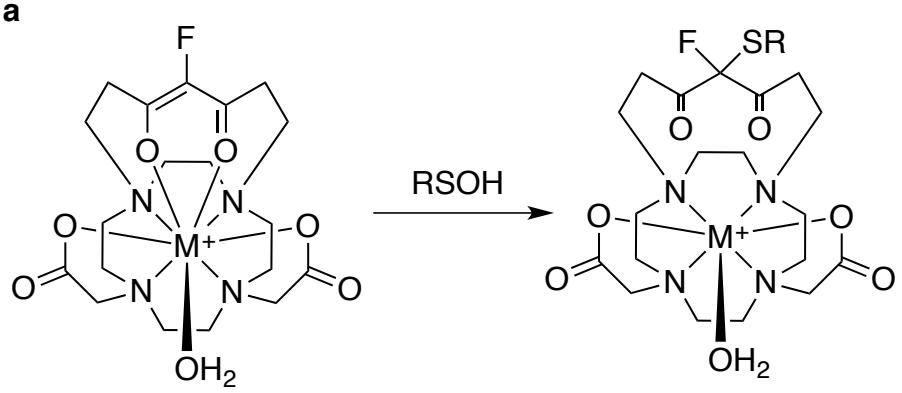

Enolate chelated Diketone unchelated

b

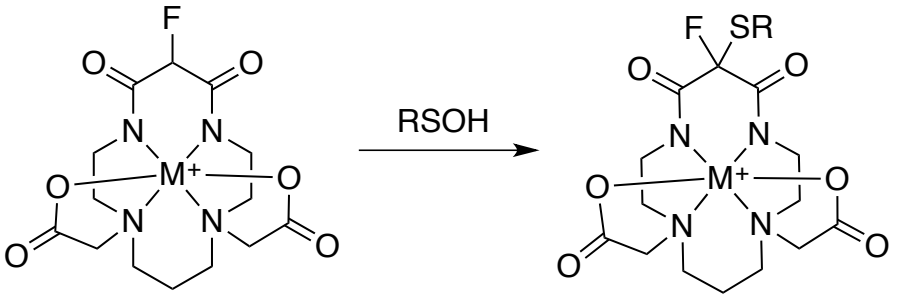

Figure 5.05. Examples of ligand-switching for lanthanide and gadolinium-based nuclear-spin probes.
a) the acetoacetate moiety is a strong metal chelate due to the negative charge on the oxygens, forming part of a dentate ligand. However, when it reacts and becomes a diketone, that binding ability decreases. b) Likewise, when a nitrogen-bound amide chelate goes from the enolate form to the diketone form, this will change the electronics and binding of the metal and ^{19}F.

Finally, should our probes find use in mouse and rat models, and sulfenylation prove to play an important role in various pathologies, ^{19}F chemical shift probes may provide a potential bioimaging clinical diagnostic tools in MRI and MRS. Broad-spectrum cysteine alkylators (iodoacetamide, maleimide) can often be toxic, and irreversible alkylation by diagnostic compounds may permanently inactivate catalytic cysteine residues that are only temporarily and reversibly deactivated by oxidation. With this in mind, it would be desirable to have reversible probes that would have lower long-term toxicity than those described above. Fluorous thiol probes (**Figure 3-10a**) form easily reducible disulfides. However, due to the putatively low inherent concentration of sulfenic acids and the high rate of disulfide exchange ($k_{on} \approx k_{off}$), sensitivity may be very low. On the other hand, it has recently been shown that linear AMCs can form reversible conjugates with sulfenic acids (**Figure 3-10b**)[208], but in these cases $k_{on} >> k_{off}$, increasing the reacted conjugate concentration while still allowing for clearance. ‘

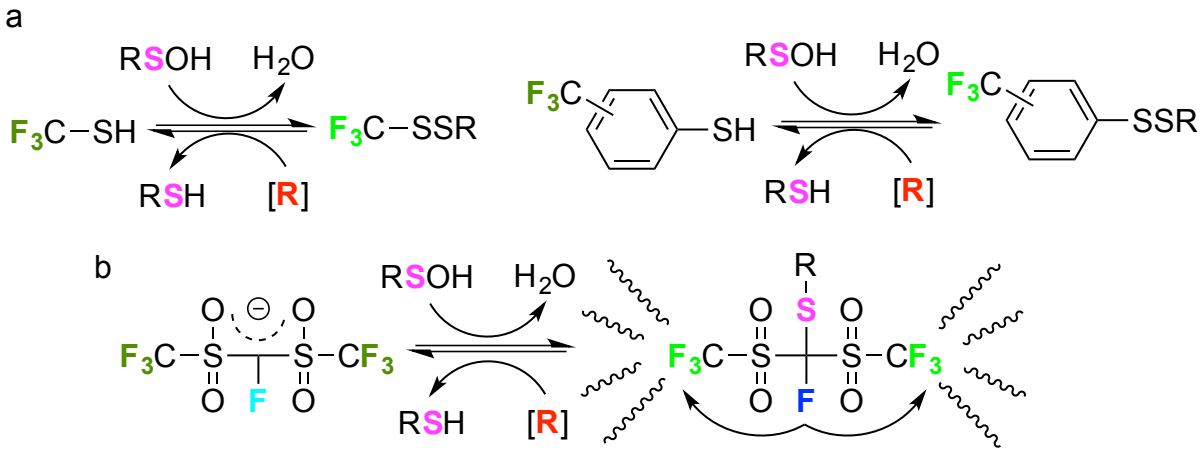

Figure 5-06. Reversible ^{19}F probes.
Irreversible cysteine alkylators such as maleimide and iodoacetamide tend to be toxic to cells and animals. Creating reversible probes, which may be metabolized and excreted,

is a much more viable solution for sulfenylation probes. a) Disulfide bonds are easily reduced by intracellular thiols. b) Linear AMCs can be cleaved by reducing agents such as DTT, TCEP, and glutathione. Such probes may lead to much lower levels of toxicity.

5.06. Sulfinic acid probes for nitrosothiols.

It was recently shown in our lab that nitrosothiols and sulfinic acids are compliments of each other in that each modifies the other. Nitrosocysteine widely implicated as a part of RNS redox stress and can inhibit palmitoylation. The resulting thiosulfonate is a highly activated disulfide and GSH attacks at the more reduced sulfur, regenerating the sulfinic acid and forming a more typical cystine-like disulfide. Electron-rich sulfinic acids will be better nucleophiles, but they'll also be more susceptible to oxidation to the sulfonic acid. Likewise, electron-poor sulfinic acids, while being worse nucleophiles, will be more resistant to overoxidation.

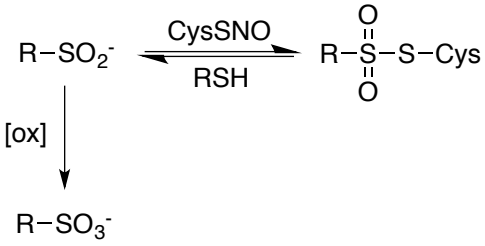

Electron-rich R

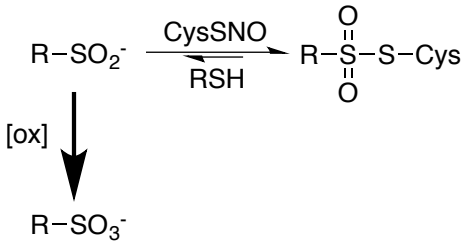

Electron-poor R

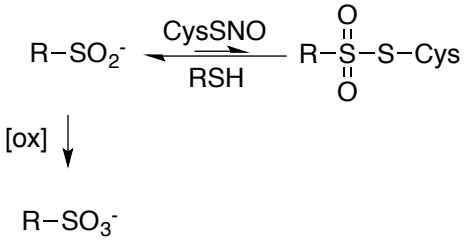

Figure 5-07. Reversible sulfinic acid probes.
These probes form thiosulfonates, which are highly reactive with thiols. Depending on the electronics of the sulfinic acid, an electron rich sulfinic acid may favor the thiosulfonates and resist cleavage, but may get rapidly and irreversibly overoxidized. The reverse is true for electron-poor sulfinic acids.

Fluorescent reversible SNO probes:

We can apply this rationale to fluorescent probes:

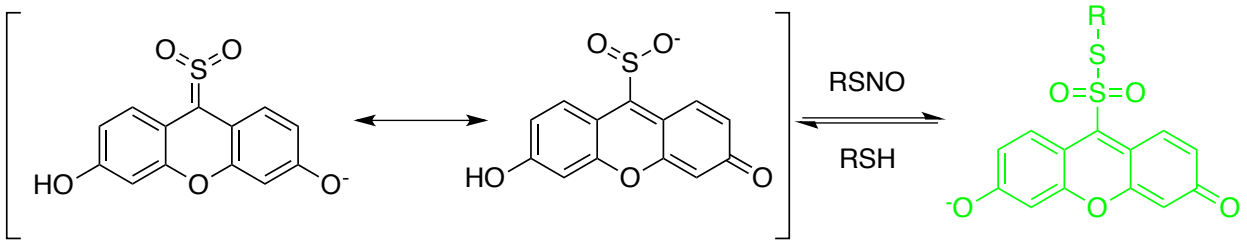

Scheme 5-11. Reversible SNO probe, FluorSO2H.

The electron rich anionic sulfinic acid moiety at the *meso* position potentially quenches fluorescence as do the reduced thiols. Upon conjugation to RSNO, this results in a thiosulfonate, restoring fluorescence to the probe. Thiosulfonates are highly reactive (MMTS is an example) so the addition would be putatively rapidly reversible.

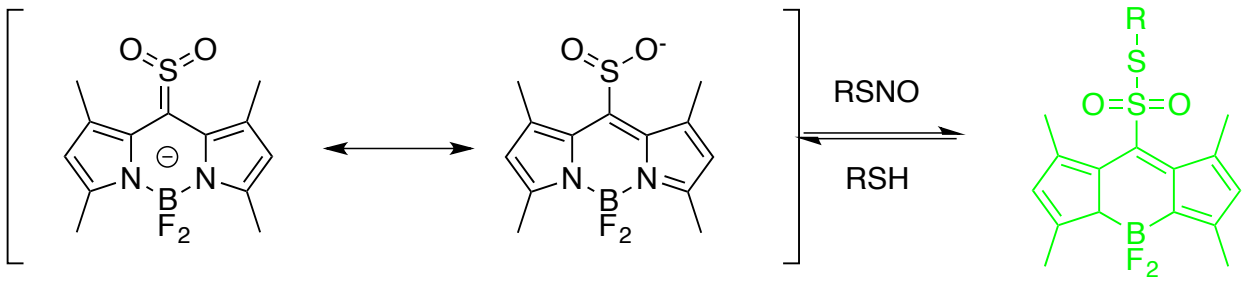

Scheme 5-12. Reversible SNO probe, BODIPY-SO_2H.

Likewise, sulfinating at the meso position of BODIPY may allow for rapid, reversible, and selective RSNO probes.

^{19}F SNO probes.

Fluorine NMR or MRI may also find use in sulfinic acid-mediated analysis nitrosocysteine. The commercially available sodium trifluoromethyl sulfinate may react with nitrosothiols. Once bound, the three fluorine atoms go from experiencing charged local microenvironment to an uncharged one, potentially shifting the ^{19}F NMR shift.,

Scheme 5-13. Reversible ^{19}F NMR/MRI RSNO probes.

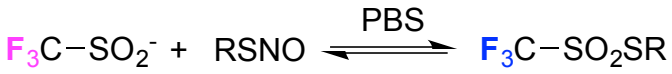

The problem with this reaction is that the strong electron-withdrawing capabilities of the trifluoromethyl group may negatively affect the reaction kinetics of the sulfinate, while also leading to a more active thiosulfonate.

Other sorts of sulfinic acid probes can likely be used. This reversibility makes it ideal for living specimens because no toxic buildup or permanent protein modifications, however because of its reversibility, the bound form may exist in only a very small concentration, too far below reasonable detection limits. Though similar strategies such as paramagnetic proximity and multiple degenerate fluorine atoms can be used, this will still likely be below the detection limit except in the case of extreme RNS overload. However, this will only be determined experimentally.

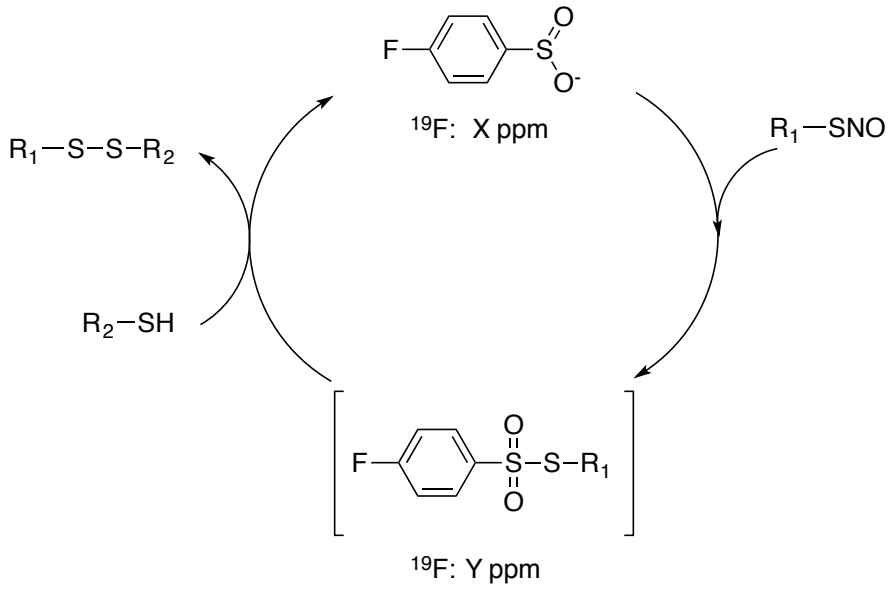

Scheme 5-14. Other reversible NMR/MRI RSNO probes.

5.07. Thioester fixation:

Thioesters are another reversible PTM of cysteine, usually appended as an acyl chain of the 16-carbon palmitic acid. This helps to localize a protein to the cell membrane or other membrane compartment. Because location informs function, this has wide implications in many aspects of cell biology that is beyond the scope to talk about in this document. However, of note, it seems that several palmitoyl acyl transferases (PATs) containing the DHHC motif, and not entirely specific for palmitic acid and indeed can accept a variety of saturated and unsaturated acids.

When palmitoylation is studied, the typical tool is to add 17-ODYA, or use the biotin switch to cleave the thioester for capture the resulting thiol. Each of these cleaves the

thioester bond, or adds exogenous reagents. Therefore, the goal of thioester fixation is to maintain the thiol-side (R_s) and the carbonyl side (R_c) and thus maintain the information held in that bond.

Nucleophilic additions to the thioester via an push-pull (umpolung) mechanism:

The thioester carbonyl is an excellent electrophile, while the sulfur is an excellent nucleophile. A reagent that can first attach the nucleophile, and then from its tetrahedreal intermediate capture the sulfur without it leaving is a difficult proposition, but there is precedent

The Bayer-Villager oxidation turns an ketone into an ester, where a nucleophilic peroxide attacks the carbonyl, and the R-group is transferred/captured intramolecularly.

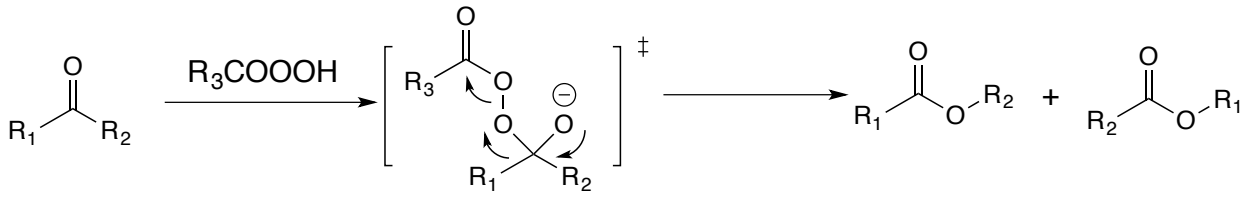

Scheme 5-15. The Bayer-Villager on esters.

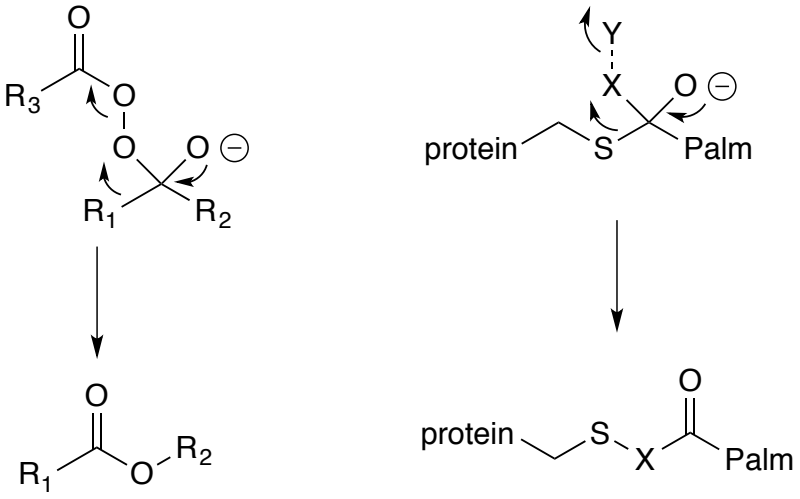

Scheme 5-16. Comparison of Bayer-Villager and a hypothetical thioester version.

Comparing them side-by-side:

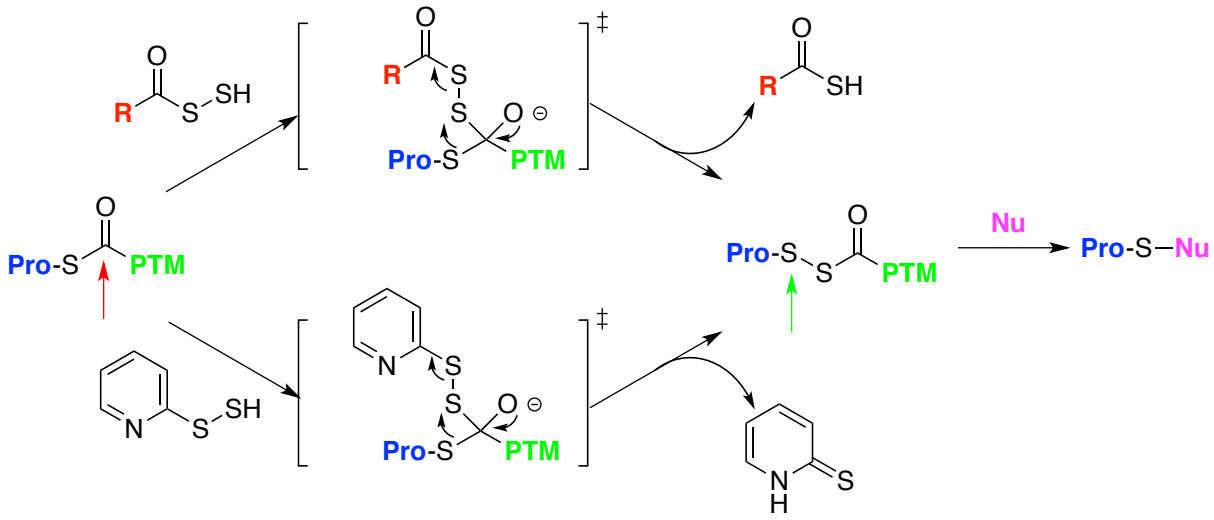

Scheme 5-17. Using persulfides to form acyl persulfides from thioesters.

Examples of each possible geometries are found below.

Geometries:

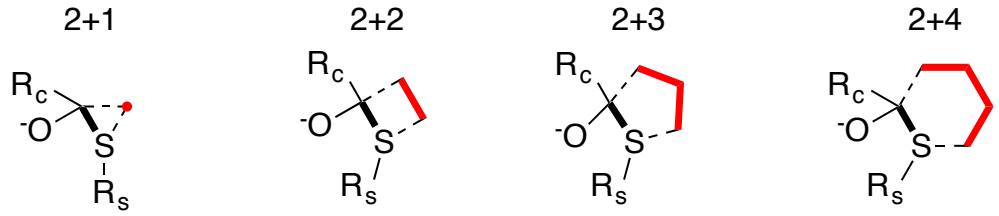

Examples:

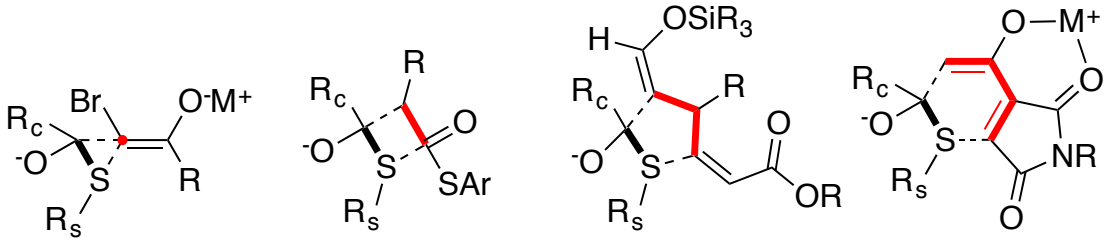

a-halo ketones | nucleophilic thioesters | John M.'s compounds | 3-Ac maleimies

Figure 5-08. Various reaction geometries of nucleophilic fixation probes.
The probe (red dot/line) can be of various length to add into the two-atom C-S bond.

The easiest analogy to the Bayer-Villager to try is the use of sulhydryl thiols (Scheme 5-17). However this leaves an activated disulfide that can either be hydrolyzed or attacked by other thiols (green arrow).

On the other hand, carbon nucleophiles have no such reversibility problem. We proposed using benzylidine compounds (R_2 = aryl) to form an anion on one of the distal carbons, assisted by Lewis acids and base. This soft anion can attack the soft thioester. Given the right metal, this can hold the intermediate in the proper orientation so that upon collapse to the thioester's tetrahedral intermediate, the sulfur transfers to the strong Michael acceptor of the benzylidine. The produce is a stable triketone-thioether.

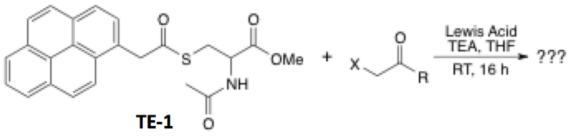

Compounds (22):

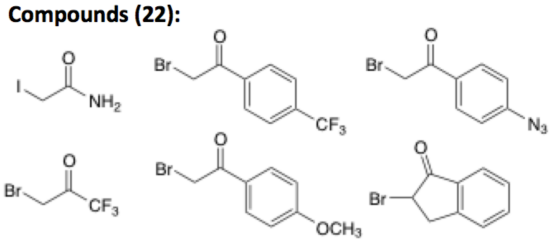

Lewis Acids (24): $TiCl_4$, BEt_3, BF_3, $FeCl_3$, $AlCl_3$, $MgBr_2$, $Eu(OTf)_3$, $Sc(OTf)_3$, $Sm(OTf)_3$, Dimesityl boronic acid, $CeCl_3$, InF_3, $InCl_3$, $Ho(OTf)_3$, $Pr(OTf)_3$, $Y(OTf)_3$, $Cu(OTf)_2$, $La(OTf)_3$, $Yb(OTf)_3$, $BiCl_3$, $Gd(OTf)_3$, $Er(OTf)_3$, $Tl(TFA)_3$, $CuOTf$

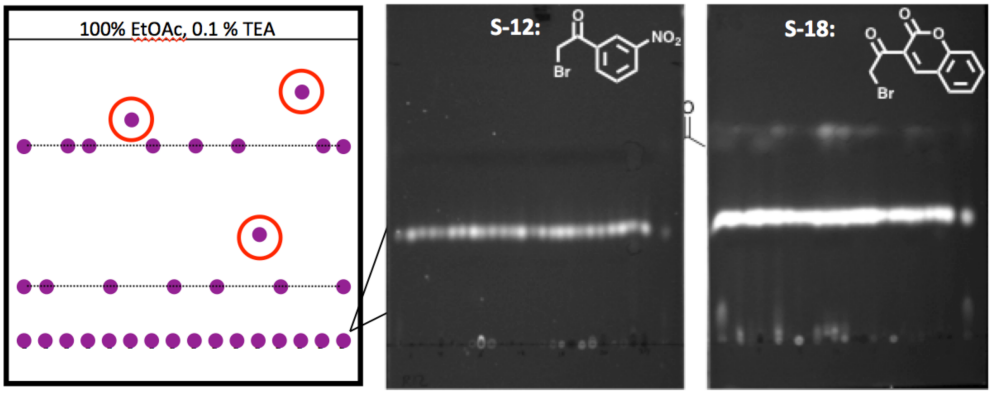

Figure 5-09. TLC profiling of α-halo ketones as 3-member transition states.

Our assay used pyrene as a floureescent reporter group and NAc-Cys-COOMe as a polar reporter, and we were looking for any spots off the two rows, the top being unreacted and the bottom being hydrolyzed thioester. After over 500 conditions, it was β-keto ester that was brought to our attention with the higher spots on the TLC plate S-18 (right) with mild conversion to a higher R_f spot. We then decided to pursue a new reaction geometry.

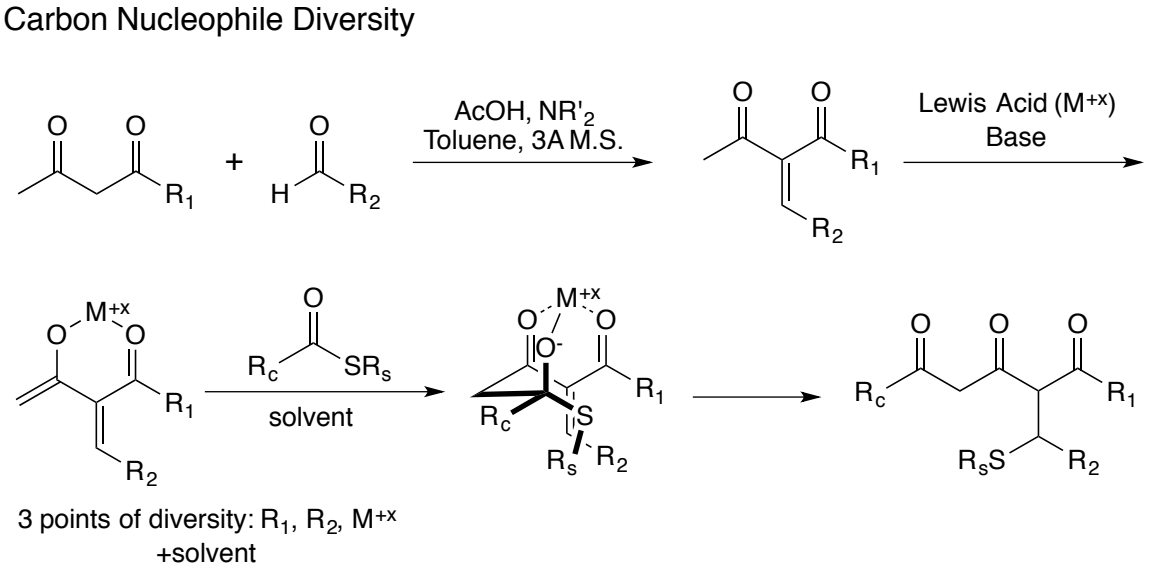

Scheme 5-18. Metal chelated *umpolung* thioester fixation probes.

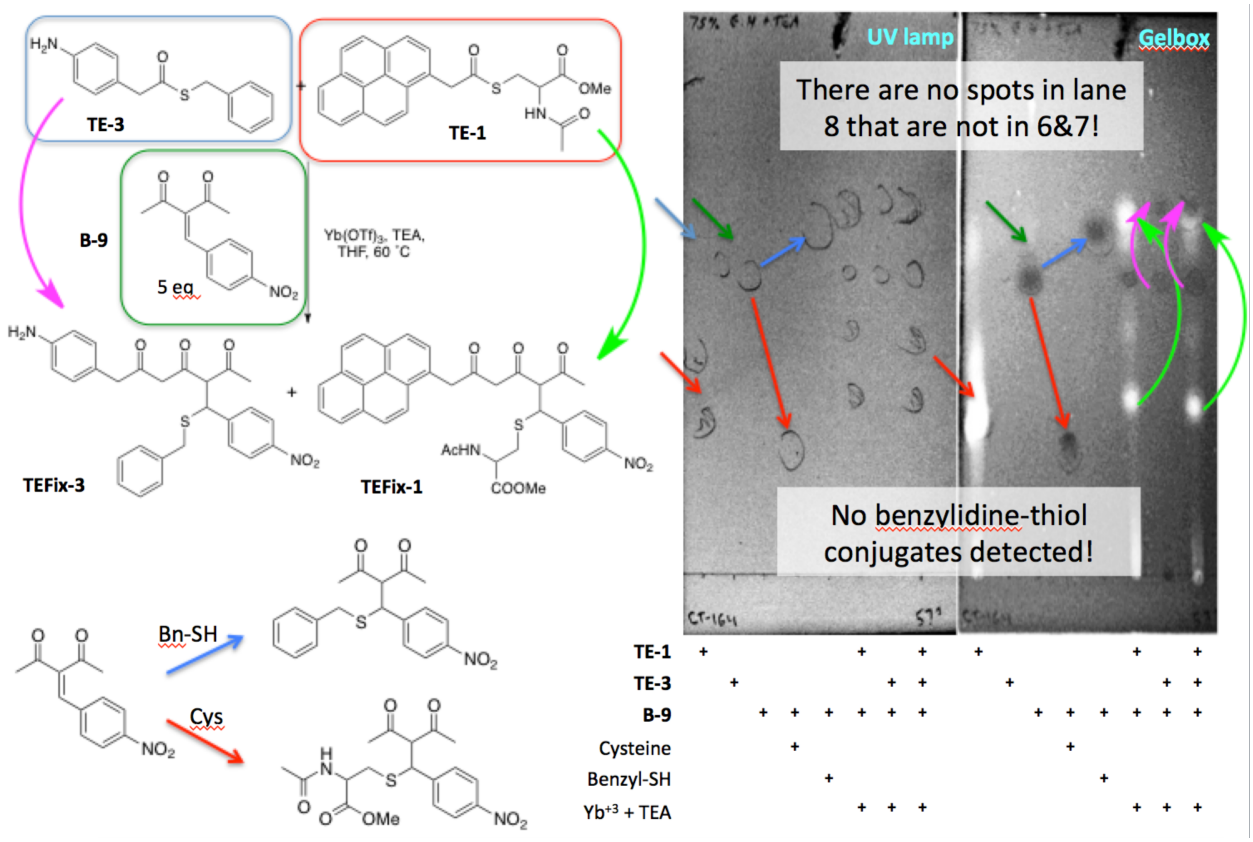

Figure 5-08. Thioester fixation is still and elusive creature.
This crossover experiment shows that it still has the potential to work. The amount of data that one can get out of this is remarkable. The pyrene fluorophore tracks the R_c of TE-1 (red box) when imaged under the gelbox, while the cysteine is a polar tracking group for R_s. The aniline of R_c of TE-3 (sky blue box) is a polar group there, while the mercaptobenzyl group of the R_s is a nonpolar one. If there were crossover between these two, it would result in a polar/polar or non-polar/non-polar pair and we would see spots well above or below beyond the R_f of the mixed polar/non-polar pairs. The benzylidine B-9 (dark green box), has a nitrophenyl moiety, that instead of fluorescing, quenches the area around it (dark green arrows; dark spots in gelbox lane). That way, we always know where that goes. Incubating B-9 with the R_s side of each thioester results in two distinct spots, the BnSH (blue arrow) increasing in R_f, while the CysSH

(red arrow) was held back. In separate experiments with TE-3 + B-9 (magenta arrows, forming TEFix-3) and TE-1 + B-9 (bright green arrows, TEFix-1), neither of these producers were seen. And, in our crossover experiment (last lane), where B-9 is incubated with both thioesers in the presence of the Lewis acid and base, both of the previous set of spots are seen, *but no new peaks are obvserved*. This indicates the potential for these reagents to yet be successful in thioester fixation, if the appropriate troubleshooting was choosen.

It is important to consider all the different geometries and which ones are considered favorable (3,6) and which ones are considered unfavorable (4,5,7). For instance, the Bayer-Villager has a 3-membered transition state, probably contributing to its success. The first example with the sulfhydrylated thiols mimicked this, and used a 3-member transition state. However, the carbon nucleophiles have a 6-member transition state between the β-carbon of the double bond, and the thiol.

Electrophilic additions from the α-carbon (aldol reaction, aldol condensation)

Perhaps a safer alternative to this nucleophilic addition is taking advantage of the unique properties the thioester for an electrophilic addition. This prevents any potential breaking of the bond. Due to the poor n = 2 and n = 3 overlap between the thioester sulfur and the carbonyl carbon, there is limited resonance between the two. This contributes to the weakness of the thioester in one sense, but also increases it nucleophilic character by allowing for a higher enolization. Because of the small amount

of resonance contribution by the sulfur, it is estimated the thioesters react much like ketones. Using the appropriate organocatalyst and appropriate aldehyde substrate may result in a product that maintains the connection of R_c to R_s, while allowing functionalization. Generally we would seek to do the following:

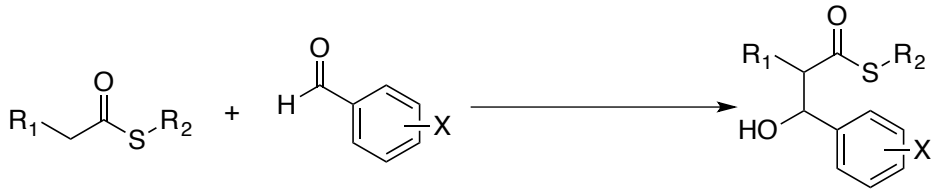

Scheme 5-19. Aldol reactions of thioesters.

Hyrolyzed EDC may provide the ideal Lewis-acid – Bronstead-base paired catalyst for the aldol condensation of thioesters and aldehydes. Because of the small amount of resonance contribution by the sulfur, it is estimated the thioesters react much like ketones. Using the appropriate organocatalyst and appropriate aldehyde substrate may result in a product that maintains the connection of R_c to R_s, while allowing functionalization.

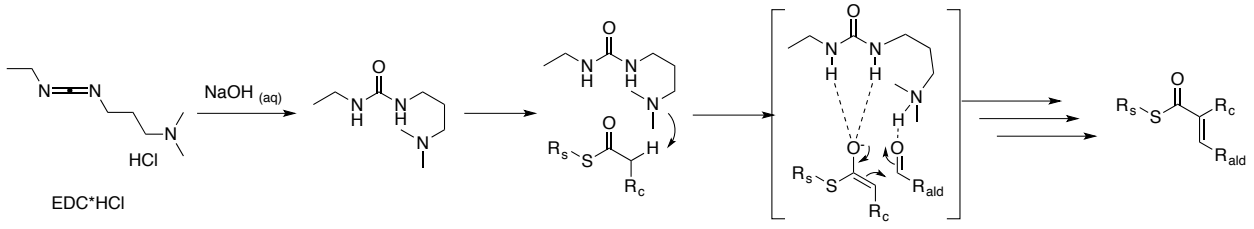

Scheme 5-20. Biomimetic organocatalysis.

Using hydrolyzed EDC as a combination Lewis-acid/Bronstead base to activate and deprotonate the thioester.

Other more complex organo-Lewis acids can be used in conjunction with an exogenous base. Such organization may help to not only deprotonate the thioester itself, but coordinate with the alhydehyde as well, bringing it into physical proximity and using hydrogen bonds to activate it/stabilize the anion intermediate.

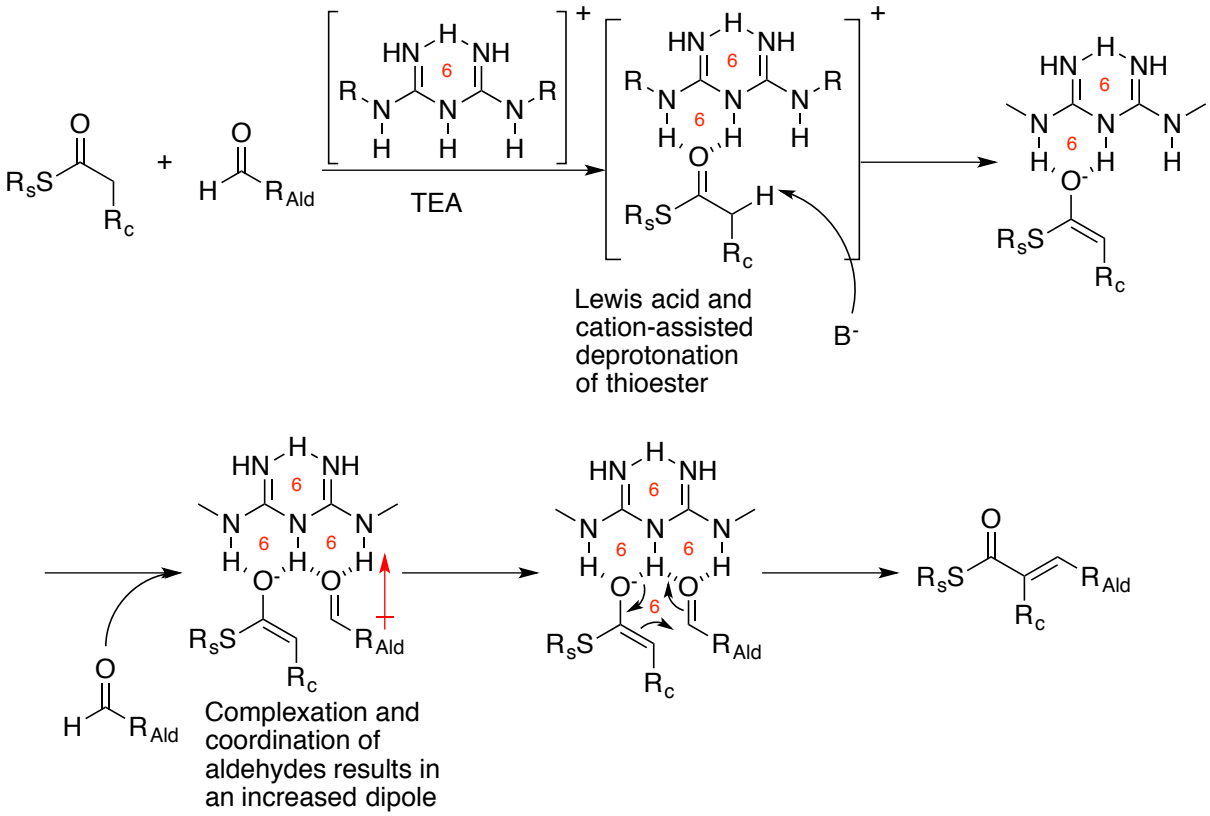

Scheme 5-21 More complex bifunctional biguanidinium Lewis acids.

This catalyst coordinates both the enolate of the thioester and the aldehyde itself in a conformationally favorable arrangement. It has strong Lewis acid character due to its positively charged group.

5.08. Random ideas.

Methods to create chemicaly uncaged sulfinic acid *in situ*

Sulfonyl chlorides

Sulfonyl chloride is a reasonably stable functional group that is slow to hydrolyze. It can be turned into a sulfenic acid by nucleophilic thiols, in which they go through a thiosulfonate intermediate, consuming one reducing equivalent (2 GSH). The problem may be that it may react with other functional groups semi-irreversibly, such as serine hydrolases. The initial product may also be fluorescent.

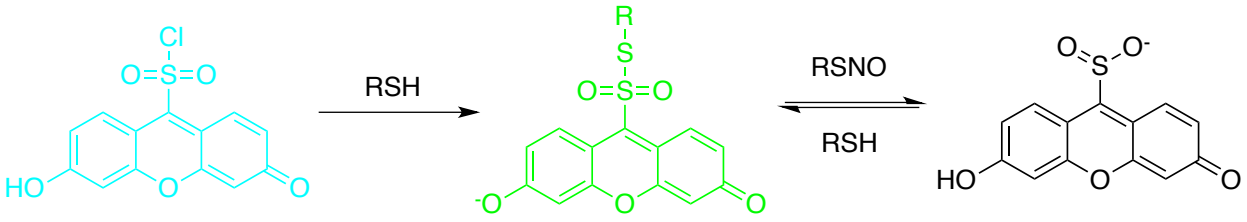

Scheme 5-22. Sulfonyl chlorides as nucleophilically uncaging groups.

Thiosulfonates

Thiosulfonates are a more mild approach, more selective for thiols, and are less prone to non-productive pathways. They can travel freely in the oxidized extracellular region, but upon exposure to the reducing environment of the cell, the high thiol content rapidly cleaves it, where it can react with nitrosothiols.

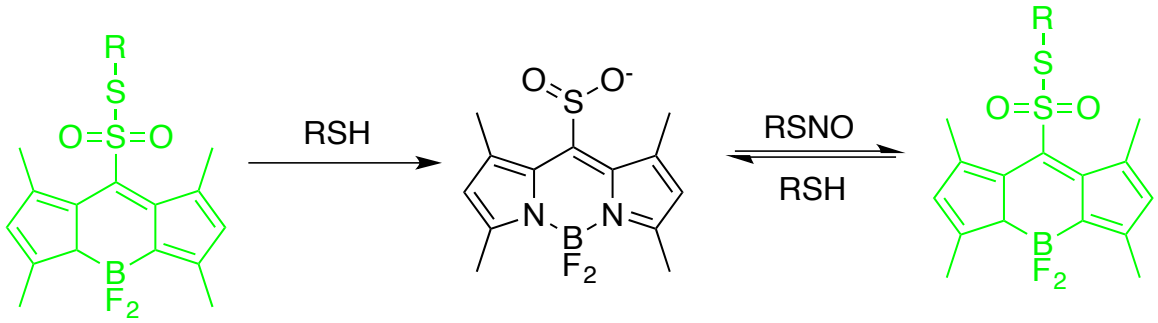

Scheme 5-23. Thiosulfonates as reducttively uncaging groups.

However, if these are both R = alkyl thiosulfonates, they will have the sample fluorescence, leading to high background. This can partially be overcome by tethering a quencher to the reduced end of the thiosulfonate.

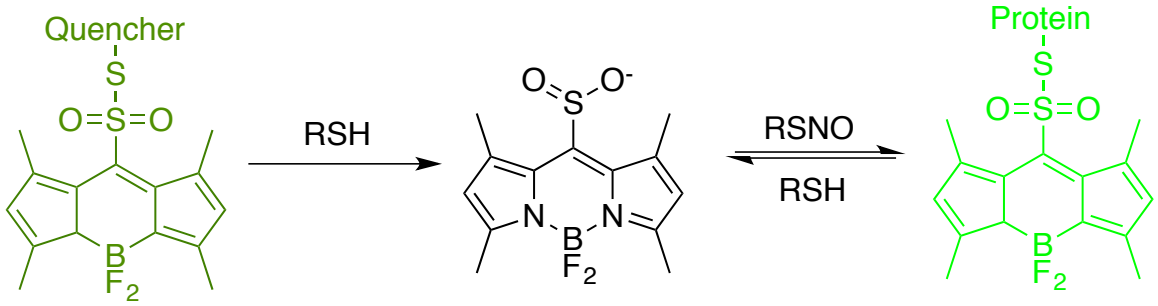

Scheme 5-24. The use of a quencher to diminish non-reduced probe background.

A method to make thiosulfonate peptides:

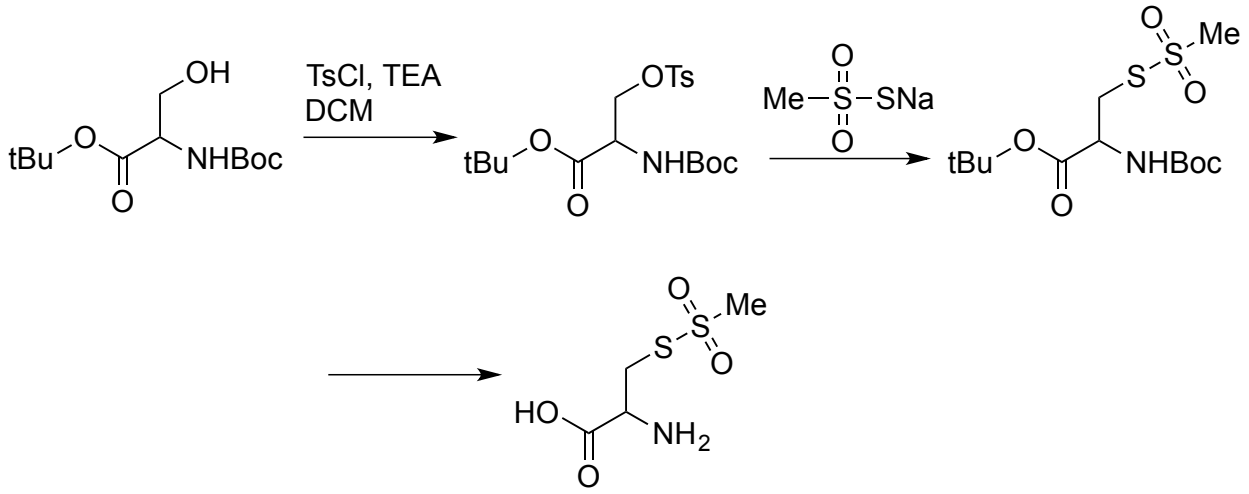

Scheme 5-25. Just in case you need it and didn't want to go through the SNO route.

Appendices

Appendix A: Rapid bioorthogonal ratiometric live-cell imaging of protein *S*-sulfenylation

Christopher T.M.B. Tom[1], Matthew B. Stone[2], Jeannie L. Hernandez[3], Yu-Hsuan Kuo[1], Kristin J. Labby[3], Lyanne Gomez-Rodriguez[1], Paul M. Jenkins[4,5], Paul M. Zimmerman[3], Sarah L. Veatch[1,2], and Brent R. Martin[1,3]*

[1]Program in Chemical Biology, [2]Department of Biophysics, [3]Department of Chemistry, [4]Department of Pharmacology, [5]Department of Psychiatry, University of Michigan, 930 N. University Ave., Ann Arbor, MI 48109.

*Correspondence should be sent to brentrm@umich.edu.

A.1. General procedures and materials for experimental methods.

All chemistry was performed with dry solvents of the highest purity available, except where noted. All glassware was flame-dried and the reactions were performed under a slight positive pressure of inert gas unless otherwise noted. 4-bromo-1,8-naphthalic anhydride was obtained from TCI Chemical. Diethyl fluoromalonate was obtained from Matrix Scientific. Zinc chloride and diethyl malonate were obtained from Alfa Aesar. Cesium carbonate, sodium azide, L-proline, copper metal, and diethyl methylmalonate were obtained from Sigma-Aldrich. Compounds were purified by normal-phase flash chromatography on silica gel (Machary-Nagel), unless otherwise noted. NMR spectra were collected on a Varian MR400 premium shielded magnet, with either a Varian 5 mm AutoX dual broadband probe or Varian autoswitchable quad probe. ^{1}H and ^{13}C drifts were corrected against residual solvent peaks[209]; ^{19}F were corrected using trifluoroacetic acid (δ = -76.5 ppm) as a standard. NMR spectra were analyzed using Mestrenova (Mestrelab Research). Low-resolution mass spectra were obtained on a Micromass LCT time-of-flight (TOF) instrument with electrospray ionization (ESI) coupled to a HPLC pump with a rheodyne loop injector. High-resolution mass spectra were collected on an Agilent Q-TOF (accuracy 1-5 ppm) with in-line photodetector array, either in direct-injection mode or through a Waters 10 cm C18 column with a 5-95% water:acetonitrile gradient, 5 mL / min, 15 minutes.

Fluorescence Spectroscopy. All spectroscopy was done in Hellma Analytics quartz precision cells 10x2 mm. Fluorescence spectra were collected on a Varian Cary Eclipse fluorescence spectrophotometer with 5 nm excitation and emission slit widths. Absorbance measurements were collected on a Varian Cary 100 Bio UV-visible

spectrophotometer. Lucifer yellow (Sigma-Aldrich) was used as a quantum yield standard by matching absorbance to DiNap at the excitation maxima, and integrating the emission intensity, correcting for refractive index as necessary.

HPLC analysis. High-performance liquid chromatography separations were performed on a Waters HPLC 1525 binary pump system with an in-line Waters 2707 autosampler, reverse-phase column, Waters 2998 photodiode array (PDA), and Waters fraction collector III. Samples were injected and run through an Atlantis prep T3 (10 x 250 mm) C_{18} column equilibrated at 5% acetonitrile / water (0.1% formic acid), held at this solvent composition for 1 min, and linearly increased to 95% until 12 min, and held at this solvent composition for 1 min before being re-equilibrated to 5% acetonitrile : water. Solvent elution was 5 mL / min. Absorption spectra were collected through the PDA, and data were analyzed using Waters Empower software. Elution traces were collected at the approximate maximum wavelength for each compound (dimedone: 280 nm; DiNaps 488 nm).

SDS-PAGE analysis. Samples were either combined immediately with loading buffer and heated to 95˚C for 10-15 min, or, as necessary, small molecules were removed by a modified trichloroacetic acid (TCA) precipitation. Briefly, proteins were precipitated by adding 0.2 volumes of a 50% w / v mixture of TCA / water, centrifuged (1000 x g for 3 minutes), and the supernatant removed. Next, the protein pellet was sonicated and washed in cold methanol (3x) and acetone (1x), and resuspended in 6 M urea in SDS gel loading buffer. Proteins were separated using pre-cast 12% acrylamide gels (BioRad) run at 160 V for 70 minutes. Western blots were transferred to Millipore Immobulon FL paper with 100 V input over 70 minutes. We found that for all AMCs

tested, there was a major cross-reaction with the polyacrylamide gel. To prevent this, samples were either first processed by TCA precipitation (Figures S4 and S6) or transferred to PVDF membranes for direct fluorescence analysis (Figures 2, 3, 4, and S5). The following antibodies were used in this study: mouse α-His_6 (Qiagen), mouse α-GAPDH (Millipore), mouse α-E-cadherin (Millipore), rabbit anti-beta-actin (Cell SIgnaling). All DiNap gel-based imaging was performed on a GE Typhoon Scanner using the 488 nm laser line using the 555 / 20 nm emission filter. Near-infrared western blot imaging was performed with an Azure Biosystems c600 system.

Mammalian cell culture. A431, HeLa, HEK293T, and MDA-MB-231 cells were grown in DMEM media with 10% FBS and penicillin / streptomycin. CH27 cells were grown in DMEM media with 15% FBS with L-Glutamine, 1 g / L glucose, and 110 mg / L sodium pyruvate with penicillin / streptomycin in the presence of 50 μM 2-mercaptoethanol. MCF10A cells were transduced with retrovirus produced from pPGS-hSnail-fl.Flag-NEO (Addgene plasmid no. 25695) and pCL-Ampho packaging vector. After two days, cells were selected with 600 μg / ml G418 (Life Technologies). MCF10A vector and Snail1 cells were cultured in DMEM / F12 base medium (Thermo) supplemented with 5% dialyzed horse serum, 20 ng / ml recombinant human epidermal growth factor (Shenandoah), 0.5 mg / ml hydrocortisone (Sigma), 100 ng / ml cholera toxin (Sigma), and 10 μg / ml insulin (Sigma). After probe incubation, cells were washed 3x with PBS and mechanically scraped from the dish. Protein levels were quantified prior to SDS-PAGE using the DC protein assay (BioRad).

Cloning and Mutagenesis of E.coli AhpC and human GAPDH. Whole genomic DNA was extracted from Top10 E.coli using TRIzol Reagent (Life Technologies) according to

manufacturer's protocol. TRIzol reagent was also used to extract RNA from HEK293T cells. cDNA was synthesized from 1 μg of total RNA using SuperScriptIII reverse transcriptase (Life Technologies). The bacterial gene for AhpC (Uniprot ID: P0AE08) was amplified from *E. coli* genomic DNA using Phusion DNA polymerase chain reaction (PCR), with primers containing BamHI and XhoI restriction sites (underlined) (5'-TTTGGATCCGTCCTTGATTAACACCAAAATTAA-3', 5'-TTTCTCGAGTTAGATTTTACCAACCAGGTCC-3'). Human GAPDH was amplified from HEK293t cDNA with the primers 5'-TTTGGATCCGGGGAAGGTGAAGGTCGGAGTC -3' and 5'- TTTCTCGAGTTACTCCTTGGAGGCCATGTG-3' containing BamHI and XhoI restriction enzyme sites (underlined). After restriction enzyme digestion, each the AhpC and GAPDH fragment was ligated (T4 DNA ligase, NEB) into pET45b between BamHI and XhoI sites to insert an N-terminal His tag. The AhpC-C166S mutant was created by quick change site-directed mutagenesis with primers 5'-CACCCAGGTGAAGTTTCCCCGGCTAAATGGAAAG-3' and 5'-CTTTCCATTTAGCCGGGGAAACTTCACCTGGGTG-3'. All sequences were confirmed by sequencing (University of Michigan DNA Sequencing Core)

Expression and Purification of AhpC-C166S and GAPDH. For large-scale recombinant expression in bacteria, 1 L of TB media with 50 μg / mL carbenicillin was inoculated with the appropriate BL21 strain and grown with shaking at 250 rpm at 37 °C. When the OD_{600} = 0.6, the cultures were induced with 0.5 mM IPTG and temperature was reduced to 22 °C. After shaking for 16 hours, *E. coli* were harvested by centrifugation. Pellets were stored at -80 °C until purification. All purification steps were carried out at 4 °C. To frozen (-80 °C) pellets from 1 L of *E. coli* culture grown in TB, 40

mL of lysis buffer (50 mM Tris pH 8.0, 150 mM NaCl, 10% glycerol) was added. Pellets were lysed by sonication, and cell debris was pelleted by centrifugation at 12,000 x g for 30 minutes. Lysate was either used at this point, or AhpC or GAPDH was purified from the supernatant using TALON (Clontech) resin according to manufacturer's protocol. Fractions containing the desired recombinant protein (as indicated by SDS-PAGE) were pooled and transferred to dialysis tubing (10,000 MWC), and dialyzed into 20 mM Tris pH 8.0 with 30 mM NaCl to remove imidazole. Protein was concentrated using 10,000 MWC spin concentrators, aliquoted and stored at -80 °C.

Rate measurements of dimedone with glyceraldehyde. Dimedone (0.5 mM final concentration) was added to PBS in an HPLC vial. To this was added a solution of from stock solutions of glyceraldehyde at 5, 10, 15, 20, 30, 40, 80 and 160 mM final concentrations. Aliquots were removed by HPLC and initial t = 0 was run, and then subsequent time points at 15 minute intervals using the standard methods. The area under the dimedone curve at 254 nm was recorded. These data were globally fit, yielding a rate constant of 0.059 ± 0.0036 M^{-1} s^{-1}.

Rate measurements for H- and F-DiNap. A 2.67 mg / mL solution of Ahpc C166S overexpressed BL21 lysate was prepared with 5, 1, 0.1, and 0.02 mM final concentation DiNap **3a** or **3c** in 0.3 mL PBS. At defined timepoints, 40 µL aliquots were added to 1.5 mL tubes containing 10 µL 100% w/v trichloroacetic acid to quench the reaction and precipitate proteins. Samples were centrifuged 5 min at 20,000 xg, and the supernatant was removed. Next, 1 mL methanol added and the samples were sonicated and centrifuged again to wash the pellet. This wash procedure was repeated 1x with MeOH and 1x with acetone. The samples were allowed to completely air-dry, before being

resuspended in 50 µL 1x loading buffer, heated at 95 ˚C for 15 minutes, and analyzed via SDS-PAGE. Protein bands were quantified using ImageJ, and protein loading was normalized using either coomassie blue staining or α-His_6 immunostaining.

Computational methods. All quantum chemical calculations were performed using the Q-Chem 4.3 ab initio quantum chemistry package.[210] Gas-phase geometry optimizations with explicit water solvent were carried out with the hybrid B3LYP density functional[211,212] in the spin restricted formulism, and the double-zeta, LANL2DZ basis set.[213-215] The ωB97X-D functional[216] was used to calculate single point energies with the PCM solvation model using water as the implicit solvent (in addition to explicit solvent). The solvent-corrected single point energies used the triple-zeta, polarized cc-pVTZ basis set.[217-219] Thermodynamic corrections were applied to the solvated energies using the B3LYP/LANL2DZ level of theory and a temperature of 298.15 K. The Growing String Method (GSM) was used to determine the exact transition state and minimum energy reaction path for each proposed elementary step.[220-222] By optimizing the reaction path, GSM provides verification that the saddle point connects the reactant to product geometries through a single transition state. GSM was considered converged when the RMS gradient at the transition state node reached less than 0.0005 HT/Å. 19 nodes along the string were used to represent the reaction paths. Natural orbital analysis was performed using the NBO 5.0 code[223] in the Q-Chem 4.3 package.

TIRF microscopy. Cells were plated on 35 mm #1.5 glass-bottomed cultuwre dishes (MatTek Corporation, Ashland, MA). Cells were incubated with 1 mM H-DiNap or F-DiNap in Tyrode's buffer. Imaging was performed on an Olympus IX81-XDC inverted microscope with a cellTIRF module, a 100X UAPO TIRF objective (NA=1.49), and

active Z-drift correction (ZDC) (Olympus America, Center Valley, PA). Images were acquired on an iXon-897 EMCCD camera (Andor, South Windsor, CT). TIRF excitation was accomplished using a 488 nm diode laser (Sapphire 488 LP, Coherent) and a 402 nm diode laser (CUBE 405-50FP, Coherent). Excitation intensities were adjusted to give approximately equal emission between UV and blue excitation. Excitation and emission was filtered using the quadband dichroic mirror LF405/488/561/635-4X-A-000 (Semrock, Lake Forest, IL). Images were analyzed using MATLAB (The MathWorks, Natick, MA).

Confocal microscopy. Cells were plated on #1.5 glass-bottomed culture dishes and imaged on a Nikon A1R+ laser scanning confocal microscope with a 60 × 1.4 Plan Apo VC oil objective. Cells were incubated with 1 mM F-DiNap in growth media for 15 minutes and imaged without washing. Sequential excitation was accomplished using 405- and 488-nm lasers, and emission was gathered through a 500-550nm bandpass filter using a pinhole diameter of 116.2 microns. A stagetop humidified incubation chamber (Okolab) was used to maintain the cells at 37 °C and 5% CO_2. Z-stacks were captured using an optical thickness of 375 nm in Z. Exposures were adjusted to the maximum dynamic range while avoiding saturation. Images were analyzed with NIS-Elements AR software (Nikon).

II. Synthetic Schemes

Scheme A1. Mechanistic rationale for α-substituted active methylene compounds. In cyclic active methylene compounds, such as dimedone, the pK_a of the α-proton is below physiological pH and is deprotonated. The enolate then reacts with a sulfenic acid to form a thioether. The second α-proton presumably has a similar, if not lower pKa and is deprotonated after sulfenic acid conjugation. From this mechanism, it is clear that the first α-deprotonation step is necessary for the reaction, but the second plays no role in sulfenic acid conjugation. Therefore, replacement of one of the α-protons with a small blocking group (Me, F) was hypothesized to allow the probe to conjugate. Probes lacking a second α-proton should be trapped in a diketone form. The enolate-to-diketone transition, and the corresponding chemical and electronic changes, is creates a chemical 'switch'.

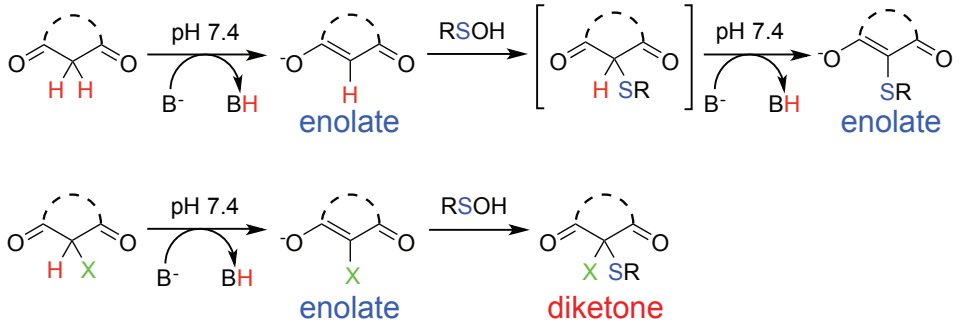

Scheme A2. General procedure for conversion of 4-bromo-1,8-naphthalic anhydride to bromo-DiNap 2a-c.

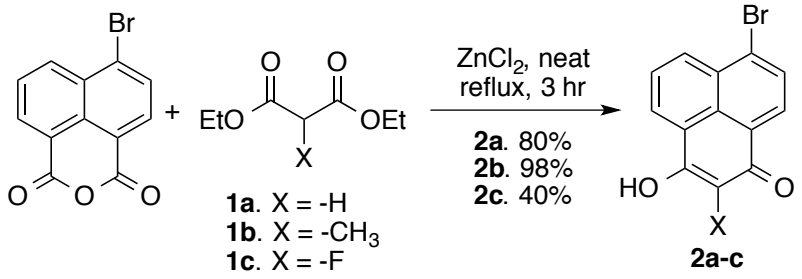

Using a modified literature procedure[224], zinc chloride (3.0 eq) was added to a round-bottom flask. The reaction flask was equipped with a magnetic stir bar, a reflux condensor, and an oil bubbler. Thionyl chloride (20 mL) was added and the heterogeneous mixture was brought to a reflux for 30 minutes, or whenever gas production ceased. The thionyl chloride was removed by rotary evaporation until the zinc chloride appeared as a free-flowing white powder. 4-Bromo-1,8-naphthalic anhydride (1.0 eq) and diethyl malonate **1** (10 eq) were added to the flask. This was outfitted with an efficient reflux condenser, and the mixture was heated to reflux (~200 ˚C) for 6 hours or until no more gas is evolved. The remaining malonate was removed by distillation under vacuum, after which point the solid was washed with 1 N HCl and filtered. The solid was dissolved in a 1:1 mixture of MeOH and 1 N NaOH, and the remaining solid was removed by filtration. The DiNap was precipitated again with 6 N HCl and filtered. The solid was dried under reduced pressure, and washed with DCM to remove residual malonate and naphthalic anhydride. As necessary, it was recrystallized from a mixture of water and methanol.

DiNapBr 2a. Zinc chloride (3.0 eq, 7.38 g, 54 mmol), bromonaphthalic anhydride (1.0 eq, 5.0 g, 18 mmol), and diethyl malonate (10 eq, 27.5 mL, 181 mmol) were used as described. 3.95 g (80%) of the title compound was collected. ^{1}H NMR (401 MHz, DMSO-d6) δ 8.34 (dd, J = 8.4, 1.2 Hz, 1H), 8.30 (dd, J = 7.3, 1.2 Hz, 1H), 8.09 – 8.01 (m, 2H), 7.83 (dd, J = 8.5, 7.3 Hz, 1H), 6.13 (s, 1H). ^{13}C NMR (100 MHz, DMSO-d6) δ 174.40, 173.84, 131.53, 130.84, 130.07, 128.30, 128.18, 128.14, 127.81, 127.75, 127.06, 126.29, 105.34. ESI-MS: [M+H] 274.9702 (predicted 274.9702)

Me-DiNapBr 2b. Zinc chloride (3.0 eq, 6.87 g, 50 mmol), bromonaphthalic anhydride (1.0 eq, 4.66 g, 17 mmol), and diethyl 2-methylmalonate (10 eq, 28.6 mL, 168 mmol) were used as described. 4.76 g (98%) of the title compound was collected. ^{1}H NMR (400 MHz, DMSO-d6) δ 8.05 (d, J = 6.7 Hz, 1H), 7.95 (d , J = 8.1 Hz, 1H), 7.79 (d, J = 7.5Hz, 1H), 7.70 (d, J = 7.6 Hz, 1H), 7.52 (t, J = 7.1 Hz, 1H), 1.94 (s, 3H). ^{13}C NMR (100 MHz, DMSO-d6) δ 163.22, 163.09, 130.43, 130.25, 129.37, 127.79, 127.49, 127.18, 127.12, 126.60, 126.18, 125.83, 113.10, 8.79. ESI-MS: [M+H] 288.8957 (predicted 288.8959)

F-DiNapBr 2c. Zinc chloride (3.0 eq, 22.1 g, 160 mmol), bromonaphthalic anhydride (1.0 eq, 15.0 g, 54 mmol), and diethyl fluoromalonate (5.0 eq, 48 g, 270 mmol) were used as described. 6.50 g, (41%) of the title compound. ^{1}H NMR (401 MHz, Methanol-d_4) δ 8.53 – 8.49 (m, 1H), 8.49 – 8.44 (m, 1H), 8.22 (d, J = 7.9 Hz, 1H), 8.04 (d, J = 7.9 Hz, 1H), 7.85 – 7.79 (m, 1H). ^{13}C NMR (100 MHz, DMSO-d6) δ 142.82, 140.44, 133.46, 133.08, 131.78, 130.95, 129.67, 128.87, 128.57, 128.24, 126.65, 125.87, 124.42. ^{13}C NMR (100 MHz, dmso) δ 142.82, 140.44, 133.46, 133.08, 131.78, 130.95, 129.67, 128.87, 128.57, 128.24, 126.65, 125.87, 124.42. ^{19}F NMR (377 MHz, Methanol-d_4) δ -

164.84. ESI-MS: [M+H] 230.0612 (230.0612 predicted).

Scheme A3. **General procedure for conversion of DiNapBr 2a-c to DiNap 3a-c**.

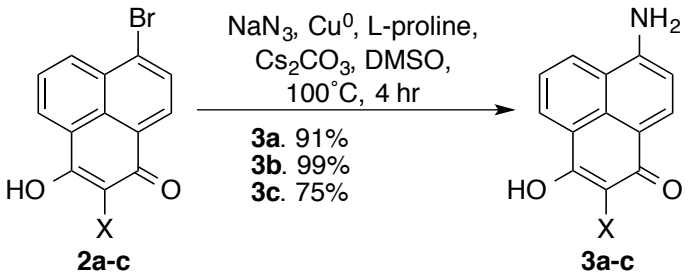

Using a modified literature procedure[225], DMSO (30 mL) was purged of gas by sonication under vacuum for a minimum of 15 minutes. **2** (1.0 eq) is added to a Schlenk flask. Next, copper metal (1.1 eq), sodium azide (3.0 eq), L-proline (1.4 eq), and cesium carbonate (2.5 eq) were added. The flask was then purged under a steady stream of nitrogen for at least 15 minutes. Degassed DMSO was then added to the dry ingredients and the mixture was put on a preheated metal block at 100 ˚C for six hours under inert gas. After the solution was cooled, 6 N HCl was added until a fluffy red precipitate was produced. The solid was filtered, washed with 1 N HCl, and eluted with methanol. The material was dry-loaded onto silica (10x mass relative to theoretical product) and eluted through a silica gel column with a 0 - 10% MeOH:DCM gradient.

DiNap 3a. Starting with **2a** (1.95 g), 1.37 g (91%) of the title compound was isolated. ^{1}HNMR (400 MHz, DMSO-d$_6$) δ 9.38 (s, 2H), 9.02 (d, J = 8.0 Hz, 1H), 8.68 (d, J = 7.6 Hz,1H), 8.38 (d, J = 9.0 Hz, 1H), 7.83 (t, J = 7.9 Hz, 1H), 6.98 (t, J = 4.5 Hz, 2H). ^{13}C NMR (100 MHz, DMSO-d$_6$) δ 170.38, 167.96, 160.48, 137.71, 132.53, 132.48, 127.33, 124.68, 121.77, 120.10, 112.36, 107.95, 100.78. ESI-MS: [M+H] 212.0705 (212.0706 predicted). Purity by HPLC >95%.

Me-DiNap 3b. Starting with **2b** (1.0 g), 0.769 g (99%) of the title compound was isolated. ^{1}H NMR (401 MHz, DMSO-d6) δ 9.39 (s, 2H), 8.86 (d, J = 8.0 Hz, 1H), 8.67 (d, J = 7.6Hz, 1H), 8.53 (d, J = 9.0 Hz, 1H), 7.70 (t, J = 7.9 Hz, 1H), 6.93 (d, J = 9.0 Hz, 1H), 2.17 (s, 3H). ^{13}C NMR (101 MHz, dmso) δ 170.50, 163.70, 158.61, 137.17, 137.11, 131.39, 130.53, 125.68, 124.31, 122.51, 119.78, 111.79, 111.75, 9.49. ESI-MS: [M+H] 226.0863 (predicted 226.0863). Purity by HPLC >95%.

F-DiNap 3c. Starting with **2c** (506 mg), 0.395 g (75%) of the title compound was isolated. ^{1}H NMR (401 MHz, DMSO-d_6) δ 8.59 (d, J = 8.2Hz, 1H), 8.33 (d, J = 6.8 Hz,1H), 8.18 (d, J = 8.5Hz,1H), 7.62 (t, J = 7.9Hz,1H), 6.83 (d, J = 8.5 Hz, 1H). ^{13}C NMR (100 MHz, DMSO-d_6) δ 163.35 (d, J = 9.9 Hz), 157.73, 151.12 (d, J = 11.7 Hz), 142.00, 139.64, 135.43, 130.28, 129.86, 124.21 (d, J = 16.2 Hz), 122.96, 119.76, 111.53, 111.40. ^{19}F NMR (377 MHz, DMSO-d_6) δ -159.34. HR ESI-MS: [M+H] 230.0609 (predicted 230.0612). Purity by HPLC >95%.

Scheme A4. General procedure to synthesize conjugated DiNap dye standards.

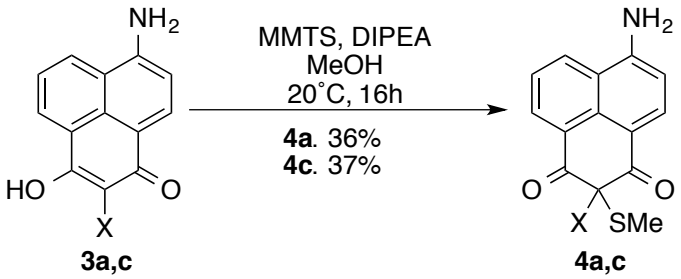

DiNap **3** (1.0 eq) was added in methanol (5 mL) to a round bottom flask, followed by addition of diisopropylethylamine (DIPEA) (1.2 eq). Next, methyl methane thiosulfonate (MMTS) (1.1 eq) was added to the flask, and the reaction was allowed to stir overnight at room temperature. Silica gel (20 times mass of **3**) was added directly to this flask and the solvent was removed under vacuum. The dry powder was added to the top of a silica gel column, and eluted with a DCM:MeOH gradient (MeOH 0-5%). The first eluted species was collected.

MeS-DiNap (4a). Starting with 86 mg of **3a**, 38 mg (36%) was isolated. ^{1}H NMR (401 MHz, DMSO-d_6) δ 10.06 (s, 1H), 8.53 (d, J = 8.2 Hz, 1H), 8.33 (d, J = 7.0 Hz, 1H), 8.12 (d, J = 8.4 Hz, 1H), 7.60 (t, J = 7.8 Hz, 1H), 7.36 (s, 2H), 6.78 (d, J = 8.4Hz,1H), 2.22 (s, 3H). ^{13}C NMR (100 MHz, DMSO-d_6) δ 226.49, 153.30, 133.06, 133.01, 129.46, 129.01, 128.36, 128.29, 128.12, 124.02, 120.37, 108.96, 108.57, 17.57. HR ESI-MS: [M+H] 258.0583 (predicted 258.0583).

MeSF-DiNap (4c). Starting with 40 mg of **3c**, 18 mg (37%) was isolated. ^{1}H NMR (401 MHz, Methanol-d4) δ 8.45 (dd, J = 8.4, 1.2 Hz, 1H), 8.32 (dd, J = 7.2, 1.2 Hz, 1H), 8.20 (d,J = 8.4Hz, 1H), 7.65–7.56 (m, 1H), 6.88 (d, J = 8.4 Hz, 1H), 2.19 (d, J = 2.3 Hz, 3H). ^{19}F NMR (377 MHz, Methanol-d4) δ -167.06. HR ESI-MS: $[M+H^+]^+$ 276.0486 (predicted

276.0489), $[M\text{-}F^-]^+$ 256.0428 (predicted 256.0428), $[M+Na^+]^+$ 298.0307 (predicted 298.0308).

Scheme A5. Probe competition with cellular thiols

a) Protein sulfenic acids (RSOH) are produced from hydrogen peroxide at a variety of different rates depending on the chemical environment of cysteine (k_1) The probe reacts (k_2) and competes with intracellular reducing agents such as glutathione GSH (k_3). b) The fraction of labeling is dependent on the rate and concentration of probe, as well as the rate and concentration of reductant. c) At 0.1 mM concentrations, and assuming that AhpC C166S reduction with 5 mM intracellular GSH is similar to the rate of glutathione reduction of HSA (*), then roughly 2% of AhpC C166S sulfenic acids should be labeled with H-DiNap **3a**. c) By contrast, under similar conditions, 95% of AhpC C166S sulfenic acids should be labeled with F-DiNap **3c** due to the thousandfold increase in reaction rate.

a

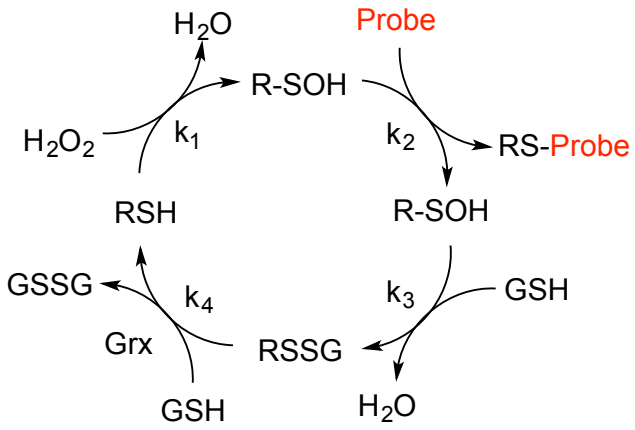

b

$$\text{frac probe reacting} = \frac{k_2[\text{probe}]}{k_2[\text{probe}] + k_3[\text{GSH}]}$$

c

0.1 mM H-DiNap with AhpC C166S with 5 mM GSH

$$2.18\% = \frac{3.24[0.0001]}{3.24[0.0001] + 2.9[0.005]^*}$$

d

0.1 mM FDiNap with AhpC C166S with 5 mM GSH

$$95.4\% = \frac{3020[0.0001]}{3020[0.0001] + 2.9[0.005]^*}$$

Scheme A6. **Sulfenylation and sources of protein carbonylation**

Proteins are typically carbonylated by one of two ways. a) In primary carbonylation, hydroxyl radicals are produced from a single-electron reduction of peroxide by Cu^{+1}/Cu^{+2} or Fe^{+2}/Fe^{+3}. These highly reactive species directly oxidize electron-rich residues in a diffusion-limited fashion, resulting in surface aldehydes. b) In secondary carbonylation, polyunsaturated fatty acids (PUFAs) such as aracadonic acid (shown) are exposed to peroxide, and through complex reaction pathways may lead to α,β-unsaturated aldehydes (enals). These react preferentially with exposed cysteine residues, but also lysine and histidine residues, decorating the exterior surface of proteins with β-linked aldehydes. c) In combination with cofactors, the functional driving input for sulfenylation, and primary and secondary carbonylation is hydrogen peroxide. Because dimedone is reactive with all three oxidative modifications, this makes it difficult to distinguish carbonylation from sulfenylation with dimedone that lacks a blocking group at the α-position.

a

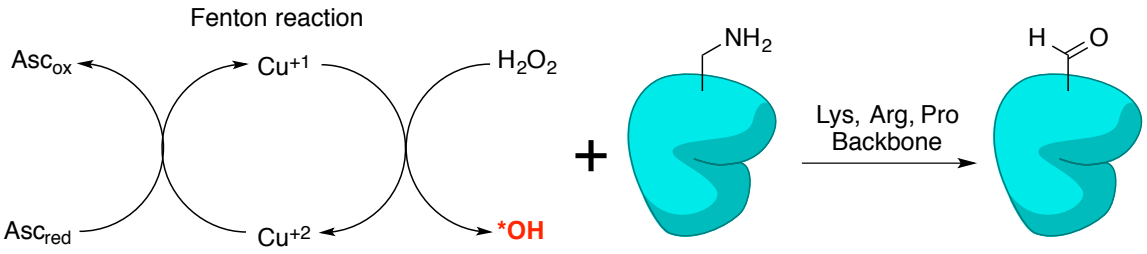

b

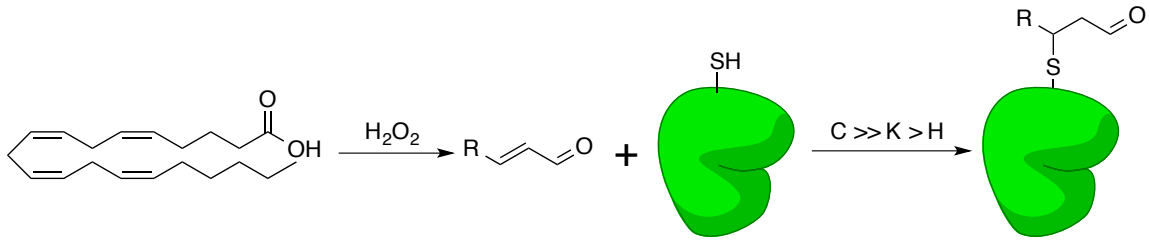
O
OH
H_2O_2
R
O
+
SH
C >> K > H
R
O
S

c

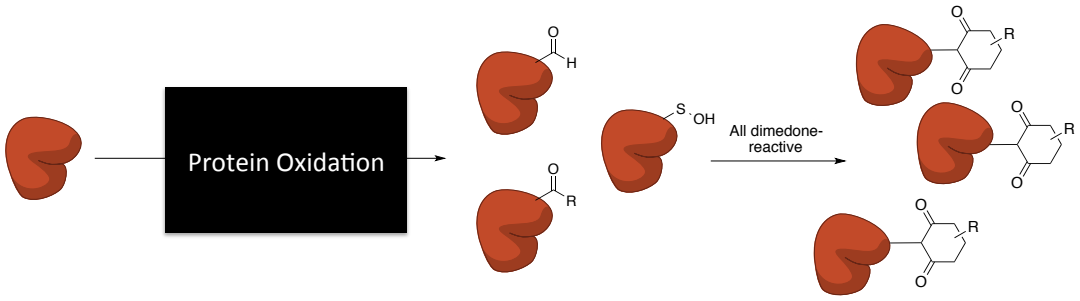
Protein Oxidation
O
H
O
R
S
OH
All dimedone-
reactive
O
R
O
O
R
O
O
R
O

A.3. Supplementary Tables

Table A-01. Fluorescence properties of DiNap probes.

Compound	No.	Excitation λ_{max} (nm)	Emission λ_{max} (nm)	solvent	ε (M^{-1} cm^{-1})	Φ (QY)
H-DiNap	3a	453	542	PBS	10270	0.175
Me-DiNap	3b	470	542	PBS	6490	0.070
F-DiNap	3c	472	544	PBS	8720	0.069
H-MeS-DiNap	4a	458	542	PBS	8680	0.031
F-MeS-DiNap	4c	448	543	MeOH	7030	0.029

Table A-02. Relative rates of protein bands reacting with **3a** or **3c**.

	Rate constant (M^{-1} s^{-1})		
Protein band	3a	3c	k_{3c}/k_{3a}
25 kDa	0.376	623	1,700
50 kDa	0.194	585	3,000
75 kDa	0.126	Too fast to measure (est.>10,000)	>80,000
80 kDa	0.0511	1144	22,000

Table A-03. Natural orbitals of α-carbon of the H- and F-DiNaps.

	FDiNap		HDiNap		ΔH-F	
Orbital	Occupancy	Energy	Occupancy	Energy	ΔOccupancy	ΔEnergy
s	0.883	-110.44	0.971	-102.28	0.088	7.96
px	0.615	-25.73	1.219	-29.49	0.604	-3.46
py	1.078	-28.24	1.068	-25.10	-0.01	3.23
pz	1.208	-79.69	1.171	-65.89	-0.037	13.74

All energies are in kcal/mol.

A.4. Supplementary Figures

Figure A-01. F-DiNap and Dyn-2 label a similar profile of proteins.
BL21 lysates (100 µg in 100 µL) overexpressing Ahpc C166S were incubated with 5 mM of F-DiNap or DYn2 for 1 hr. The reaction was stopped by TCA precipitation, at which point the DYn-2 sample was treated with 1 mM $CuSO_4$, 1 mM TCEP, 1 mM Tris[(1-benzyl-1H-1,2,3-triazol-4-yl)methyl]amine, and 50 µM rhodamine azide, and analyzed by SDS-PAGE. Though there were minor difference, as some proteins were labeled with F-DiNap more effectively, and some were labeled with Dyn-2 more effectively, the overall profile is similar.

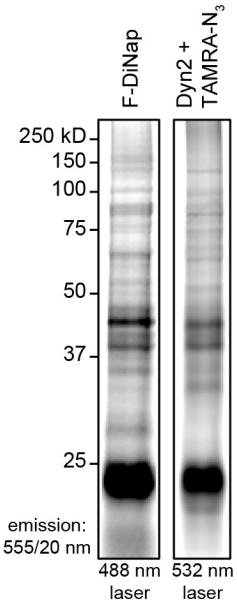

Figure A-02. 3c reacts in an oxidation-dependent manner.
F-DiNap labeling of BL21 cell lysates overexpressing AhpC (C166S) is oxidation dependent, nearly eliminating labeling after treatment with 5 mM TCEP for 1 hour. A slight increase is observed upon peroxide treatment, indicating that most of the protein is in the oxidized state basally in bacterial cell lysates. NT = no treatment.

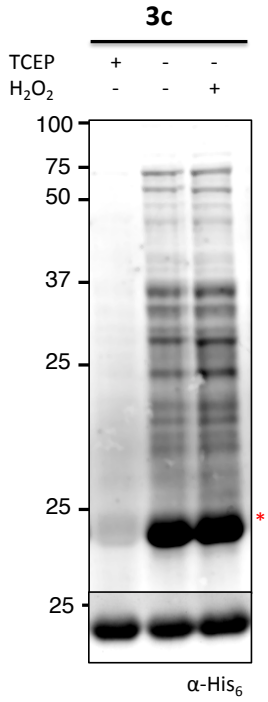

Figure A-03. Peroxide diminishes labeling at higher concentrations.
Pre-treatment of BL21 cell lysates overexpressing AhpC (C166S) for 1 hr at 37˚C followed by 1 mM F-DiNap for 1 hr indicates a decreased labeling at higher peroxide concentrations, perhaps due to overoxidation to sulfinic (RSO_2^-) and sulfonic (RSO_3^-) acids. It is interesting to note that it seems difficult to oxidize the unmodified protein to any large extent, indicating that it already exists in a stable oxidized form.

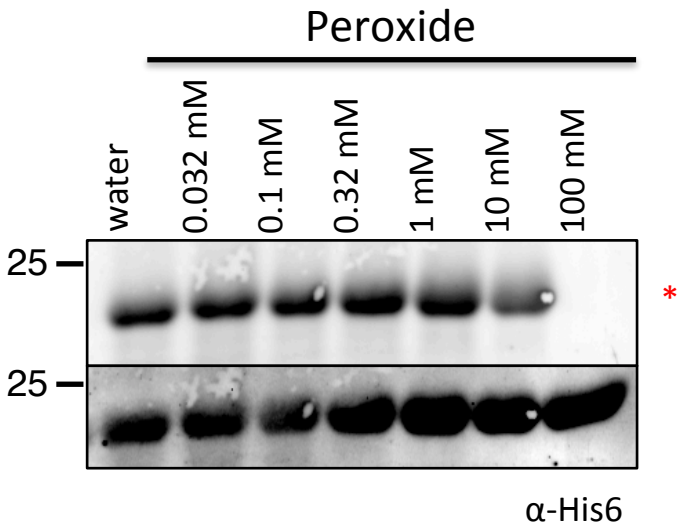

Figure A-04. Dimedone competes with FDiNap for labeling.
Pre-treatement of BL21 cell lysates overexpressing AhpC (C166S) with dimedone in the indicated amounts for 1 hr at 37˚C followed by 1 mM F-DiNap at 37˚C for 1 hr. At higher concentrations, dimedone competes with F-DiNap for labeling.

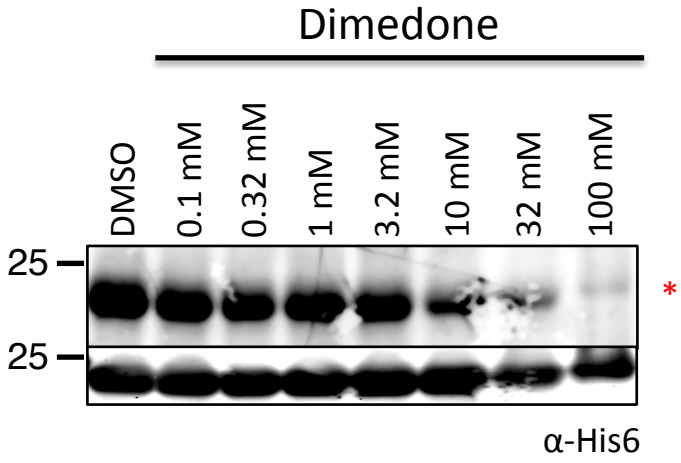

Figure A-05. F-DiNap reacts with a sulfenamide standard.
A cyclic sulfenamide MeOVal-CysSA-Cbz was prepared by literature procedure[158]. DiNap **3c** (100 mM stock in DMSO; final concentration, 1 mM) was added to the sulfonamide (100 mM stock in DMSO; final concentration, 1 mM) was reacted in PBS for 1 hr. HPLC analysis reveals the formation of a new species, as confirmed by HRMS XXXX.

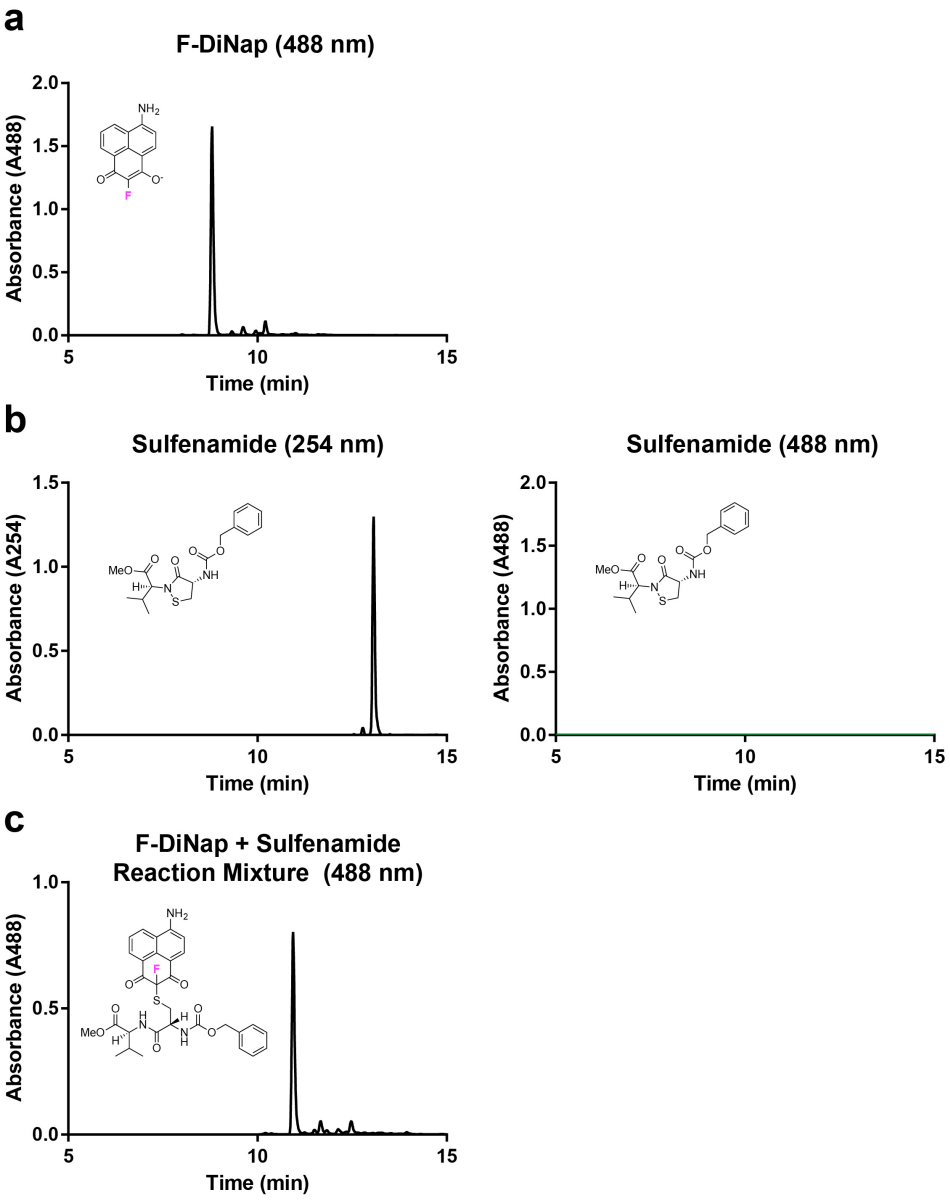

Figure A-06. F-DiNap shows a ^{19}F NMR shift upon conjugation in aqueous buffer. To a mixture of 10% D_2O in PBS (pH 7.4) was added with 33 μM trifluoroacetic acid (TFA) and DiNap **3c** (100 mM stock in DMSO; final concentration, 1 mM). (a) The ^{9}F NMR of F-DiNap and TFA. (b) Subsequently the cyclic sulfonamide MeOVal-CysSA-Cbz (100 mM stock in DMSO; final concentration, 1 mM) was reacted for 1 hr with F-DiNap. (c) Fluorine is sensitive to chemical environment, and F-DiNap shifts from -170.52 to -120.69 ppm upon reaction.

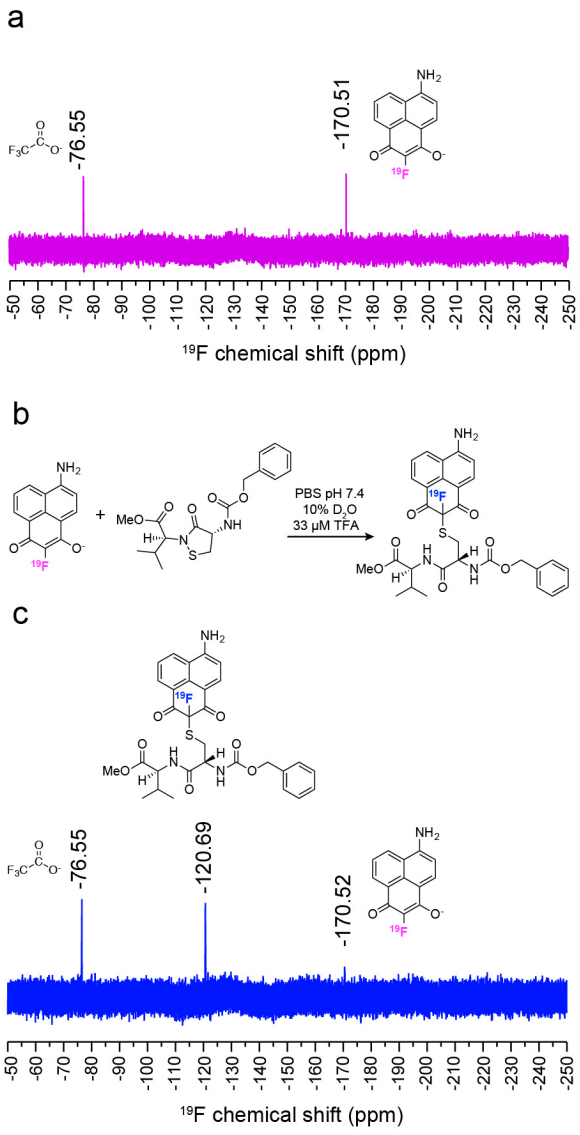

Figure A-07. Dimedone reacts with MMTS in aqueous buffer.
Dimedone (5 mM) or F-DiNap (5 mM) and MMTS (15 mM) were combined in PBS, incubated for 30 minutes, and analyzed by HPLC using a photodiode array detector.

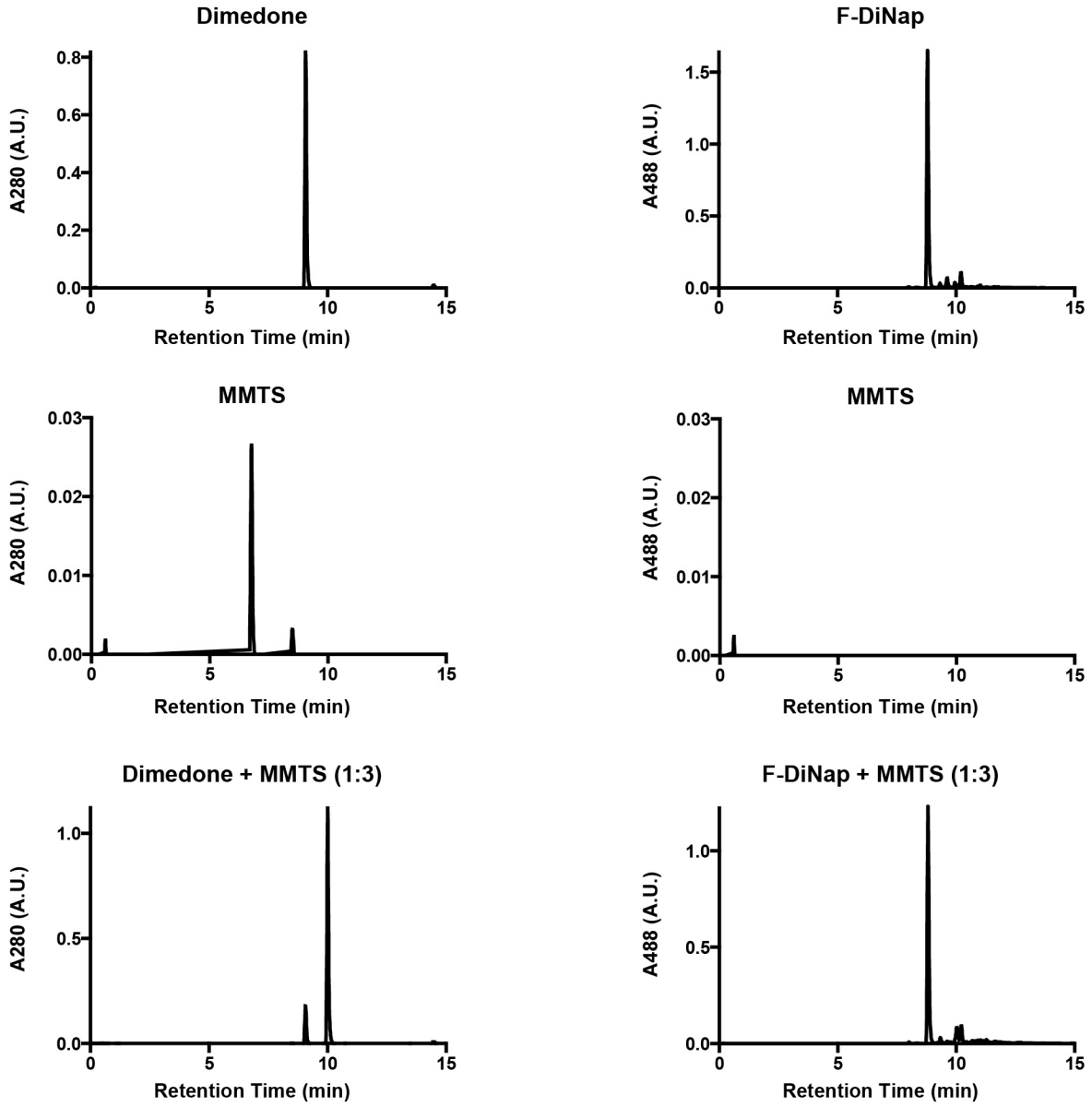

Figure A-08. Fluorescence spectra of **3a** and **4a**.
(a) The 400 nm excitation of **3a** is reduced after sulfenic acid conjugation (**4a**). (b) Hypothetical model for the reduction in 400 nm excitation after conjugation. We hypothesize the free enolate electrons donate into the empty *d*-orbitals of sulfur, which can alter absorption from the dimedone portion of the molecule.

a

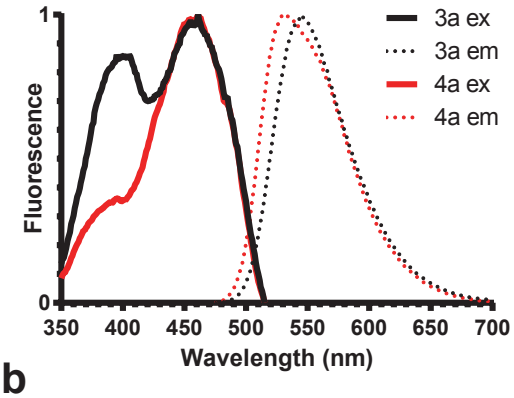

b

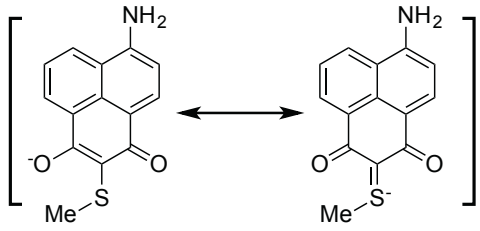

Figure A-09. F-DiNap changes its fluorescence excitation spectra below the probe pKa. Data is normalized to 1 to highlight changes in the peak excitation. Excitation spectra were collected by monitoring emission intensity at 550 nm. Emission spectra were collected by exciting at the maximum wavelength of each pH (pH 7.4: 450 nm; pH 2: 495 nm).

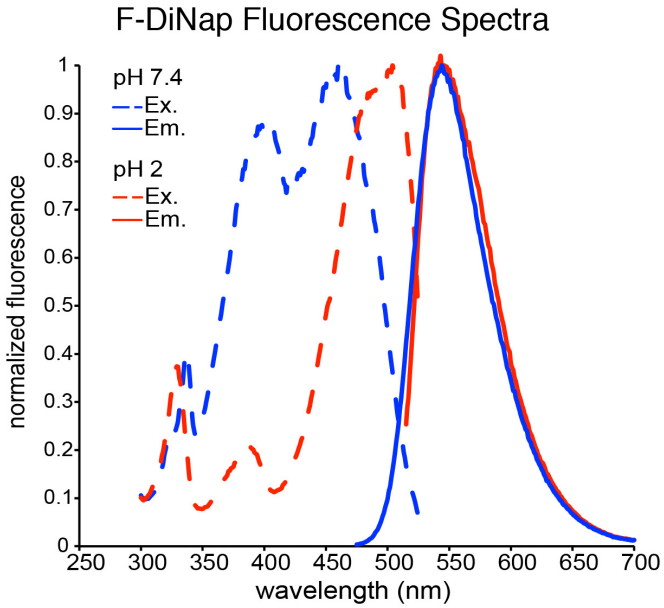

Figure A-10. DiNap probe pKa values.

Measurements were acquired from 100 μM solutions of each DiNap probe in buffered solutions at the defined pH values. The ratio of the 488 nm fluorescence excitation intensity was divided by the 405 nm excitation intensity, plotted and fit to sigmoidal curve with the half-max inflection point taken as the pK_a. .

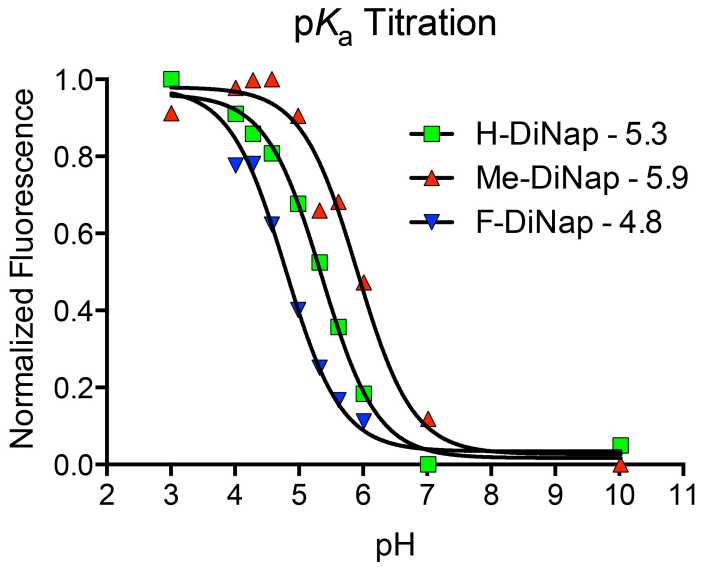

Figure A-11. Reaction rates of DiNaps in BL21 lysates.

F-DiNap shows an accelerated rate over H-DiNap with towards other unidentified proteins n bacterial cell lysates. In all cases, H-DiNap reacts on the order of minutes and hours, while F-DiNap reacts on the order of seconds to minutes. In some cases, as with the 75 kDa band, the reaction rate exceeded our ability to measure, even at 20 μM. Additional protein bands were collected, with an overall average rate constant of 0.11 M^{-1} s^{-1} for H-DiNap, while F-DiNap had an average rate constant of 380 M^{-1} s^{-1}.

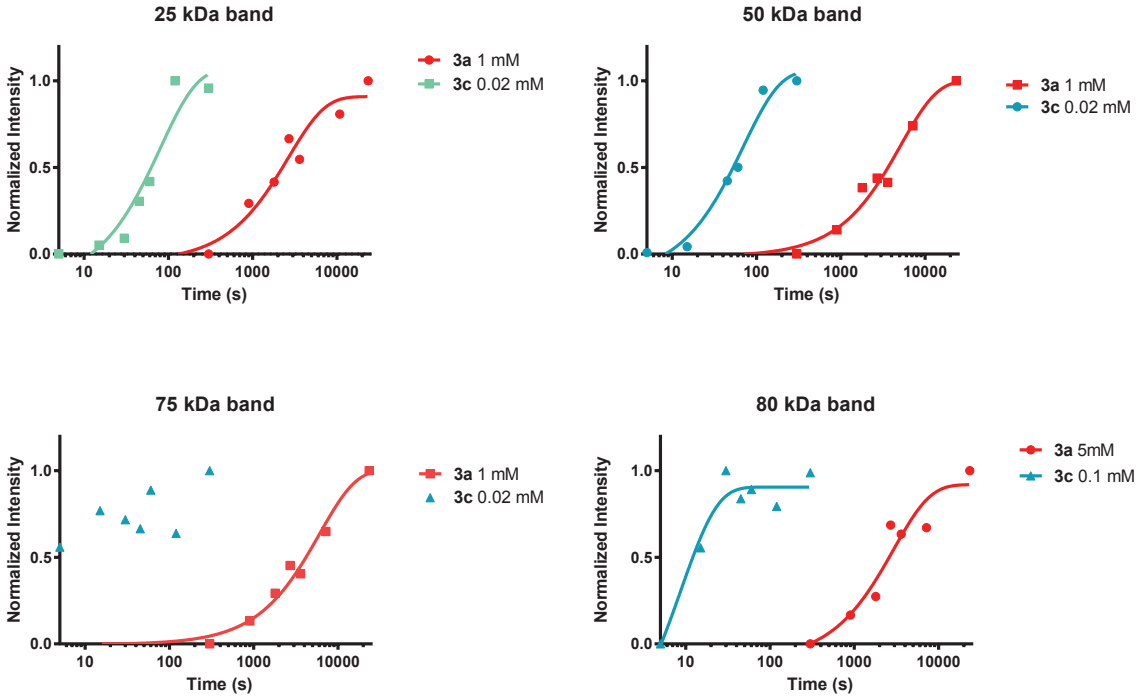

Figure A-12. Chemical simulation of a sulfenic acid and F-DiNap.

In silico calculations were performed to model the reaction of methyl sulfenic acid with DiNap probes to determine the basis for the observed rate enhancement. This analysis revealed the positioning of water molecules is critical to protonate the sulfenic acid hydroxyl prior to substitution. Direct substitution of the sulfenic acid hydroxyl without protonation was prohibitive (ΔG of +60 kCal/mol). In the presence of proximal waters, the simulation reported a $\Delta\Delta G^{\ddagger}_{3a\text{-}3c}$ of 10.1 kCal/mol, yielding a theoretical $2x10^7$ rate increase, yet this acceleration was not caused by hydrogen bonding between the sulfenic acid and fluorine. Instead, the most obvious difference between H-DiNap and F-DiNap was the observation that the F-DiNap fluorine bends out of plane and distorts from sp^2 geometry, yielded simulated dihedral angles at the α-carbon of 119.9˚ for H-DiNap, and 116.7˚ for F-DiNap. We hypothesize that the high electron density of fluorine adjacent to the electron-rich dimedone enolate leads to an electrostatic repulsion effect in which the 2p-π C-F overlap is partially destabilized. The C-F bond is also much longer than is typical for an sp^2 or aromatic carbon (1.36-1.38 vs 1.404 Å for F-DiNap). Fluorine carbanions situated between one or two strongly electron-withdrawing groups may adopt structures more closely resembling sp^3 tetrahedra[226], leading us to hypothesize that the α-carbon becomes a mixed sp^2-sp^3 center in which the sp^3 character destabilizes the carbanion and increases its reactivity. However, analysis of the natural bond orbitals shows that there is virtually no sp^3 character on the α-carbon (**Table S3**). Instead, the C-F p_x strongly *decreases* the occupancy of the α-carbon, while the p_z mildly back-donates. The net effect is that the p_z on the α-carbon decreases by 0.6 eV (13.8 kCal/mol). We speculate that this decrease in energy allows the purely sp^2-

hybridized center to more readily rehybridize to sp^3 upon proximity to an appropriate nucleophile (**Figure S8c**). Therefore, the pseudo-tetrahedral center is primed for attack and transition to full nucleophile. Furthermore, F-DiNap has a driving force of 5.4 kCal/mol larger than H-DiNap, which according to the Bell-Evans-Polanyi principle also brings down its $\Delta G^{\ddagger}$. As our model only accounted for an aqueous environment, each protein's local microenvironment may lead to suboptimal conditions to take full advantage of the higher reactivity of the fluorous probe. Nevertheless, rate enhancements of up to 20,000x are observed.

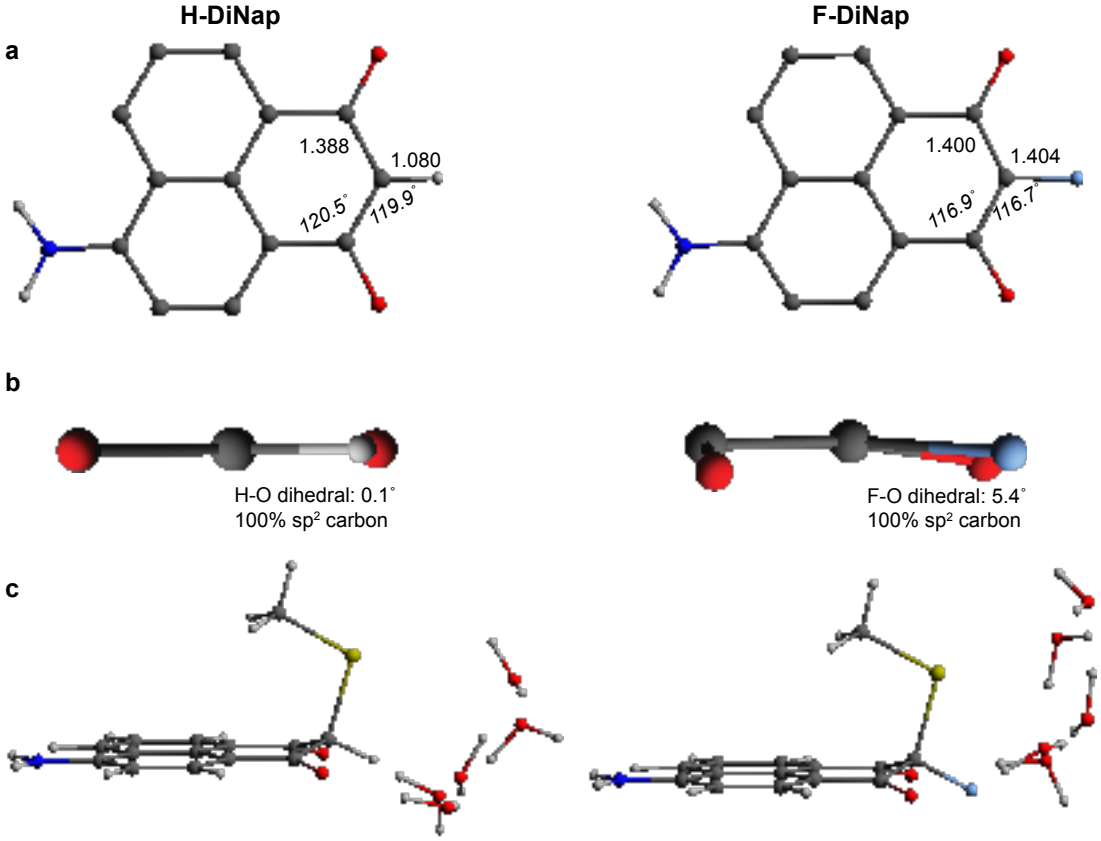

Figure A-13. Dimedone reacts with pyridoxal.

Dimedone (5 mM final) or F-DiNap (5 mM final) and pyridoxal (15 mM final) were added in PBS, incubated for 30 minutes, and subsequently analyzed by HPLC using a photodiode array detector. The same solution was analyzed on LC-HRMS to confirm the presence of the single and double adduct.

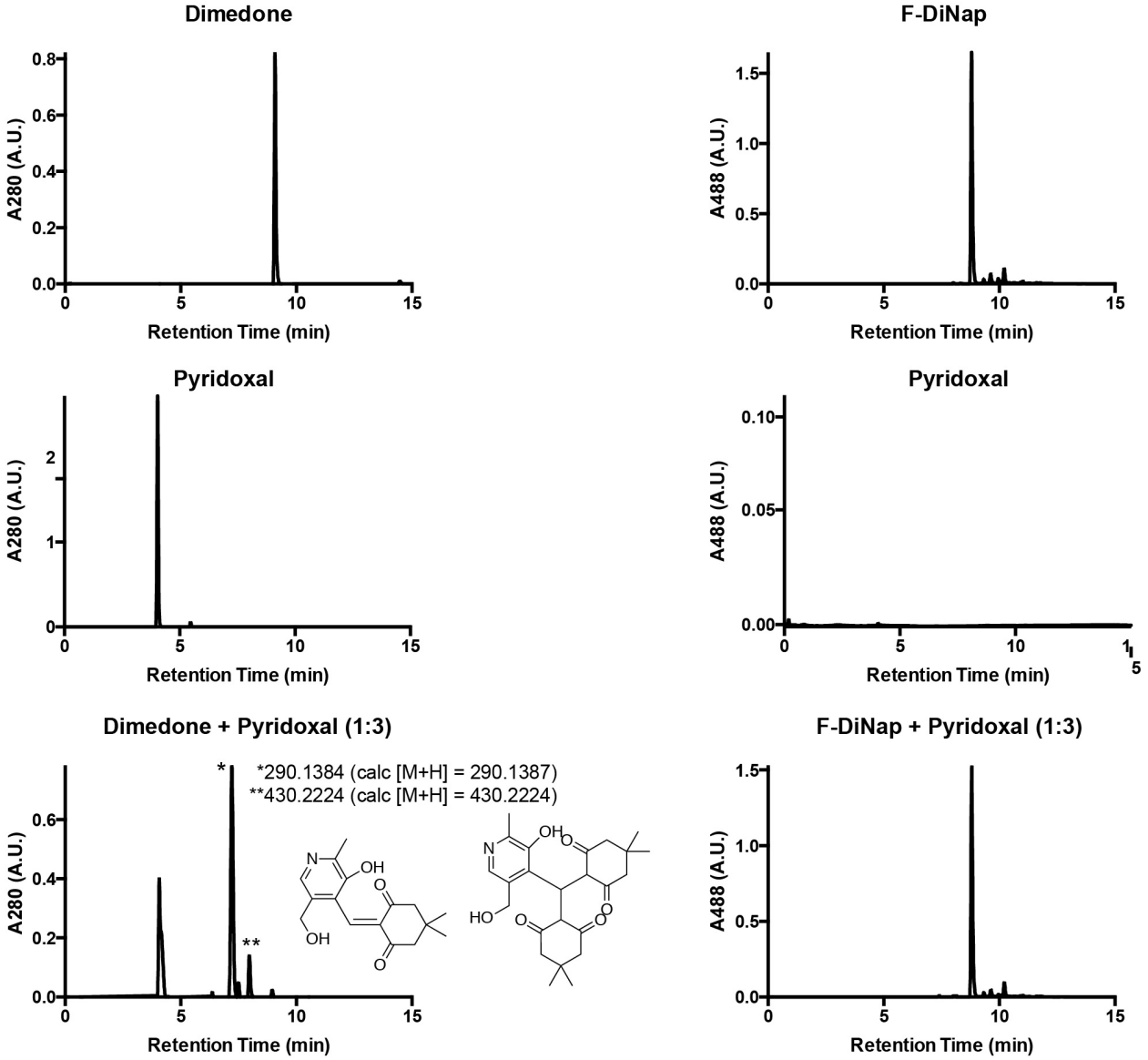

Figure A-14. Dimedone reacts with glyceraldehyde.

Dimedone (5 mM final) or F-DiNap (5 mM final) and glyceraldehyde (15 mM final) were added in PBS, incubated for 30 minutes, and subsequently by HPLC using a photodiode array detector. The same solution was analyzed on LC-HRMS to confirm the presence of the single adduct.

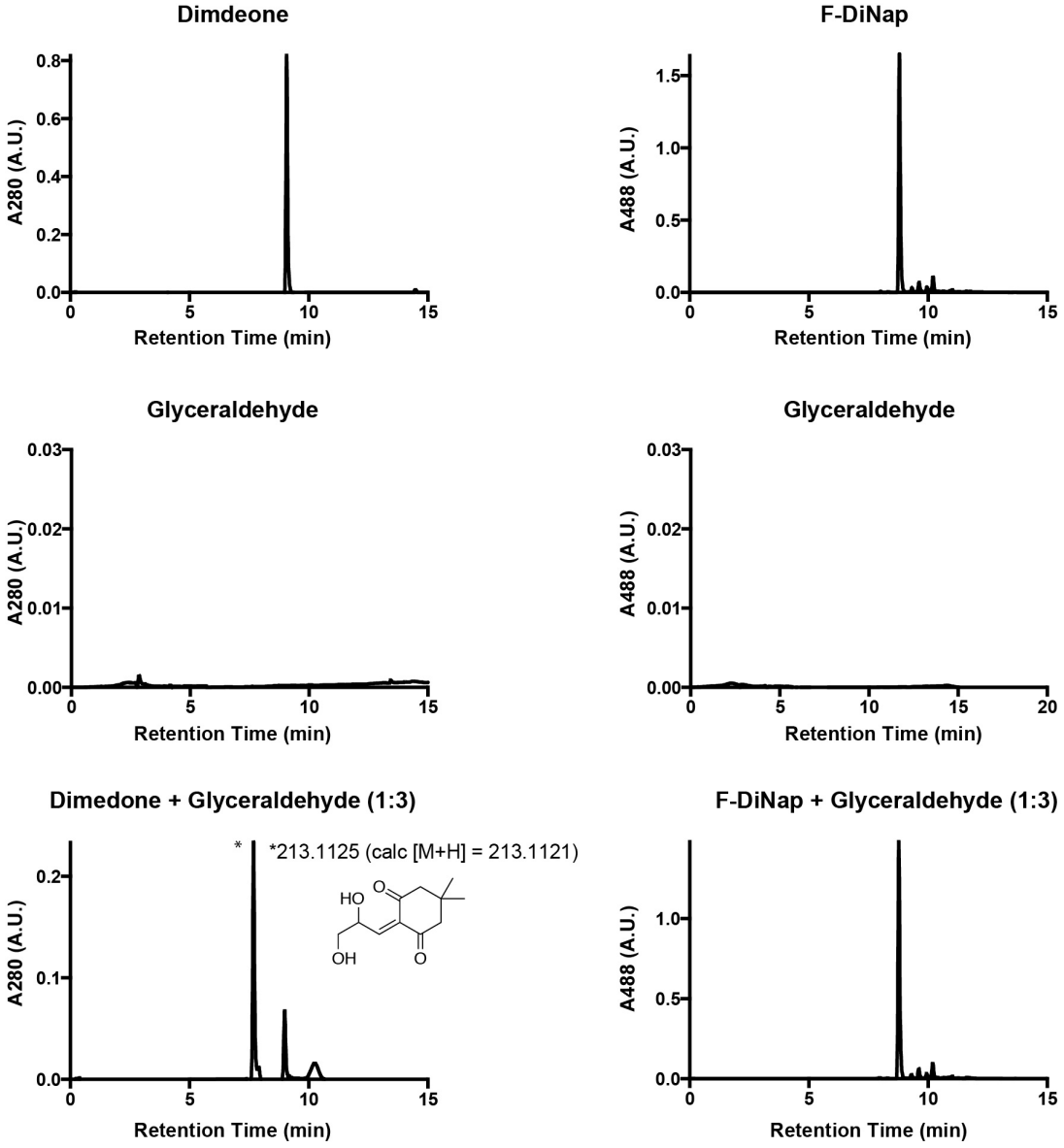

Figure A-15. Rates of dimedone condensation with glyceraldehyde.

0.5 mM dimedone (final concentration) was added to a HPLC vial. To this was added a solution of glyceraldehyde at varied concentrations. An initial t = 0 was run, and then subsequent time points at 15 minute intervals. The area under the dimedone curve at 254 nm was recorded. These data were globally fit, yielding a rate constant of 0.059 ± 0.0036 M^{-1} s^{-1}.

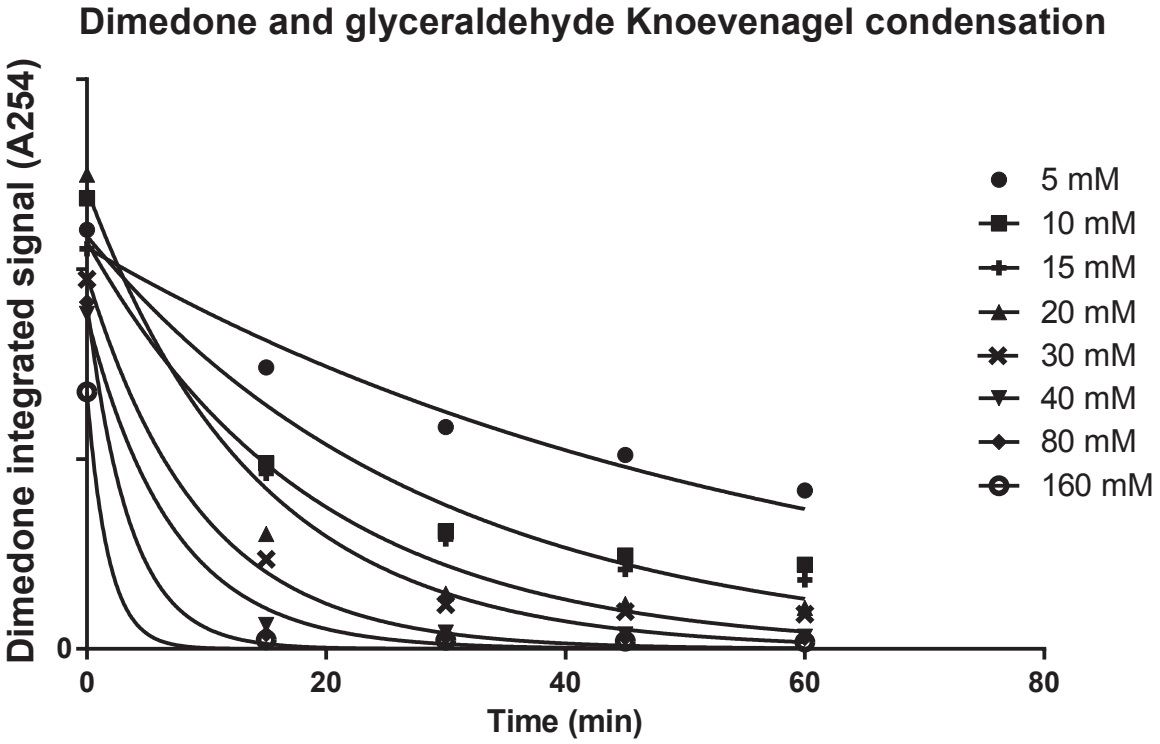

Figure A-16. Dimedone reacts with ene-als.

Dimedone (5 mM final) or F-DiNap (5 mM final) and acrolein or acrolein + N-acetyl cysteine (5 mM final each) were added in PBS, incubated for 30 minutes, and analyzed using by HPLC using a photodiode array detector.

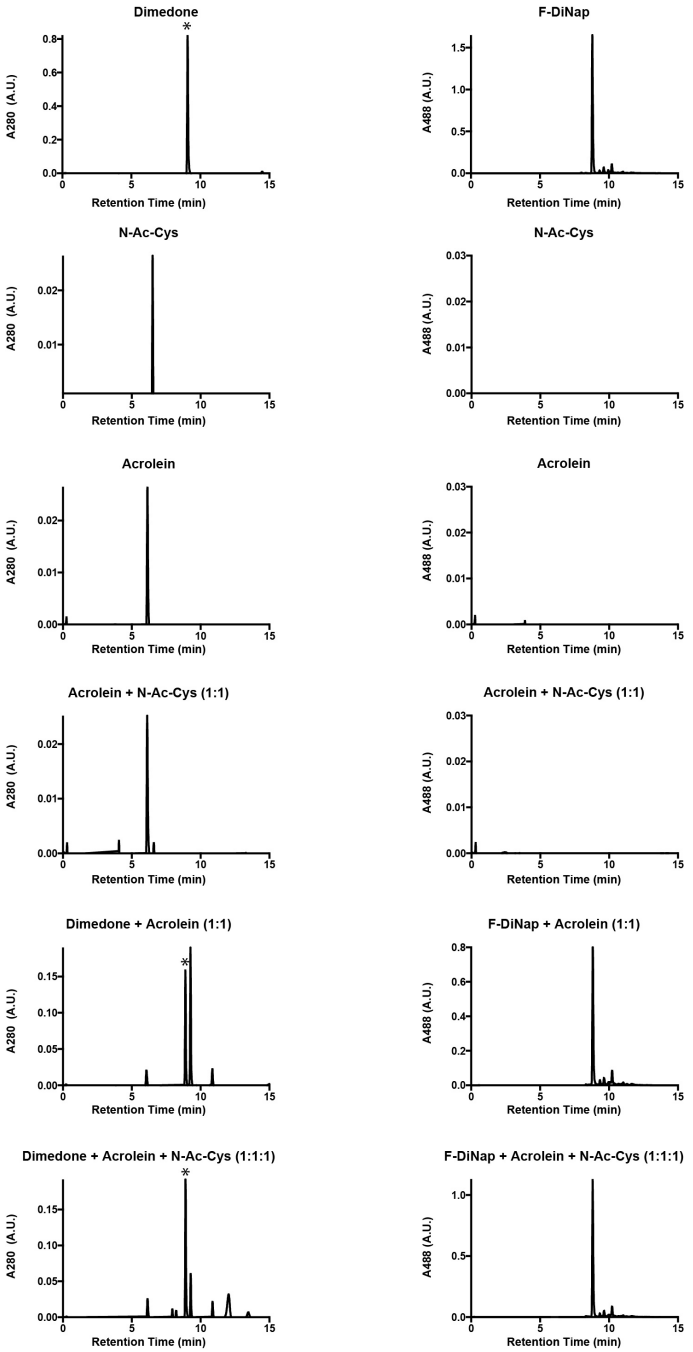

Figure A-17. Hexenal and acrolein form stable protein conjugates with H-DiNap

A 5 mM solution of the each of the probes below was added to BL21 cell lysates overexpressing AhpC (C166S) for 1 hr at 37˚C followed by 5 mM **3a** or **3c**. No aldehydes on their own contributed to additional labeling, however, hexenal and acrolein (but not cinnamaldehyde) lead to a large increase in labeling for H-DiNap but not F-DiNap, indicating some mechanism of the α,β-unsaturated aldehydes.

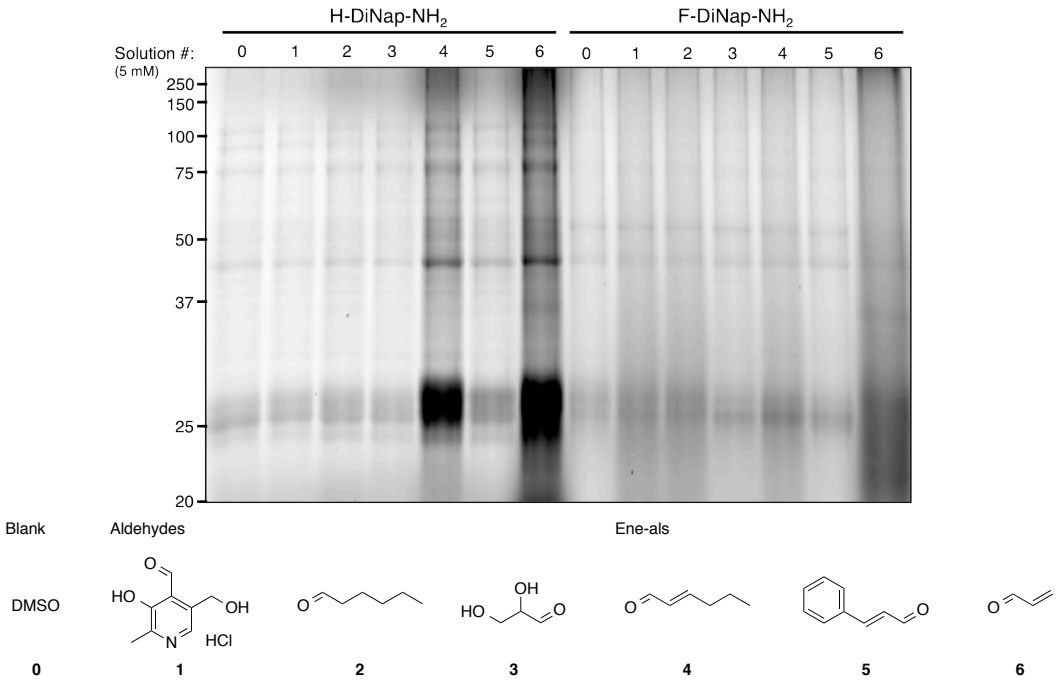

Figure A-18. F-DiNap profiling of S-sulfenylation in different cell lines.

Cells were labeled with F-DiNap (5 mM) for 1 hour at 37 ˚C, washed with PBS, collected by scraping form the dish, and lyzed by sonication. After normalizing for protein concentration, lysates were separated by SDS-PAGE and transferred to PVDF membrane for GAPDH western blotting (Cy5) and F-DiNap (Ex: 488 nm, Em: 555/20 nm) fluorescence imaging.

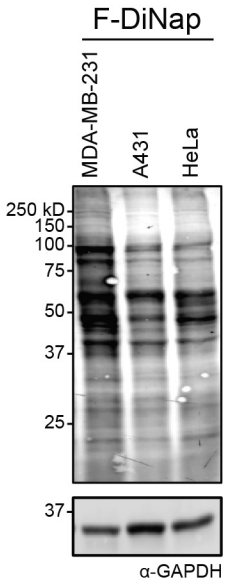

Figure A-19. Time-dependent ratiometric labeling of CH-27 B-cells.

Adherent cells were labeled with H-DiNap or F-DiNap (1 mM) and ratiometric images (image collected with 488 nm excitation / image collected with 405 nm excitation) were measured at 2-minute increments at room temperature in Tyrodes buffer. Image size is 81 μm x 81 μm. Below is a histogram of the ratio increase by pixel.

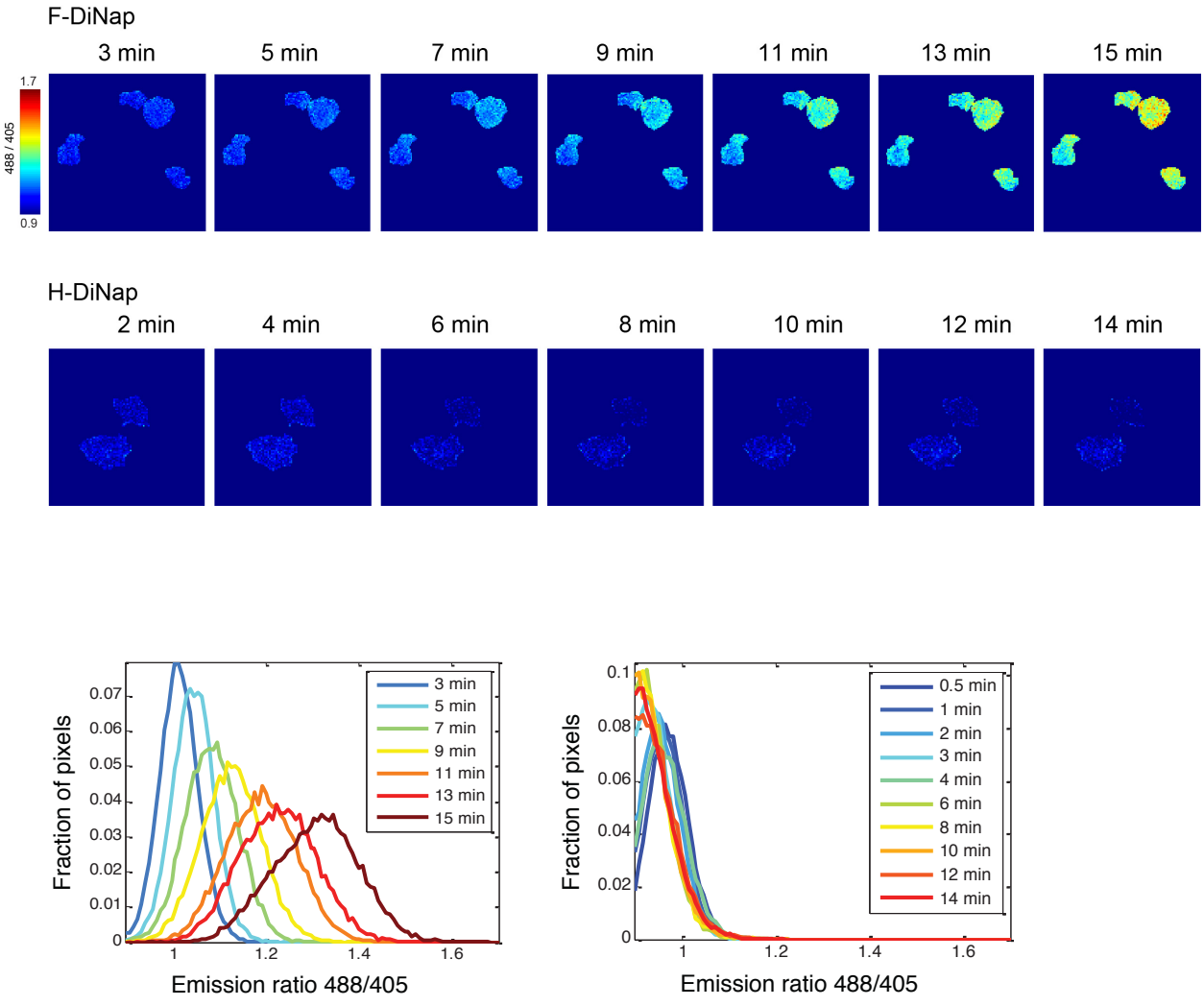

Figure A-20. Hydrogen peroxide rapidly increases F-DiNap ratios.

CH27 B-cells were treated with F-DiNap (1 mM) for 15 minutes prior before stimulation and imaged by TIRF microscopy. To stimulate redox stress, hydrogen peroxide (1 mM final) was added. An immediate increase is observed in the 488 nm / 405 nm excitation ratio. Scale bar = 20 μm.

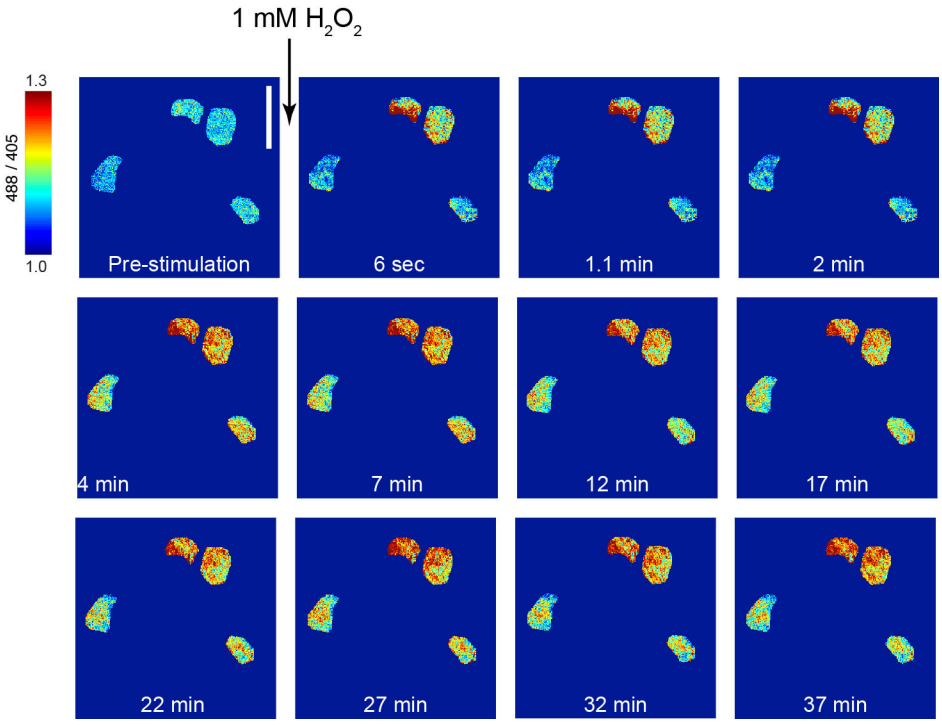

Figure A-21. F-DiNap selectivity panel.

F-DiNap is highly selective against every reactant tested, which includes oxidants, reductants, and electrophile classes that are either biological relevant or used in biochemical manners. F-DiNap was tested at 1 mM and each additive was added at 5 mM, incubated for an hour at 25 ˚C. The solvent gradient was with MeCN (B) and H_2O (A), each with 0.1% formic acid. that was run is 0-2 min 5% B, run to 95% B at 12 min, then hold at 95% B until 15 min.

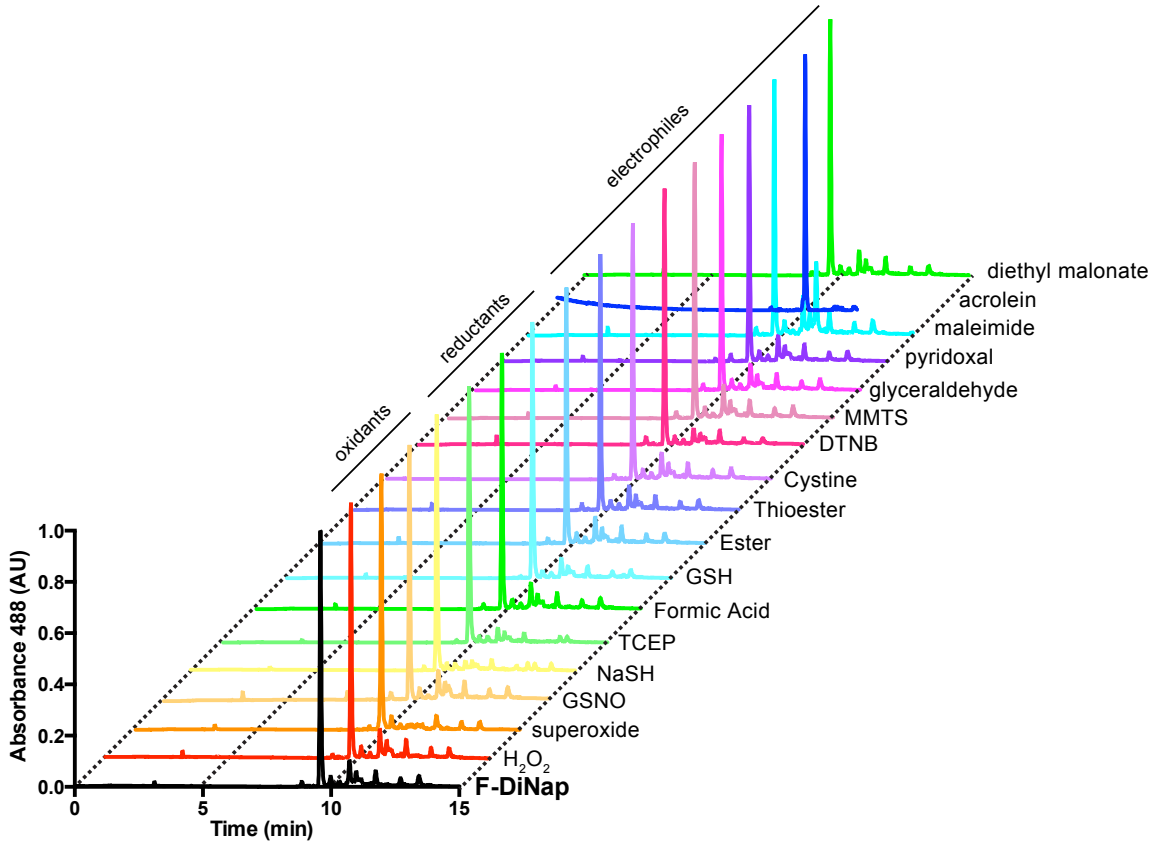

A.5. NMR spectra

^{1}H NMR: DiNapBr (**2a**)

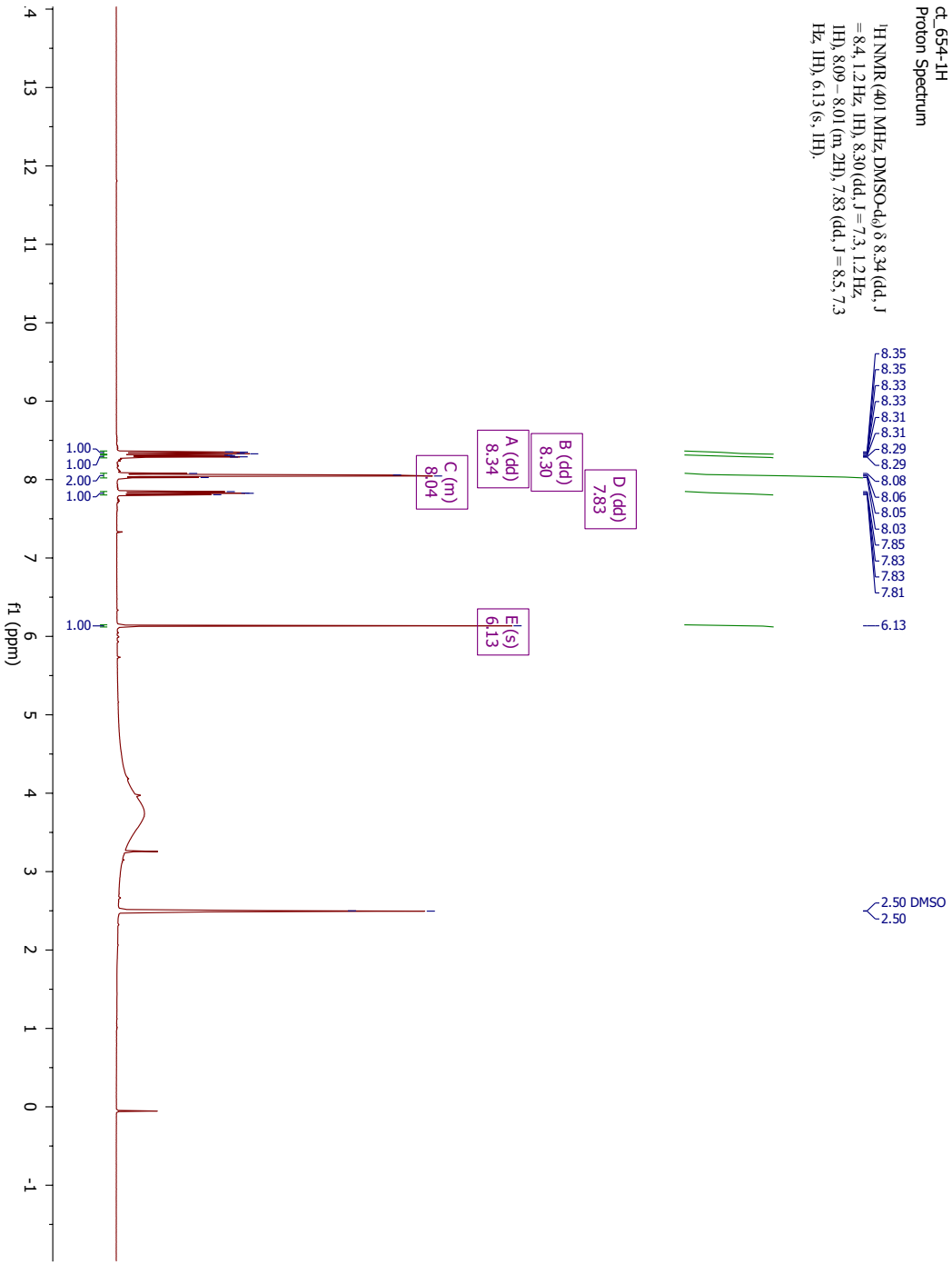

^{13}C NMR: DiNapBr (**2a**)

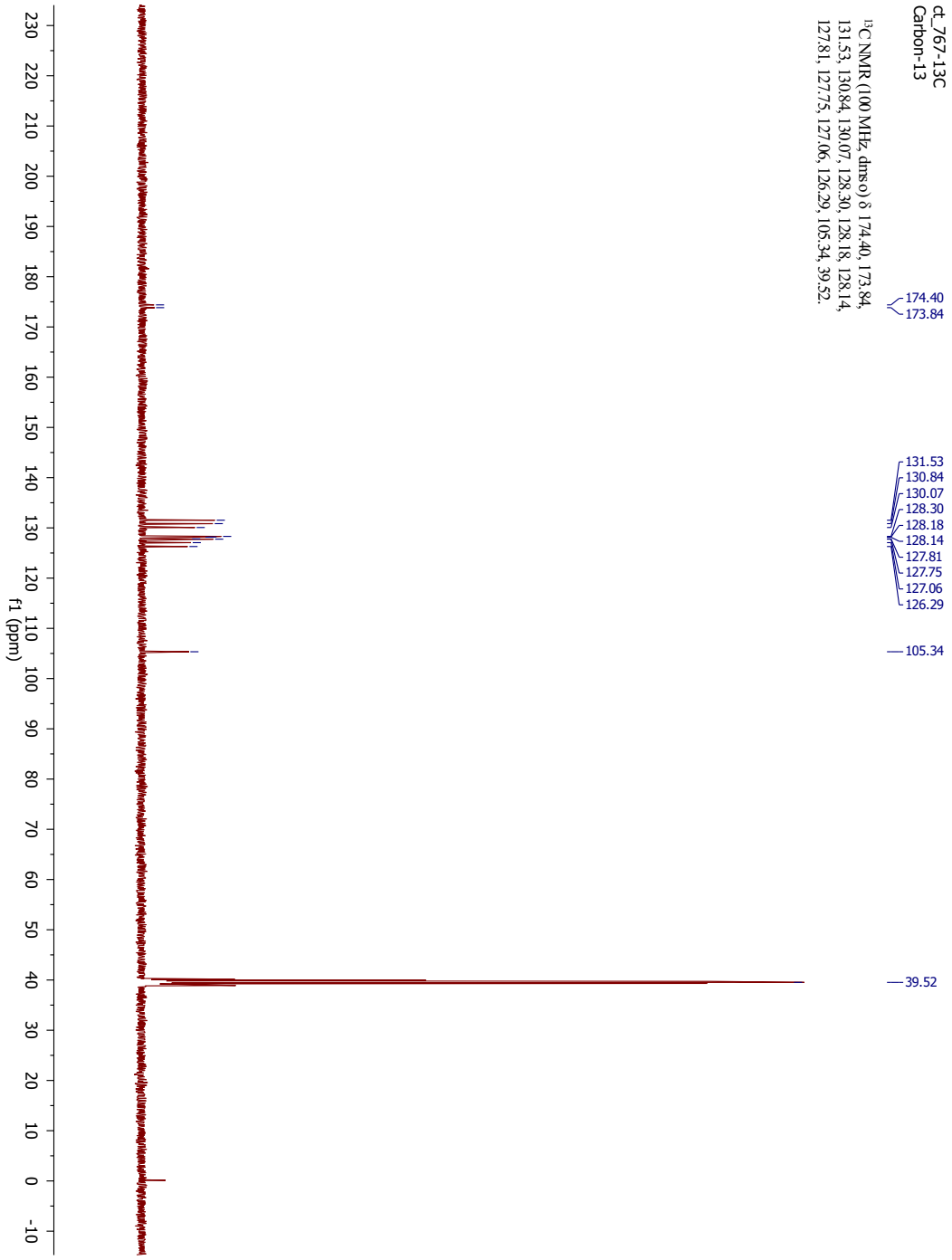

^{1}H NMR: Me-DiNapBr (**2b**)

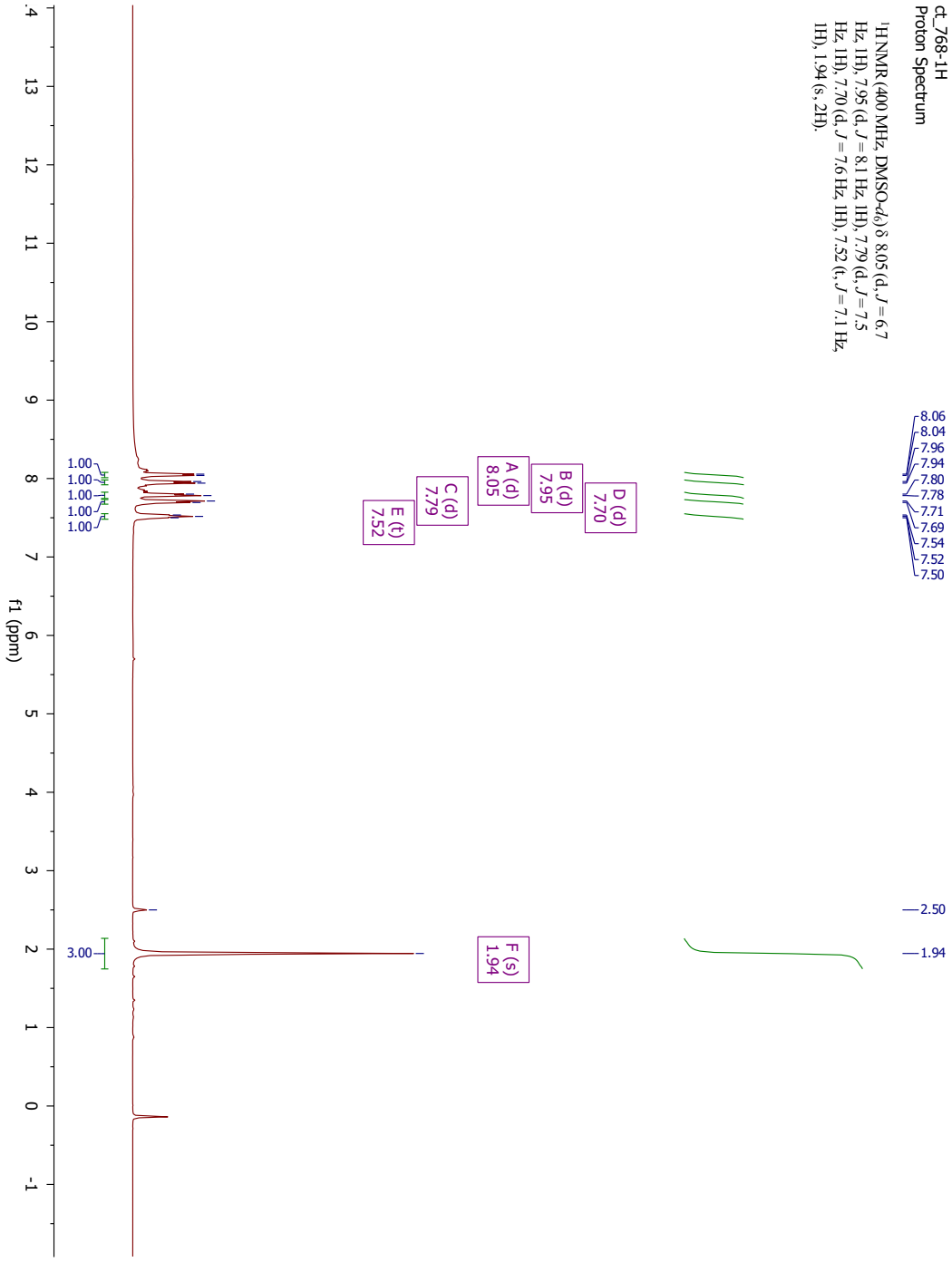

^{13}C NMR: Me-DiNapBr (**2b**)

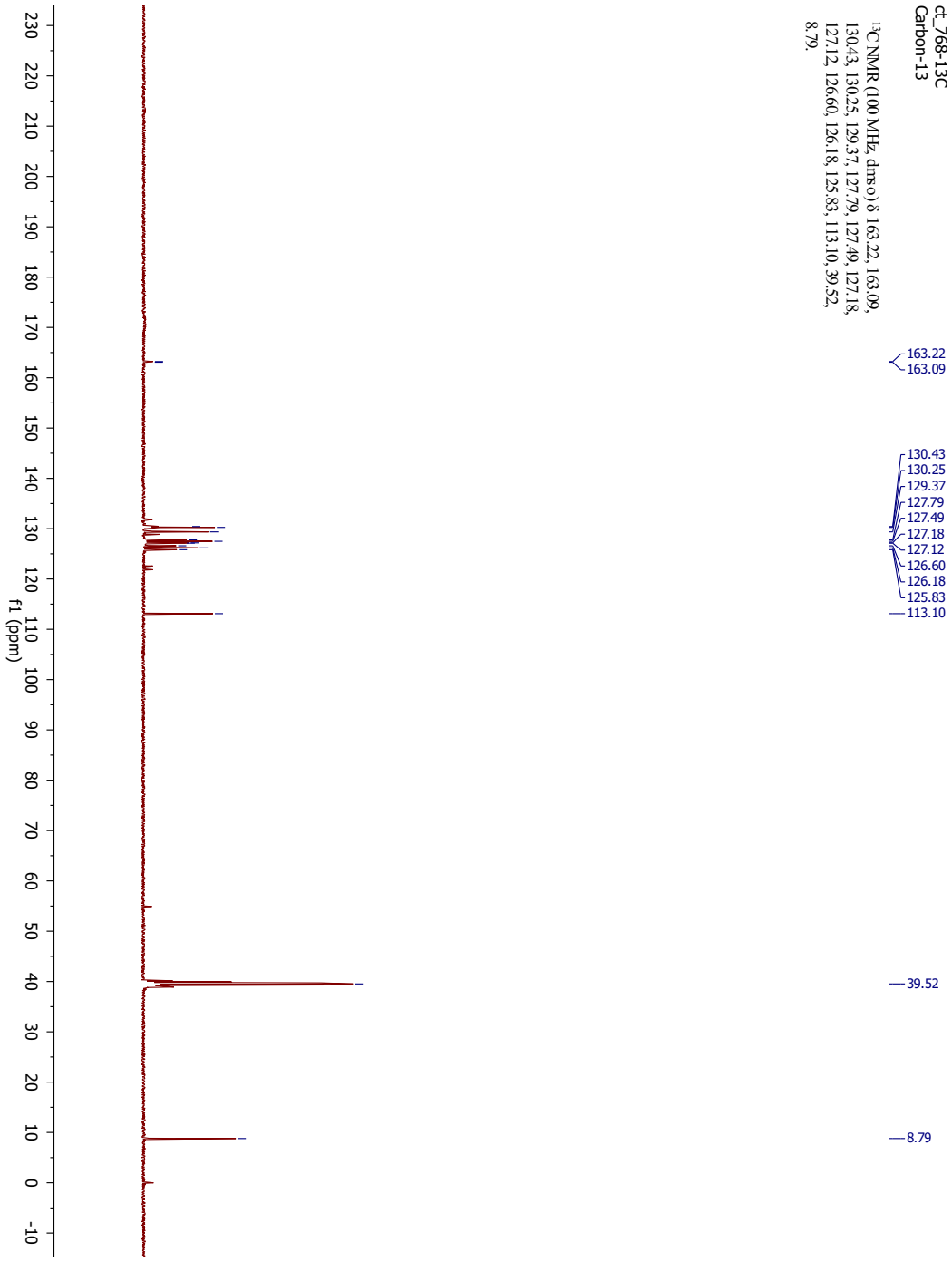

^{1}H NMR: F-DiNapBr (**2c**)

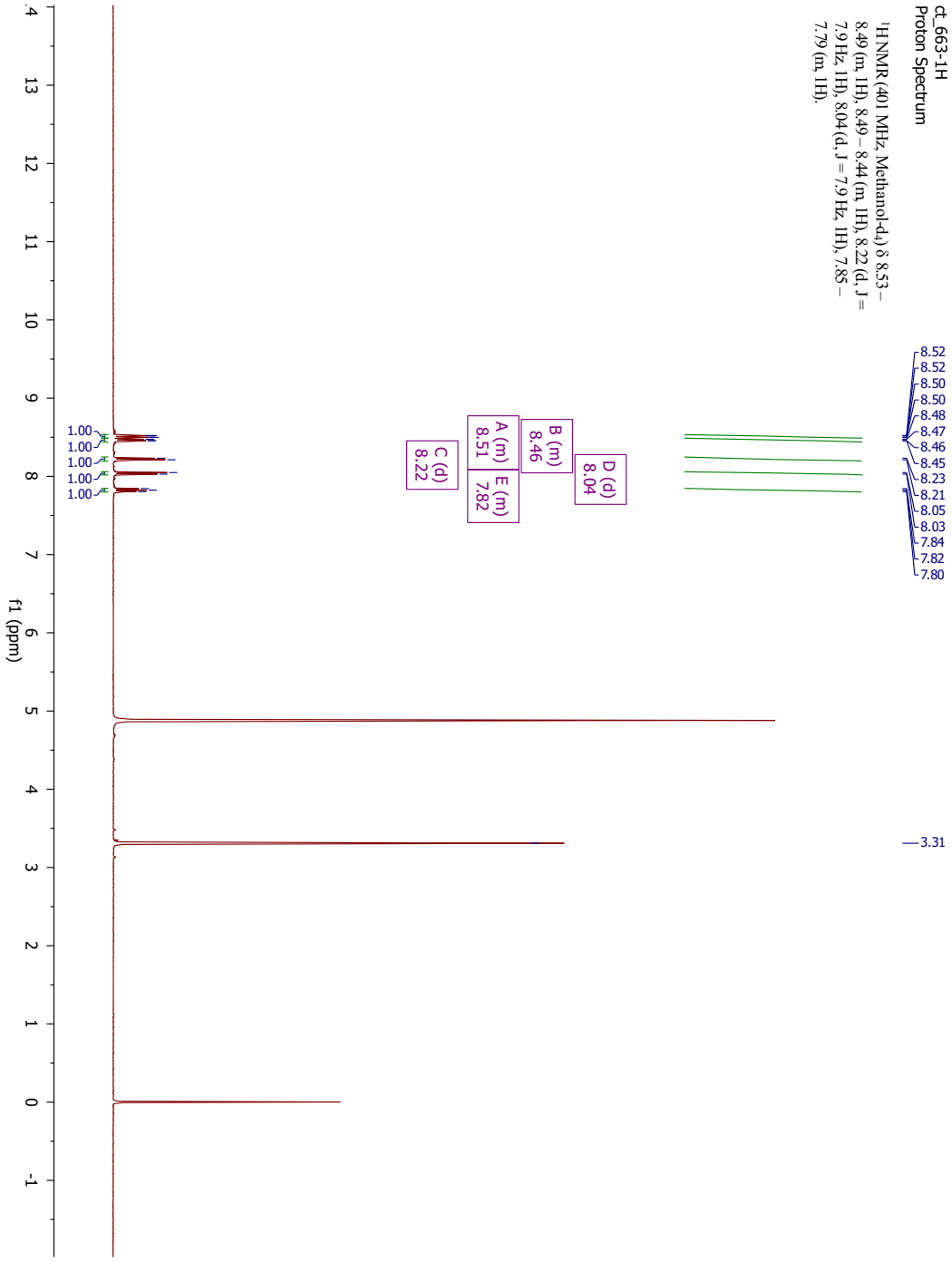

^{13}C NMR: F-DiNapBr (**2c**)

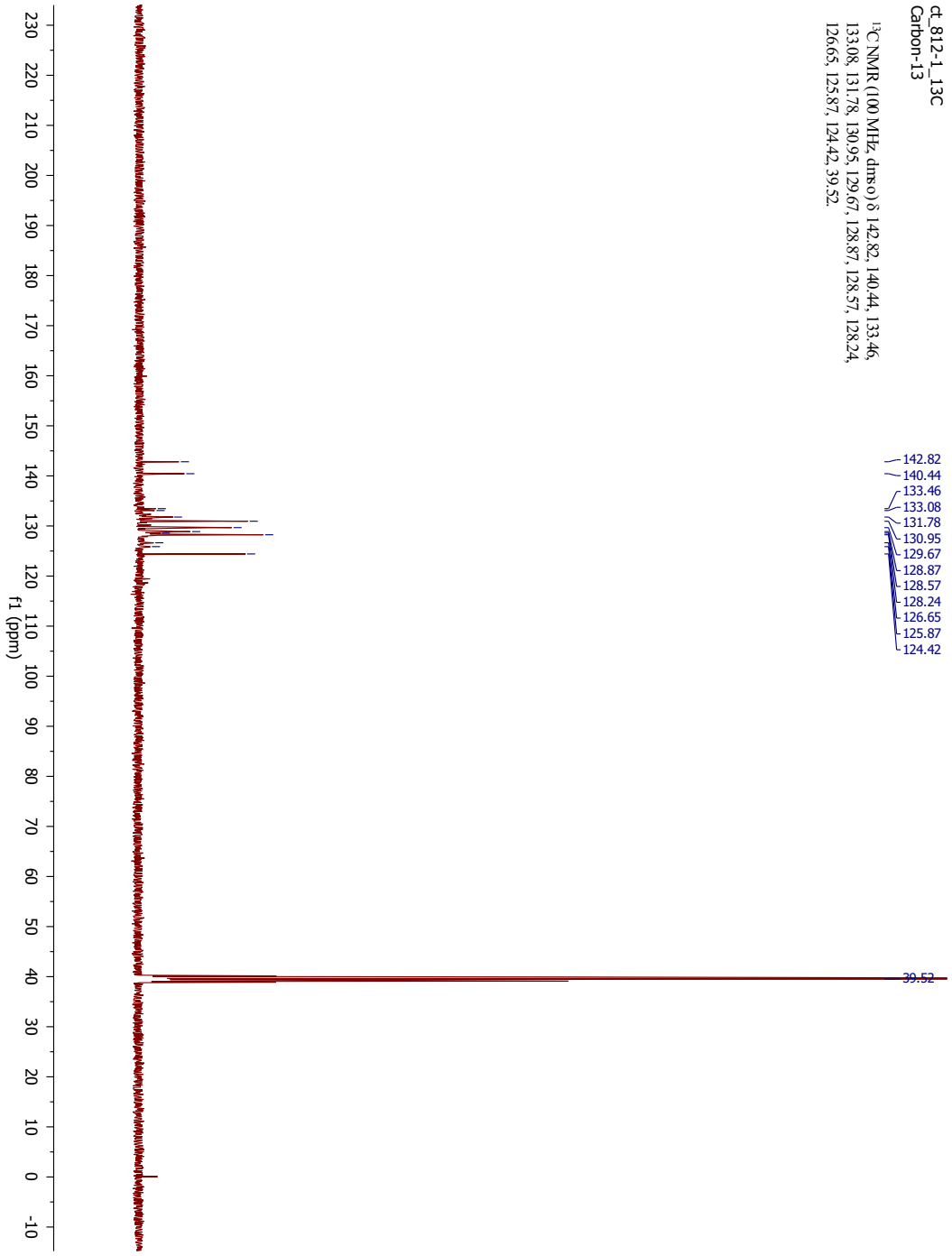

^{19}F NMR: F-DiNapBr (**2c**)

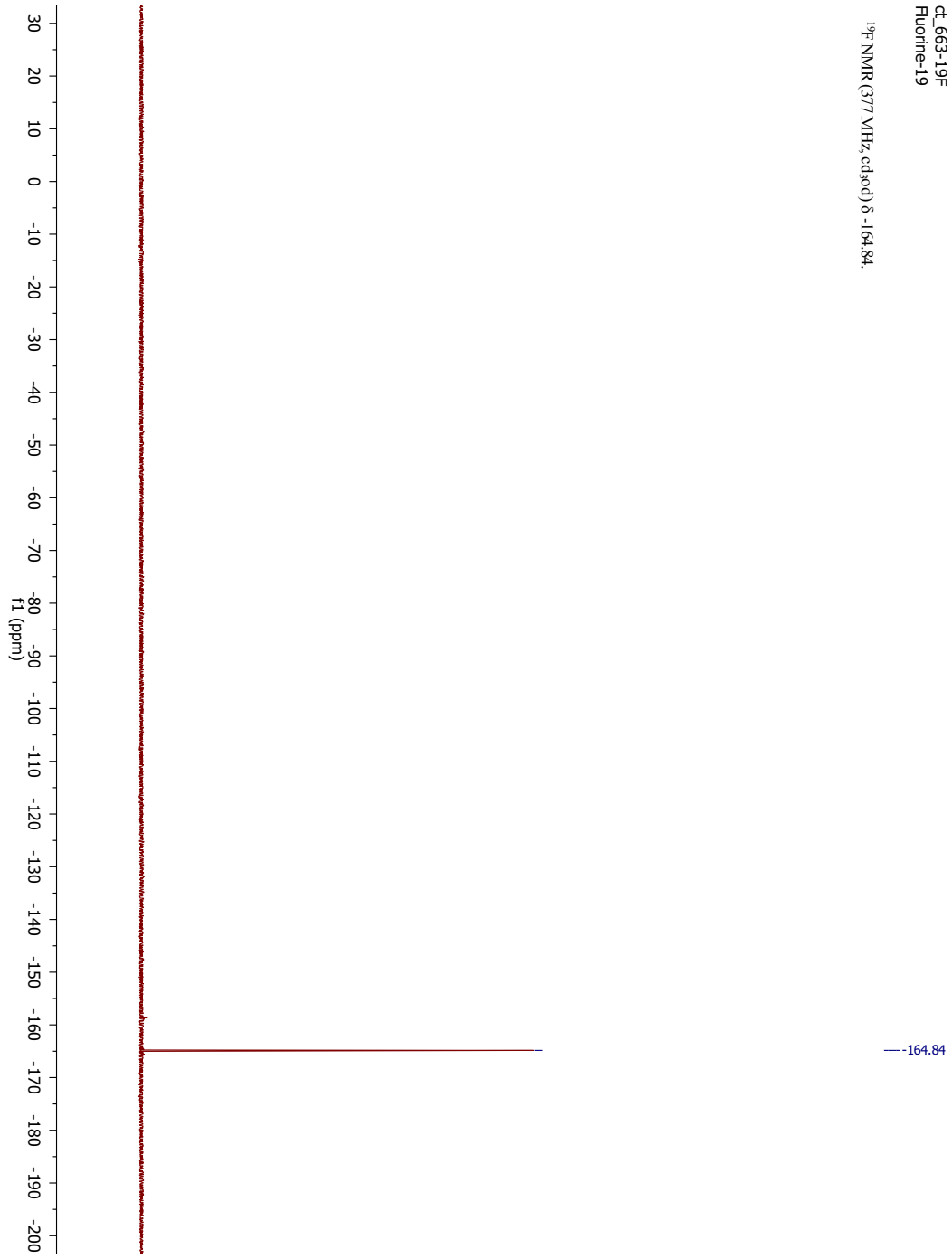

^{1}H NMR: H-DiNap (**3a**)

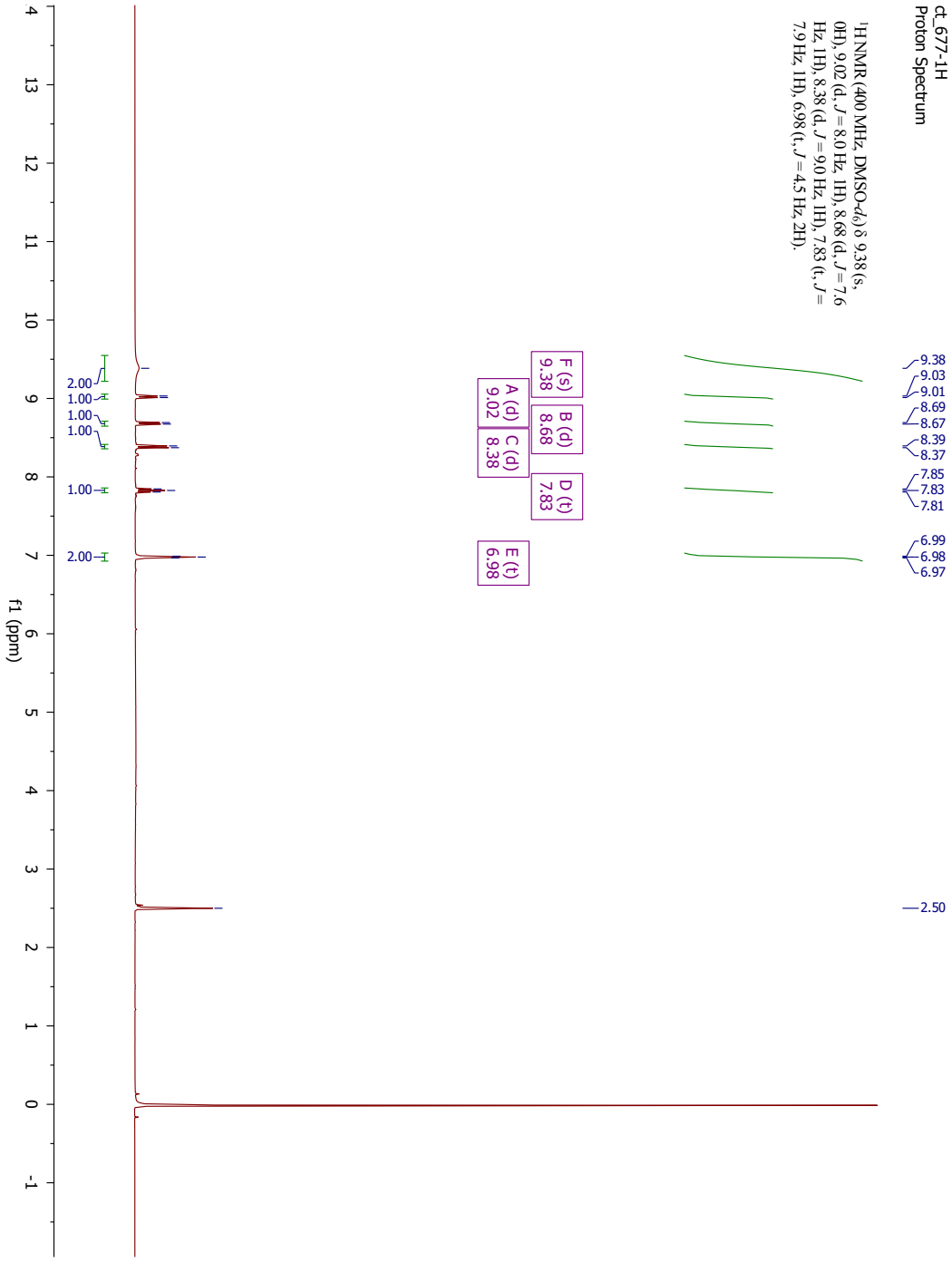

^{13}C NMR: H-DiNap (**3a**)

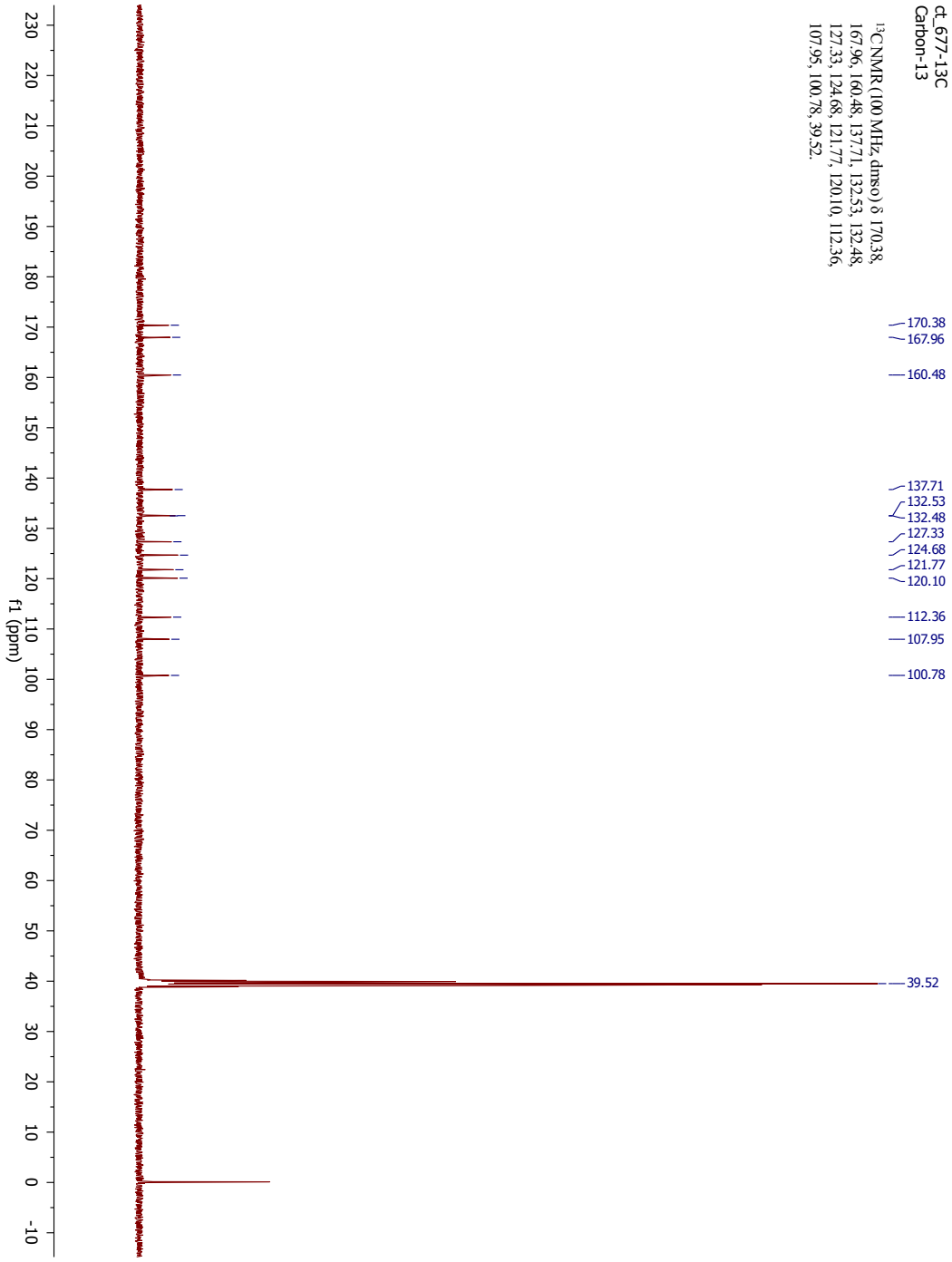

^{1}H NMR: Me-DiNap (**3b**)

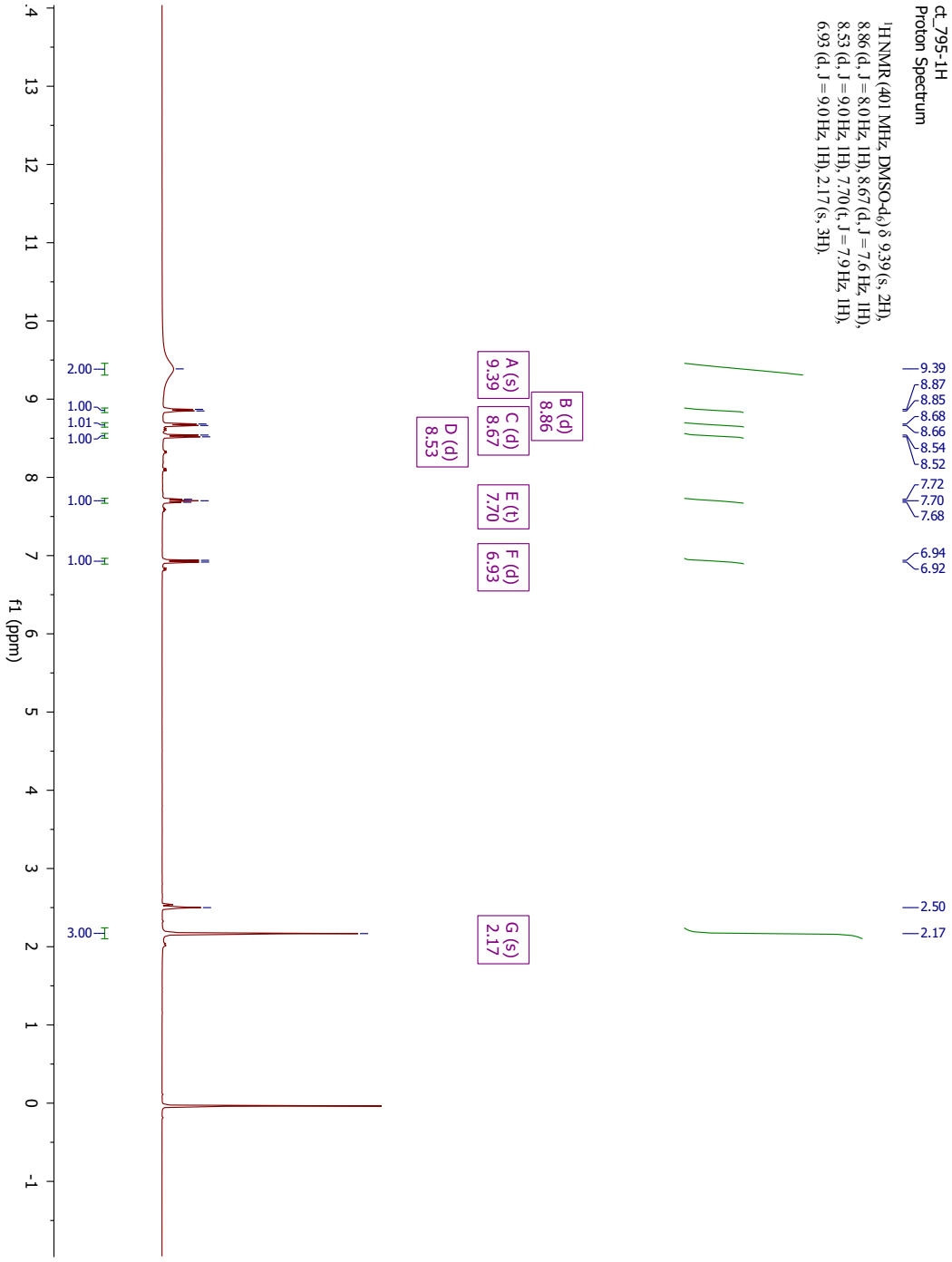

^{13}C NMR: Me-DiNap (**3b**)

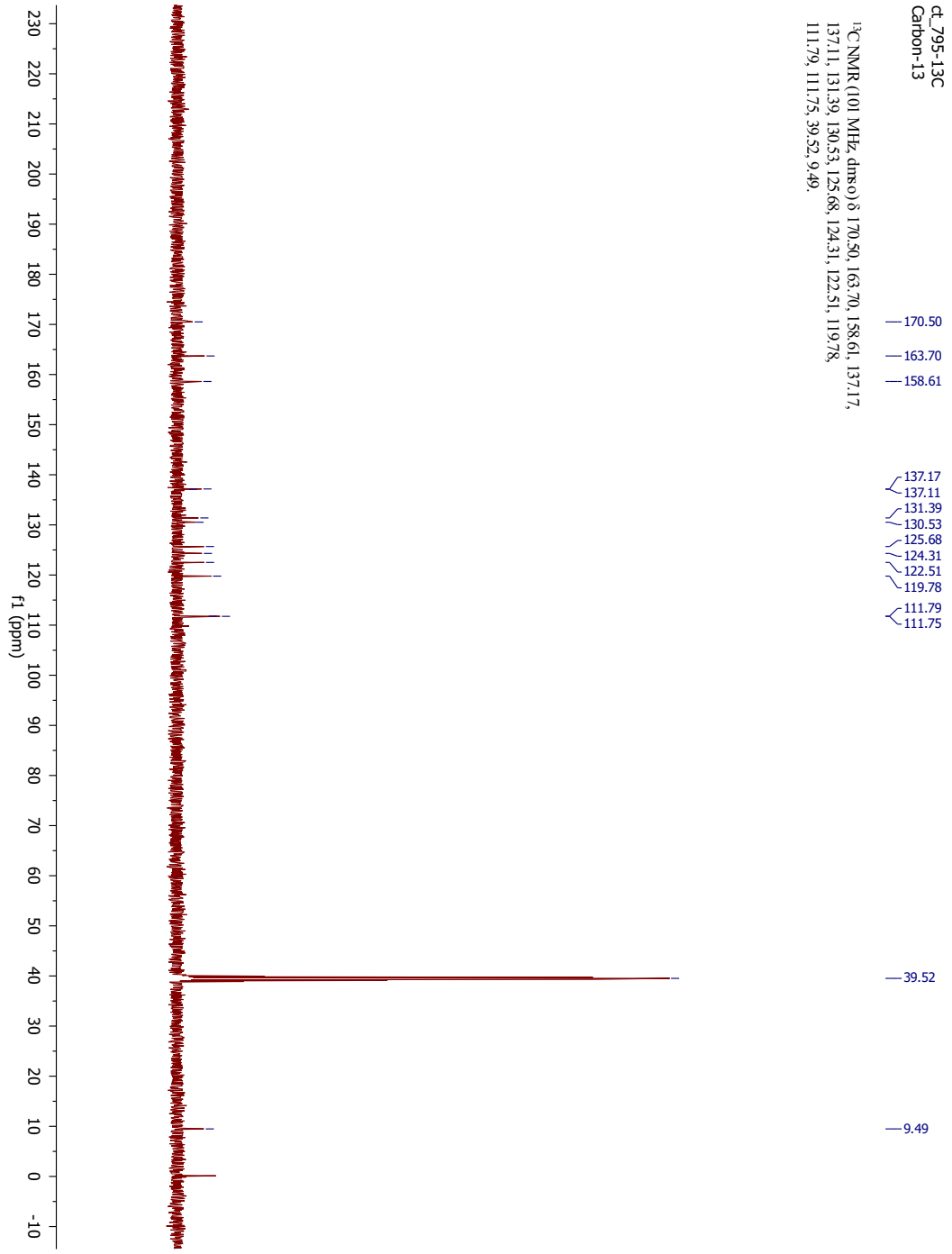

^{1}H NMR: F-DiNap (**3c**)

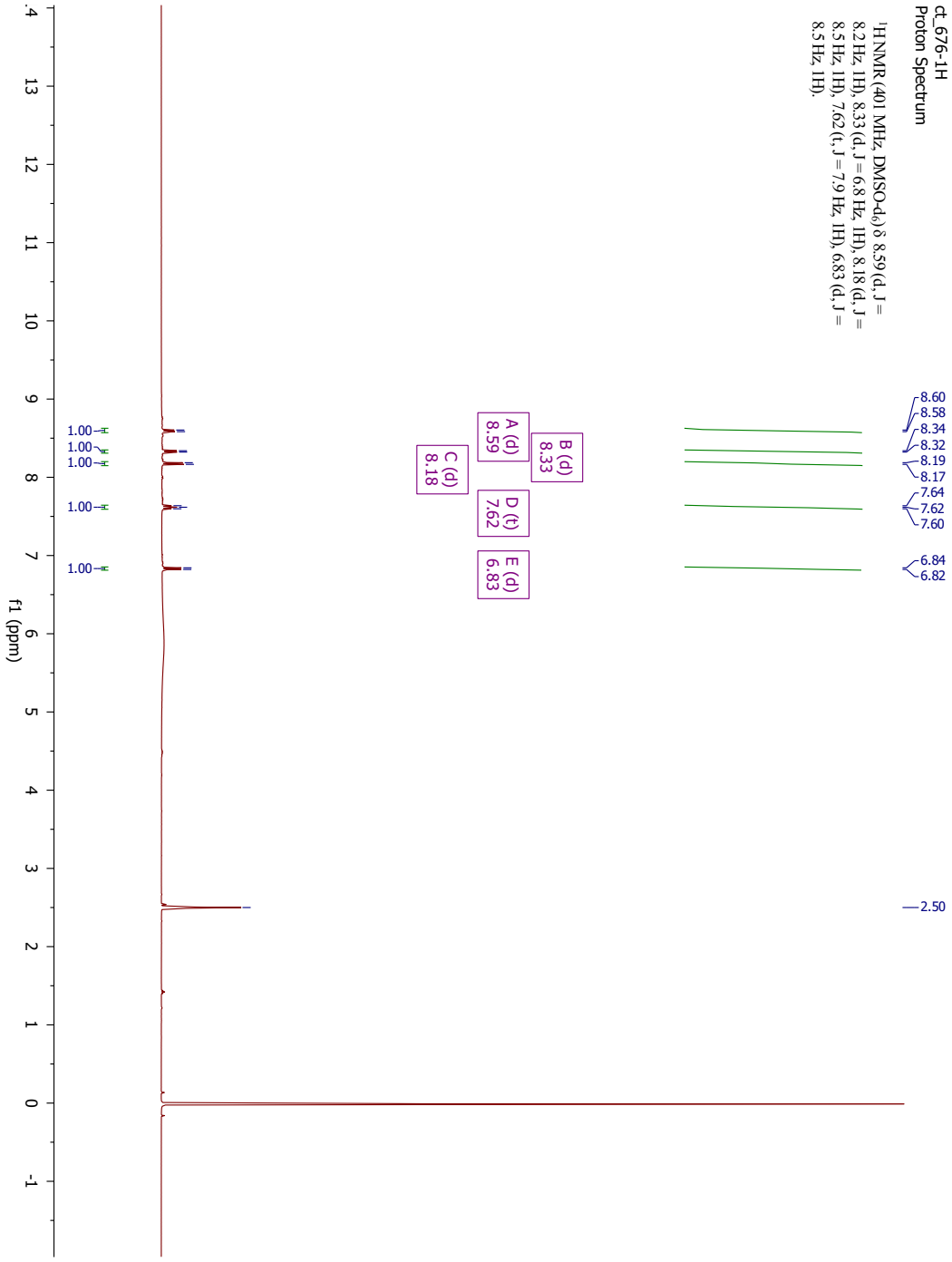

^{13}C NMR: F-DiNap (**3c**)

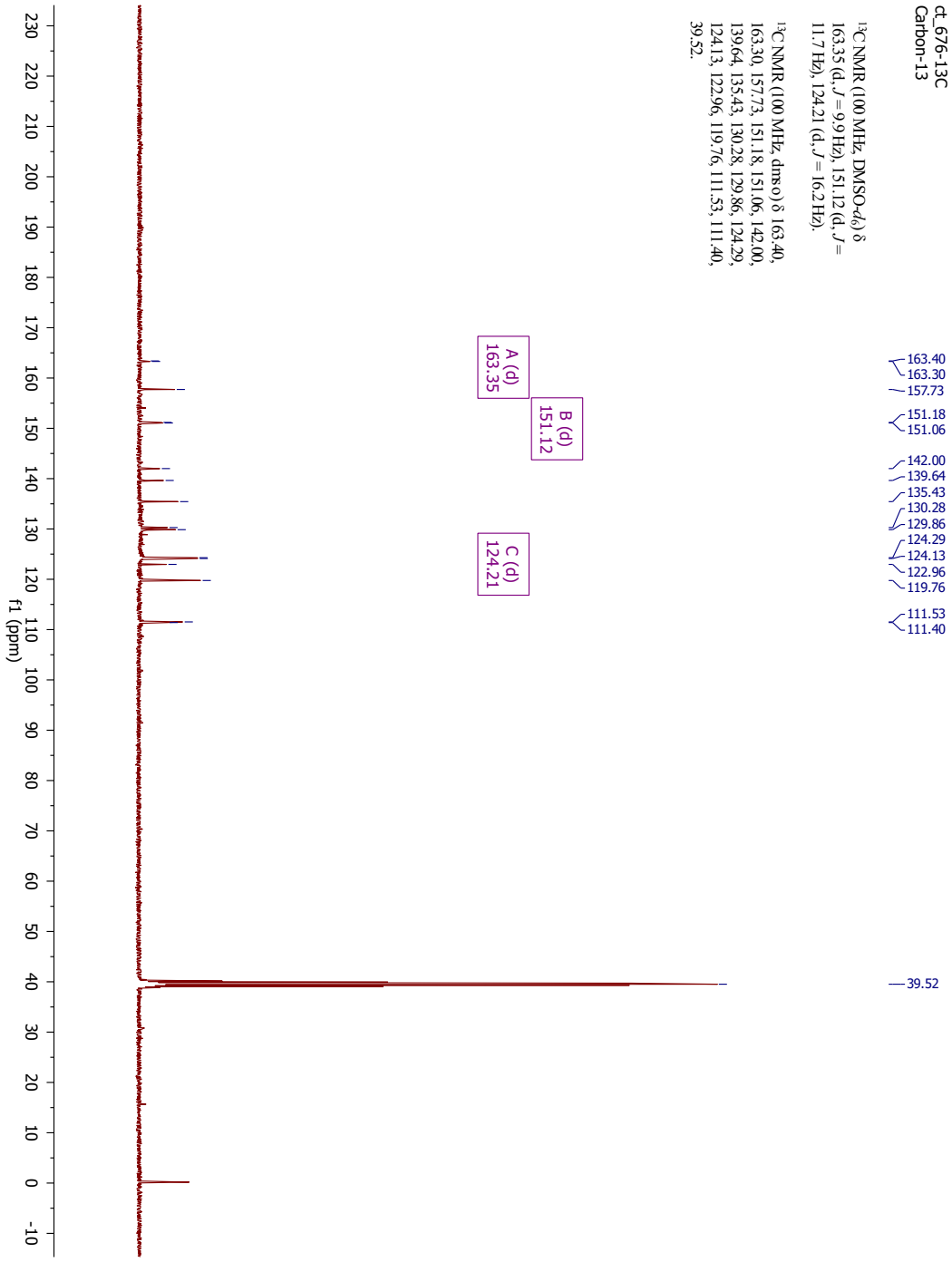

^{19}F NMR: F-DiNap (3c)

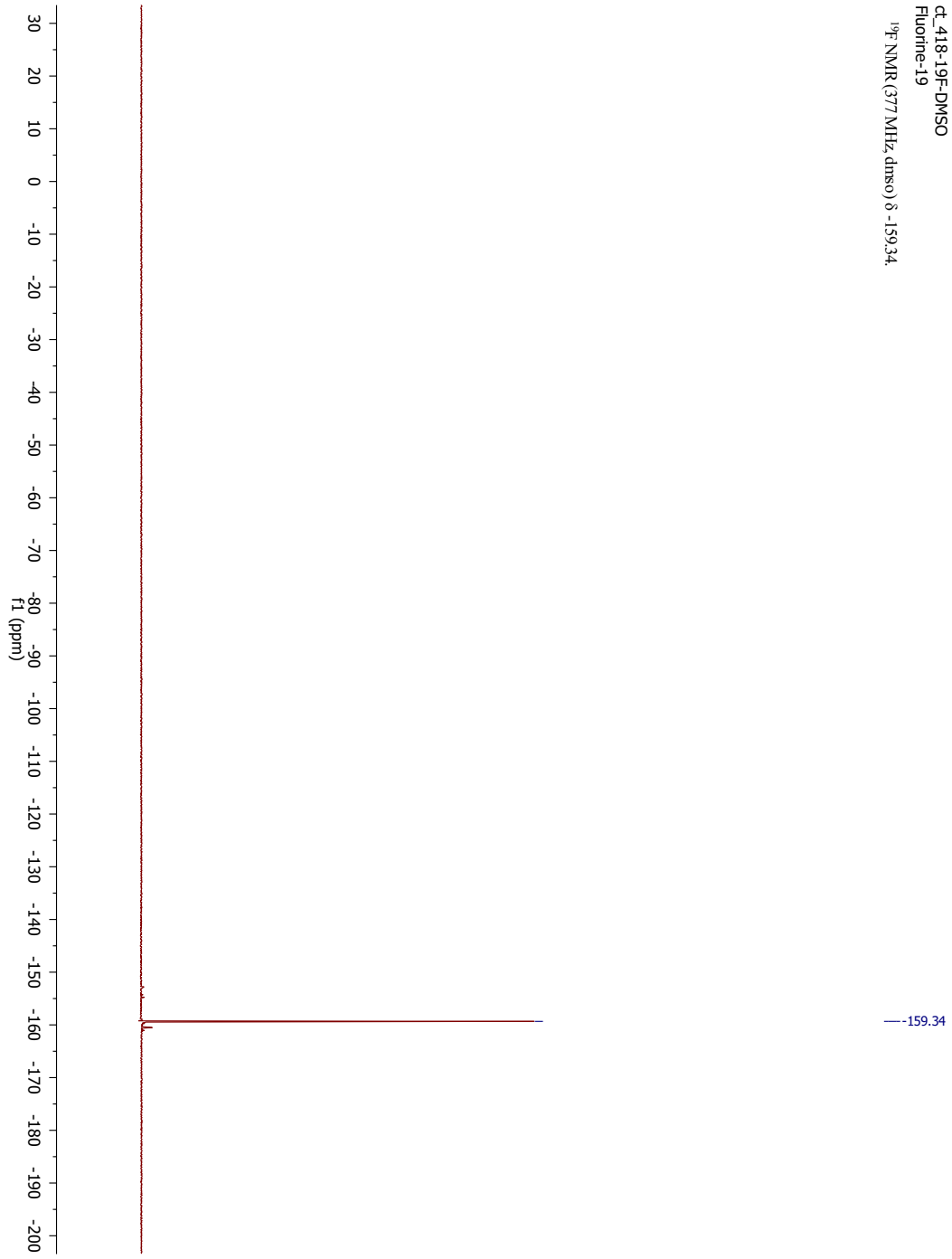

^{1}H NMR: H-MeS-DiNap (**4a**)

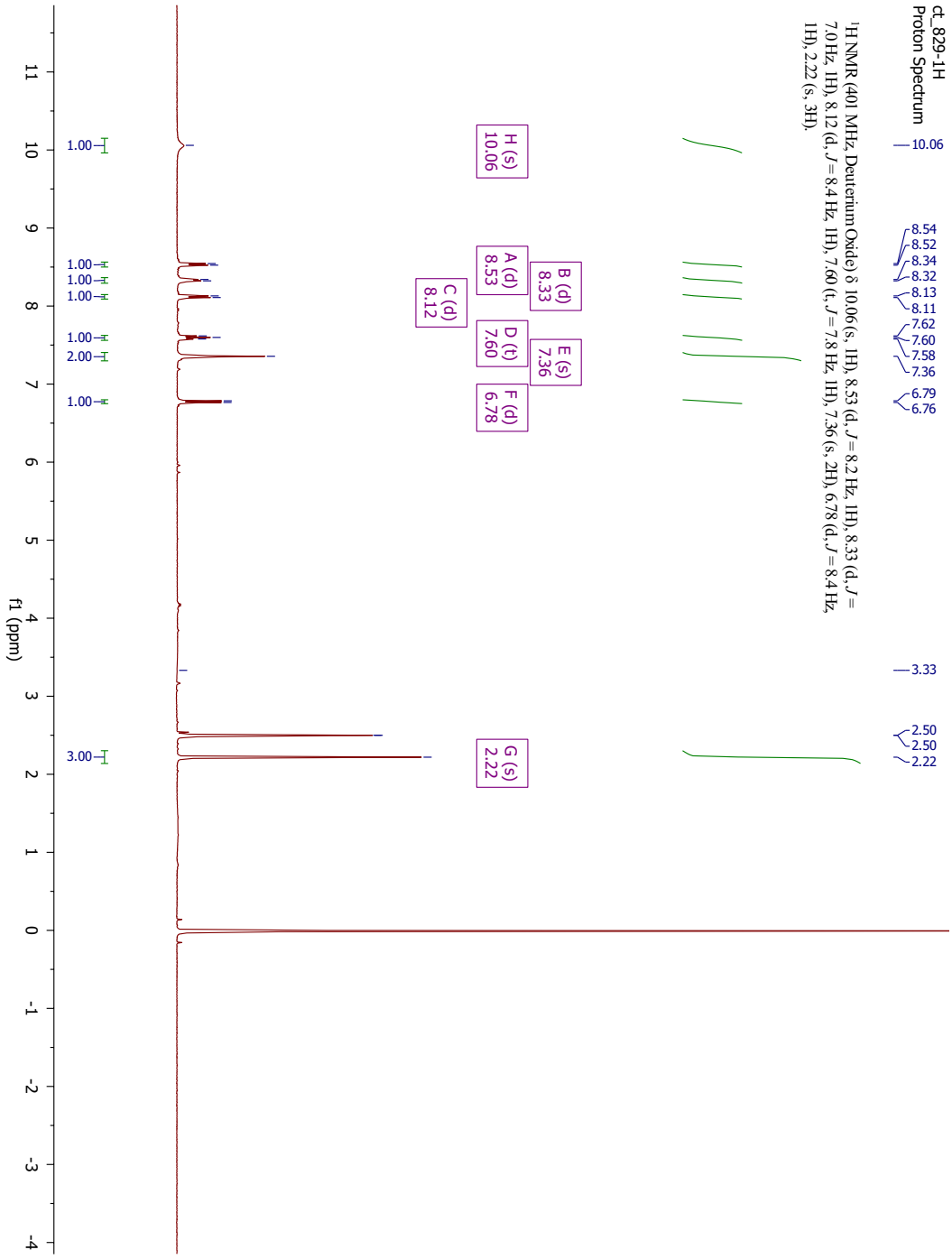

^{13}C NMR: H-MeS-DiNap (**4a**)

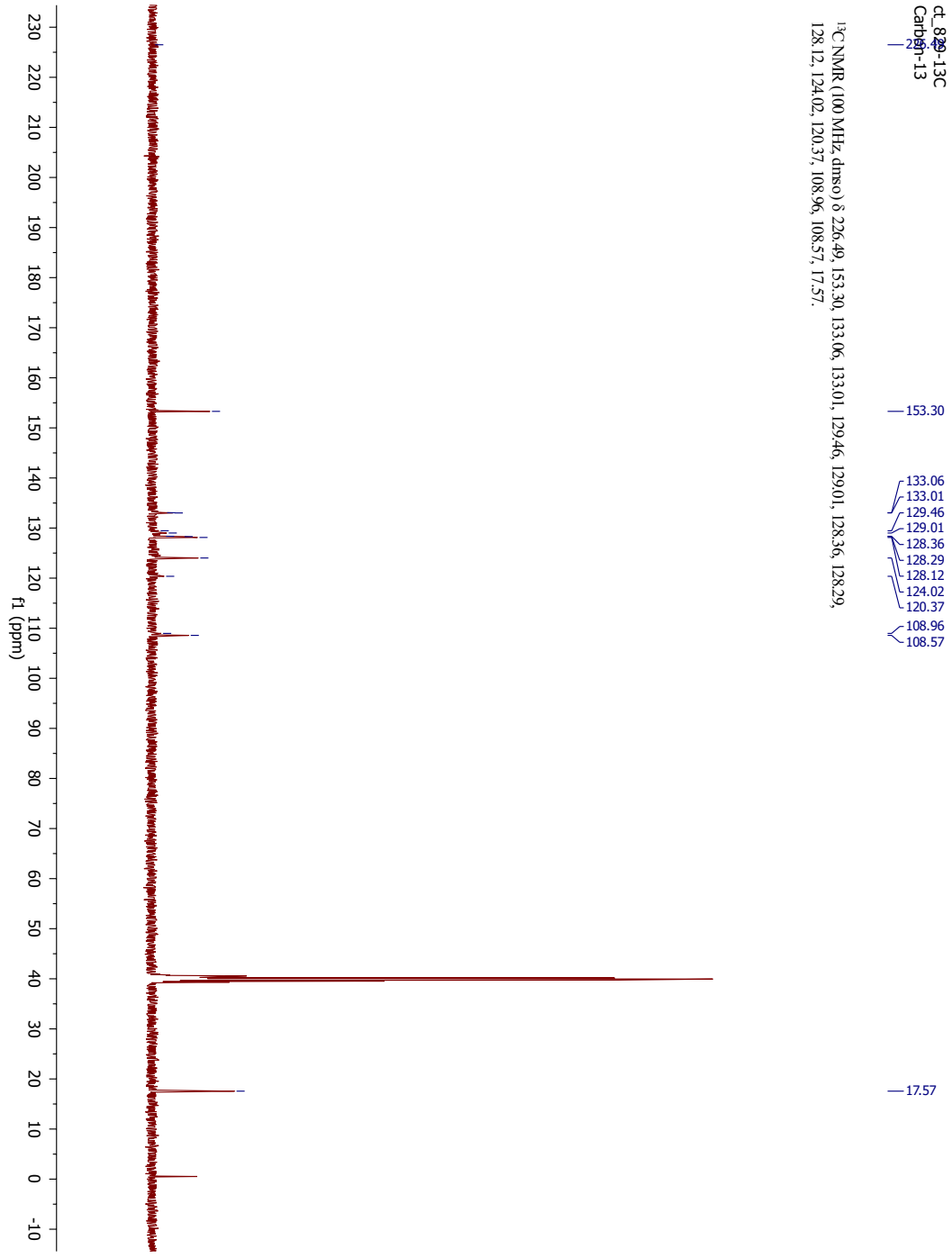

^{1}H NMR: F-MeS-DiNap (**4c**)

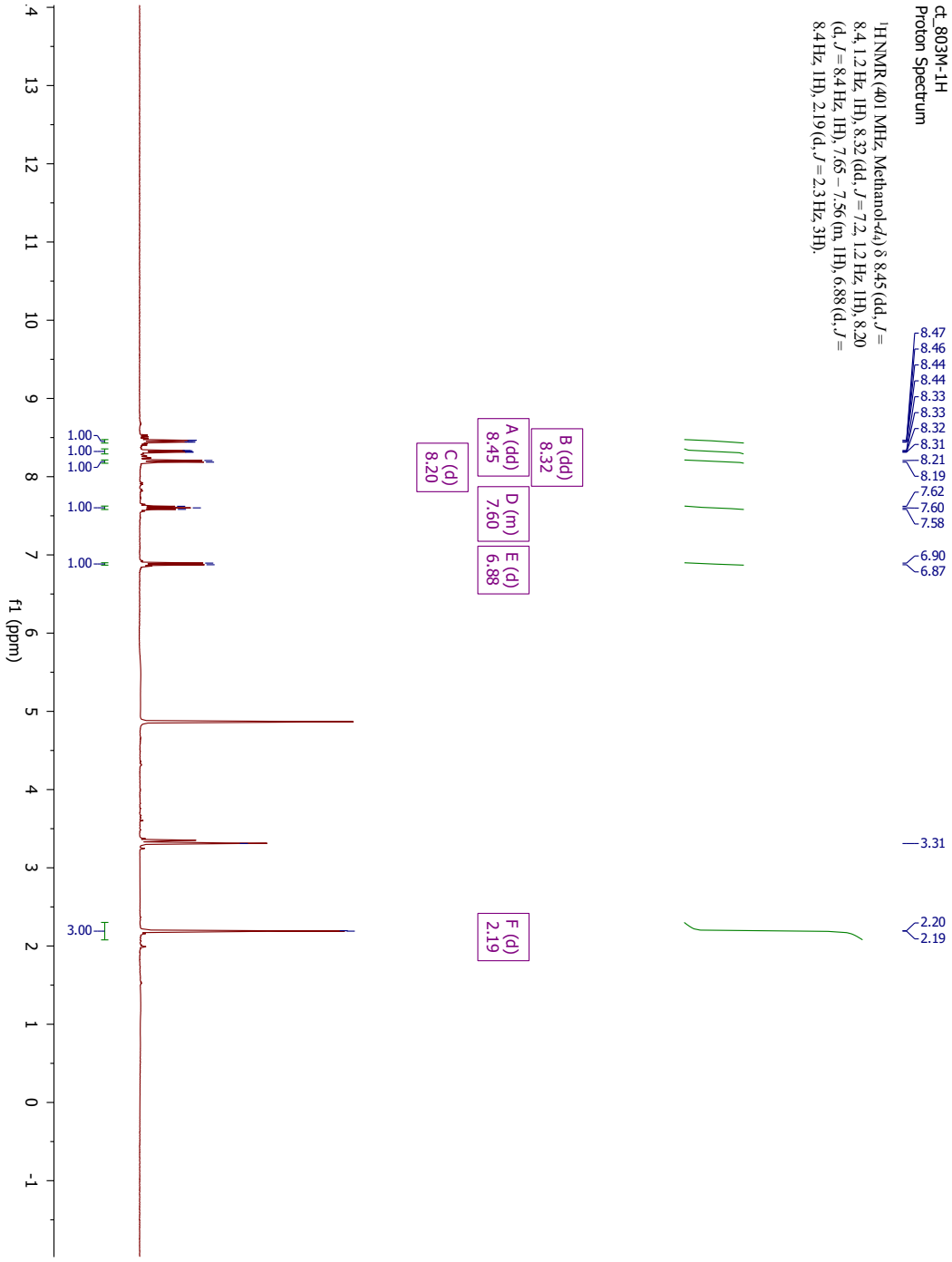

^{19}F NMR: F-MeS-DiNap (**4c**)

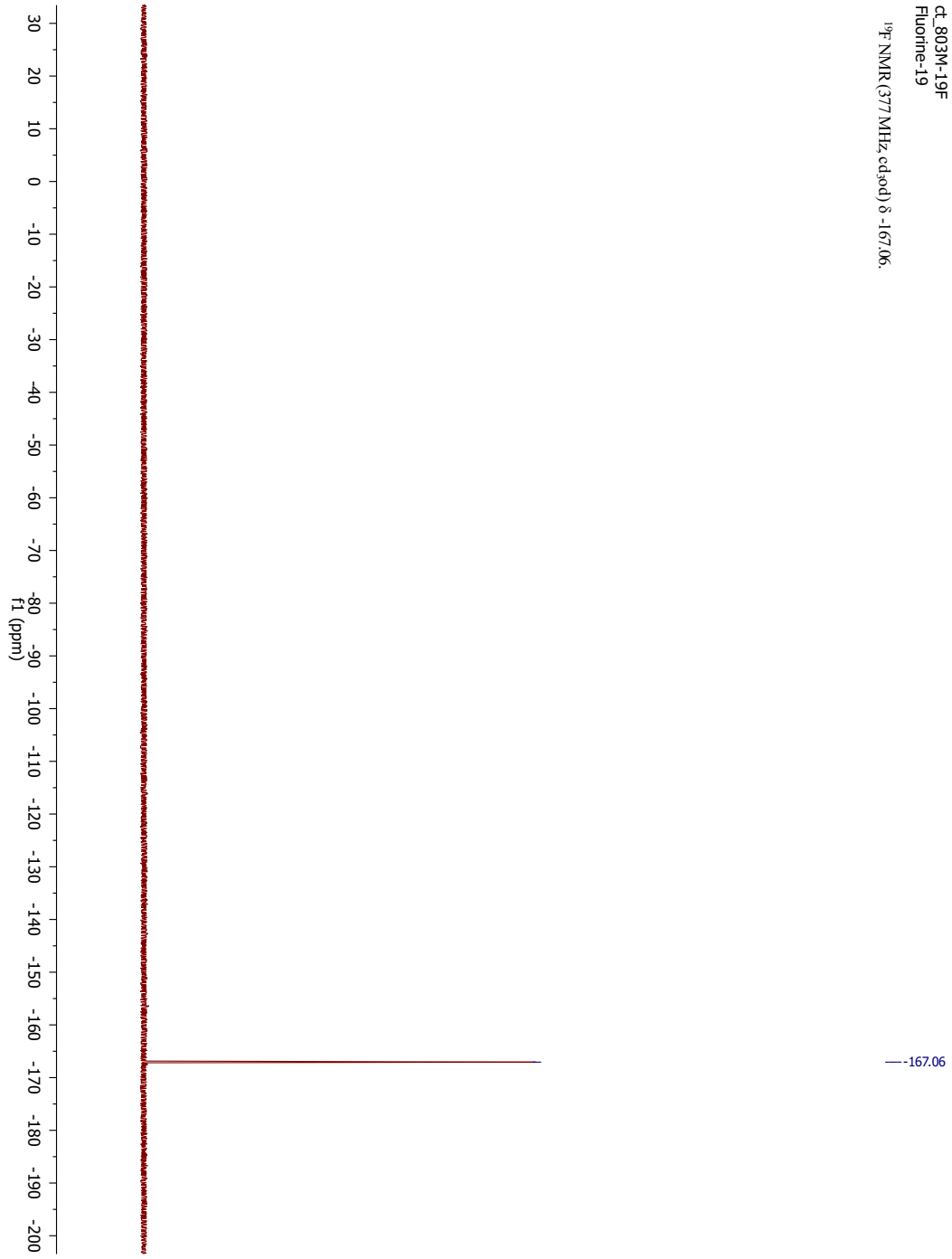

^{19}F NMR: FDiNap (**3c**) in PBS / 10% D_2O

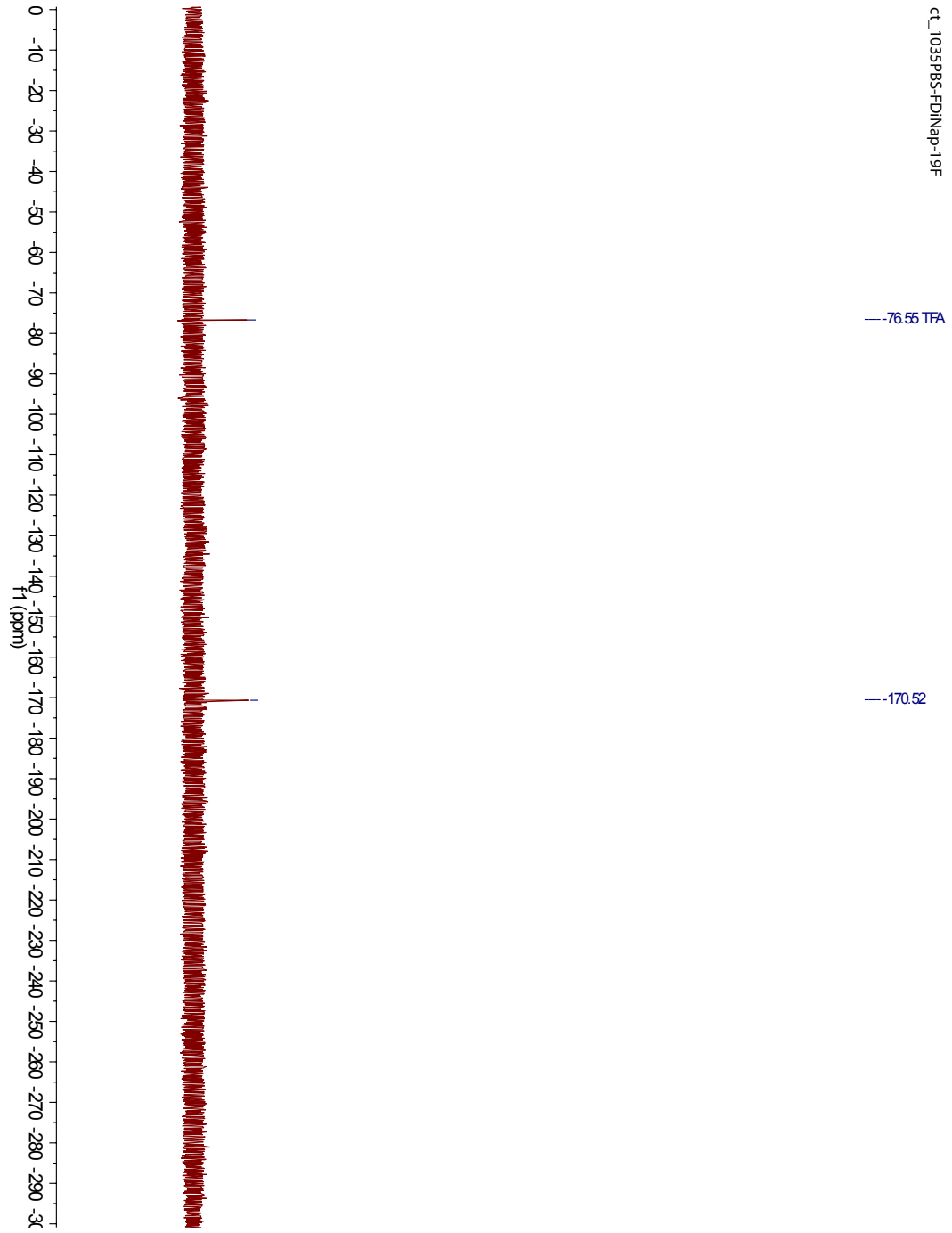

^{19}F NMR: Pep-FDiNap (**5c**) in PBS / 10% D_2O

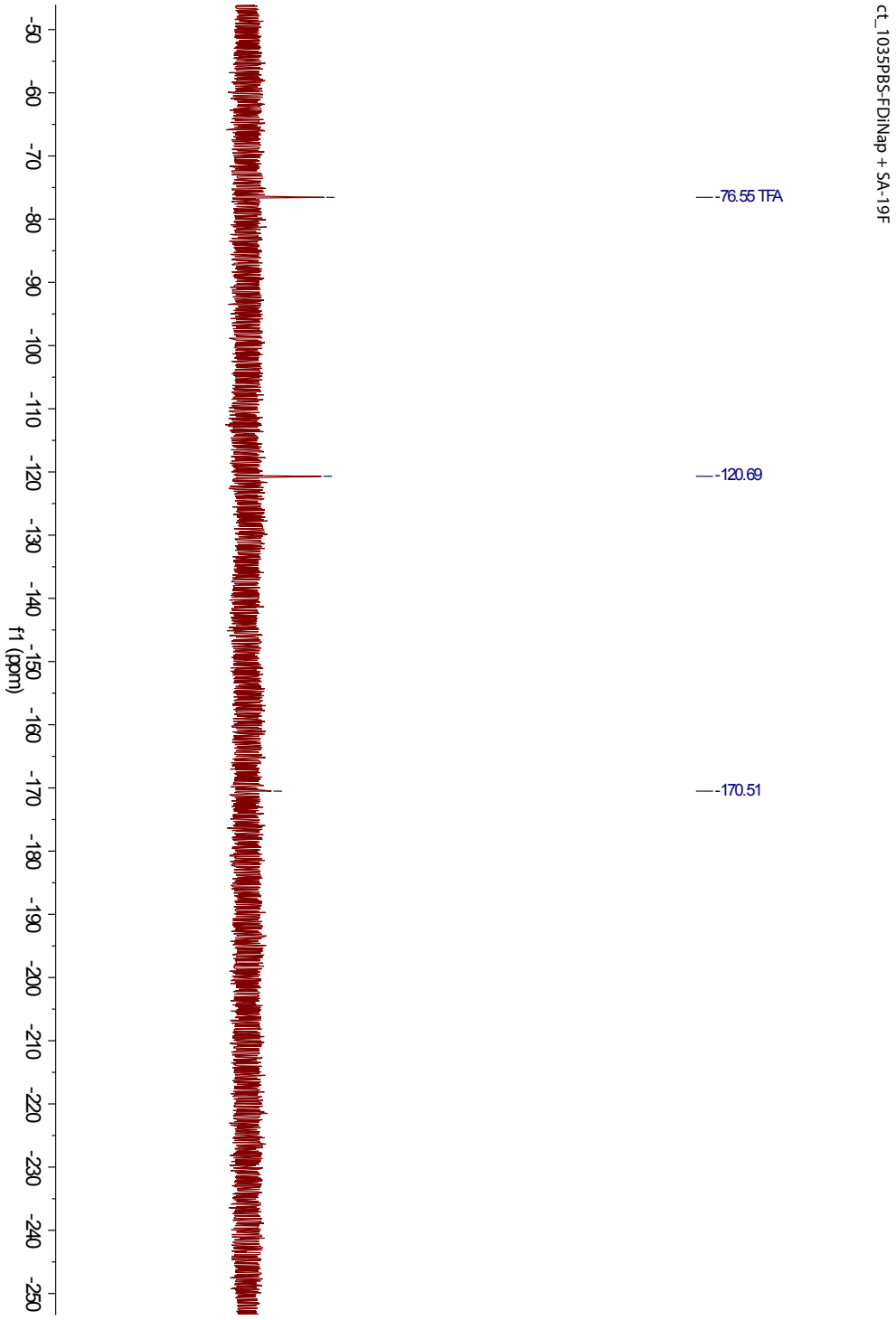

A.6. HPLC Spectra

HPLC trace of H-DiNap (3a). Absorbance at 488 nm.

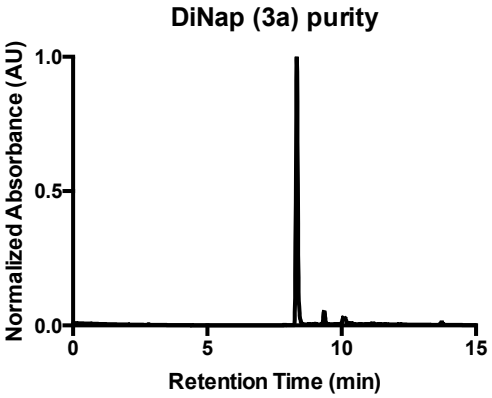

HPLC trace of Me-DiNap (3b). Absorbance at 488 nm.

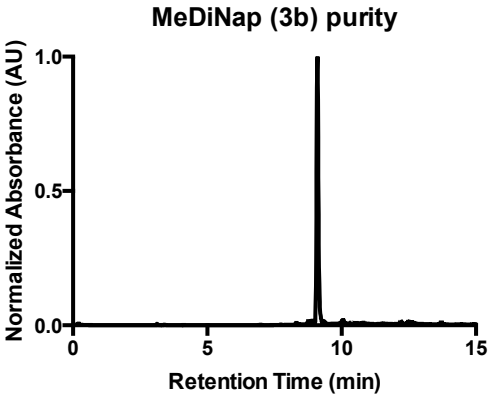

HPLC trace of F-DiNap (3c). Absorbance at 488 nm.

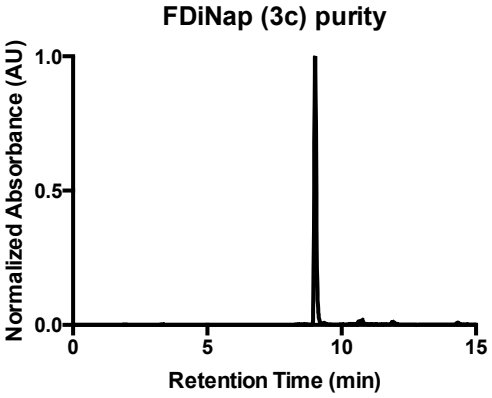

Appendix B: ^{19}F probes for the study of sulfenylation in nuclear-spin instrumentation

B.1. General procedures and materials for experimental methods.

All chemistry was performed with dry solvents of the highest purity available, except where noted. All glassware was flame-dried and the reactions were performed under a slight positive pressure of inert gas unless otherwise noted. Diethyl fluoromalonate was obtained from Matrix Scientific. Ethyl fluoroacetoacetate was obtained from Acros Organics. Compounds were purified by normal-phase flash chromatography on silica gel (Machary-Nagel), unless otherwise noted. NMR spectra were collected on a Varian MR400 premium shielded magnet, with either a Varian 5 mm AutoX dual broadband probe or Varian autoswitchable quad probe. NMR spectra of biological samples were collected on a 500 MHz (11.7 Tesla) premium shielded magnet possessing two high band and one low band radio frequency channels; 14 bit 80 MHz ADC provides effective 20 bit dynamic range at 10 kHz spectral width. The instrument has two probes: a Varian 5 mm PFG OneNMR probe and a Varian 5 mm PFG H/F/[X] triple resonance AutoX probe. ^{1}H and ^{13}C drifts were corrected against residual solvent peaks[209] and/or TMS (0.0 ppm); ^{19}F were corrected using trifluoroacetic acid (δ = -76.5 ppm) as a

standard. NMR spectra were analyzed using Mestrenova (Mestrelab Research). Low-resolution mass spectra were obtained on a Micromass LCT time-of-flight (TOF) instrument with electrospray ionization (ESI) coupled to a HPLC pump with a rheodyne loop injector. High-resolution mass spectra were collected on an Agilent Q-TOF (accuracy 1-5 ppm) with in-line photodetector array, either in direct-injection mode or through a Waters 10 cm C18 column with a 5-95% water:acetonitrile gradient, 5 mL / min, 15 minutes.

HPLC analysis. High-performance liquid chromatography separations were performed on a Waters HPLC 1525 binary pump system with an in-line Waters 2707 autosampler, reverse-phase column, Waters 2998 photodiode array (PDA), and Waters fraction collector III. Samples were injected and run through an Atlantis prep T3 (10 x 250 mm) C_{18} column equilibrated at 5% acetonitrile / water (0.1% formic acid), held at this solvent composition for 1 min, and linearly increased to 95% until 12 min, and held at this solvent composition for 1 min before being re-equilibrated to 5% acetonitrile: water. Solvent elution was 5 mL / min. Absorption spectra were collected through the PDA, and data were analyzed using Waters Empower software. Elution traces were collected at the approximate maximum wavelength for each compound (dimedone: 280 nm; DiNaps 488 nm).

SDS-PAGE analysis. Samples were either combined immediately with loading buffer and heated to 95˚C for 10-15 min, or, as necessary, small molecules were removed by a modified trichloroacetic acid (TCA) precipitation. Briefly, proteins were precipitated by adding 0.2 volumes of a 50% w / v mixture of TCA / water, centrifuged (1000 x g for 3 minutes), and the supernatant removed. Next, the protein pellet was sonicated and

washed in cold methanol (3x) and acetone (1x), and resuspended in 6 M urea in SDS gel loading buffer. Proteins were separated using pre-cast 12% acrylamide gels (BioRad) run at 160 V for 70 minutes. Western blots were transferred to Millipore Immobulon FL paper with 100 V input over 70 minutes. We found that for all AMCs tested, there was a major cross-reaction with the polyacrylamide gel. To prevent this, samples were either first processed by TCA precipitation (Figures S4 and S6) or transferred to PVDF membranes for direct fluorescence analysis (Figures 2, 3, 4, and S5). The following antibodies were used in this study: mouse α-His_6 (Qiagen), mouse α-GAPDH (Millipore), mouse α-E-cadherin (Millipore), rabbit anti-beta-actin (Cell SIgnaling). All DiNap gel-based imaging was performed on a GE Typhoon Scanner using the 488 nm laser line using the 555 / 20 nm emission filter. Near-infrared western blot imaging was performed with an Azure Biosystems c600 system.

Mammalian cell culture. A431, HeLa, HEK293T, and MDA-MB-231 cells were grown in DMEM media with 10% FBS and penicillin / streptomycin. CH27 cells were grown in DMEM media with 15% FBS with L-Glutamine, 1 g / L glucose, and 110 mg / L sodium pyruvate with penicillin / streptomycin in the presence of 50 μM 2-mercaptoethanol. MCF10A cells were transduced with retrovirus produced from pPGS-hSnail-fl.Flag-NEO (Addgene plasmid no. 25695) and pCL-Ampho packaging vector. After two days, cells were selected with 600 μg / ml G418 (Life Technologies). MCF10A vector and Snail1 cells were cultured in DMEM / F12 base medium (Thermo) supplemented with 5% dialyzed horse serum, 20 ng / ml recombinant human epidermal growth factor (Shenandoah), 0.5 mg / ml hydrocortisone (Sigma), 100 ng / ml cholera toxin (Sigma), and 10 μg / ml insulin (Sigma). After probe incubation, cells were washed 3x with PBS

and mechanically scraped from the dish. Protein levels were quantified prior to SDS-PAGE using the DC protein assay (BioRad).

Cloning and Mutagenesis of E.coli AhpC and human GAPDH. Whole genomic DNA was extracted from Top10 E.coli using TRIzol Reagent (Life Technologies) according to manufacturer's protocol. TRIzol reagent was also used to extract RNA from HEK293T cells. cDNA was synthesized from 1 µg of total RNA using SuperScriptIII reverse transcriptase (Life Technologies). The bacterial gene for AhpC (Uniprot ID: P0AE08) was amplified from *E. coli* genomic DNA using Phusion DNA polymerase chain reaction (PCR), with primers containing BamHI and XhoI restriction sites (underlined) (5'-TTTGGATCCGTCCTTGATTAACACCAAAATTAA-3', 5'-TTTCTCGAGTTAGATTTTACCAACCAGGTCC-3'). Human GAPDH was amplified from HEK293t cDNA with the primers 5'-TTTGGATCCGGGGAAGGTGAAGGTCGGAGTC -3' and 5'- TTTCTCGAGTTACTCCTTGGAGGCCATGTG-3' containing BamHI and XhoI restriction enzyme sites (underlined). After restriction enzyme digestion, each the AhpC and GAPDH fragment was ligated (T4 DNA ligase, NEB) into pET45b between BamHI and XhoI sites to insert an N-terminal His tag. The AhpC-C166S mutant was created by quick change site-directed mutagenesis with primers 5'-CACCCAGGTGAAGTTTCCCCGGCTAAATGGAAAG-3' and 5'-CTTTCCATTTAGCCGGGGAAACTTCACCTGGGTG-3'. All sequences were confirmed by sequencing (University of Michigan DNA Sequencing Core)

Expression and Purification of AhpC-C166S and GAPDH. For large-scale recombinant expression in bacteria, 1 L of TB media with 50 µg / mL carbenicillin was inoculated with the appropriate BL21 strain and grown with shaking at 250 rpm at 37 °C.

When the OD_{600} = 0.6, the cultures were induced with 0.5 mM IPTG and temperature was reduced to 22 °C. After shaking for 16 hours, *E. coli* were harvested by centrifugation. Pellets were stored at -80 °C until purification. All purification steps were carried out at 4 °C. To frozen (-80 °C) pellets from 1 L of *E. coli* culture grown in TB, 40 mL of lysis buffer (50 mM Tris pH 8.0, 150 mM NaCl, 10% glycerol) was added. Pellets were lysed by sonication, and cell debris was pelleted by centrifugation at 12,000 x g for 30 minutes. Lysate was either used at this point, or AhpC or GAPDH was purified from the supernatant using TALON (Clontech) resin according to manufacturer's protocol. Fractions containing the desired recombinant protein (as indicated by SDS-PAGE) were pooled and transferred to dialysis tubing (10,000 MWC), and dialyzed into 20 mM Tris pH 8.0 with 30 mM NaCl to remove imidazole. Protein was concentrated using 10,000 MWC spin concentrators, aliquoted and stored at -80 °C.

^{19}F NMR studies. A standardized solution of 10% D2O in PBS and 33 μM TFA was prepared. A 100 mM F-Barb stock in DMSO was added to the solution (1 mM final concentration), followed by either MeO-Val-CysSA-Cbz or a protein. These were measured on a ^{19}F NMR.

B.2. Synthetic Schemes

Scheme B1: potential 19F AMCs based on 1,3-dicarbonyl compounds. 0a and 0b are commercially available. **0c** is not commercially available, but theoretically accessible.

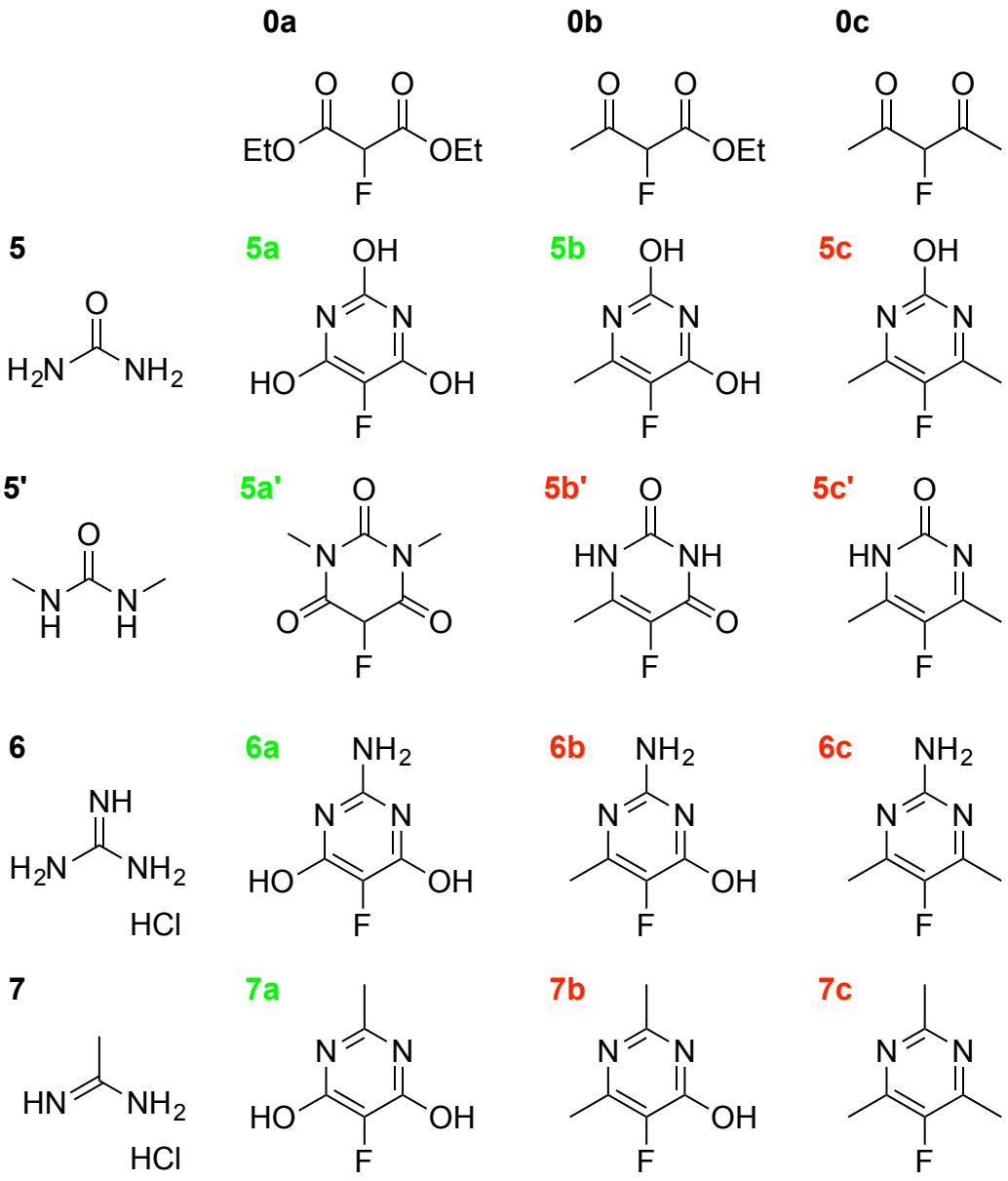

Scheme B2. Synthesis of ^{19}F AMC probes.

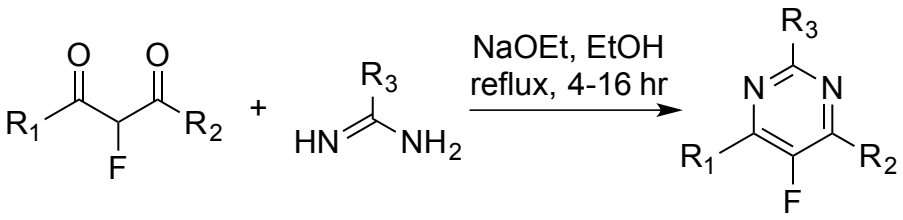

General procedure for the synthesis of cyclic AMCs 5a, 5a', and 5b[195-197,201]

To a solution of urea (1.0 eq) was added NaOEt (1.2 eq). After stirring at reflux (78˚C) for 5 minutes, the α-fluoro-β-carbonyl ester was added in one portion (1.1 eq). A precipitate formed rapidly, and the reaction was allowed to stir at reflux for 4-16 hr, at which point the reaction is quenched with concentrated HCl, adjusting the pH to 3. The reaction is filtered with a Buchner funnel, gently rinsed with a small amount of cold water, then thoroughly washed with ethanol, acetone, and diethyl ether and allowed to dry.

General procedure for the synthesis of cyclic AMCs 6a, 7a[198-200]

To a solution of containing suspensions of the HCl salts of guanidine or amidine (1.0 eq) was added NaOEt (2.4 eq). After stirring at reflux (78˚C) for 5 minutes, the α-fluoro-β-carbonyl ester was added in one portion (1.1 eq) to the heterogeneous solution. The reaction was allowed to stir at reflux for 4-16 hr, at which point the reaction is quenched with concentrated HCl to pH 3. The reaction is filtered with a Buchner funnel, gently rinsed with a small amount of cold water, then thoroughly washed with ethanol, acetone, and diethyl ether and allowed to dry.

5a. (5-fluoropyrimidine-2,4,6(1*H*,3*H*,5*H*)-trione): Starting with 0.85 g urea, 1.80 g (87%) of **5a** was recovered. ^{1}H NMR (401 MHz, DMSO-d_6): 11.40 (d, J = 11.40, 2H), 9.15, (s, br, 1H), 6.01 (d, J = 6.06, 5.95, 1 H). ^{19}F NMR (377 MHz, DMSO-d_6): -216.01, -210.21. ^{19}F NMR (377 MHz, D_2O): -203.66, -120.67. ^{19}F NMR (377 MHz, PBS / 10% D_2O): -203.65. HRMS ESI: m/z 147.0181 [M+H] (expected 147.0201).

5a'. (5-fluoro-1,3-dimethylpyrimidine-2,4,6(1*H*,3*H*,5*H*)-trione): Starting with 1.54g dimethyl urea, 2.07g (83%) of **5a'** was recovered. ^{1}H NMR (401 MHz, DMSO-d_6): 3.08 (br, s, 6H). ^{19}F NMR (377 MHz, DMSO-d_6): -211.55, -205.37, -168.92. ^{19}F NMR (377 MHz, D_2O): -189.89, -178.34, -120.68. ^{19}F NMR (377 MHz, PBS / 10% D_2O): -198.90. HRMS ESI: m/z 175.0498 [M+H] (expected 175.0514).

6a. (2-amino-5-fluoropyrimidine-4,6-diol) Starting with 1.27 g of guanidine HCl, 1.52 g (79%) of **6a** was recovered. ^{1}H NMR (401 MHz, DMSO-d_6): 7.24 (2H), 5.11 (d J = 5.17 5.05). ^{19}F NMR (377 MHz, DMSO-d_6): -199.68, -140.79. ^{19}F NMR (377 MHz, D_2O): -120.68. ^{19}F NMR (377 MHz, PBS / 10% D_2O): -196.19. HRMS ESI: m/z 146.0346 [M+H] (expected 146.0360).

7a. (5-fluoro-2-methylpyrimidine-4,6-diol) Starting with 1.43 g of methyl amidine HCl, 1.34 g (62%) of **7a** was recovered. ^{1}H NMR (401 MHz, DMSO-d_6) 2.03 (s, 3H): ^{19}F NMR (377 MHz, DMSO-d_6): -200.65, -189.14. ^{19}F NMR (377 MHz, D_2O): -187.98, -178.49, -120.68. ^{19}F NMR (377 MHz, PBS / 10% D_2O): -187.99. HRMS ESI: m/z 145.0399 [M+H] (expected 145.0408).

5b (5-fluoro-6-methylpyrimidine-2,4(1*H*,3*H*)-dione) Starting with 1.50 g of urea, 703 mg (19%) of **5b** was recovered. ^{1}H NMR (401 MHz, DMSO-d_6): 11.04 (s, 1H), 10.36 (s, 1H), 1.96 (s, 3H). ^{19}F NMR (377 MHz, D_2O): -173.18, -120.71. ^{19}F NMR (377 MHz, PBS / 10% D_2O): -120.67. HRMS ESI m/z 145.0402 [M+H] (expected 145.0408).

Scheme B3 Synthesis of MeOVal-CysSA-Cbz

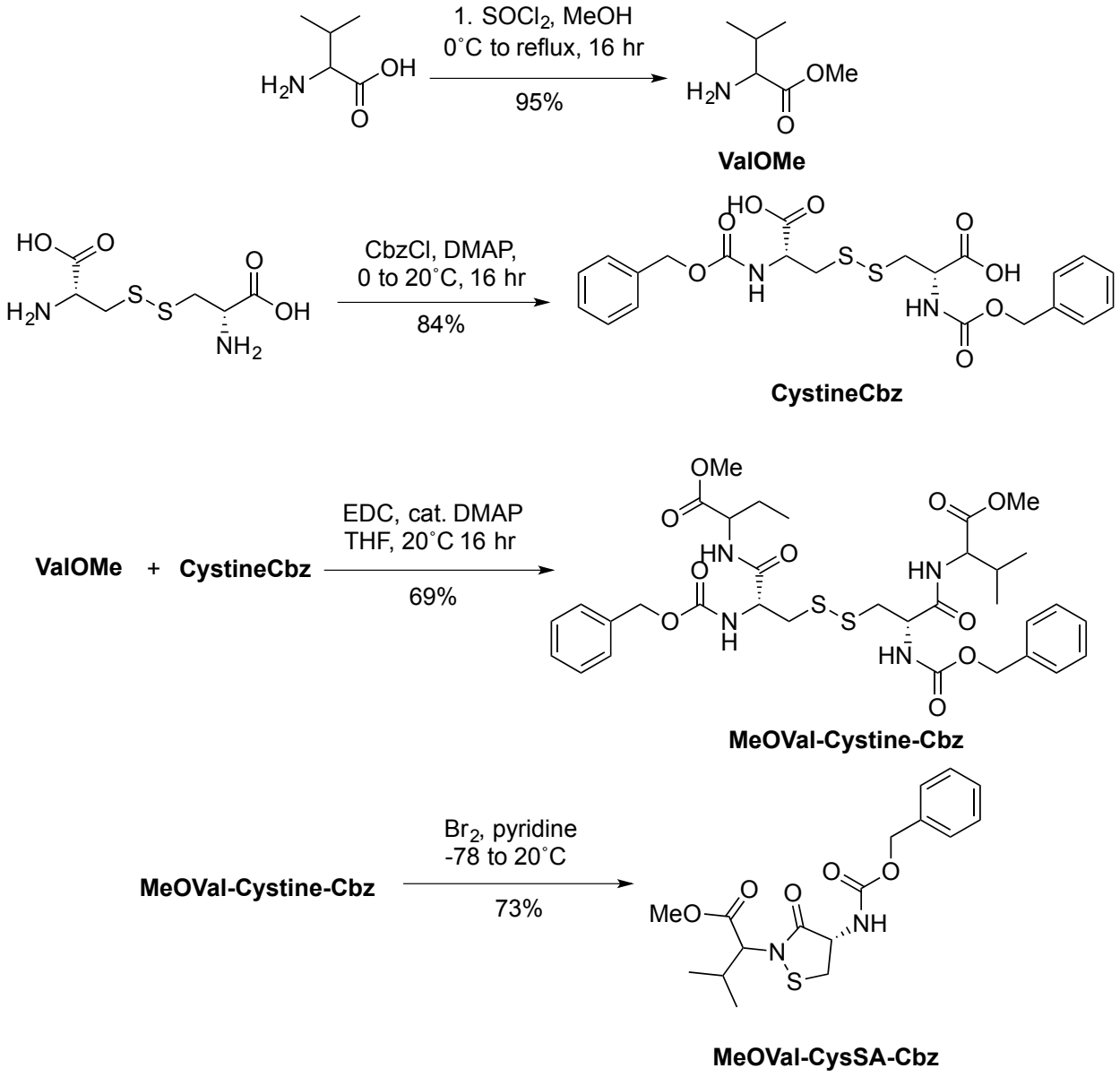

MeOValCysSACbz was synthesized according to modified literature procedures[158]:

ValOMe. To a 250 mL flask was added 50 mL of MeOH. This was cooled with ice and (6.46 g, 4.46 mL, 1.2 eq) of thionyl chloride was added dropwise with rapid stirring. The evolution of gas was monitored (SO_2) and when this ceased the solution was stirred for another half-hour before L-valine was added in one portion. The reaction was brought to reflux for 16 hrs, cooled, the volume was reduced by rotary evaporation. The reaction was taken up into 150 mL EtOAc, rinsed with 3 x 50 mL portions of 1 N NaOH, and 1 x 50 mL portion of brine. The organic layer was dried over $MgSO_4$, filtered, and collected, and then he solvent was removed by rotary evaporation, and further removed under high vaccum (< 0.1 torr). Spectral information matched that of published literature.

CystineCbz. Cystine (2.5 g) and sodium carbonate (2.76 g, 2.5 eq) was added to 50 mL 1:1 H_2O / MeOH and cooled on ice. Catalytic DMAP was added (0.1 eq). To this was dropwise added Cbz-Cl (4.44 g, 3.70 mL 2.5 eq) and allowed to warm to room temperature and react for 16 hrs. The volume was reduced and the mixture slowly acidified with 6 N HCl to pH 2. 200 mL of EtOAc was added, and this was extracted with 3 x 50 mL portions of 1 N HCl, rinsed with water, and then with brine. The organic layer was dried over $MgSO_4$, filtered, and collected, and then the solvent was removed by rotary evaporation, and further removed under high vaccum (< 0.1 torr). Spectral information matched that of published literature.

MeOVal-Cystine-Cbz. To a 250 mL round-bottom flask was added 100 mL THF and 5.3 g cysteine-Cbz, 3 g Val-OMe (2.2 eq), 5.0 g EDC*HCl (2.5 eq), and 636 mg DMAP (0.5 eq). This reaction was allowed to stir overnight at room temperature, after which the volume is reduced, and the reaction taken up in EtOAc, and extracted with 1 N HCl (3 x 50 mL portions) and 10% $NaHCO_3$ (3 x 50 mL portions), and washed with brine. The organic fractions were dried with $MgSO_4$, and filtered, and collected, and then the solvent was removed by rotary evaporation, and further removed under high vaccum (< 0.1 torr). 5.15 g was recovered (69%) and spectral information matched that of published literature.

MeOVal-CysSA-Cbz. To a flame-dried round-bottom flask was added 560 mg of MeOVal-Cystine-Cbz and dry DCM (20 mL). To this was added dry pyridine (502 µL, 8 eq) and the reaction vessel was cooled to -78˚C in an efficient Dewar and a large amount of dry ice in acetone. Bromine (88 µL, 2.2 eq) was dissolved in 5 mL dry DCM and added dropwise to the reaction mixture under nitrogen. This was allowed to warm to room temperature slowly and react overnight. 10 g of silica was added to the vessel and the reaction was dried down. This was dry-loaded onto a silica gel column and purified with a 0-50% acetone:DCM gradient. 415 mg (73%) of product was collected, and spectral information matched published data.

Scheme B4. Synthesis of Pyr-SEt

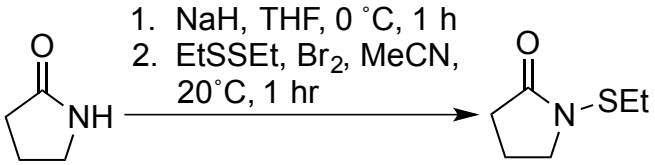

Pyr-SEt

Pyr-SEt. In a modified literature procedure[227], to a 100 mL flame-dried two-neck round-bottom flask was added sodium hydride as a 60% suspension in mineral oil (1.337 g, 34 mM, 4.2 eq), which was thoroughly washed with hexanes (3 x 25 mL portions) under nitrogen. This was suspended in 25 mL dry THF and cooled on an ice bath. 2-pyrrolidinone (2.50 mL, 33 mM, 4 eq), was added dropwise to this solution with stirring and allowed to equilibrate for 1 hr with the evolution of gas. In a separate 25 mL flame-dried round-bottom flask, to a solution of ethyl disulfide (1 g, 8.2 mM, 1 eq) and dry acetonitrile (10 mL) was added elemental bromine (1.31 g, 8.2 mM, 1 eq), and this was allowed to react for 1 hr. Following this, the solution was added dropwise via cannula to the suspension of sodium pyrrolidinonate, which was accompanied by a loss of color. This was allowed to warm to room temperature, and left to react for one hour. Hexanes (100 mL) was added to the heterogeneous reaction, which was then filtered through a plug of glass wool to remove pyrrolidinate and other salts. The solvent was removed under vacuum, and the crude mixture was purified by flash chromatography on a 0-2% methanol gradient in dichloromethane. Fractions were combined, and 1.56g (66%) was collected as a light brown liquid. ^{1}H NMR (401 MHz, Chloroform-d) δ: 3.58 (t, J = 7.1 Hz, 2H), 2.79 (q, J = 7.4 Hz, 2H), 2.40 (t, J = 8.1Hz, 2H), 2.04 (tt, J = 7.8, 6.8Hz, 2H), 1.22 (t, J = 7.4Hz, 3H). ^{13}C NMR (101 MHz, $CDCl_3$) δ 177.87, 77.33, 77.01, 76.69, 52.85, 30.96, 30.24, 18.83, 13.16. HRMS ESI^{+} 146.0634 (M+H^{+} calc 146.0640)

Scheme B5. Reaction of **5-7** with **MeOVal-CysSA-Cbz:**

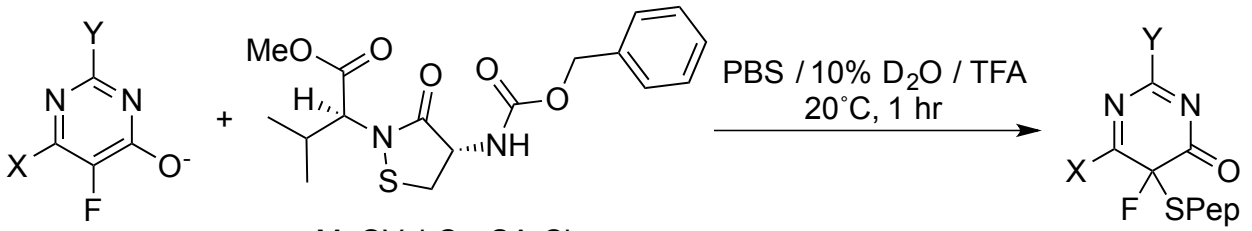

General procedure for the 19F NMR evaluation of the reactivity of 5-7 with MeOVal-CysSA-Cbz:

To a 1.5 mL Eppendorf tube was added 980 uL of a standard solution of PBS with 10% D_2O and TFA as an internal standard. To this was added 10 µL of a 100 mM solution of **5-7** in DMSO, and then quickly 10 µL of a 100 mM solution of **MeOVal-CysSA-Cbz** in DMSO was added and the solution mixed thoroughly. After 1 hr, the solution was transferred to an NMR tube and analyzed.

General procedure for the LC-HRMS evaluation of the reactivity of 5-7 with MeOVal-CysSA-Cbz:

To a 1.5 mL Eppendorf tube was added 980 uL PBS. To this was added 10 µL of a 100 mM solution of 5-7 in DMSO, and then quickly 10 µL of a 100 mM solution of MeOVal-CysSA-Cbz in DMSO was added and the solution mixed thoroughly. After 1 hr, the solution was injected on the LCMS and analyzed.

General procedure for the evaluation of the rates of reaction of 5-7 by LC-HRMS with MeOVal-CysSA-Cbz:

To a 1.5 mL Eppendorf tube was added 980 uL PBS. To this was added 10 µL of a 100 mM solution of **5-7** in DMSO, and then quickly 10 µL of a 100 mM solution of MeOVal-CysSA-Cbz in DMSO was added and the solution mixed thoroughly. Immediately, a 100 µL portion aliquot was removed and put into a 100 µL vial with AcOH. This is repeated for the described number of timepoints, and these are analyzed by LC-HRMS. The mass peak for each compound is extracted and the ion count is collected. As possible, this is fit to a one-phase association curve, in which the k_{obs} is extracted and the k_{rxn} is determined.

Scheme B6. Structures of 5-pep – 7-pep:

5a-pep

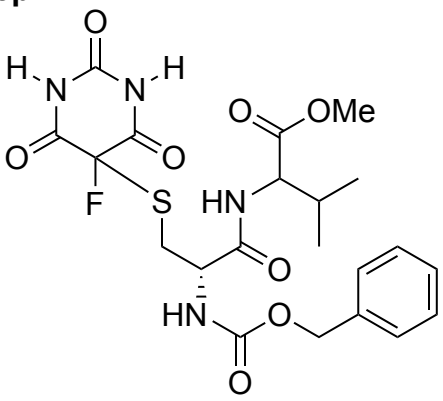

5a'-pep

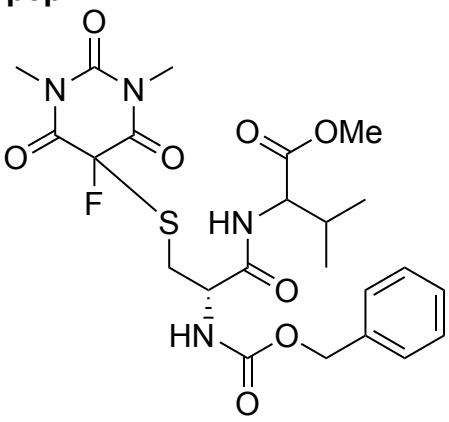

5b-pep

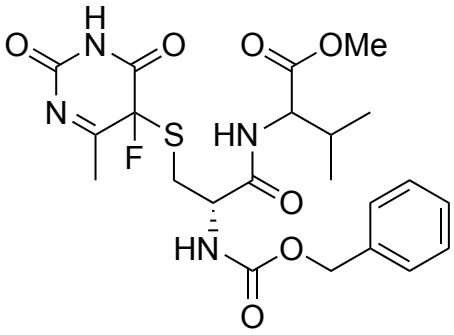

6a-pep

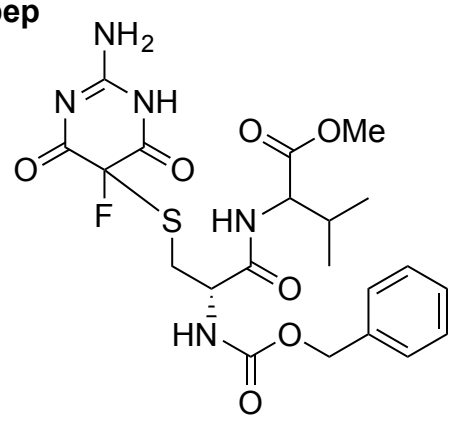

7a-pep

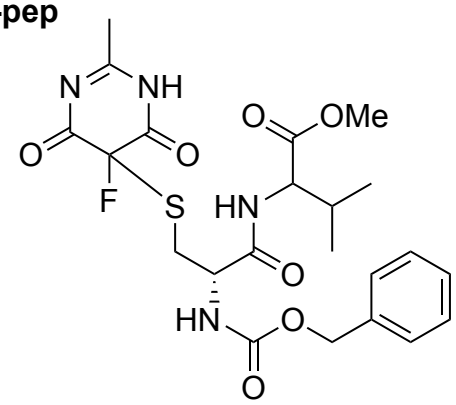

Scheme B7. Reaction of Pyr-SEt with 5a

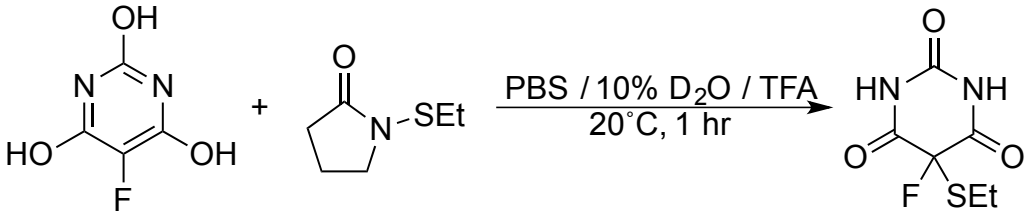

5a **Pyr-SEt** **5a-SEt**

To a 1.5 mL Eppendorf tube was added 980 uL of a standard solution of PBS with 10% D_2O and TFA as an internal standard. To this was added 10 µL of a 100 mM solution of **5-7** in DMSO, and then quickly 10 µL of a 100 mM solution of **Pyr-SEt** in DMSO was added and the solution mixed thoroughly. After 1 hr, the solution was transferred to an NMR tube and analyzed.

Scheme B8. Planned procedure for the conversion of hydroxy-19F AMC probes to amino-19F AMC probes[197,198]

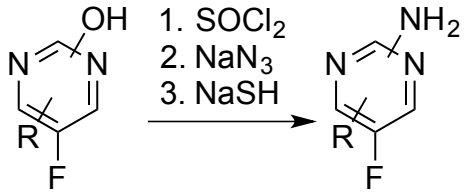

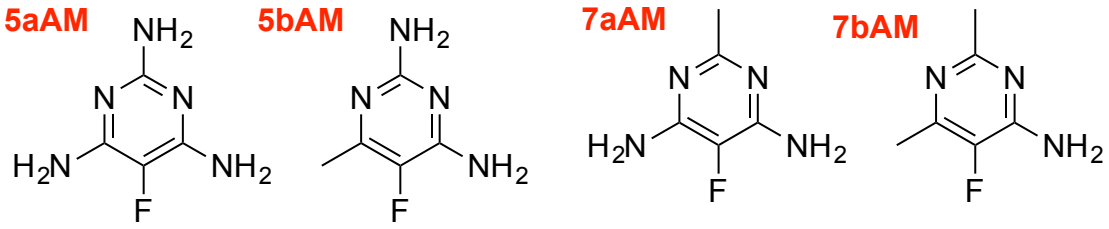

To a solid amount of an hydroxy-pyrimidine was added neat thionyl chloride at room temperature. This reaction was brought to reflux and the evolution of gas was monitored. When no more gas (-$SOCl_2$ and -HCl) is produced, the reaction is cooled, and the remaining thionyl chloride is carefully removed by rotary evaporation. The resulting perchloro pyrimidine was dissolved in THF, and a number of equivalents of sodium azide is added equal to the number of chlorines plus an additional half. This is allowed to stir for 4 hours, and conversion is checked by TLC. If necessary, the reaction is heated to reflux overnight. Following this, a number of equivalents of sodium sulfide is directly added to the same solution equal to the number of chloro sites plus one. The evolution of gas is monitored (-N_2). The THF is removed, and the reaction is taken up into EtOAc, and the reaction is then extracted with 1 N NaOH to remove inorganics.

Scheme B9. Other potential expanded ^{19}F AMC derivatives based on diethyl fluoromalonate.

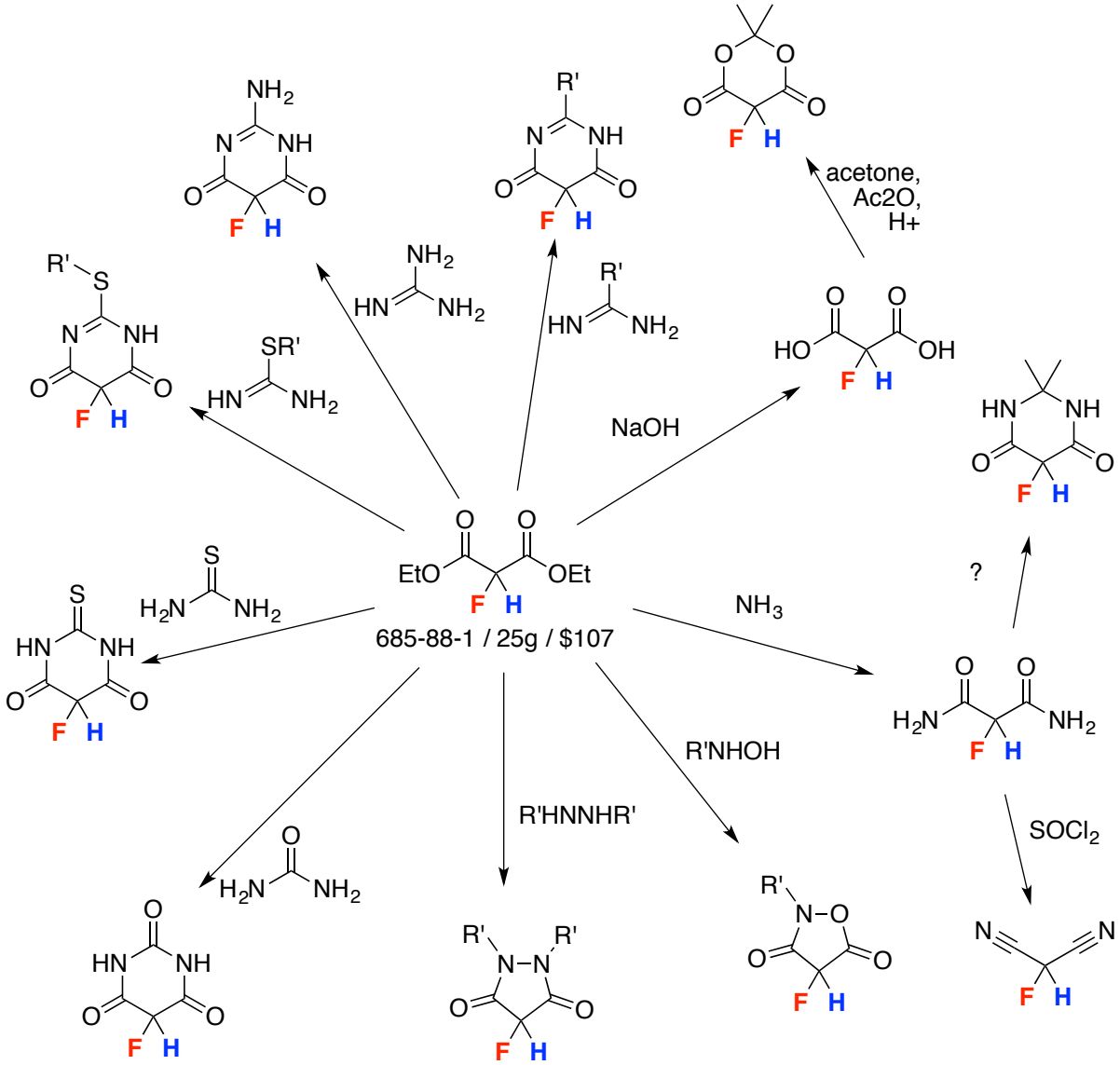

Scheme B10. Other potential scaffolds based on ethyl fluoro acetoacetate

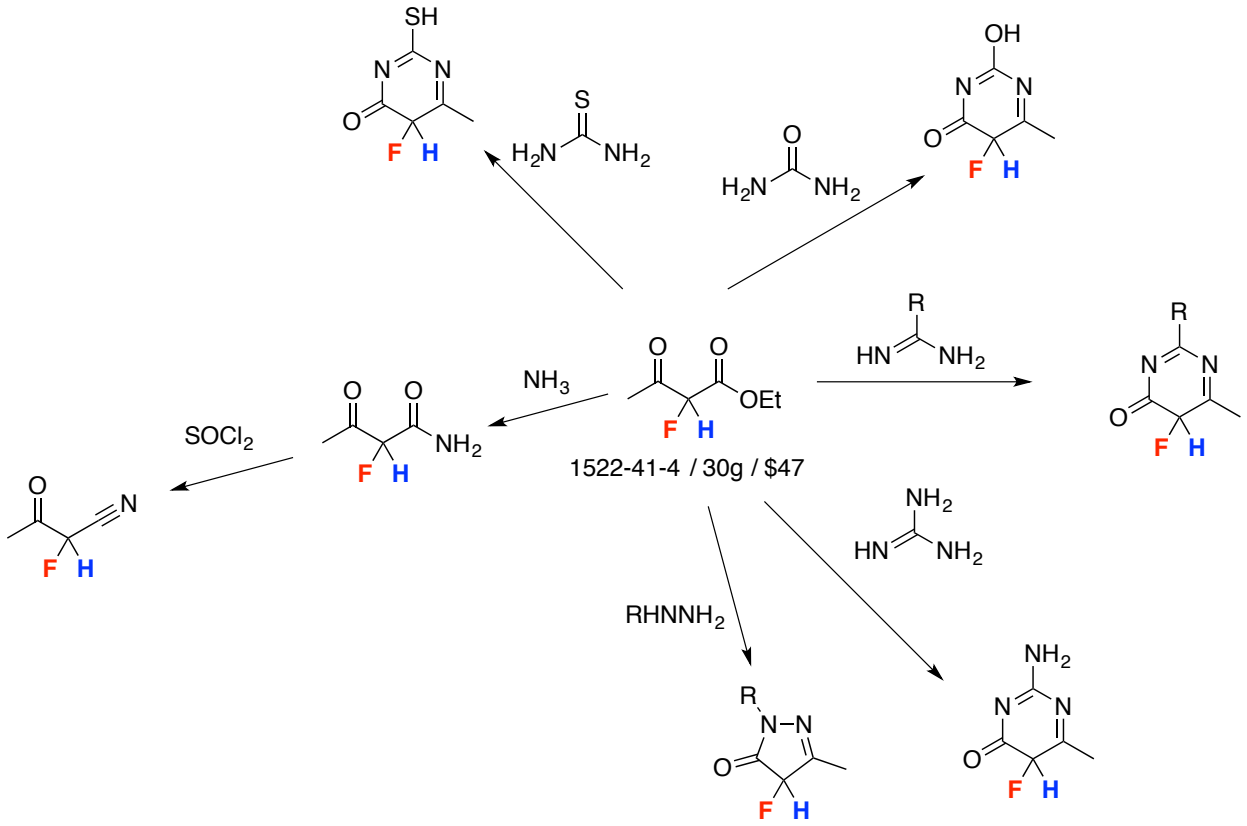

Scheme B11. Proposed synthesis of 6a-yne

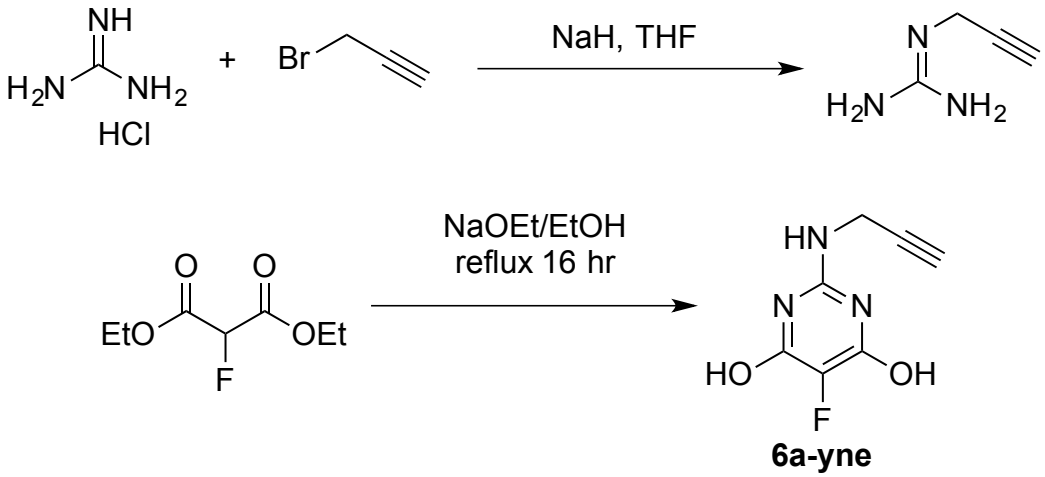

6a-yne

B.3. Supplementary Tables

Table B1. Chemical shifts before and after MeOVal-CysSA-Cbz treatment

19F chemical shifts, in ppm

	Starting material	post- MeOVal-CysSA-Cbz:	result
5a	-203.65	-120.68 ppm	complete conversion
5a'	-198.90	-198.92, -120.68 ppm	partial conversion
6a	-196.19	-120.69 ppm	complete conversion
7a	-187.99	-188.01 ppm	no reaction
5b	-120.67	-120.67 ppm	no reaction

B.4. Supplementary Figures

Figure B-01. Rate measurements of ^{19}F AMCs with MeOVal-CysSA-Cbz.
Into a 1.5 mL Eppendorf tube was added 880 µL of PBS. To this, 100 µL of a 100 mM DMSO stock of **5-7** was added, and then 10 µL of a 100 mM DMSO stock of MeOVal-CysSA-Cbz was added, then the reaction was immediately quenched at given time points with AcOH, and the pseudo-first order kinetics was calculated if possible. a) **5a** shows a rapid increase, and then degradation. b) The initial time points of **5a** show a rapid (1700 M^{-1} s^{-1}) increase. c) **5a'** also shows the same rapid increase, followed by a degradation. d) **6a** shows a clean kinetics curve, with first-order kinetics of 215 M^{-1} s^{-1}. e) **7a** produced no expected products, consistent with ^{19}F NMR studies.

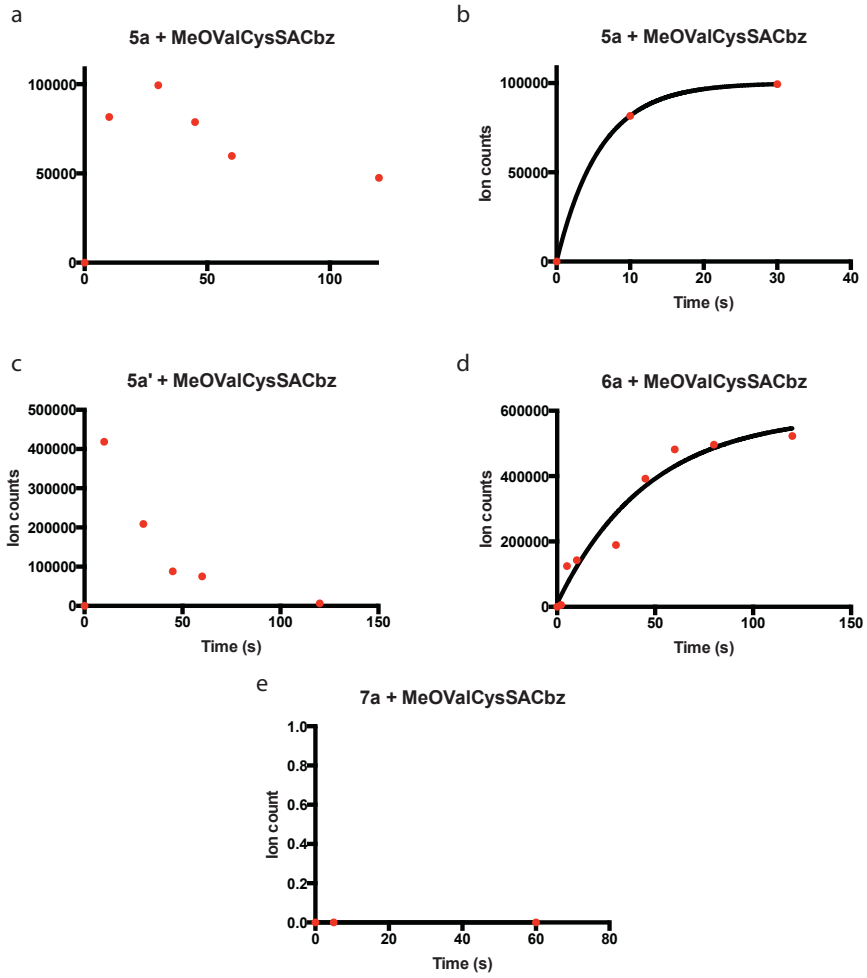

Figure B-02. Toolkit for the α-fluorination of dimedone and dimedone analogues

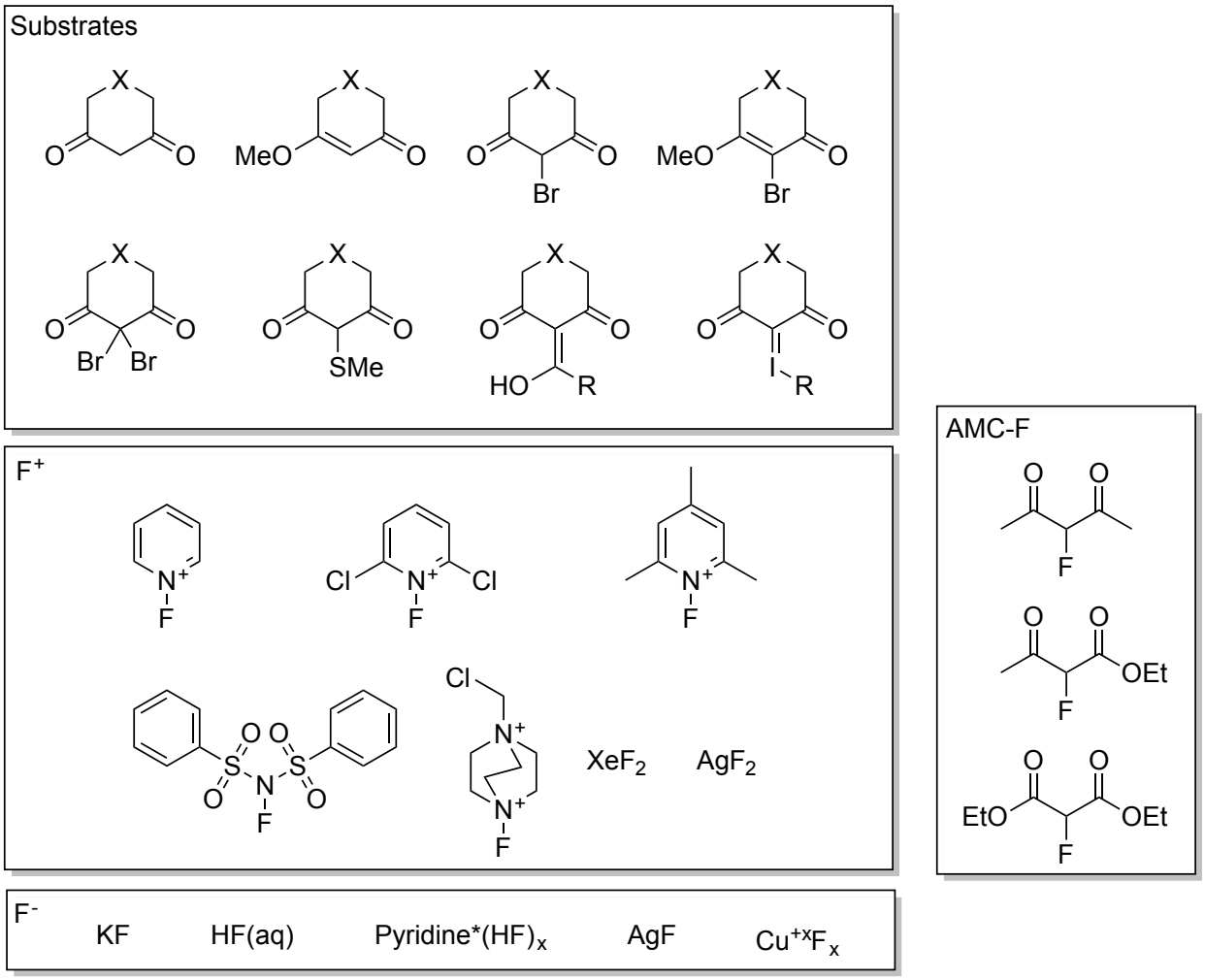

B.5. NMR spectra

^{1}H NMR: MeOVal-CysSA-Cbz in $CDCl_3$

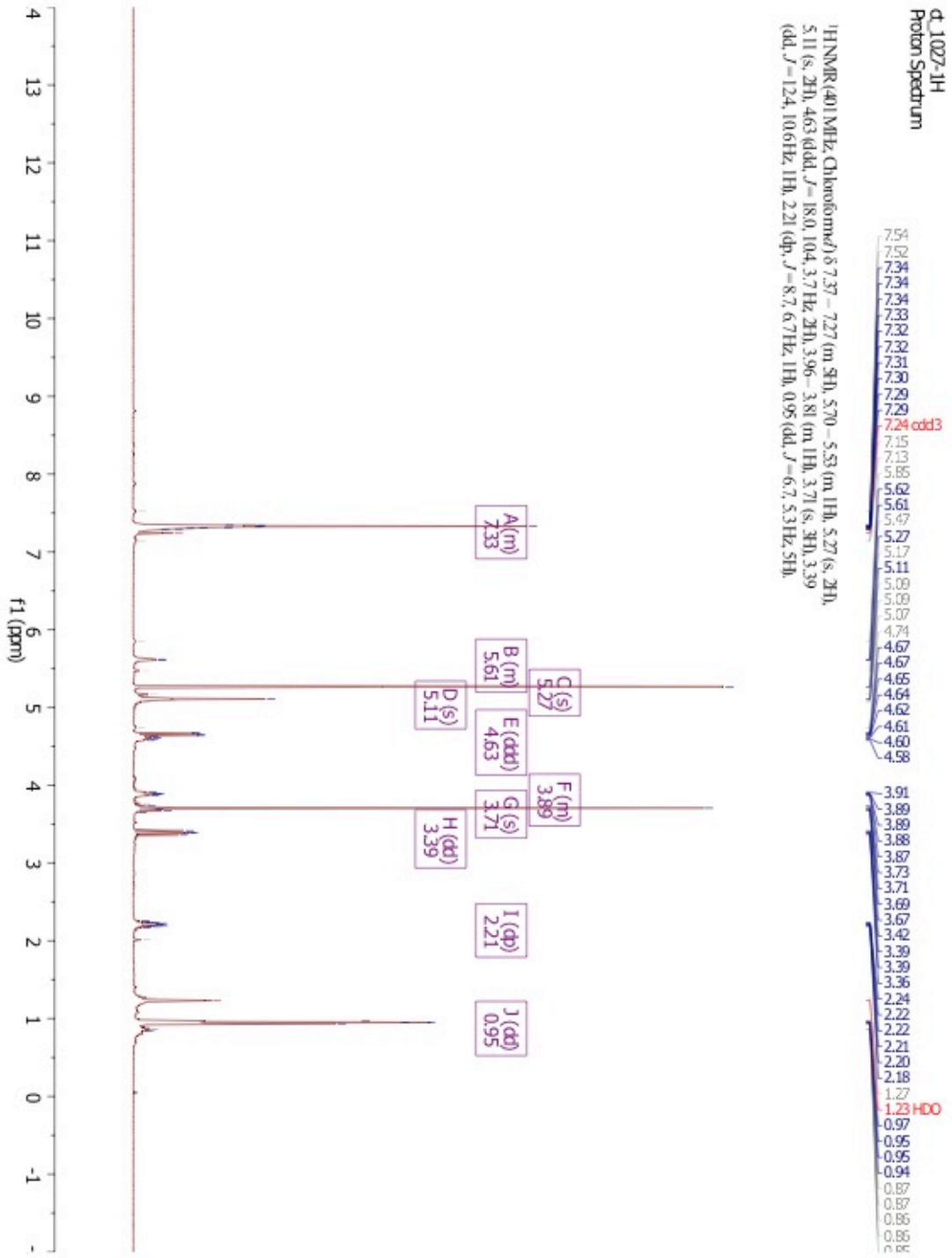

^{13}C NMR: MeOVal-CysSA-Cbz in $CDCl_3$

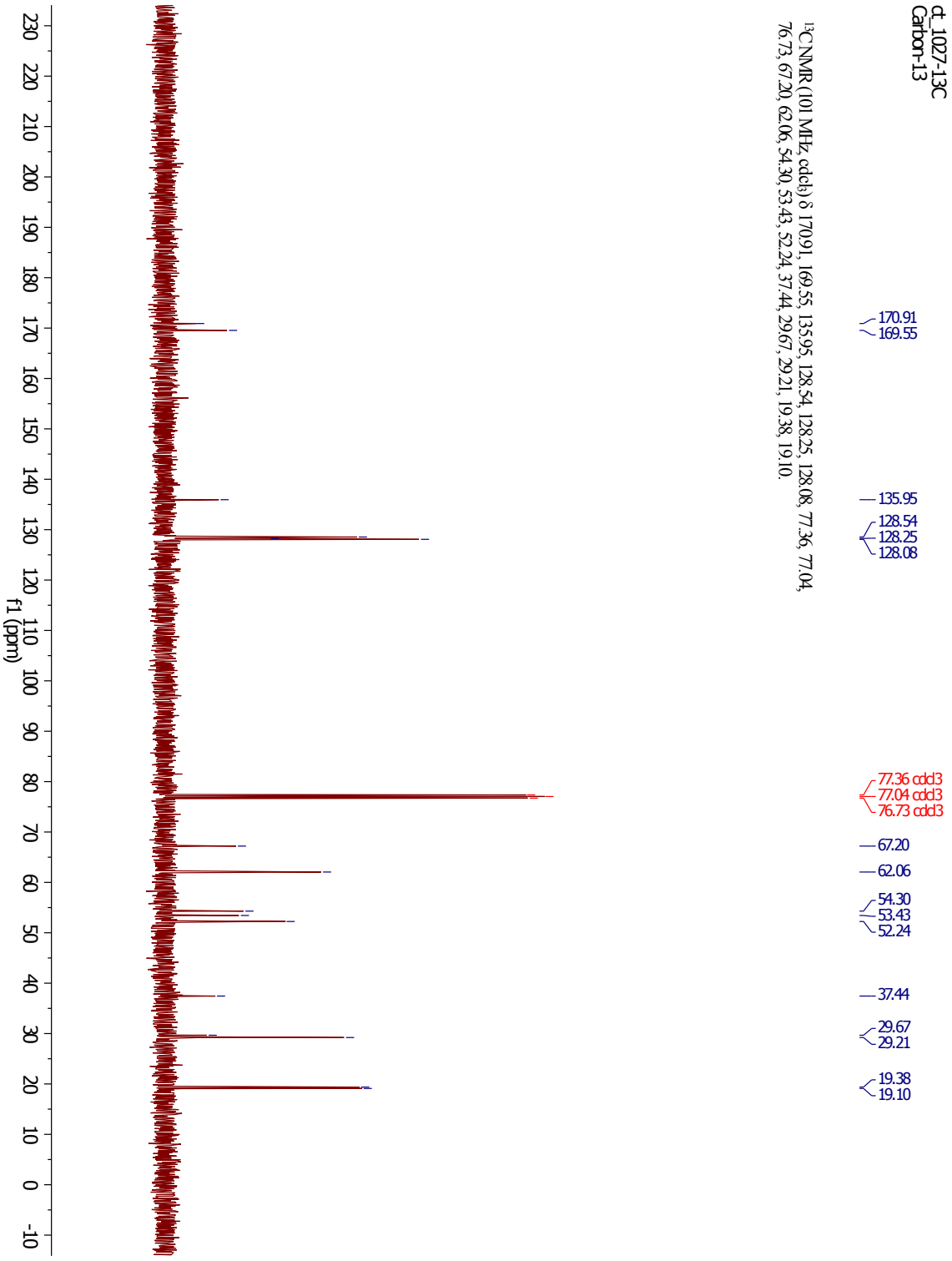

^{1}H NMR: **5a** in DMSO

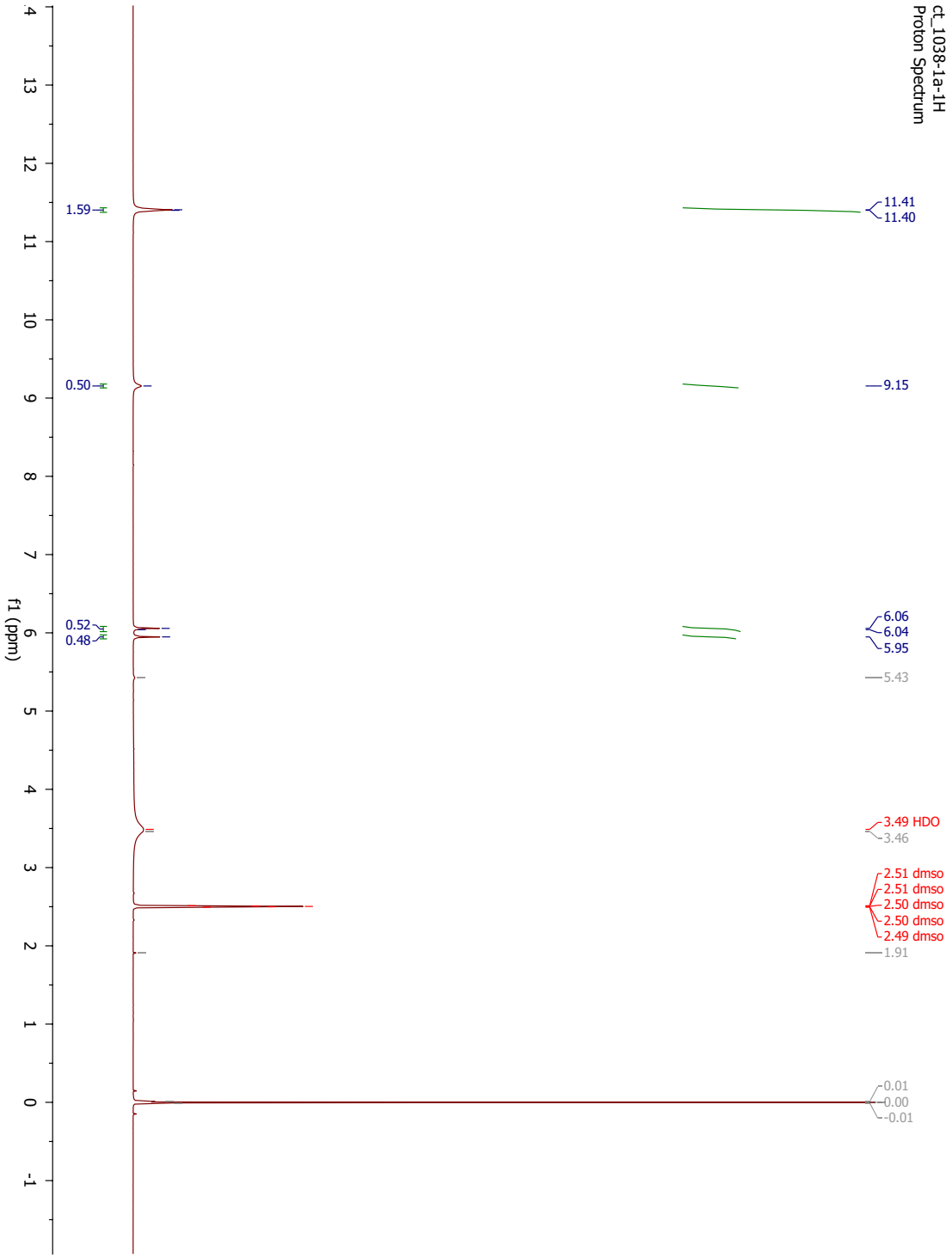

^{19}F NMR: **5a** in DMSO

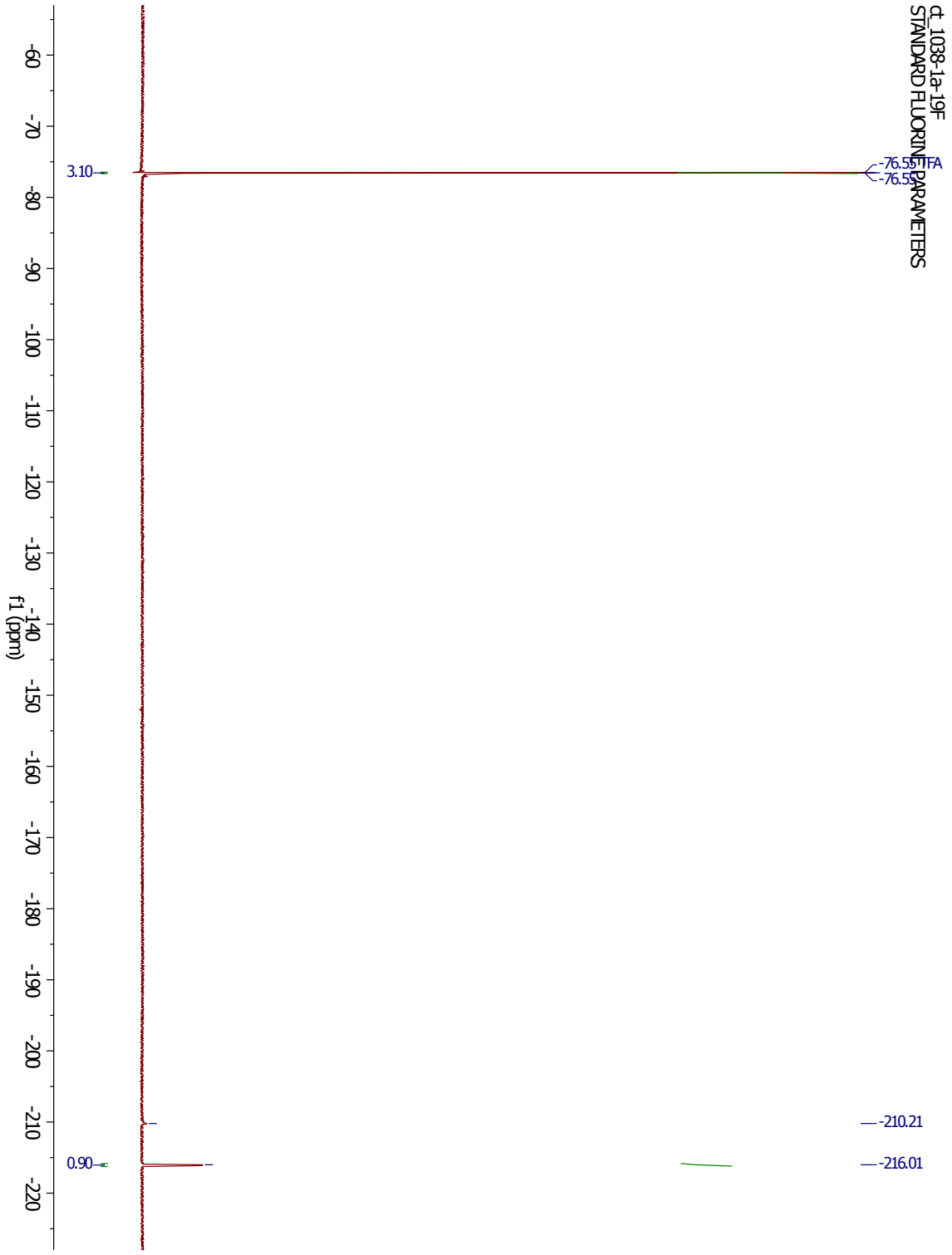

^{19}F NMR: **5a** in D_2O

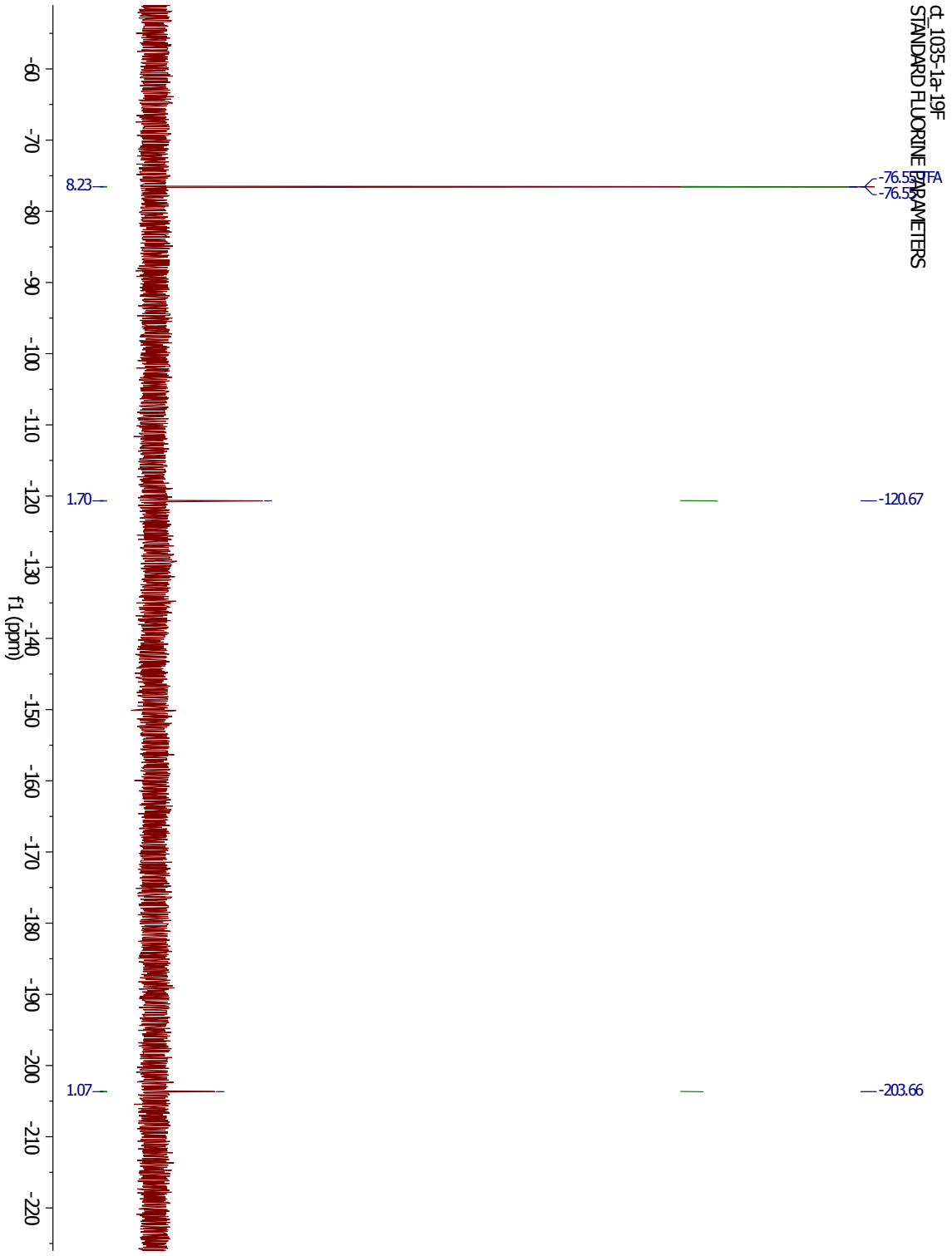

^{19}F NMR: **5a** in PBS / 10% D_2O

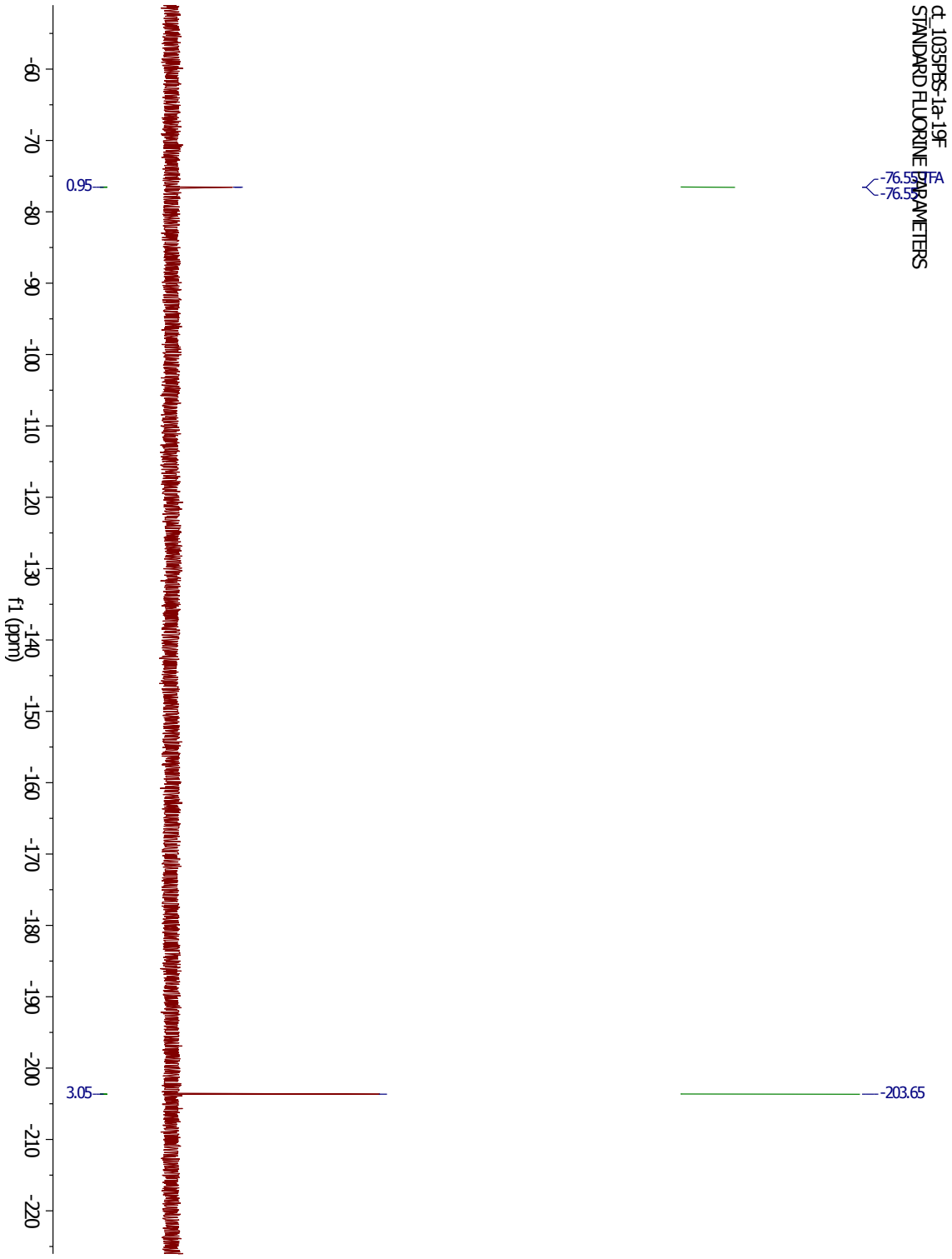

^{19}F NMR: **5a-pep** (**5a** + MeOVal-CysSA-Cbz) in PBS / 10% D_2O

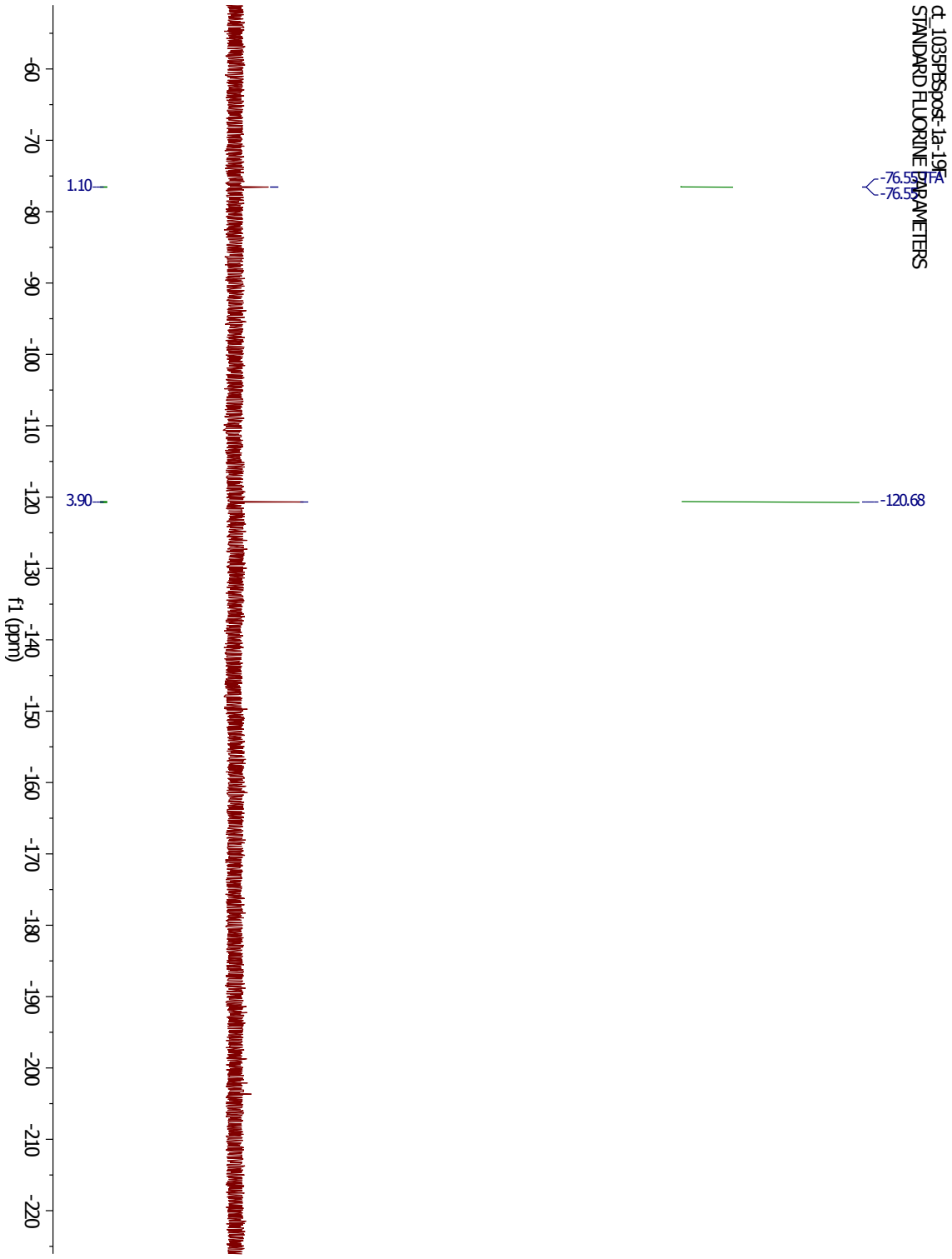

^{19}F NMR: **5a'** in DMSO

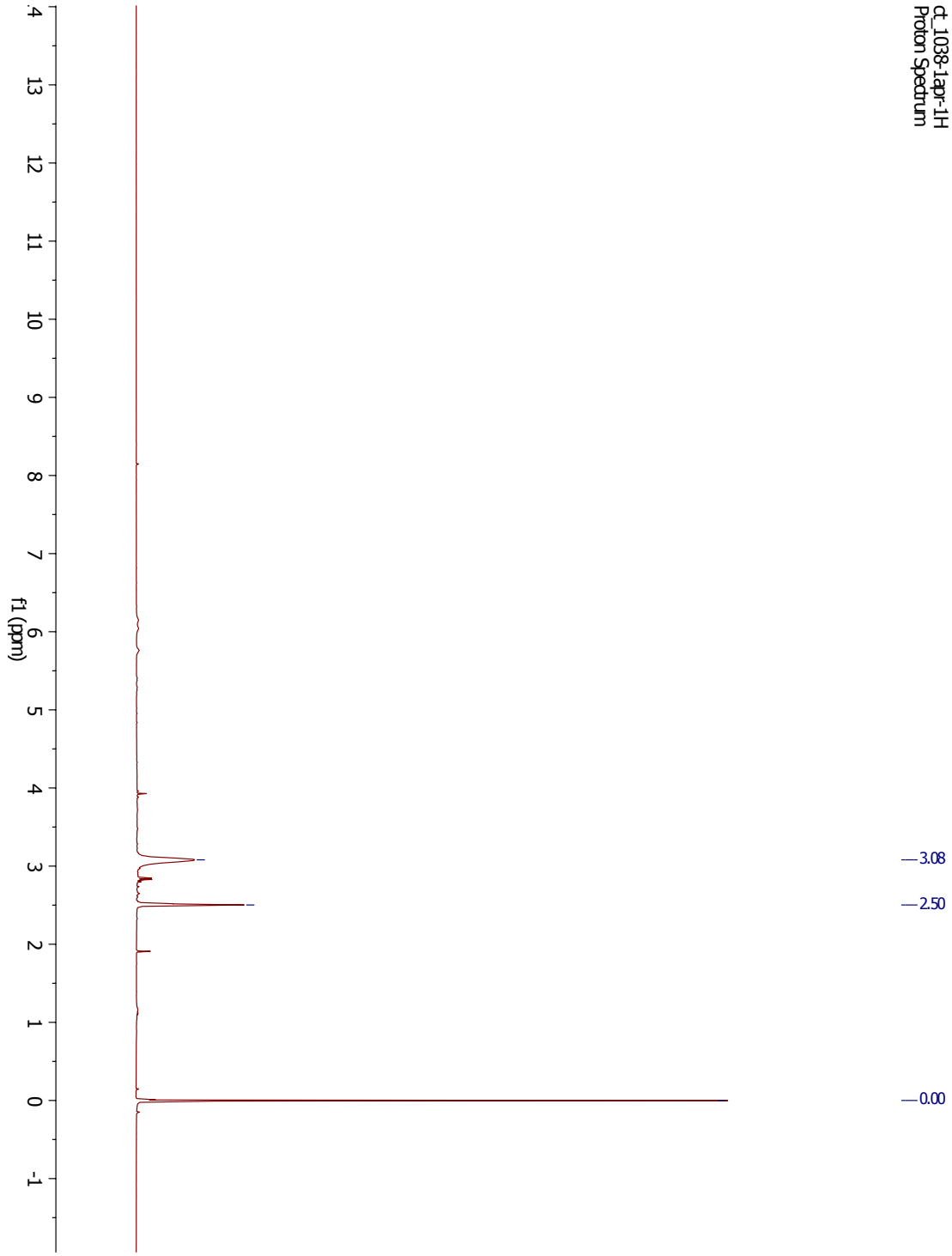

^{19}F NMR: **5a'** in DMSO

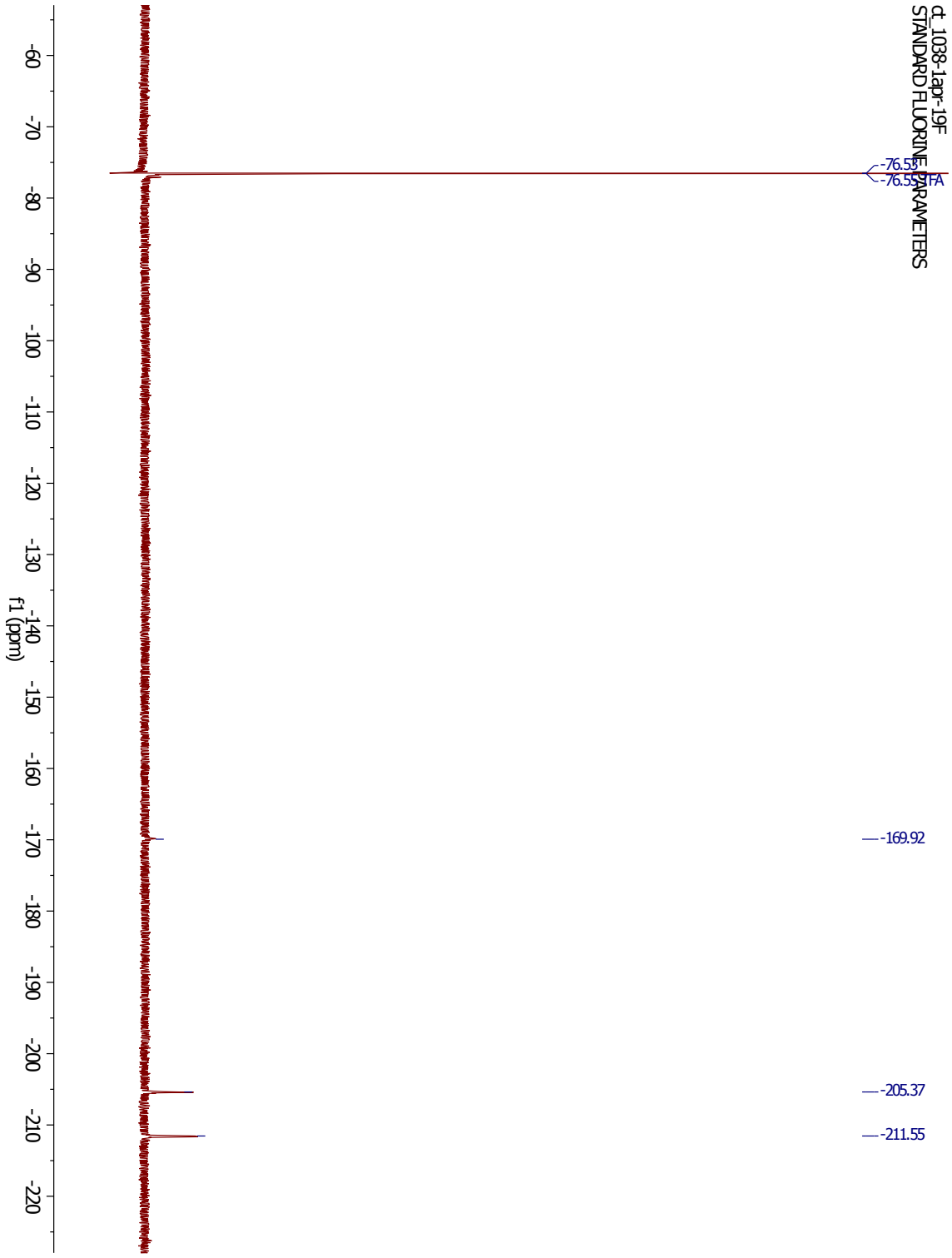

19F NMR: 5a’ in D2O

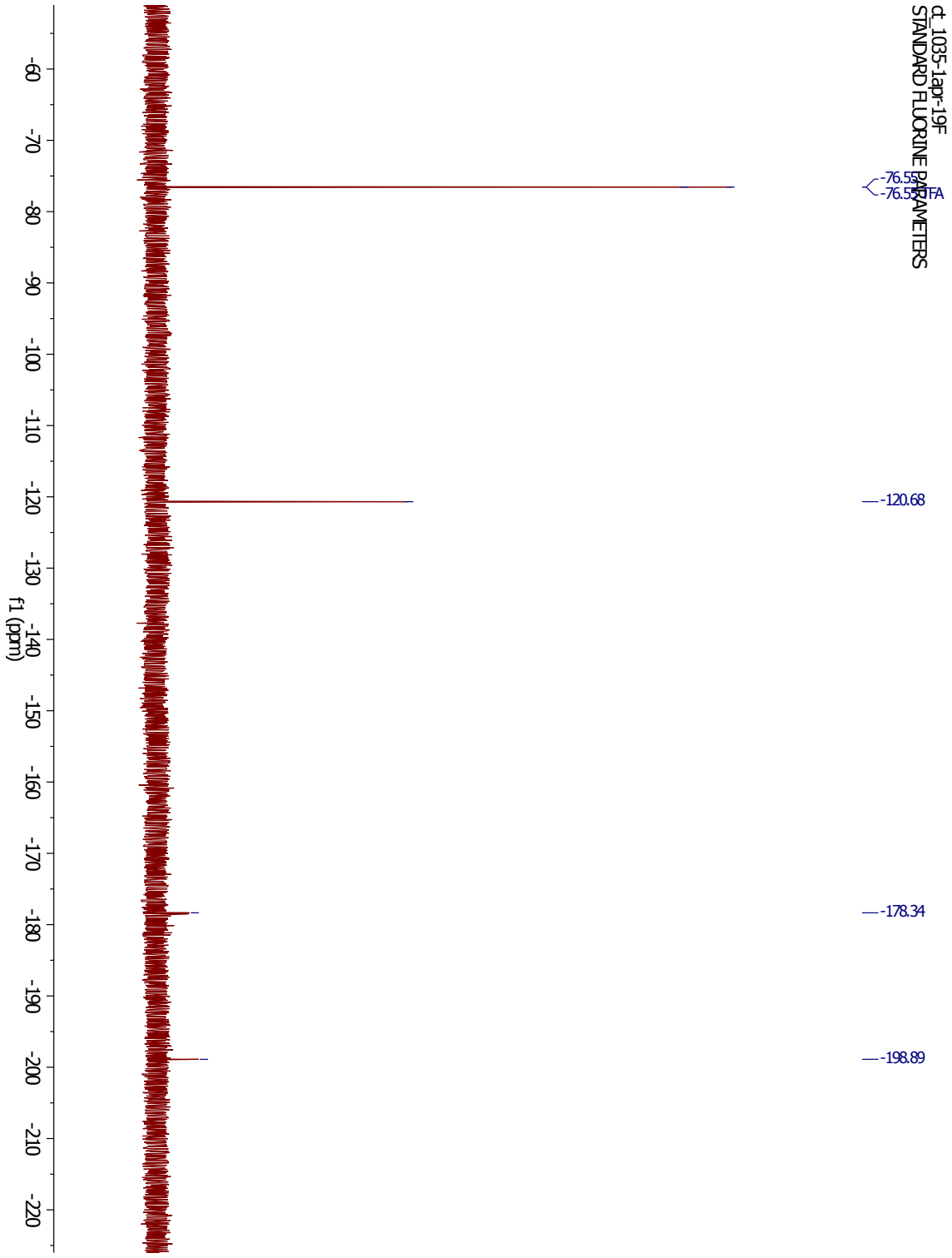

19F NMR: 5a’ in PBS / 10% D2O

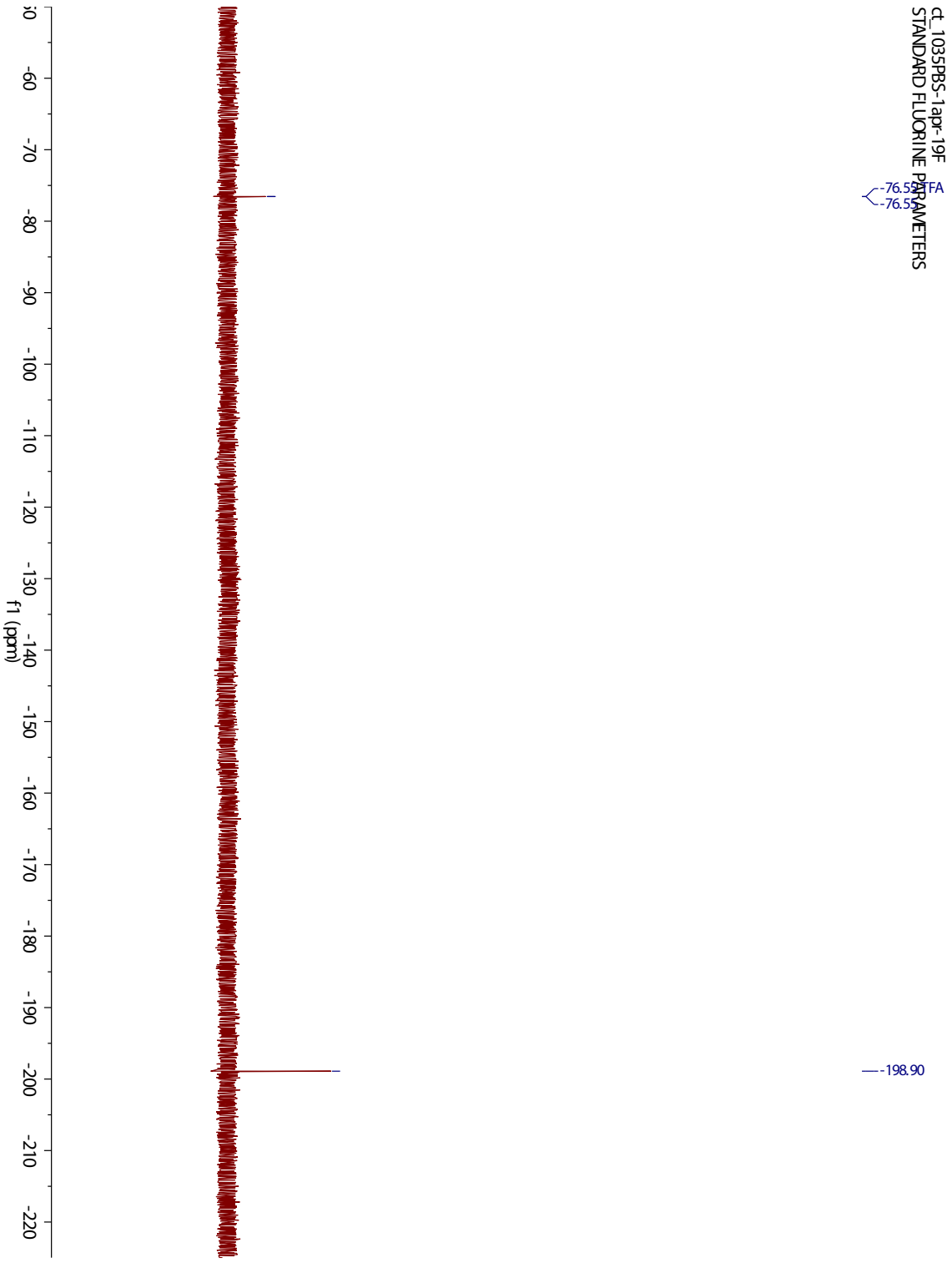

19F NMR 5a'-pep (5a' + MeOVal-CysSA-Cbz) in PBS / 10% D2O

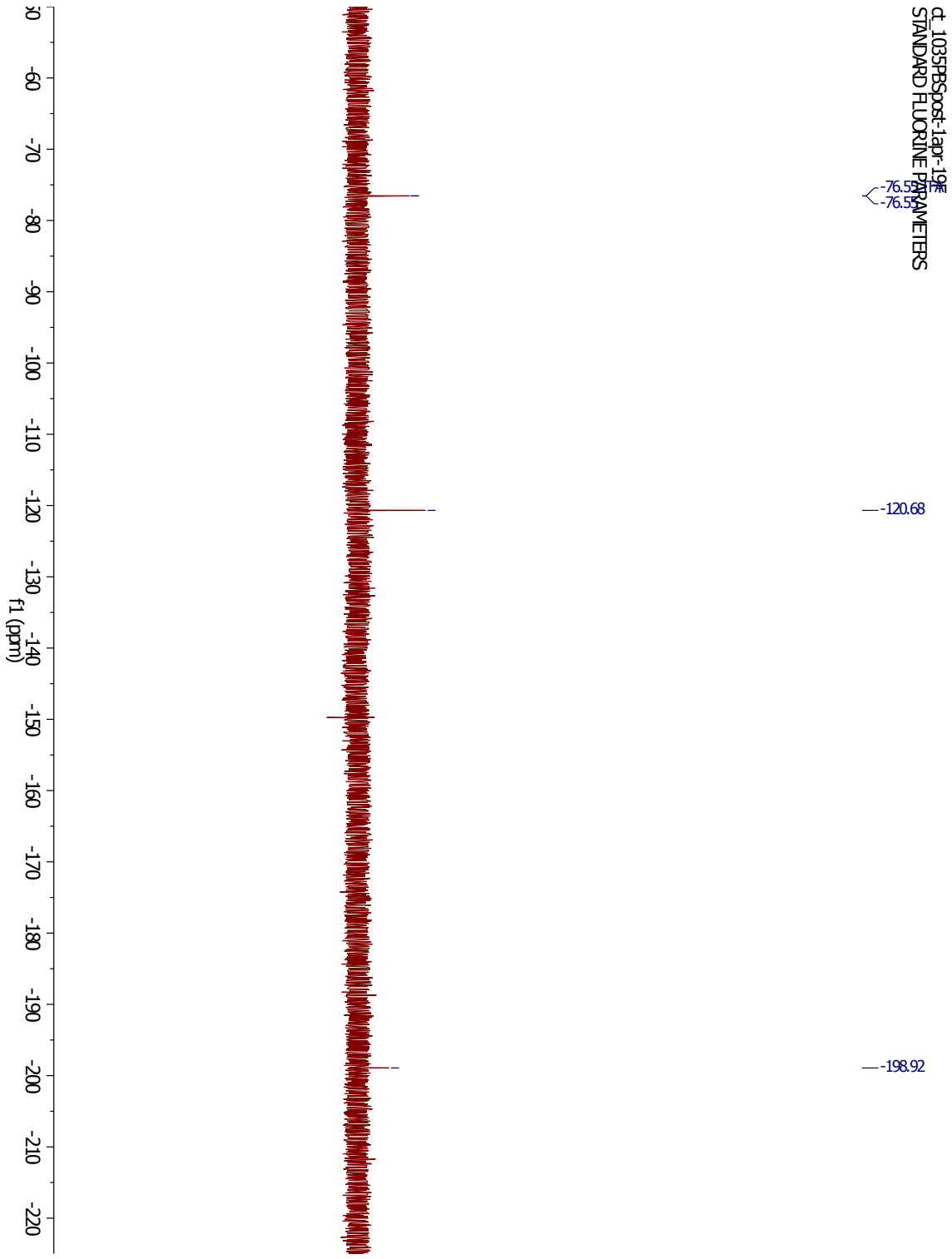

1H NMR: 6a in DMSO

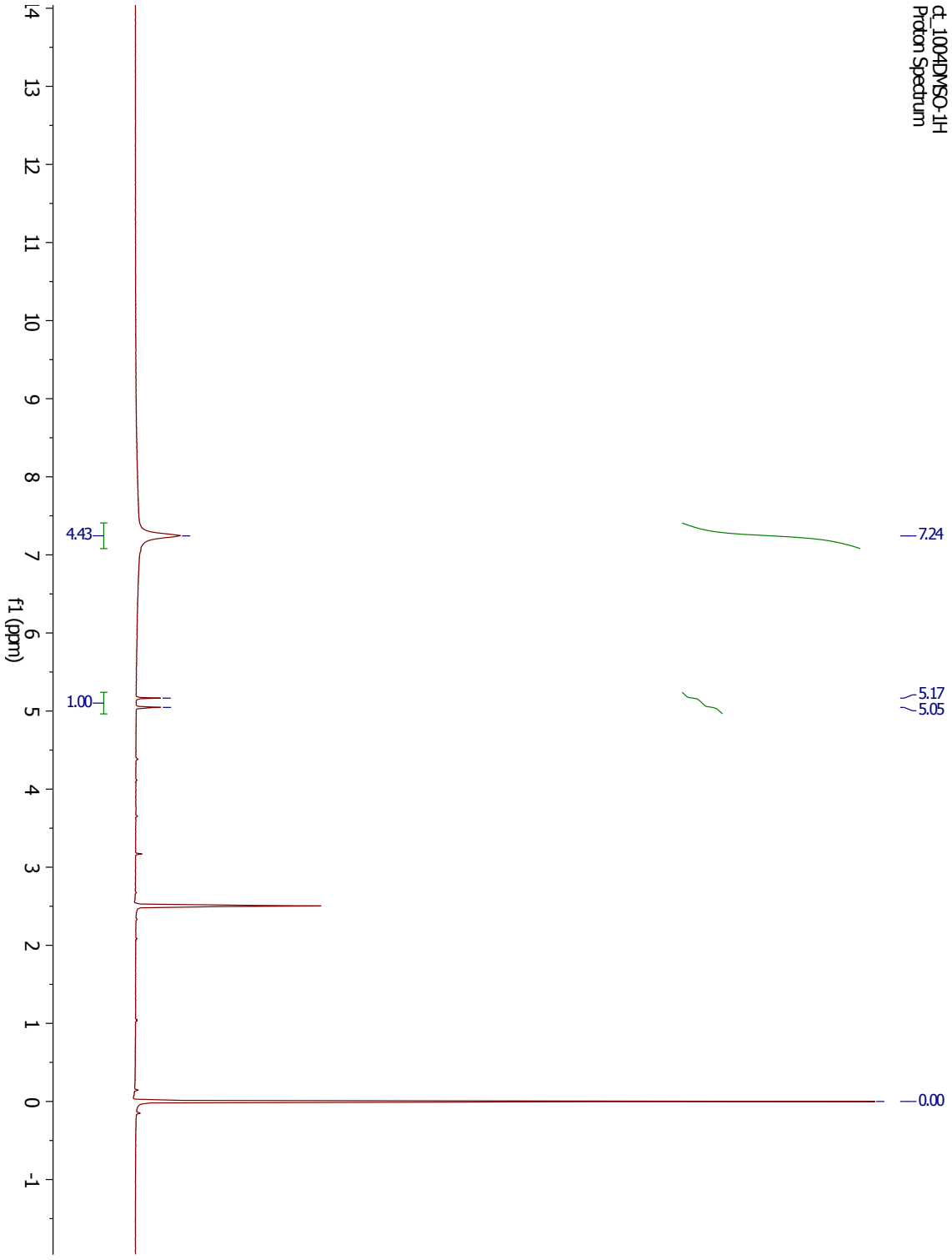

^{19}F NMR: **6a** in DMSO

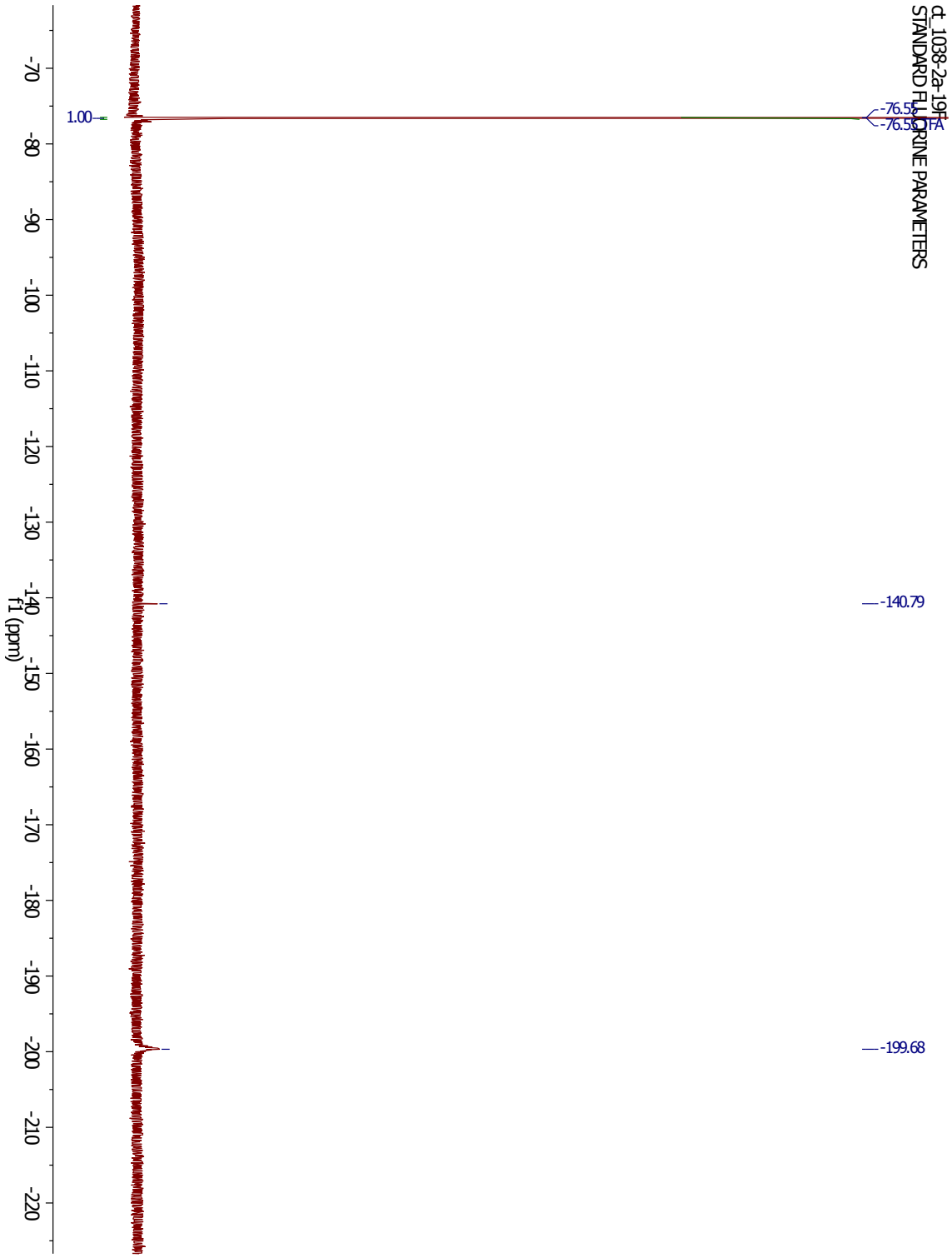

^{19}F NMR: **6a** in D_2O

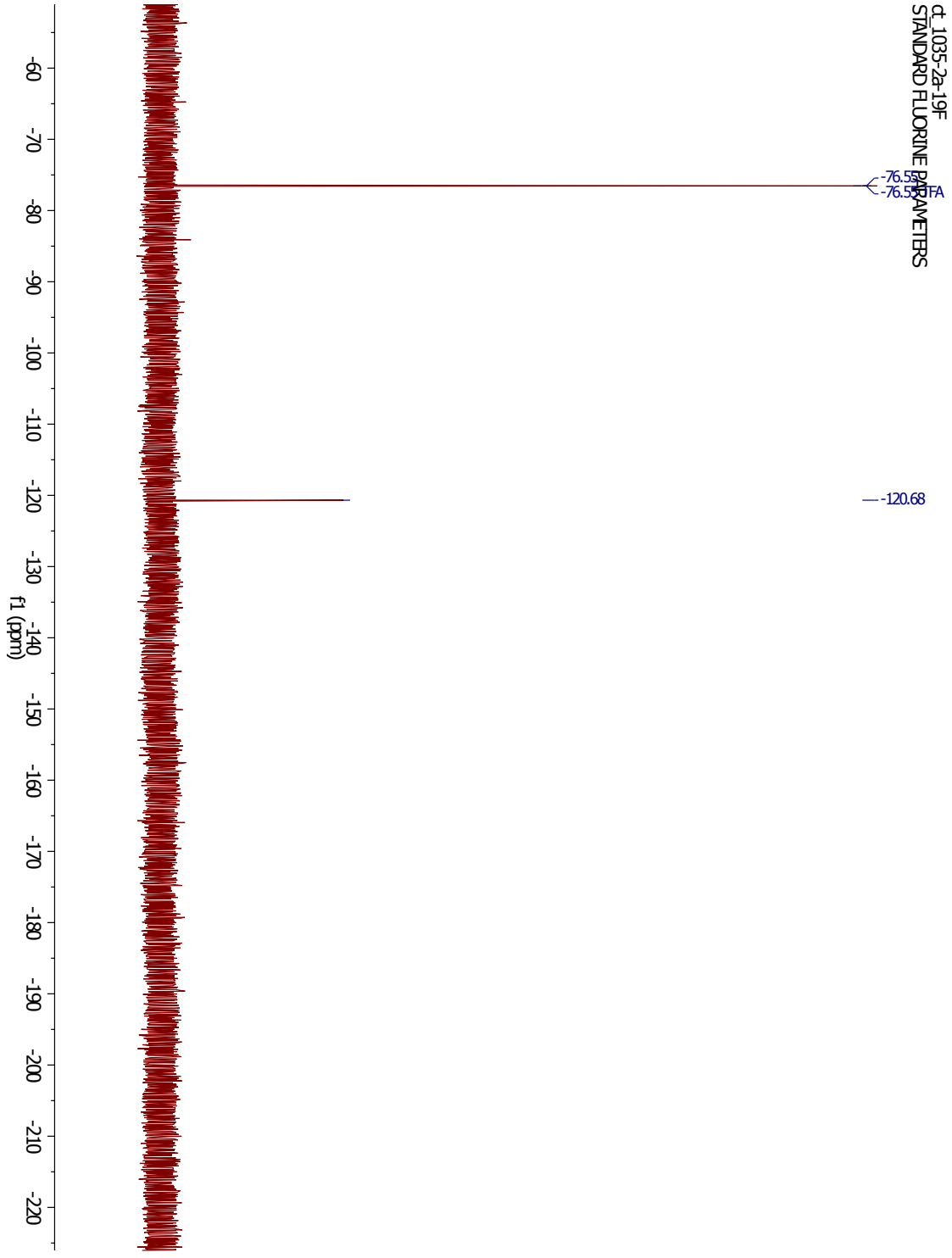

^{19}F NMR: **6a** in PBS / 10% D_2O

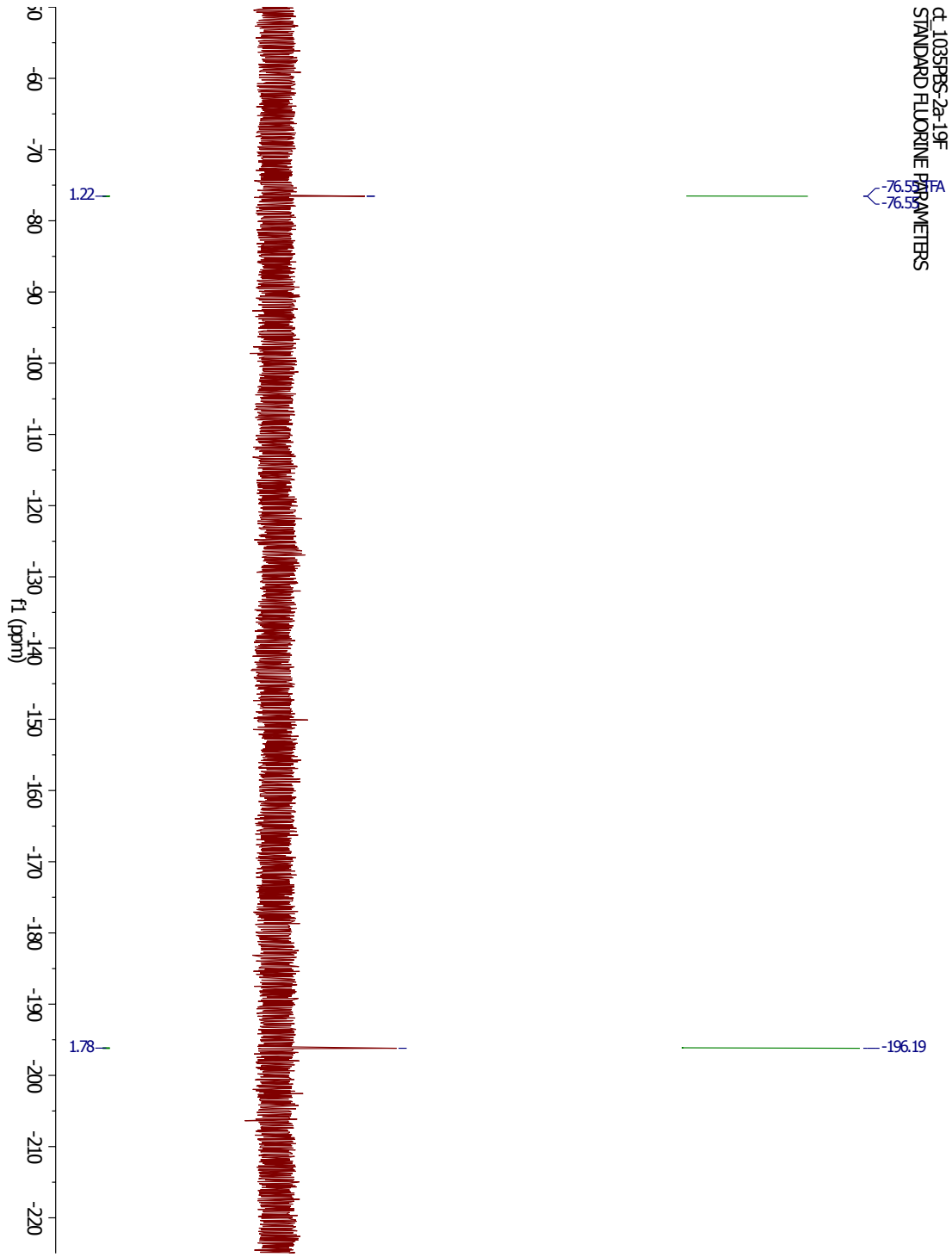

^{19}F NMR: **6a-pep** (**6a** + MeOVal-CysSA-Cbz) in PBS / 10% D_2O

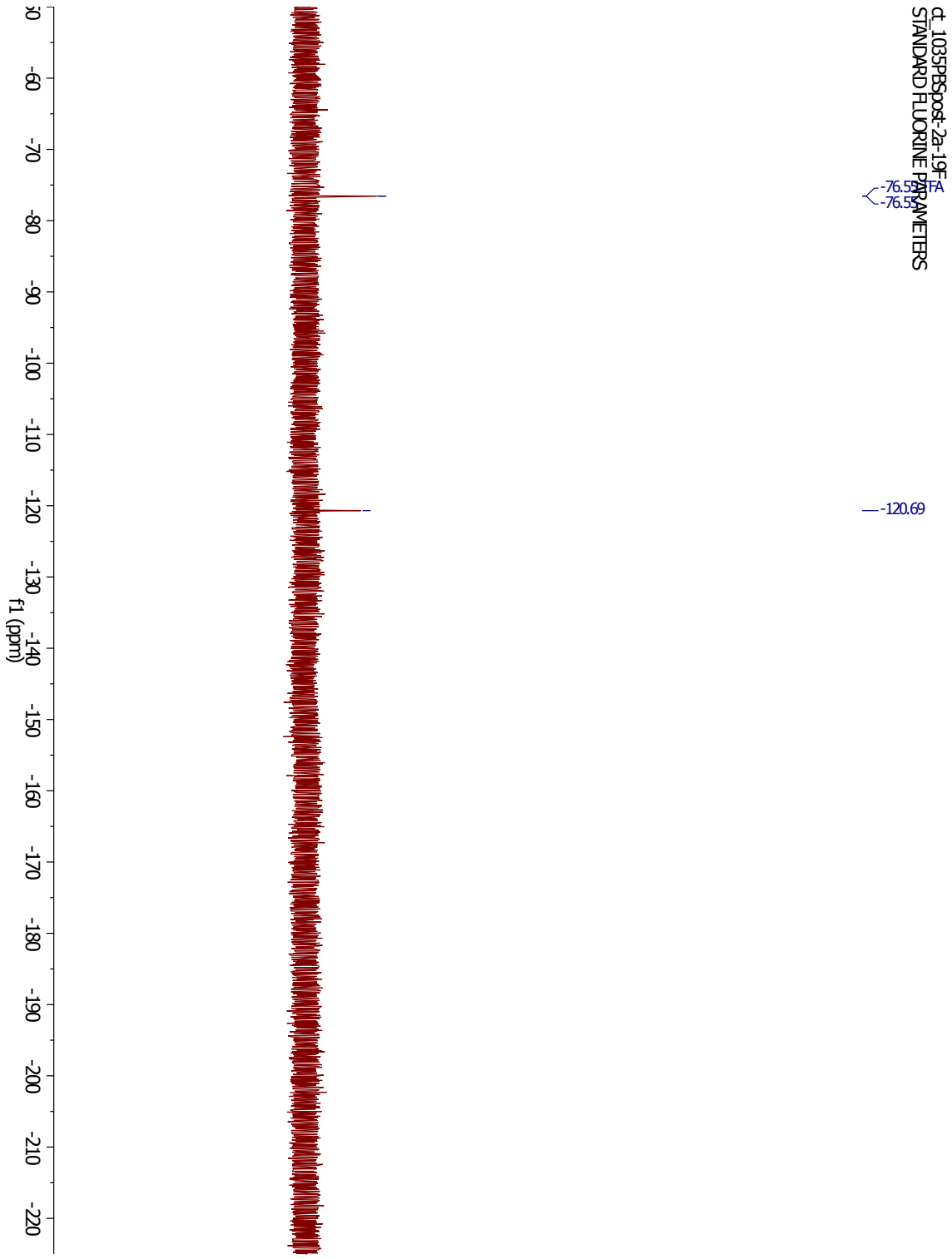

^{19}F NMR: **6a-pep** (**6a** + MeOVal-Cys-Cbz) in PBS / 10% D_2O after 5 min

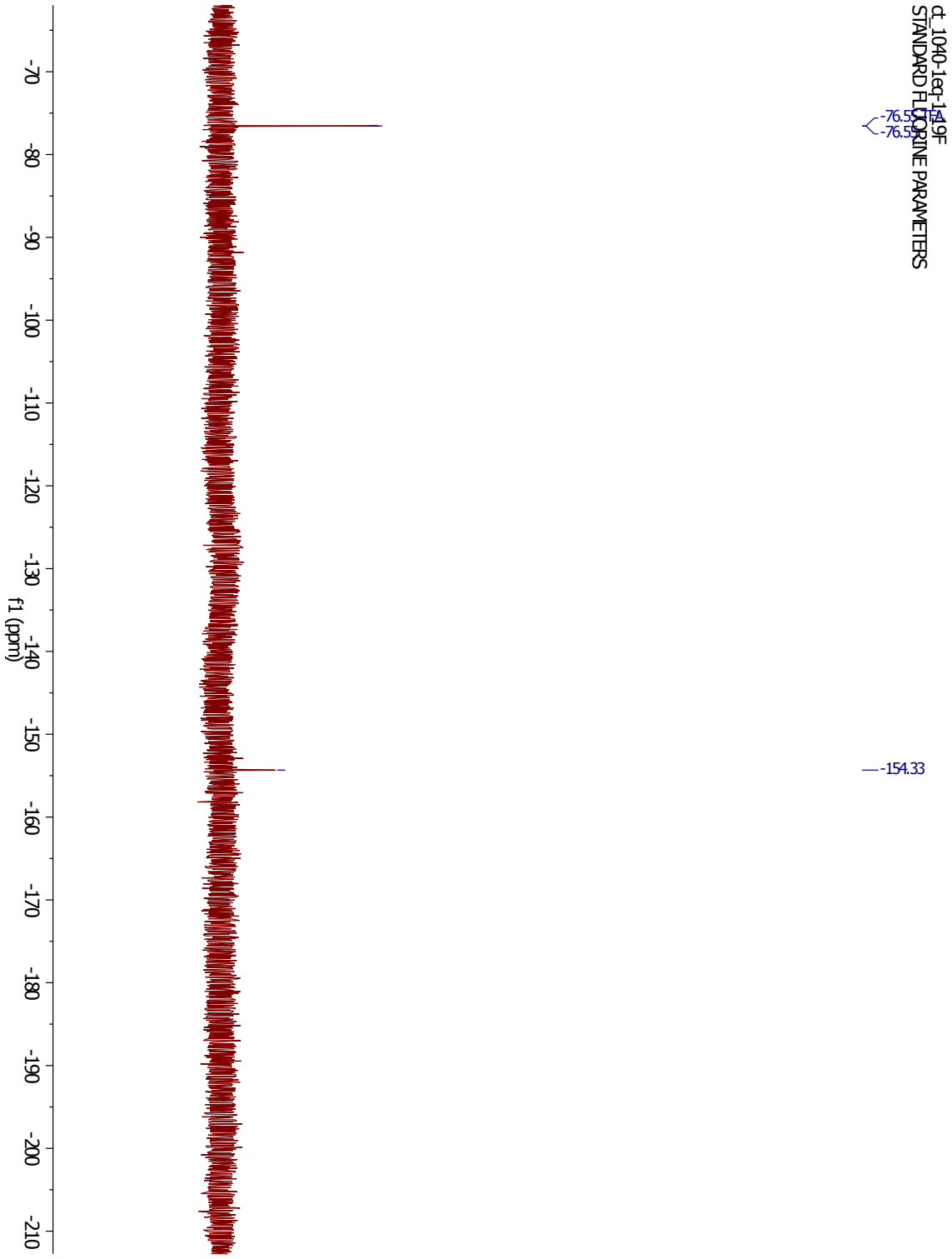

^{1}H NMR: **7a** in DMSO

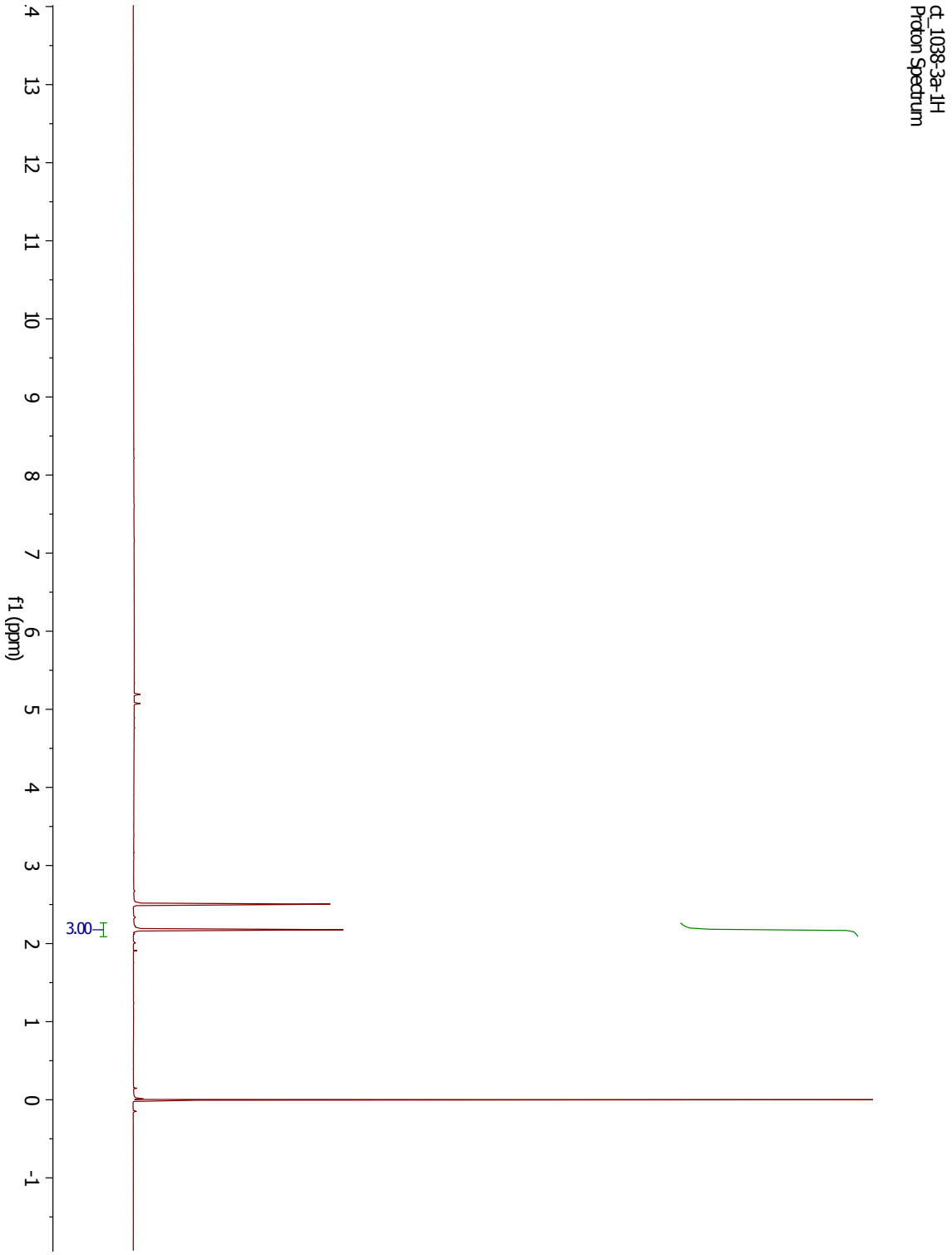

^{19}F NMR: **7a** in DMSO

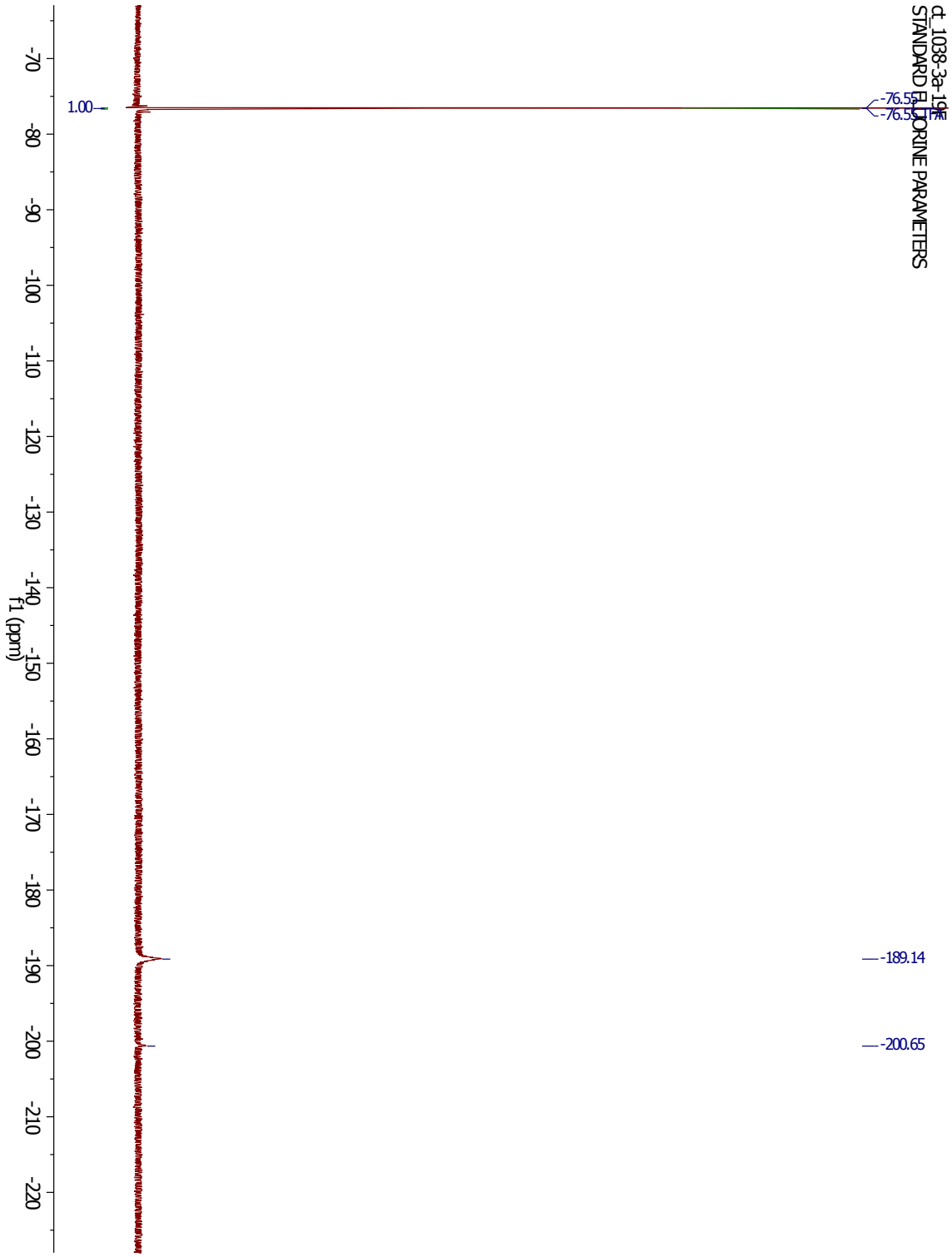

^{19}F NMR: **7a** in D_2O

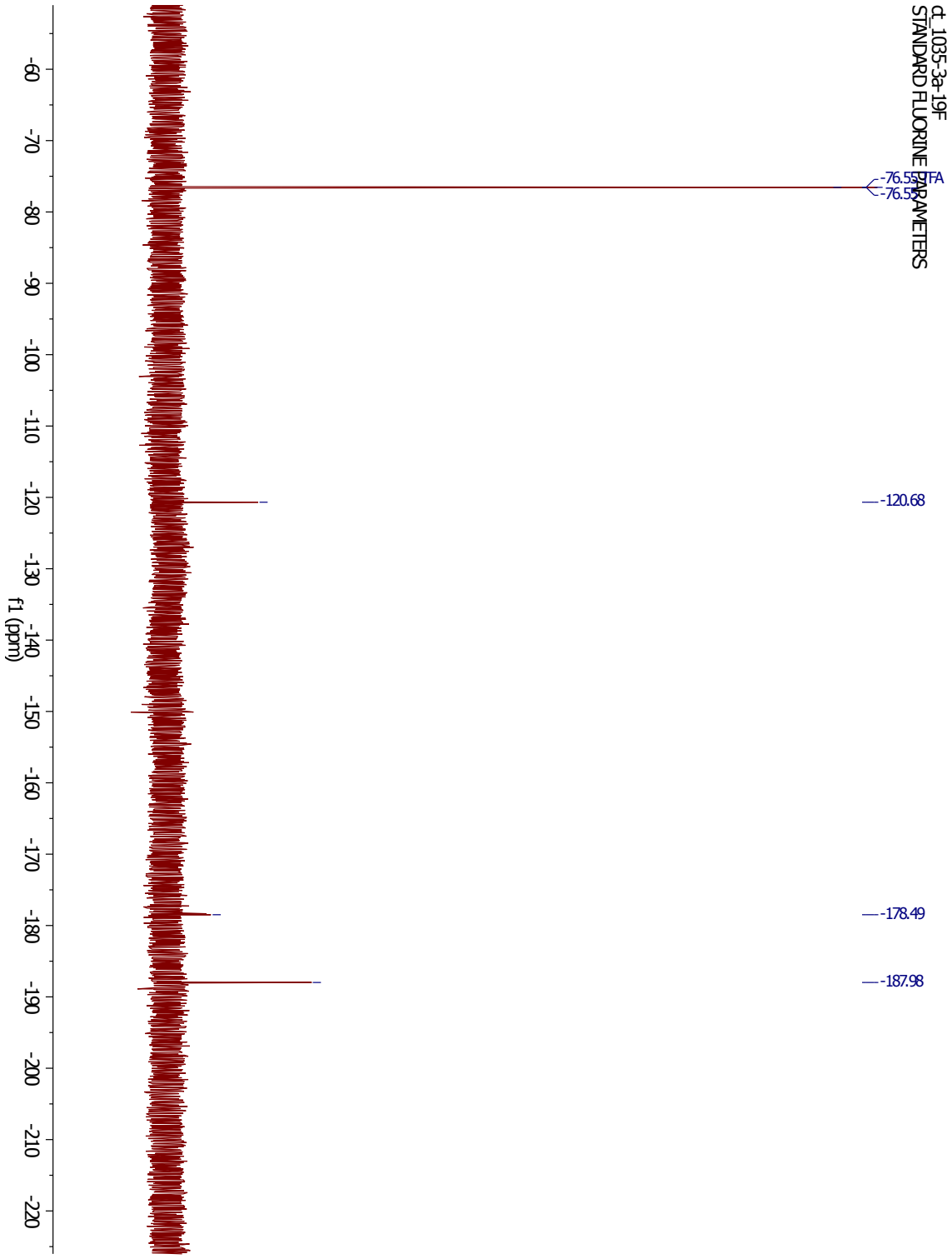

^{19}F NMR: **7a** in PBS / 10% D_2O

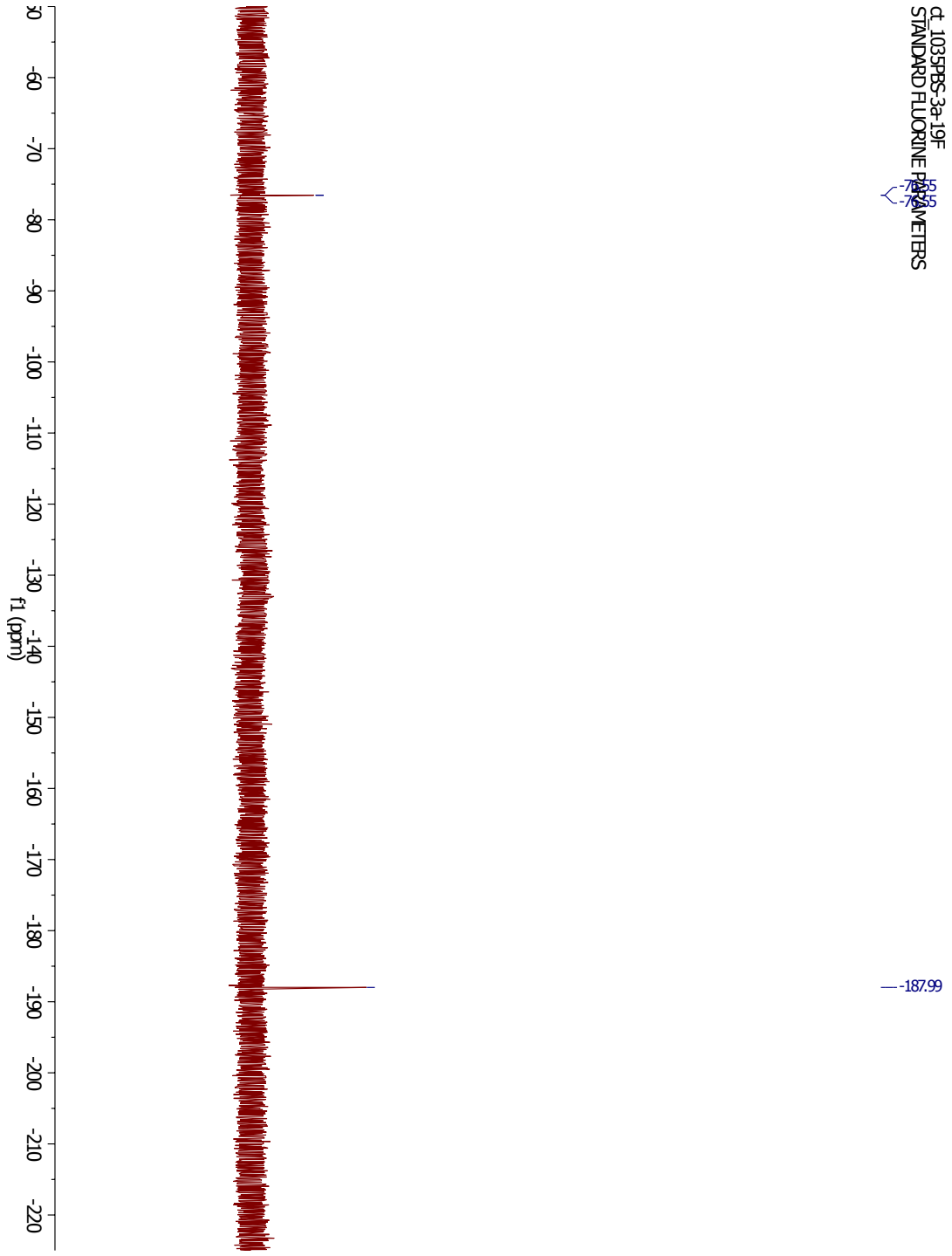

^{19}F NMR: **7a-pep** (**7a** + MeOVal-CysSA-Cbz) in PBS / 10% D_2O

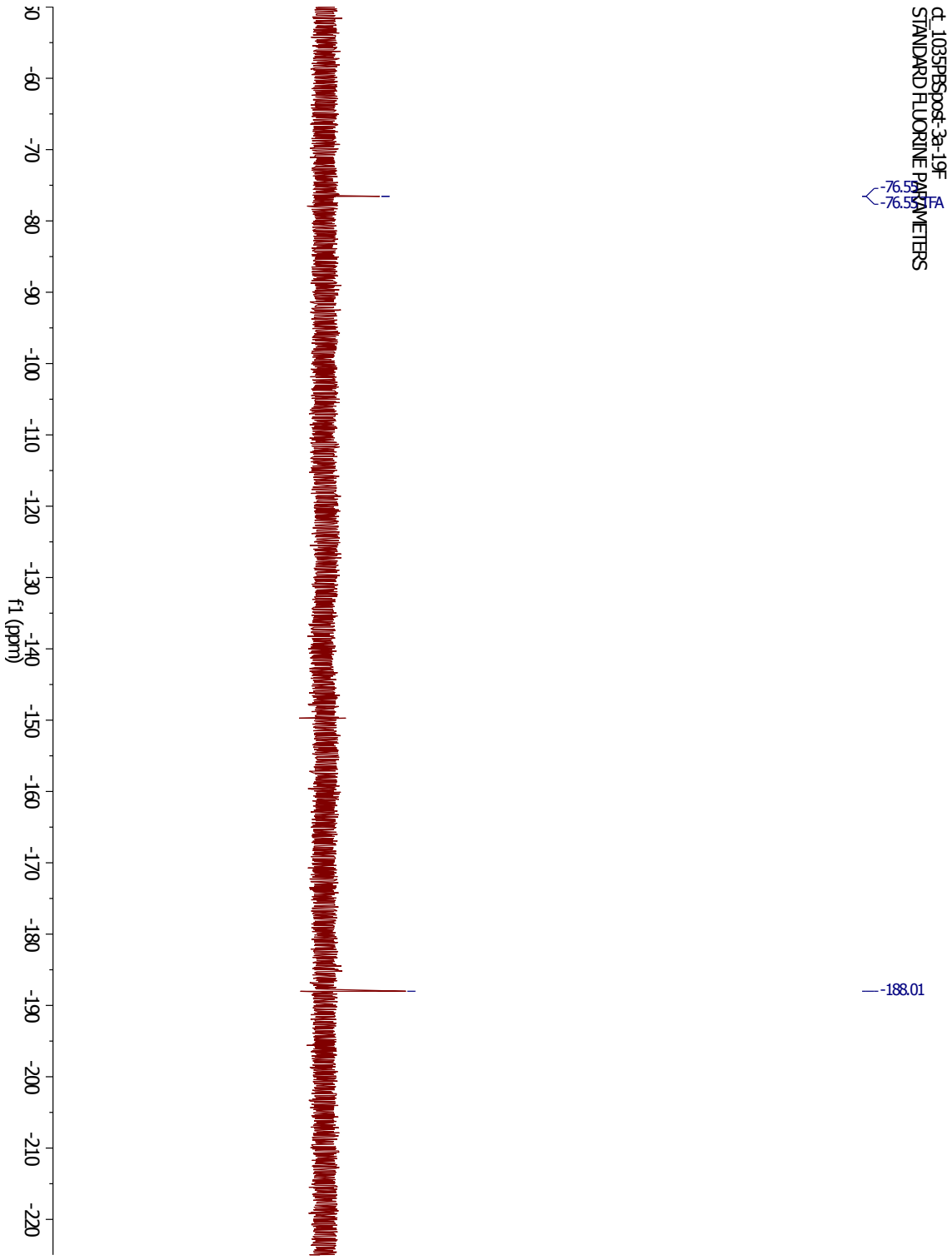

^{1}H NMR: **5b** in DMSO

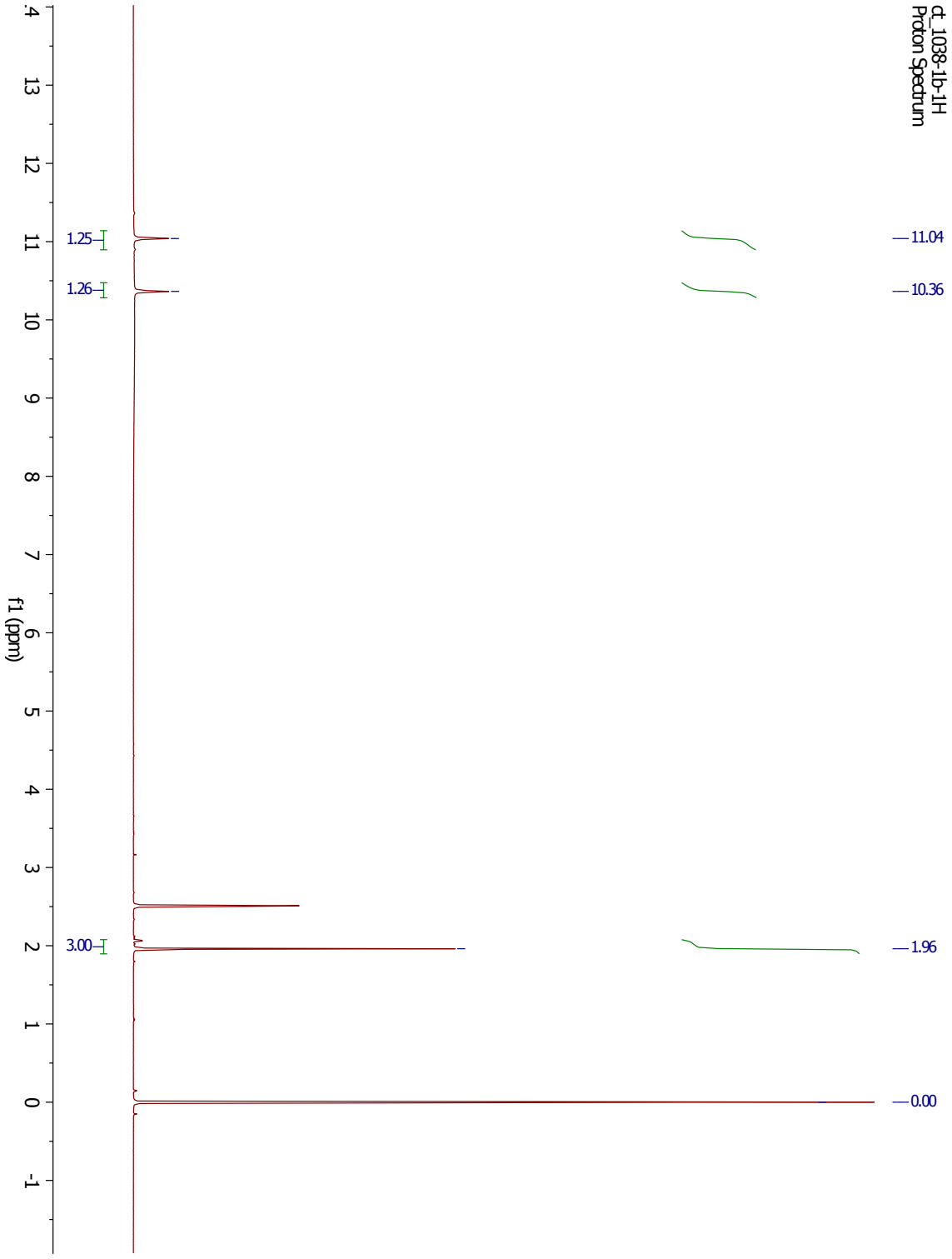

^{19}F NMR: **5b** in D_2O

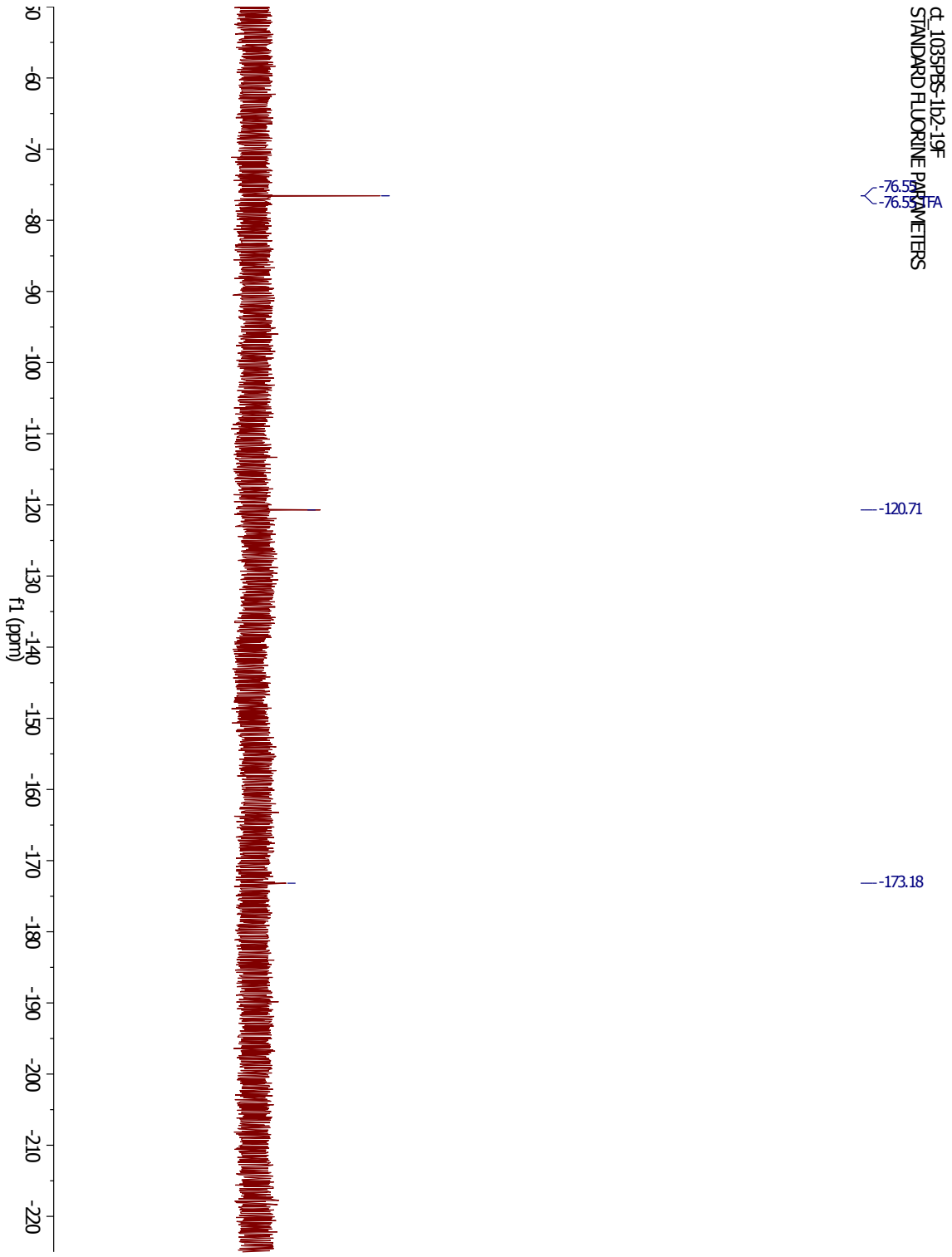

^{19}F NMR: **5b** in PBS / 10% D_2O

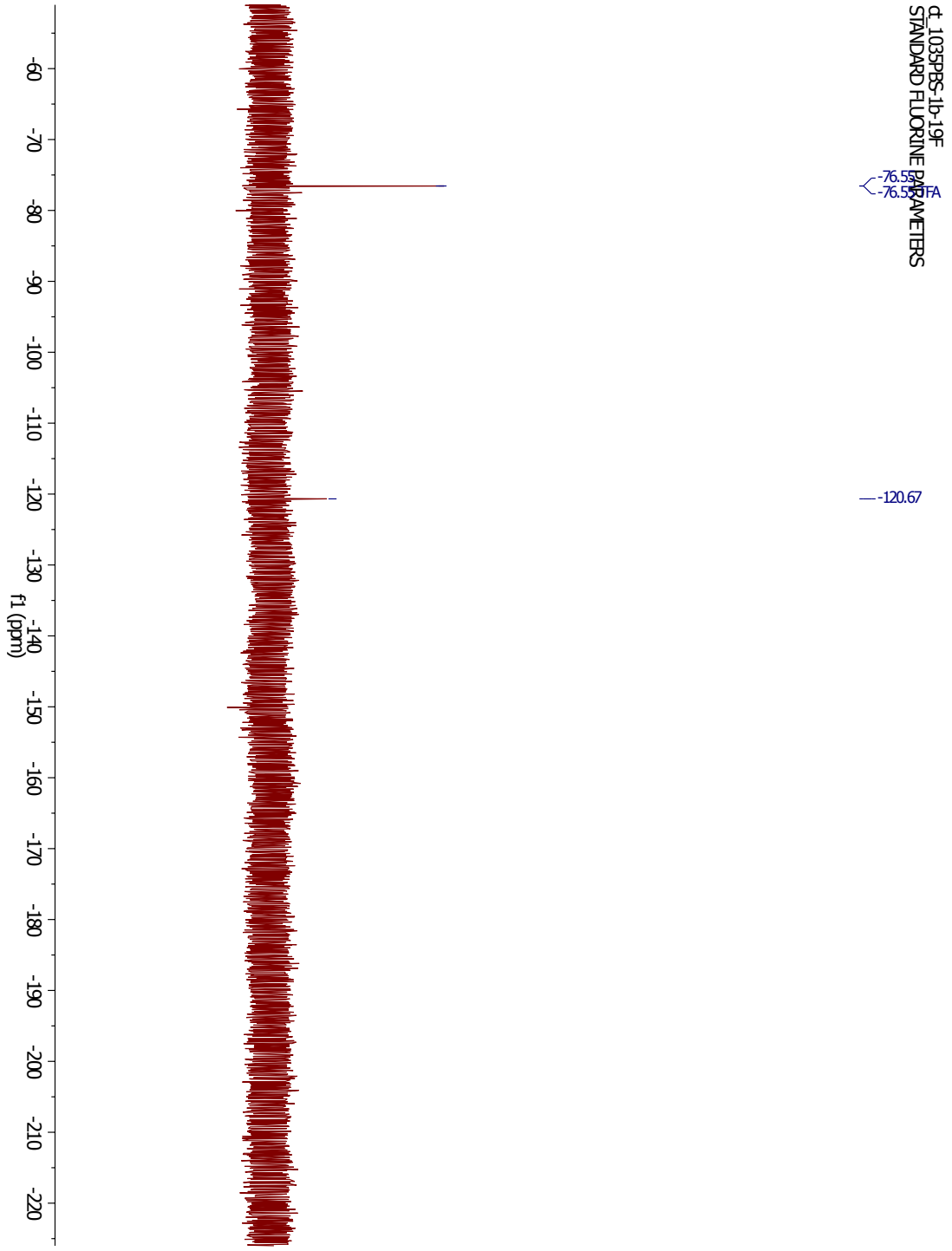

^{19}F NMR: **5b-pep** (**5b** + MeOVal-CysSA-Cbz) in PBS / 10% D_2O

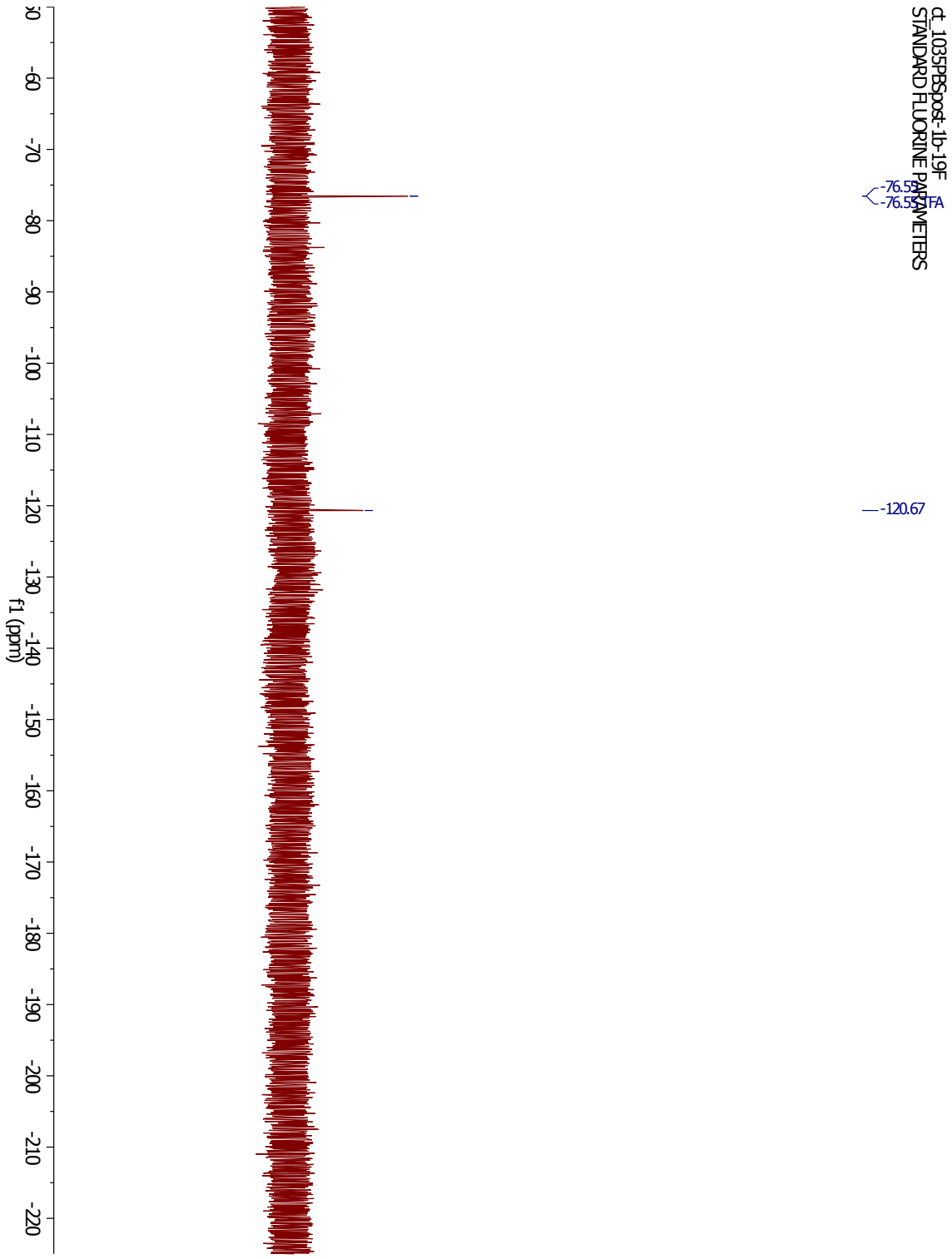

^{19}F NMR: PyrSEt + 6a

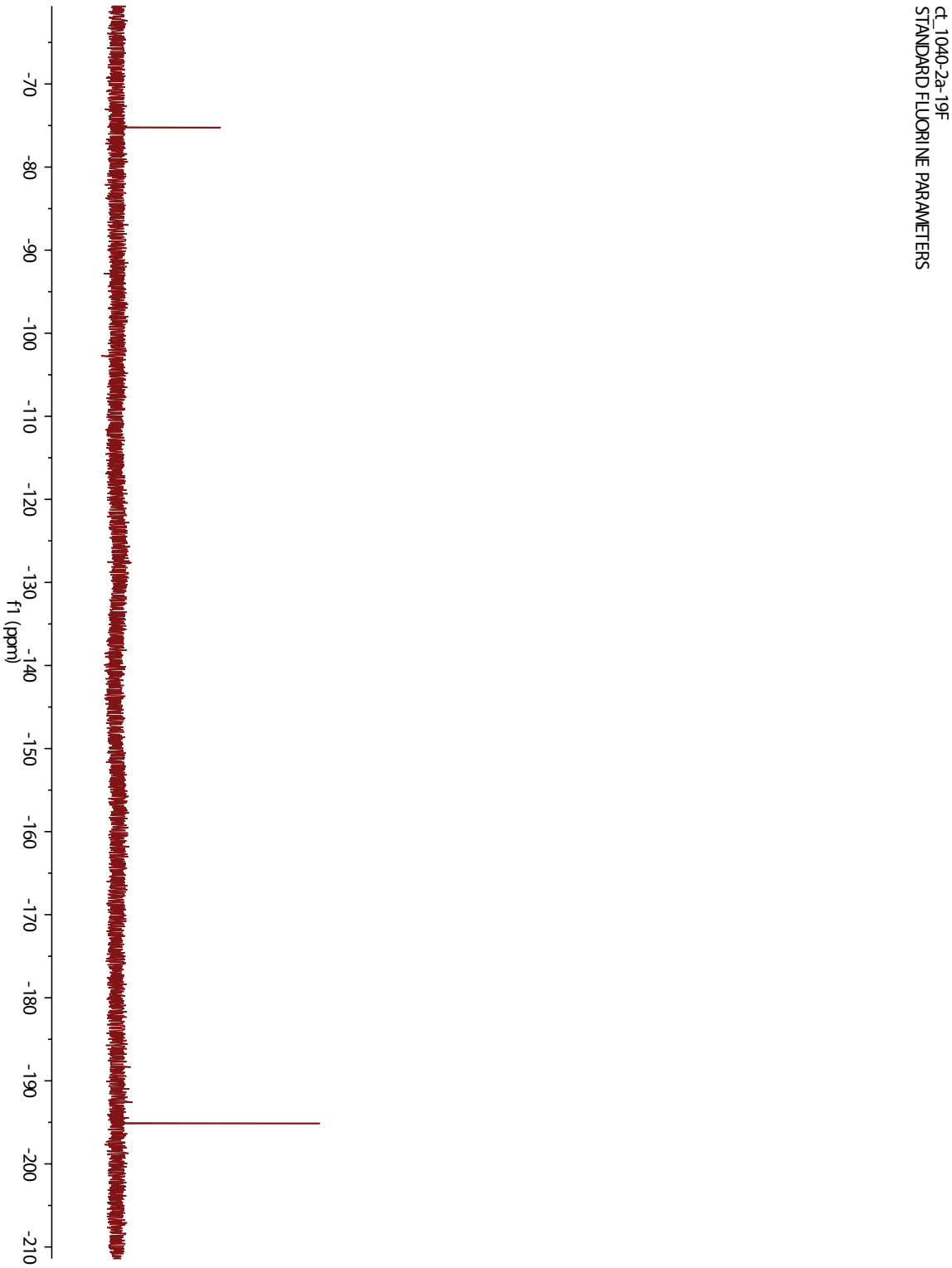

^{19}F NMR: BL21 cell lysates o/e AhpcC166S + NaSH (1 mM) + 6a (1 mM)

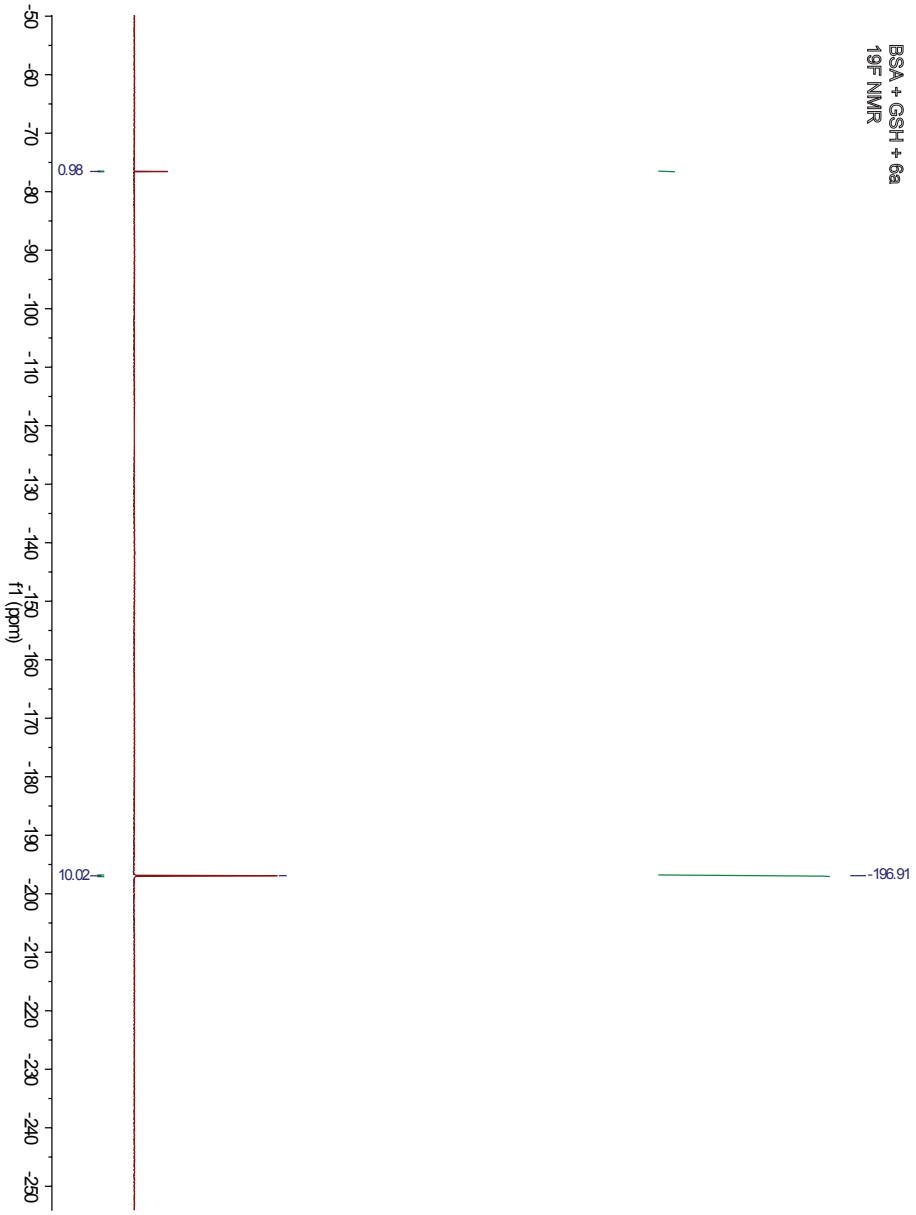

^{19}F: NMR. BL21 cell lysates o/e AhpcC166S + NaSH (1 mM) + 6a (1 mM)

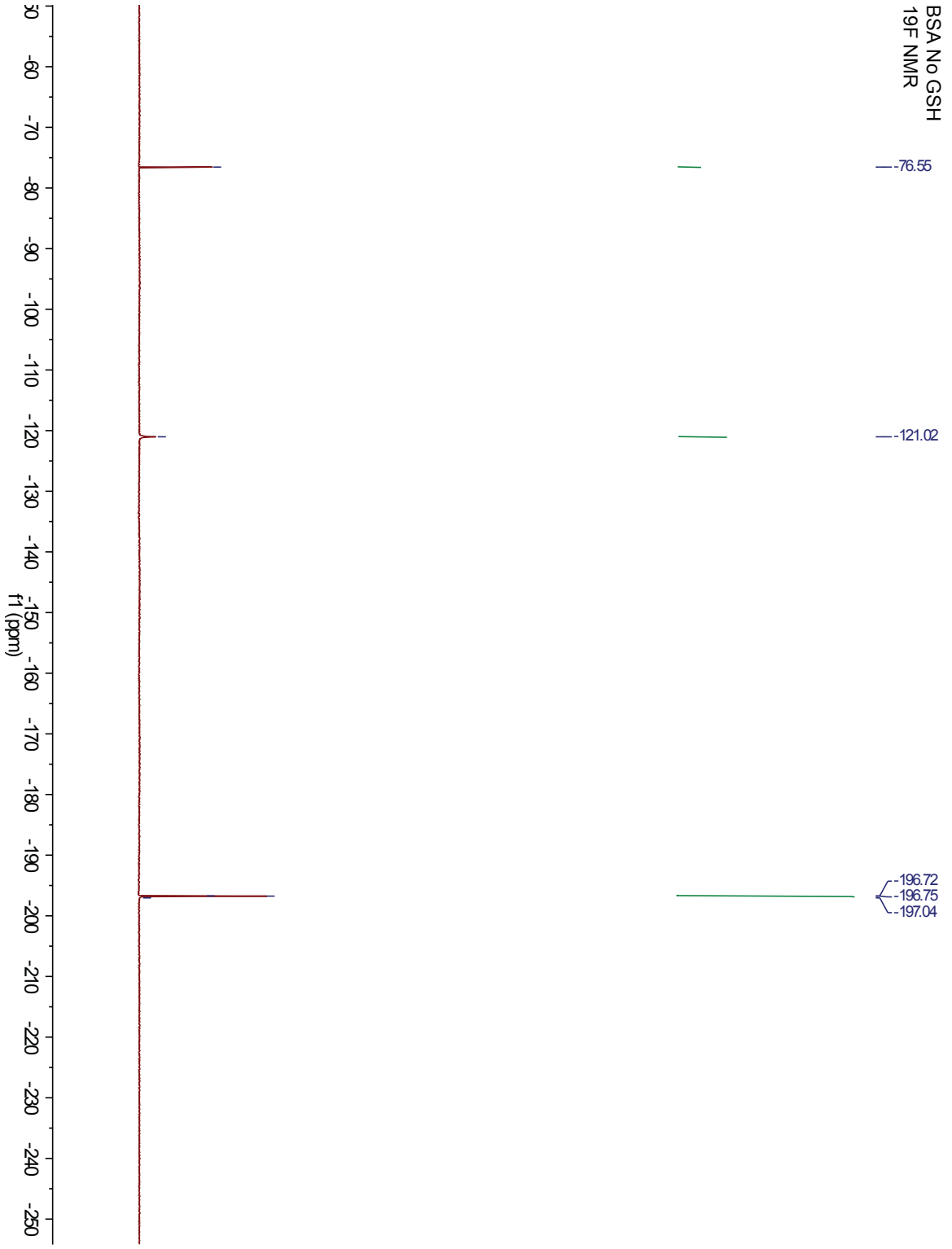

^{19}F NMR: BL21 cell lysates o/e AhpcC166S, fluorine background

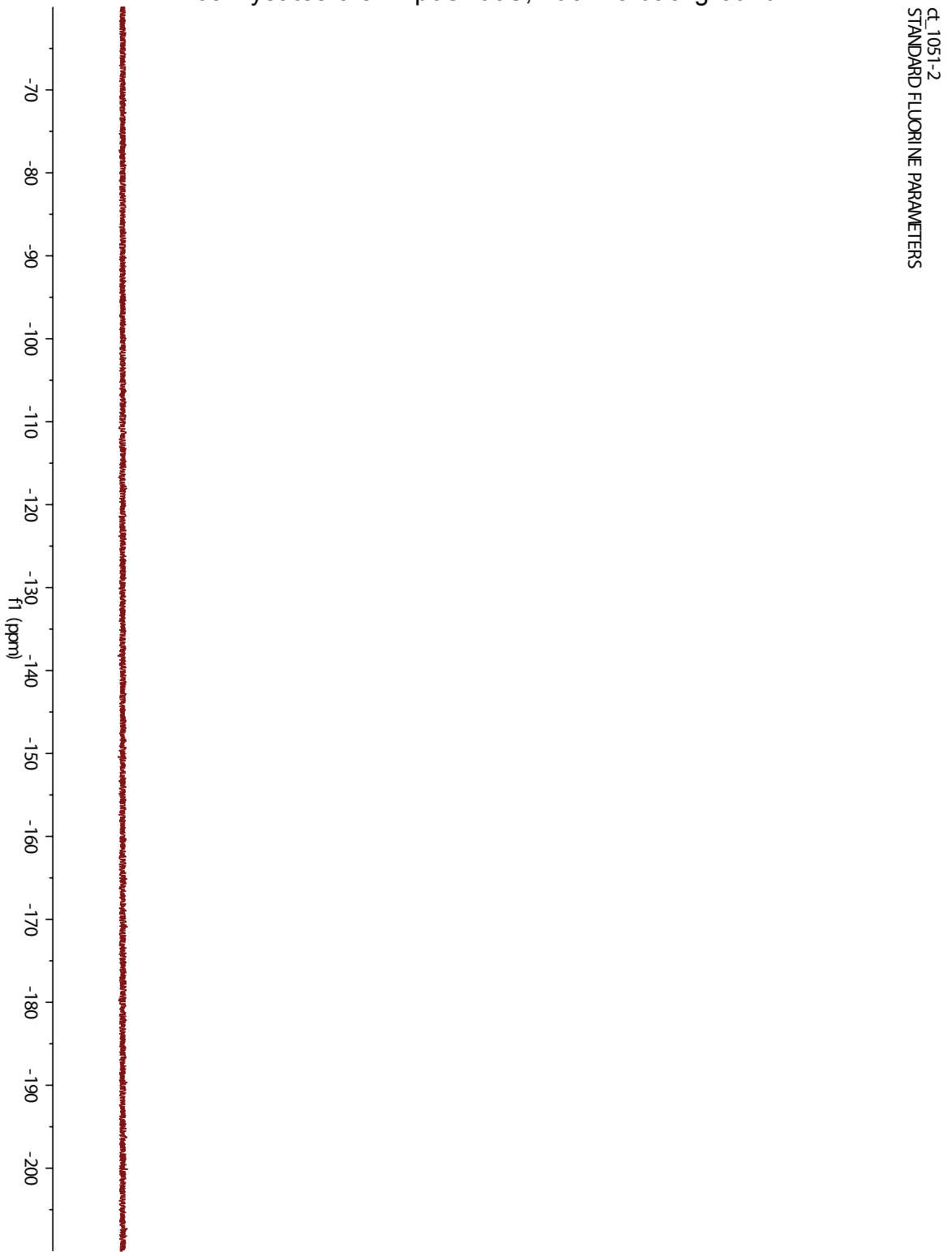

^{19}F NMR: 6a in PBS, stability

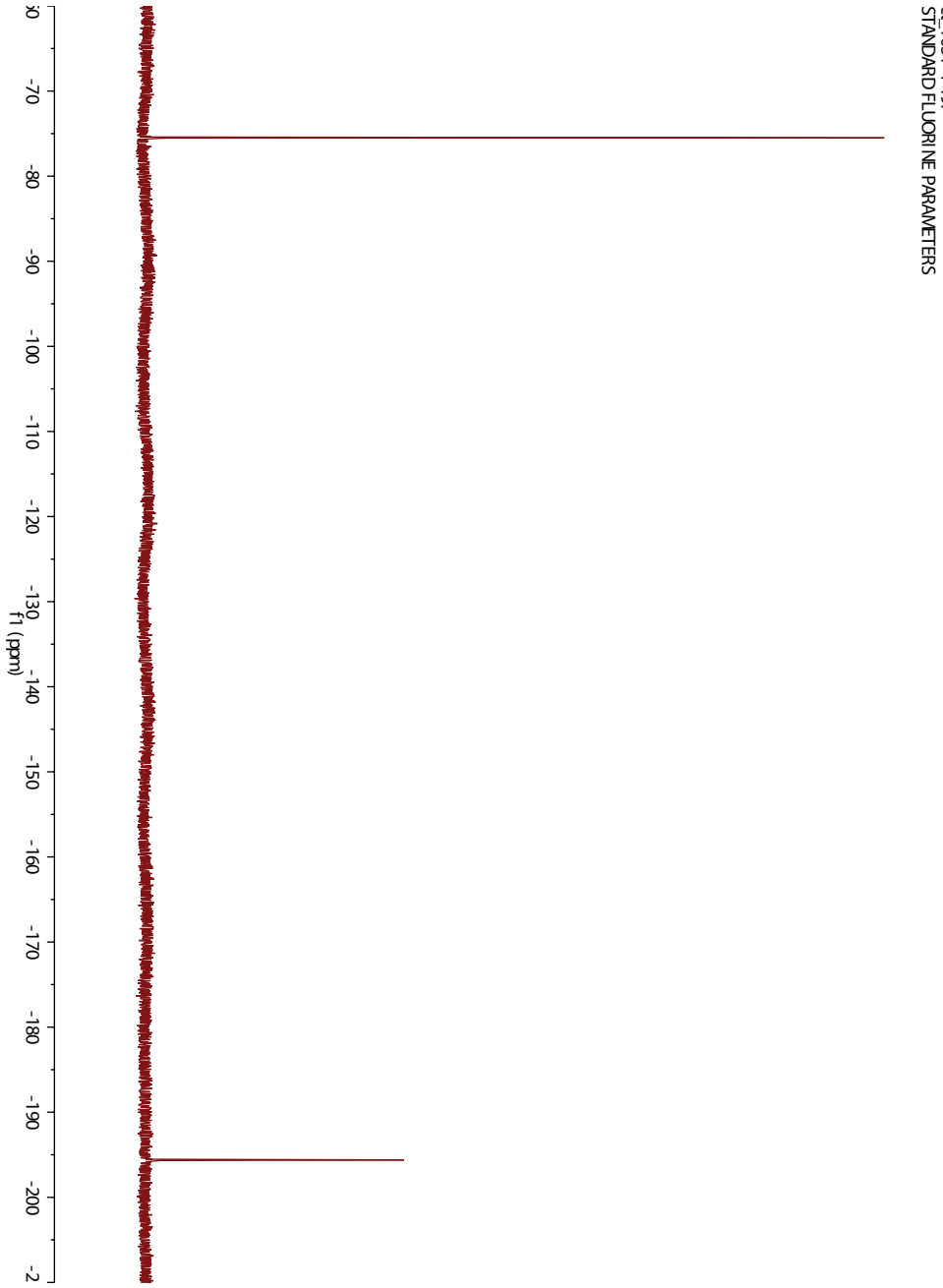

^{19}F NMR: BL21 cell lysates o/e AhpcC WT + GSH + 6a in PBS

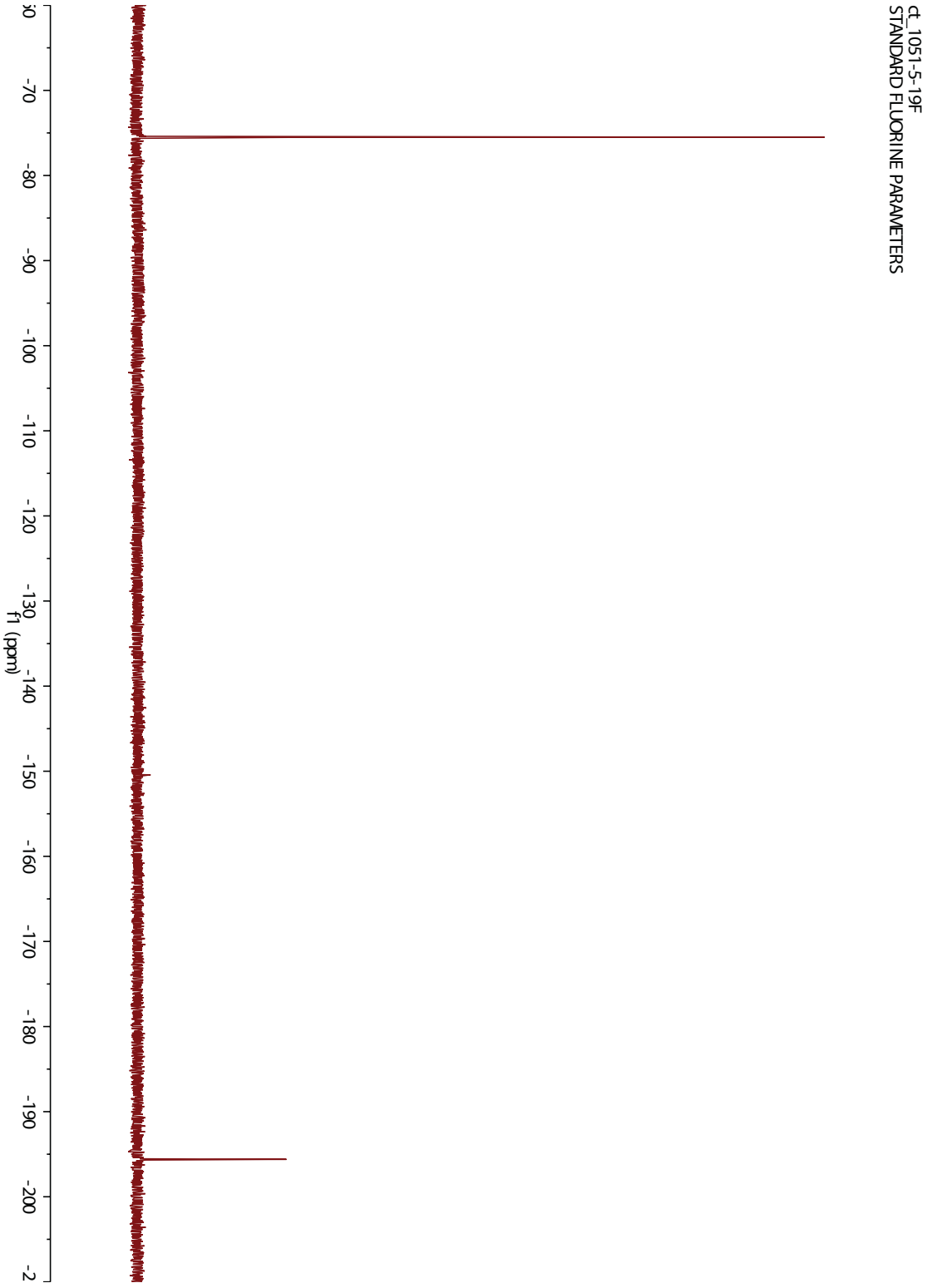

^{19}F NMR: BL21 cell lysates o/e AhpcC WT - GSH + 6a in PBS

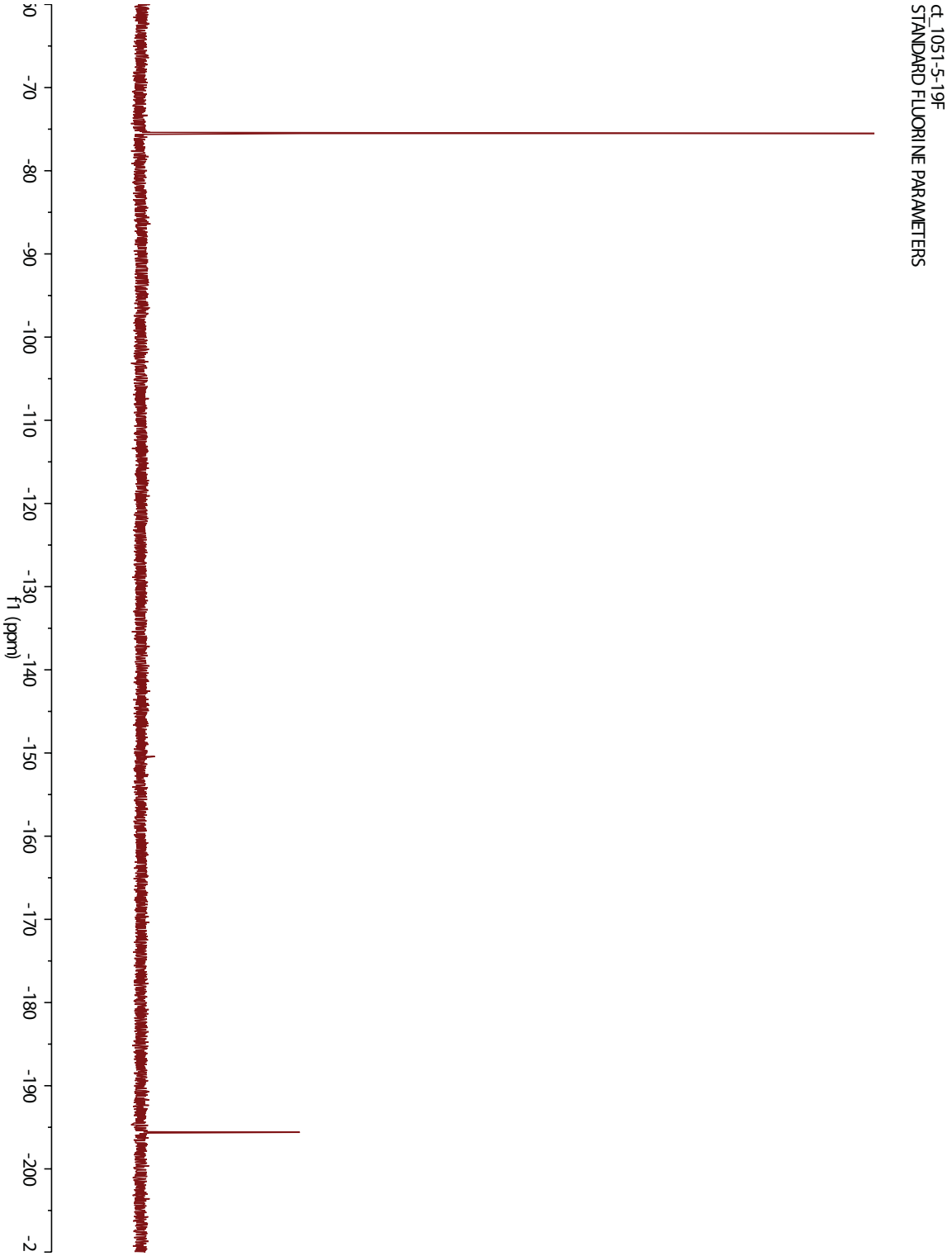

^{19}F NMR: BL21 cell lysates o/e AhpcC C166S + GSH + 6a in PBS

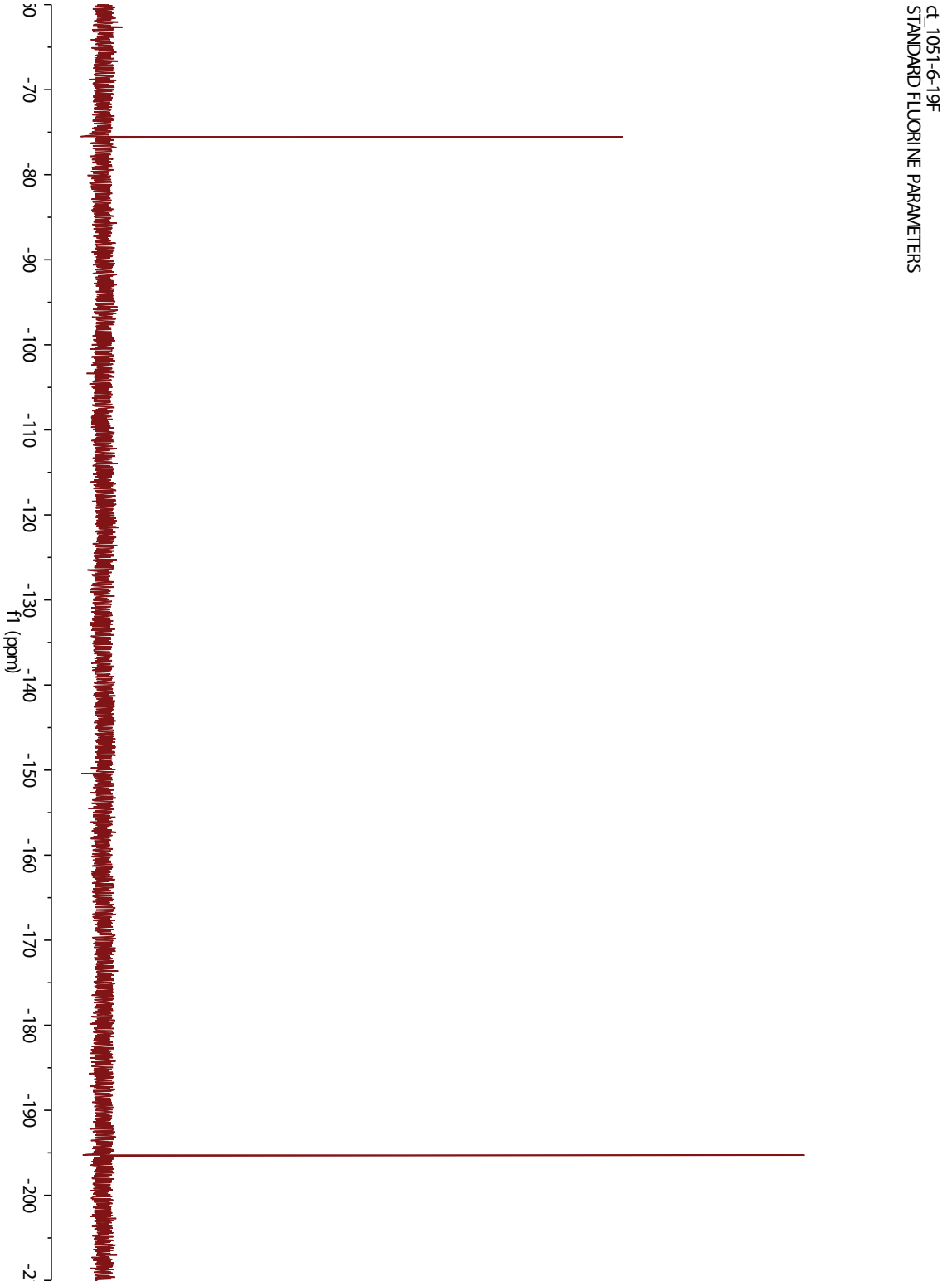

^{19}F NMR: BL21 cell lysates o/e AhpcC C166S - GSH + 6a in PBS

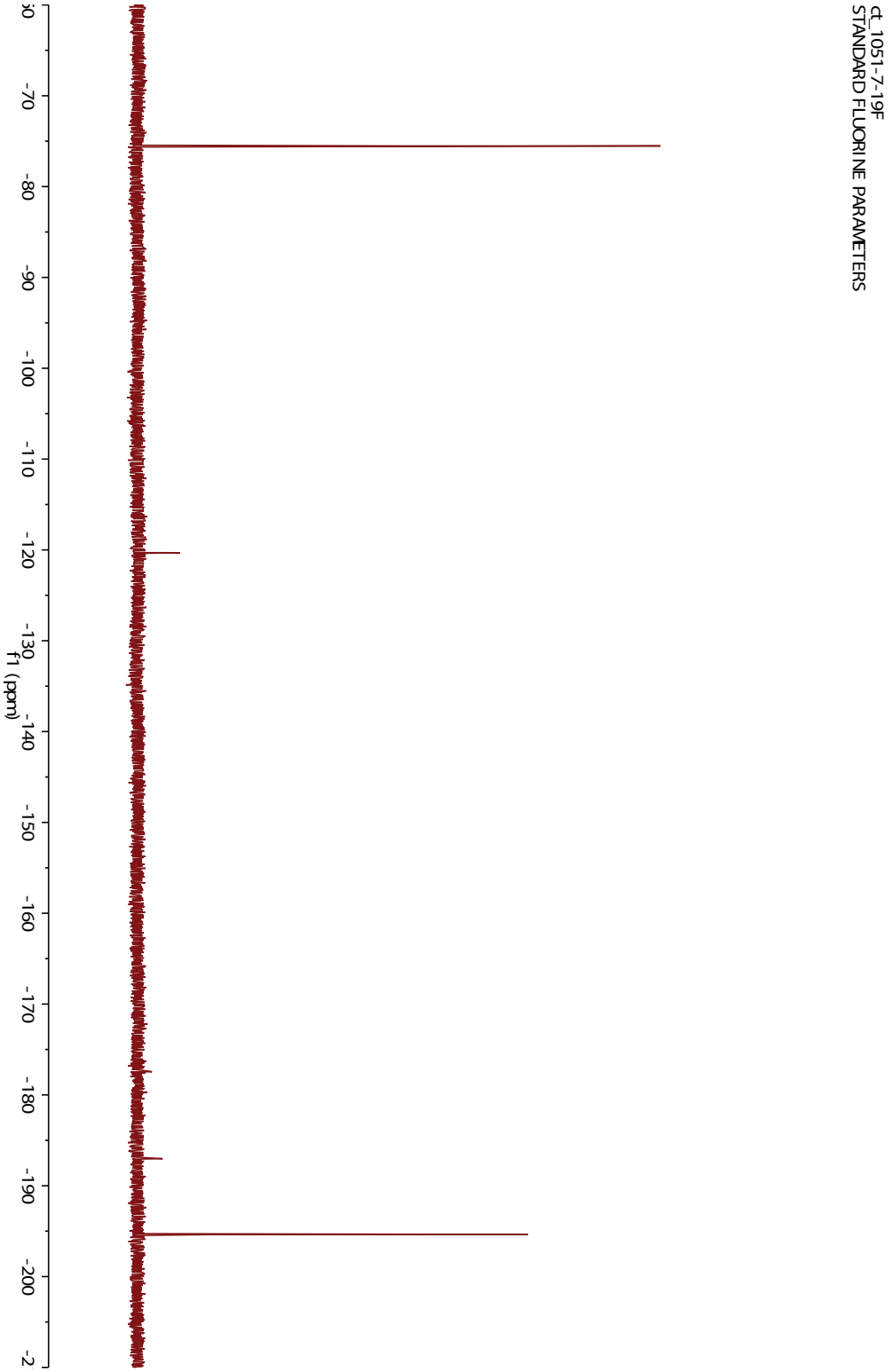

B.6 Mass Spectra

Time course of 10 µM MeOVal-CysSA-Cbz with 100 µM **6a**

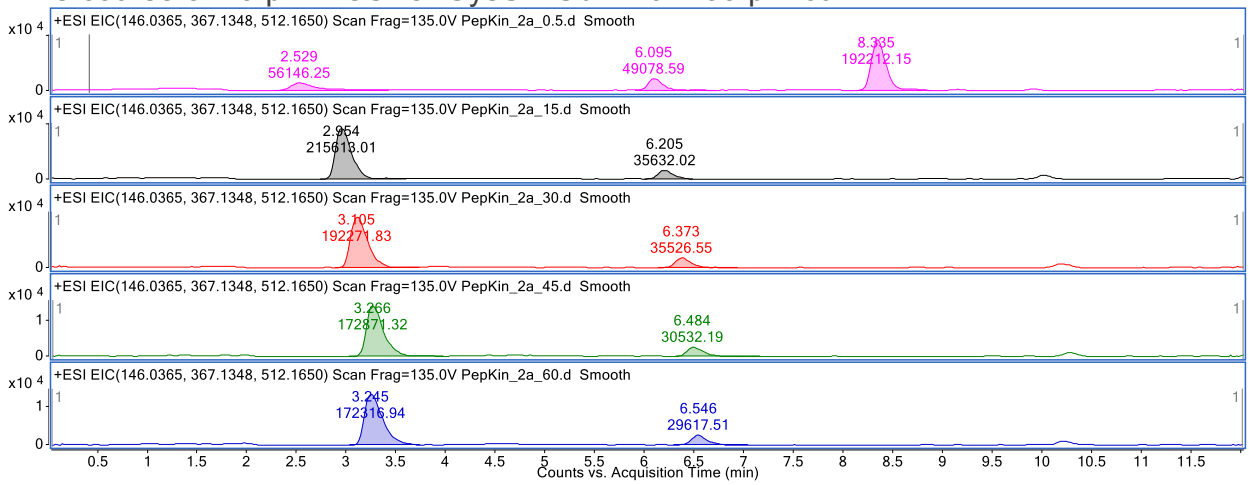

Time course of 100 µM MeOVal-CysSA-Cbz with 1000 µM **6a**

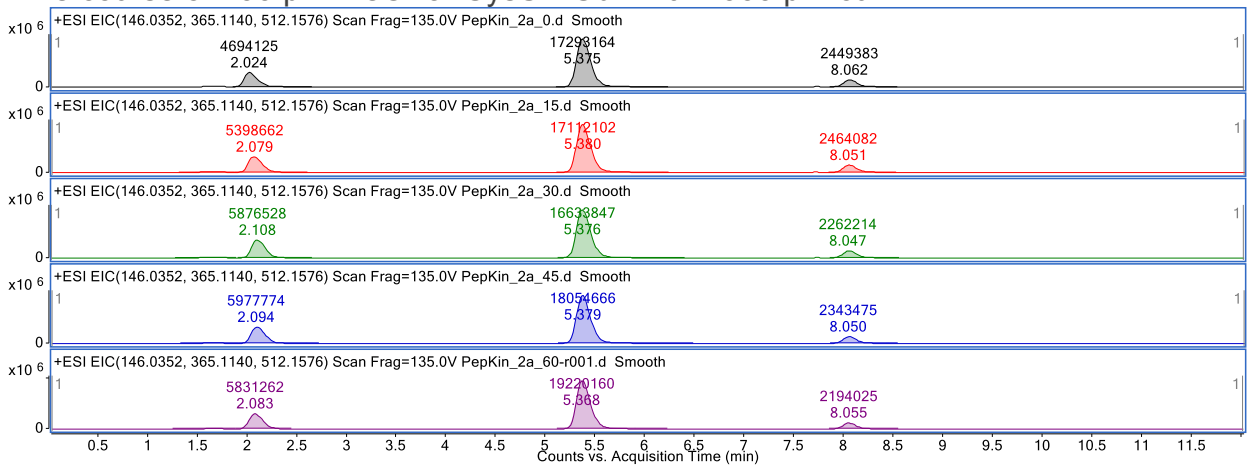

6a + MeOVal-CysSA-Cbz

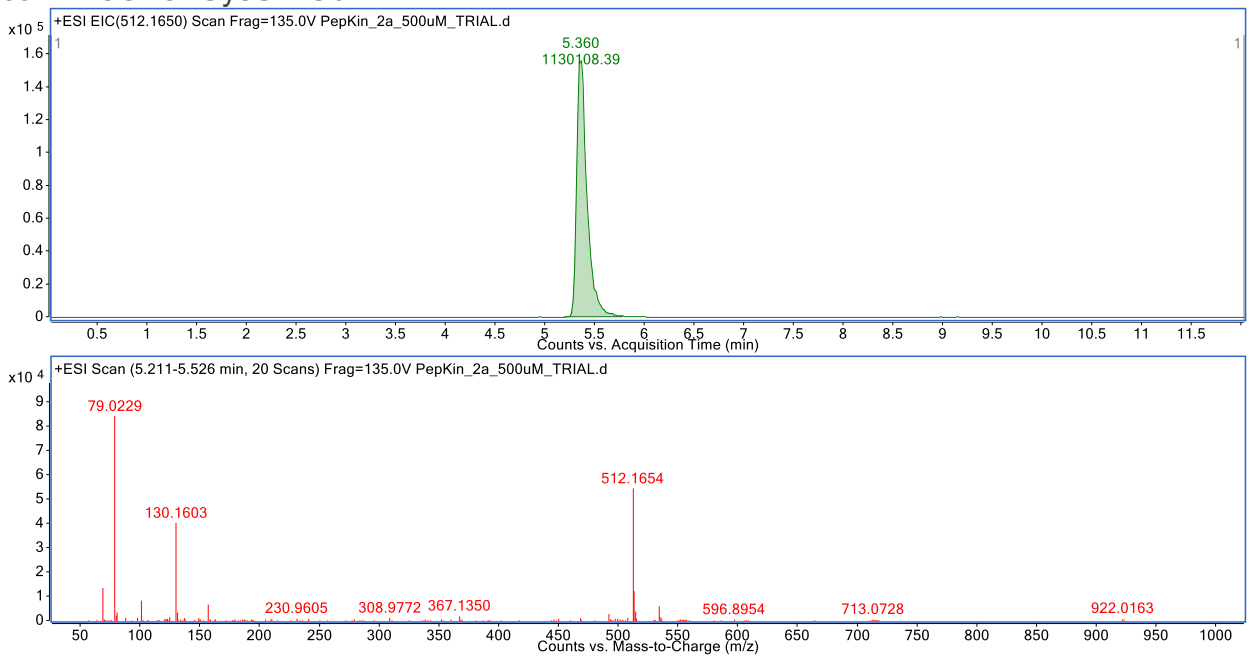

6a standard, 100 µM

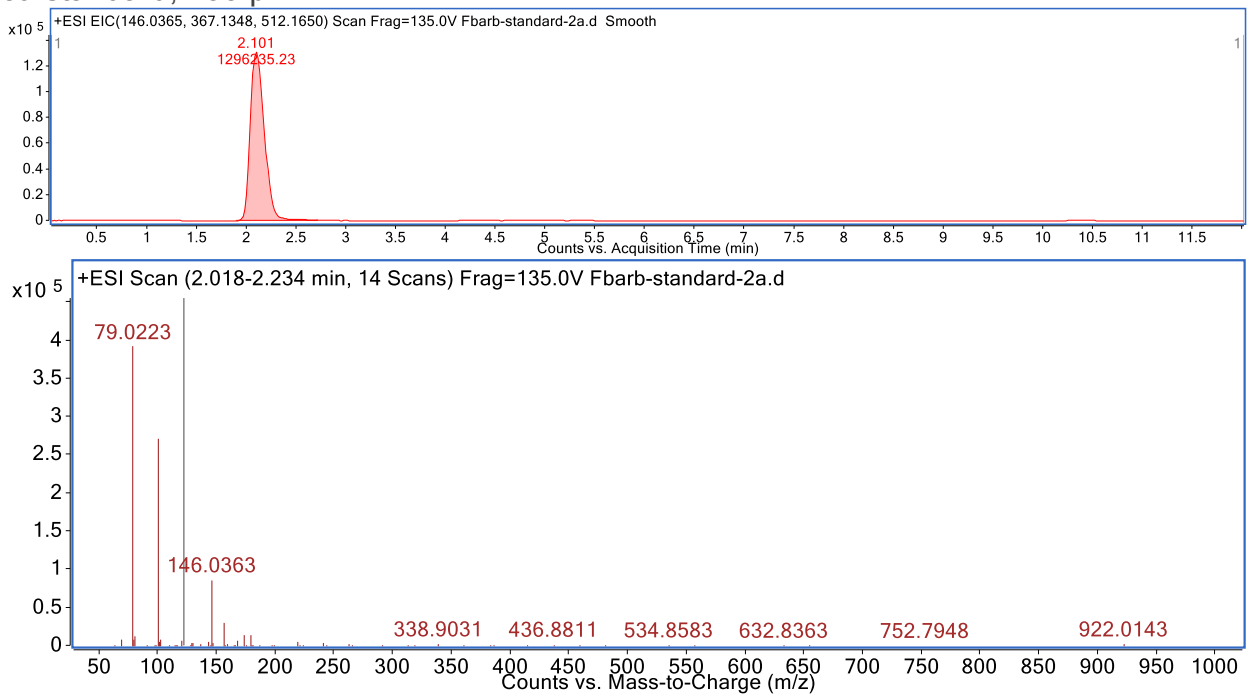

MeOVal-CysSA-Cbz standard, 100 µM

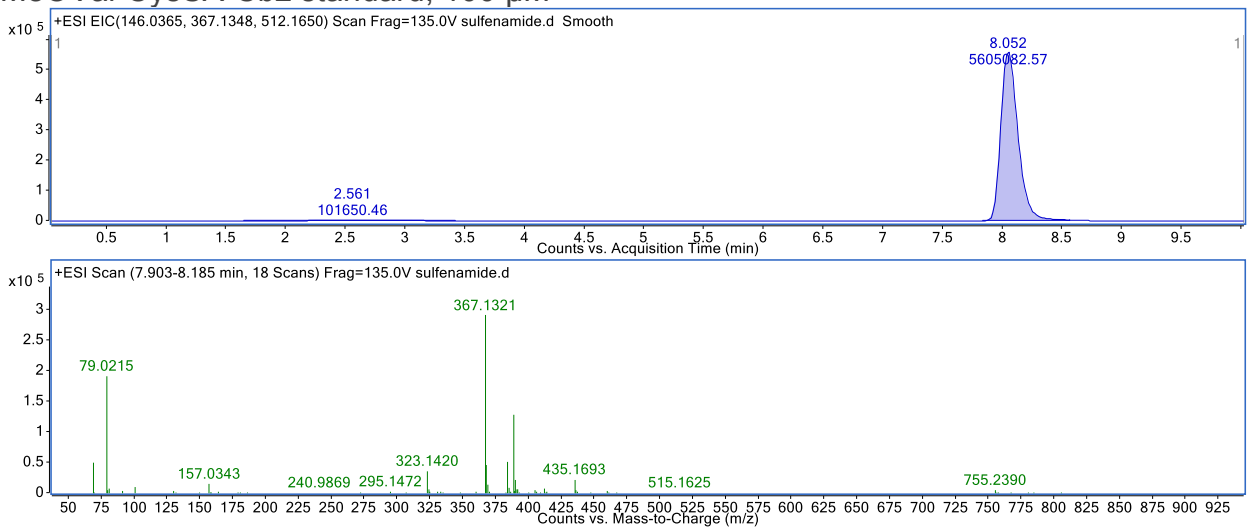

LCMS Sensitivity trials

Testing the detection limits for the 6a-pep. The samples were mixed with a 1:10 ratio of 6a to MeOVal-CysSA-Cbz, and were immediately analyzed. a) 25 μM **6a**. b) 50 μM **6a**. c) 100 μM **6a**. d) 250 μM **6a**. e) 500 μM **6a**.

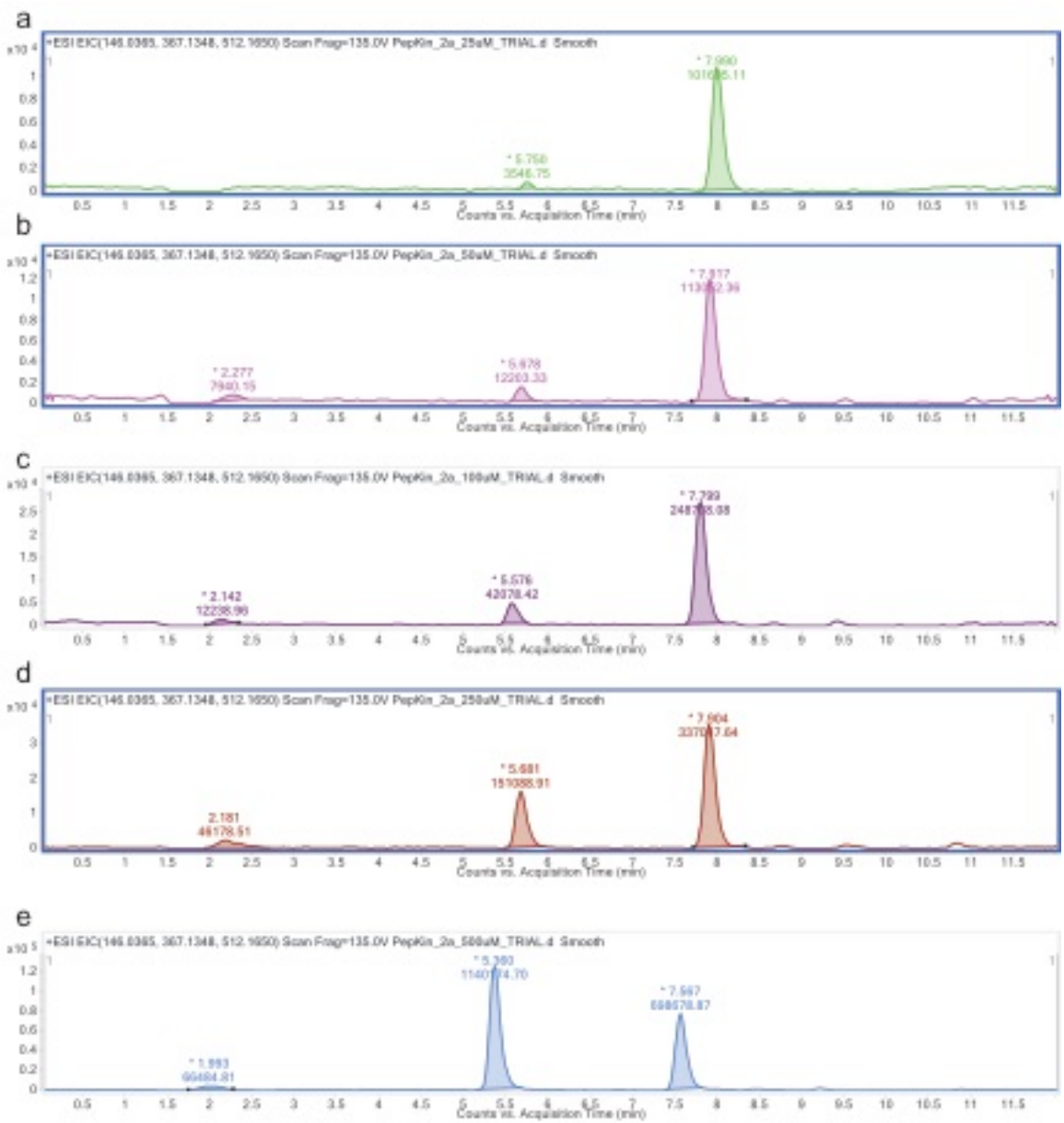

Appendix C: Additional proteins involved in the redox regulation of the cell

For instance, the redox balance of the ER is one of the most precarious in the cell, as it governs the transition from the reducing environment of the intracellular space that favors cysteine thiol to the oxidative environment of the extracellular space, which favors cysteine disulfides. This oxidative modification is an integral part of extracellular protein structure; however, proteins with multiple-to-numerous cysteine residues may have many incorrect disulfide possibilities that a rapidly overoxidizing environment may disrupt[228]. This is corrected by chaperones known as protein disulfide isomerases (PDIs)

One such chaperone is Ero1 (ER oxidoreductin 1), and it is implicated in maintaining endoplasmic reticulum redox balance and proper protein folding[228]. When Ero1 is knocked down, translated proteins accumulate[229] and demonstrate a higher levels of unfolded protein response, implying that Ero1 helps properly arrange disulfide bonds and fold the protein and/or provides the oxidizing equivalents to another PDI which helps to chaperone the nascent protein (Figure 1-Xa)[228]. Ero1 contains four active-site cysteine residues coupled to a proximal flavin cofactor, which in conjunction with molecular oxygen provides the necessary oxidation equivalents to form proper

disulfides. A distal pair of cysteines far from the catalytic site regulates the activity; when the oxidizing environment of the ER is at appropriate levels, these residues remain as free thiols and the PDI and substrate thiol oxidation activity is maintained[230]. However, when the oxidative environment is high, these distal cysteine residues form a disulfide, which inhibits the oxidative PDI activity, slowing the formation of peroxide and mediating the rate at which disulfides can form. Cells expressing the dual cysteine-to-alanine mutants of the regulatory cysteines showed an increase in the UPR and decreased viability, Glutathione levels in the ER play a role in reducing these cysteines and letting Ero1 sense redox state.

Critically, for every disulfide bond formed by Ero1, one equivalent of H_2O_2 is formed and two equivalents of O_2 consumed. Thus during high levels of production of secretory proteins, Ero1 can account for nearly 25% of the ROS production in the cell[228,231,232]. So during low levels of oxidation, Ero1 is active, helping to form disulfide bonds and creating ROS, helping to maintain levels of ROS needed to function as a PDI. In this sense, Ero1 it is self-regulating, with negative feedback resulting from overactivity and/or oxidation. In most cases, it appears as though the majority of Ero1 is in the oxidized, inactive form, thereby limiting the amount of peroxide formed[230]. This explains the various levels of redox-mediated regulation: disulfide sensing, disulfide exchange, and ROS production.

Within the oxidizing environment of the endoplasmic reticulum (ER) and the Golgi apparatus, where proteins destined for the extracellular domain are folded and disulfide bonds are formed, sulfenic acids are the putative intermediate for this[233]. Given that Ero1 produces peroxide, which induces disulfide formation, this seems likely. Thus

regulation of oxidative environments and protein oxidation has implications in secreted protein folding, which accounts for an estimated ⅓ of all translated proteins, so on a macroscopic level, sulfenic acids are of enormous importance[231].

Linking the ER stress to the rest of the cell, Sestrin2 can help mediate cellular response in the rest of the cell. The Sestrin family of proteins (SESN) includes three redox-sensing isoforms (Sestrin1, Sestrin2, Sestrin3) that help govern antioxidant response (Figure 1-xb and 1-xc). Each member is widely implicated in the complex and diverse redox-balance activities throughout the cell[234].

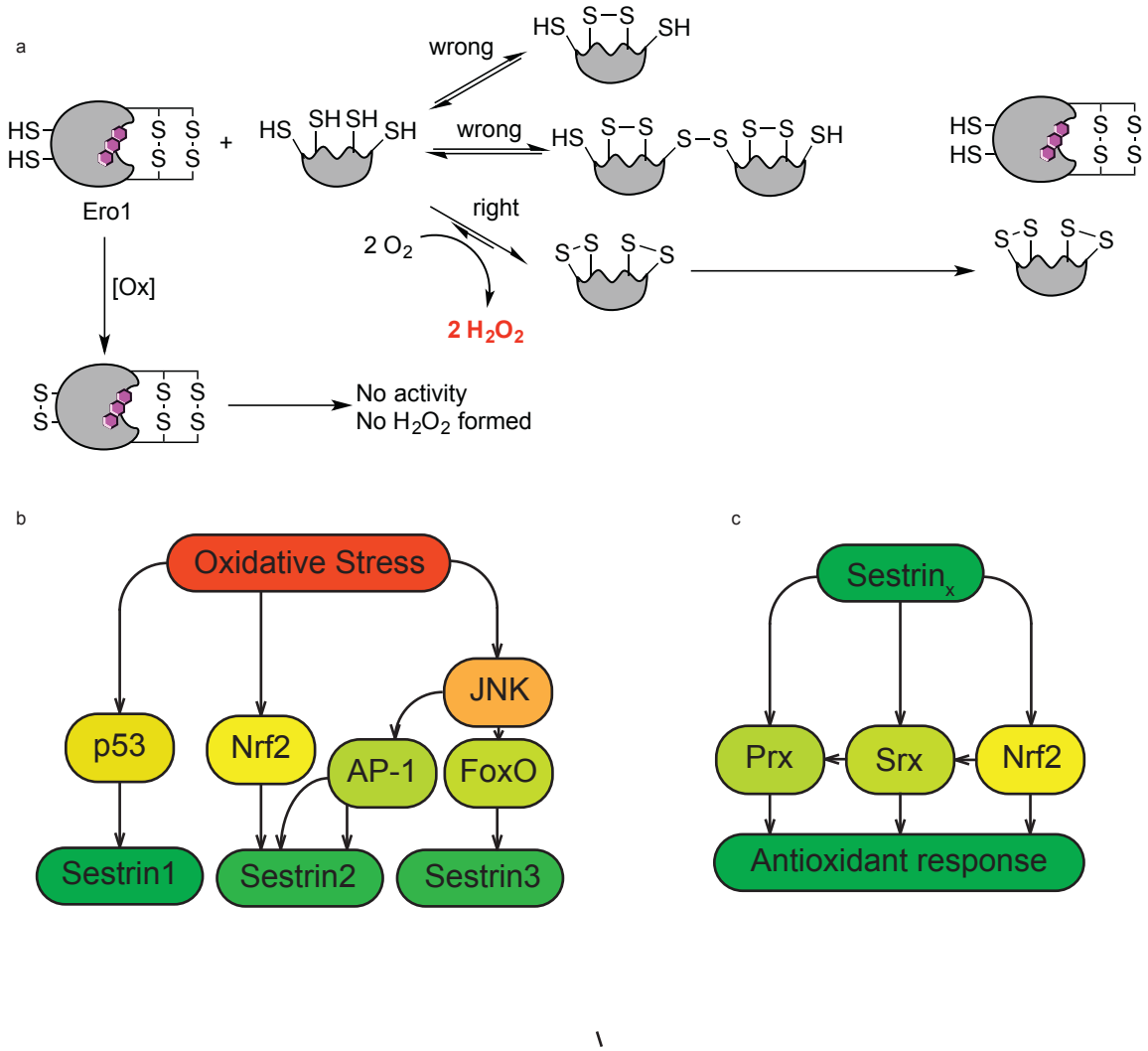

Figure C-01. The antioxidant and redox response proteins of the cell.
a) Ero1 modulates the redoxi balance of the ER though its ROS-producing PDI activity. As the oxidative load of he ER increases, the PDI-capacity and ROS generation decreases. Pink group is a flavin cofactor. b) Oxidative stress activates a number of different pathways, many o which lead to the activation of the Sestrin family of proteins. c) The Sestrins activate several different antioxidant pathways, including Nrf2, which induces a positive antioxidant feedback loop with Sestrin 2.

Sestrin2 is involved in ER stress and this stress induces Sestrin2 and helps to increase the survivability of a cell. When too much protein is being made and the UPR is activated, IRE1α and PERK go on to activate the mTORC1 pathway, shutting down

protein synthesis and increasing autophagy[235]. When Sestrin2 is blocked, protein biosynthesis continues, and exacerbates the stress on the ER.

Sestrins can be induced by a number of pathways responding to oxidative stress. Sestrin1 is induced by hydrogen peroxide in a p53-dependant manner[234]. Sestrin2 is partially determinate on p53, but can also be induced by NMDA-receptor signaling in neurons[234,236], which produces ROS. Sestrin2 can also be induced by activation of the transcription factor Nrf2, and by the JNK/AP-1 signaling cascade[234,236-240]. Nrf2 increases the antioxidant program of the cell, which can be stimulated by oncogenes[241]. Sestrin3 is stimulated by the oxidative damage and activation of the of FoxO transcription factors[234].

Silencing any of the Sestrins by siRNA results in increased accumulation of ROS and decreased survivability[234]. There exists a sequence with small but definitive homology to *Mycobacterium tuberculosis* protein AhpD, which helps to regenerate the bacterial peroxyredoxin AhpC. Though Sestrins do not directly regenerate Prx, it may help form complexes with other reductases, such as sulfiredoxin (Srx)[234,237]. Further upstream, Sestrins can increase Nrf2 expression, which can induce Srx expression, which can increase the concentration of active Prx by reducing the buildup of overoxidized, inactive Prx[104].

Indeed, the sestrin family of proteins (SESN) family of proteins is one of the primary redox-sensing proteins that help govern antioxidant response. It widely implicated in many redox-balance activities throughout the cell.

In the nervous system, reactive oxygen species are involved in chronic neuropathic pain response. Both H_2O_2 and $O_2^{\circ -}$ are involved pain sensitization, and suppressing

NADPH oxidase isoforms NOX2 and NOX4 diminishes pain response[242]. Upon pain stimulation, Sestrin2 helps modulate the pain response through its antioxidant properties, and helps activate the activating transcription factor 3 (ATF3) after sensory nerve injury (SNI)[242].

When small-molecule mitochondrial inhibitors of electron transport chain complex I (piericidin A) and III (myxothiazol) were applied to cells, the gene encoding for Sestrin2, SESN2 was upregulated[236]. The activating transcription factor 4 (ATF4) plays a key roles in the integrated stress response (ISR), and it was found that blocking ISR blocked SESN2 expression[236]. This indicates that SESN2 plays a key regulatory role in mitochondrial health and stress.

In macrophages, Sestrin2 almost completely diminished the Toll-Like Receptor (TLR) response to lipopolysaccharide (LPS) stimulation and release of NO° by iNOS and H_2O_2 by NOX[239]. In these cells, high levels of both ROS and RNS are produced in a so-called 'resparatory burst' that play an antibioltic role endogenously. The high expression of both types of species is sufficient to produce other species including peroxynitrite ($ONOO^-$) and myeloperoxidase can convert peroxide to hypochlorite. Expression of pro-inflamatory cytokines TNF-α, IL-6, and IL-1β was reduced as well[239]. This seems to happen by inhibition of MAPK/P38/JNK, preventing downstream activation of ROS/RNS sources and AP-1 (c-jun)[239].

Sestrins, as described above, are implicated in many forms of antioxidant response, across different cell lines and are necessary for the health of various organelles, especialy those with strong oxidative potential.

Small heat-shock proteins such as Hsp25 and Hsp 27[243], which at times double as

redox chaperone proteins, can upregulate the amount of glutathione by increasing the amount of glucose-6-phosphate dehydrogenase[244]. They also may increase the amount of glutathione reductase and glutathione transferase[245].

Under low-to-moderate degrees of oxidative stress, heat shock factor 1 (HSF1) is liberated from binding to Hsp's, where it then goes to act as a transcription factor to upregulate Hsp production levels[245]. Overoxidation levels, however, inhibit this transition and DNA binding, preventing this activity. HSF1 activation also leads to an increase in reduced gluathione levels (GSH), which helps reestablish the appropriate redox balance[245].

The caspases are a family of aspartate-specific cysteine proteases that are often associated with cell death. Their catalytic cysteine needs to be free for activity; alkylating agents can block their action[246]. The cell-death initator protein caspase-9 is a pro-apoptotic protease that has a catalytically active redox-sensitive cysteine in its active site[247]. Oxidation of this cysteine causes it to associate with the apoptotic protease-activating factor 1 (Apaf1), which leads to more pro-apoptotic events. This binding association occurs through a intermolecular disulfide bond to Apaf1, which would explain why ROS induces this association. Interestingly, RNS and nitrosylation at these catalytic cysteines of caspases blocks its catalytic and apoptotic potential[248-250] from upstream apoptotic factors such as cytochrome c. However, it seems as other factors such as Fas can denitrosylate other caspases, such as caspase-3[249]. Caspase-3, however, is activated by thioredoxin and other antioxidants[246]. Caspase-2 blocks ROS stress and is activated by ROS[251]. *Casp2*$^{-/-}$ knockout mice show phenotypic signs of advanced aging and reduced resistance to oxidative pressure. Without the

antioxidant properties of Caspase-2, *Casp2*$^{-/-}$ mice experience ROS accumulation and the activation of the FOXO-Nrf2 pathway leading to reduced levels of SOD and Prx-GSH, as well as Jnk activation leading to increased IL-6 and IL 1β levels. [251,252]

Peroxyredoxins, while playing the role of primary antioxidant protein, can also play a role in redox signaling cascades[253]. Cytokine-induced oxidation of Prx2 results in the formation of a disulfide, which is traditionally thought to be reduced by Trx. Instead, the oxidative equivalent gets transferred to the transcription factor STAT3, which after disulfide formation goes on to form dimers and tetramers and increases its activity.

YajL/DJ1 is an antioxidant protein that has a conserved cysteine that is modified as a stable sulfinic acid in crystal structures. YajL/DJ1 has been found to protect cells against sulfenylation and form mixed disulfides with sulfenic acids on proteins[254]. Mutations to this cysteine are implicated in early-onset Parkinson's disease and parkinsonism[255] and trigger global cellular response across many types of antioxidant proteins[256].

And finally, the catalytic cysteine of glyceraldehyde-3-phosphate dehydrogenase (GAPDH) is susceptible to oxidation[257], where it forms either disulfides on Cys152 (cat) and Cys156, or cysteic acid (sulfonic acid) on Cys152. When this occurs it interferes with critical phase of glycolysis where glyceraldehyde-3-phosphate is oxidatively transformed into 1,3-bisphosphoglycerate. This halts the production of pyruvate and the subsequent production of ATP through the mitochondrial electron transport train, which is a key source of oxidative stress and drain on the supply of NADPH. Instead, it reroutes metabolism through to the pentose phosphate pathway, generates reducing

units of NADPH that is a key cofactor and electron source for the rexodins and glutathione reductase.

Appendix D: Non-invasive methods of imaging tissues and chemical state *in vivo*

D.01. X-Rays and Computed Tomography

Two-dimensional X-rays, and more recently, X-ray CT (X-CT computed tomography), was the first technology to enable the non-invasive imaging of macrostructures[258-261]. The high-energy photons are able to penetrate bodily tissue and are particularly useful for studying both differences in density between tissues and the hard skeletal structures (**Figure 3-1a**). These can be enhanced by the use of contrast agents, particularly barium for the gastrointestinal track and a variety of iodine[262] compounds are used to image the vasculature and other body compartments. However, the ability to image non-metal elements on second- and third-row of the periodic table is severely restricted, and without the addition of contrast agents is unable to image the transparent proteins.

D.02. Positron emission tomography

By contrast, Positron Emission Tomography (PET) is a highly sensitive technique. It involves the introduction of isotopes that undergo an anti-electron i.e. positron (β^+) decay, which upon collision and annihilation with an electron produces a pair of high-

energy γ particles (always 511 keV due to the $\beta/\beta^{=}$ annihilation energetics) that are detected by the instrument (**Figure 3-1b**)[263-265]. The location of decay is computed and the three-dimensional structure is reconstructed. β^{+}-emitting isotopes include ^{11}C ($t_{1/2}$ ~20 min), ^{13}N ($t_{1/2}$ ~10 min), ^{15O} ($t_{1/2}$ ~2 min), etc., with the most common being ^{18}F ($t_{1/2}$ ~110 min)[266,267]. There are also numerous other nuclei[267,268] with different β^{+}-emission energies.

The production of these isotopes occurs in a cyclotron where the appropriate progenitor nuclei are bombarded by high-energy particles. For $^{20}Ne \rightarrow {}^{18}F$, the particle energy can be quite low (0-2 MeV), as opposed to higher-energy transitions such as $^{68}Ge \rightarrow {}^{68}Ga$, which occurs only on national-lab scale beamlines operating at greater than 100 MeV[266].

The β^{+}-emission energy determines the average path length before decay, which correlates in a non-linear manner to the β^{+}-emission energy, usually in the realm of MeV. The full-width at half-max (FWHM) for a β^{+} particle ejected from ^{18}F has 0.64 MeV of energy and travels, on average, 0.54 mm before it loses enough of that energy to capture an electron and annihilate. For a β^{+} particle ejected from ^{82}Rb at 3.35 MeV, the FWHM is 6.14 mm. A single grain of ^{18}F would appear to be 1.2 mm with perfect instrumentation; a single grain of ^{82}Rb would appear to be 1.2 cm. Thus the energy of the ejection / lifetime of the decay is the fundamental limiting factor on the spacial resolution[202].

For the reason of ease of production, and one of the shortest β^{+}-decay path and highest resolution, ^{18}F is one of the most popular radionuclei for PET. ^{18}Fluordeoxyglucose (FDG) is the prevalent radiotracer in 90% of PET scans, and is

used as a metabolic sensor of rapidly-dividing oncogenic cells[269]. Such energy-consuming tumors uptake the sensor, which is then trapped inside cells by phosphorylation with hexokinase and is thus unable to diffuse or be transported outside the cell, leading to a selective bioaccumulation of radionuclei[270].

Due to the expense of producing these radioisotopes, it is typically a secondary imaging technique should X-ray/CT fail to observe abnormal physiological structures. Thus, strong practical limitations of this technique include the requirement that short-lived radioisotopes must be produced on-site by cyclotrons and subsequently synthetically incorporated into the radiotracer and rapidly purified. This chemistry, particularly the ^{18}F chemistry, has the difficulty of always racing the uphill battle against rapid nuclear decay for incorporation into the sensor that is necessary to ensure the sensitivity of the technique. This decay leads to much of the potential radiolabel is lost by the time the synthesis and purification is done, paradoxically decreasing the sensitivity of the technique. Given this additional constraint, many of the typical rules for organic synthesis no longer apply: consider a hypothetical organic chemical reaction that ideally gets a quantitative chemical conversion after 9 hours with ^{19}F, with a two-hour purification and one hour for analysis resulting in ~100% yield. However, this timeframe represents roughly nearly seven half-lives for ^{18}F, which will only result a radioyield of product of ~1%. This necessitates specialized chemistry to be developed for rapid incorporation the sensor[271]. Thus expensive and mandatory on-site production of the radionuclei, rapid decay, and lack of access to an enormous range of reactions that a synthetic organic chemist has access to remains a great drawback.

From our perspective, the most significant drawback is that while information on the

spacial position and concentration/bioaccumulation are have reasonably high resolution and sensitively collected, the technique itself is an indirect measurement of ejected positrons that decay into the gamma rays. These gamma particles contain no information about the chemical environment of the nuclei before its two-step decay, always emitting at 511 keV, limiting its use to *only* determining the location of bioaccumulation and clearance.

D.03. Nuclear Magnetic Resonance, Magnetic Resonance Imaging

Magnetic Resonance Imaging (MRI) and Magnetic Resonance Spectroscopy (MRS) utilize high-field magnets and radio frequency pulses to probe the nuclear spin-state and chemical environment of receptive nuclei (**Figure 3-1c**).

MRI and NMR operate on the same principles (**Figure 3-1d**), an excellent review of all pertinent topics can be seen here[272]. First, a sample containing a nuclei with a non-zero magnetogyric spin state. Active spin ½ nuclei include, but are not limited to: ^{1}H, ^{13}C, ^{11}B, ^{15}N, ^{29}Si, ^{31}P, and ^{19}F. The sample is then subjected to a strong magnetic field (for a 400 MHz magnet this is 9.4 T, roughly 150,000 times the strength of the earth's magnetic field), which aligns the nuclei into two states: a lower-energy α, and a higher-energy β. The α population is aligned with the field, and the β against. Upon excitation with radio frequency (R_f) light, some of the α transfers to β, which produces a nuclear magnetic resonance response, i.e. the chemical shift tensor[273]. This response can probe for the chemical environment of the nuclei i.e local chemical structure. Other forms of information that can be collected are the T1 (spin-lattice) and T2 (spin-spin) relaxation times, which are two different phenomena that result in the degradation of the

NMR/MRI signal. T1 is the decrease in the population of β back to α as signal intensity in the *z* plane normal to the magnetic field B_0. This results from the population of magnetic spin states approaching parity after excitation and repopulating their non-excited form. It is essentially how fast the excited β nuclei return to the α state, and typically having a short T1 is favorable because once the nuclei have relaxed, another pulse can be applied. T2 involves the loss of the coherence of the magnetization in the *xy* plane perpendicular to B_0, contributing to signal line broadening. T2 is like a top that begins to wobble off axis, which diffuses the nuclear alignment spin state in the measured *z* direction.

	In 1.5 T magnet	
Tissue	T1 (ms)	T2 (ms)
Adipose tissues	240-250	60-80
Whole blood (deoxygenated)	1350	50
Whole blood (oxygenated)	1350	200
Cerebrospinal fluid (similar to pure water)	4200 - 4500	2100-2300
Gray matter of cerebrum	920	100
White matter of cerebrum	780	90
Liver	490	40
Kidneys	650	60-75
Muscles	860-900	50

Table D-01. T1 and T2 relaxation times of 1H under a 1.5 T field strength.
Different tissues have different relaxation times due to the concentration of other small molecules present in the matrix[274].

Simply put, a short T1 decay leads to the ability to take an increased number of scans in a given amount of time and thus a higher effective sensitivity, while a low T2 leads to rapid decoherence and broadening in the signal, which causes a decrease in the S/N. Repeated pulses increase the S/N by a factor of $n^{½}$. Thus increasing the number of scans from 16 to 32 will yield roughly a 41% increase in S/N. A decrease in

T2 is often correlated with larger molecules such as proteins, micelles, or solid- or pseudosolid-state material. Thus, a high T2/T1 is a desirable “on” state for the sensor/probe to ensure the highest S/N in the shortest amount of time. In practice, T2 can never be longer than T1 due to the fact that after T1 relaxation, the nucleus is relaxed into a stable alignment with the B_0. In MRI and MRS, the chemical shift (environment), intensity (concentration in a given environment), T1 and T2 relaxation times can all be used to gather clinically useful information (**Table 3-1**). These factors depend on not only the covalent chemical environment of the probed nuclei, but also the small-molecule and biological macromolecule composition of the tissue. For instance, the increased T2 of oxygenated whole blood over deoxygenated whole blood is due to the paramagnetic electron spin state of the unpaired electrons in molecular oxygen. Thus nuclear-spin techniques represent an extremely versatile means to evaluate parallel factors in chemical environment.

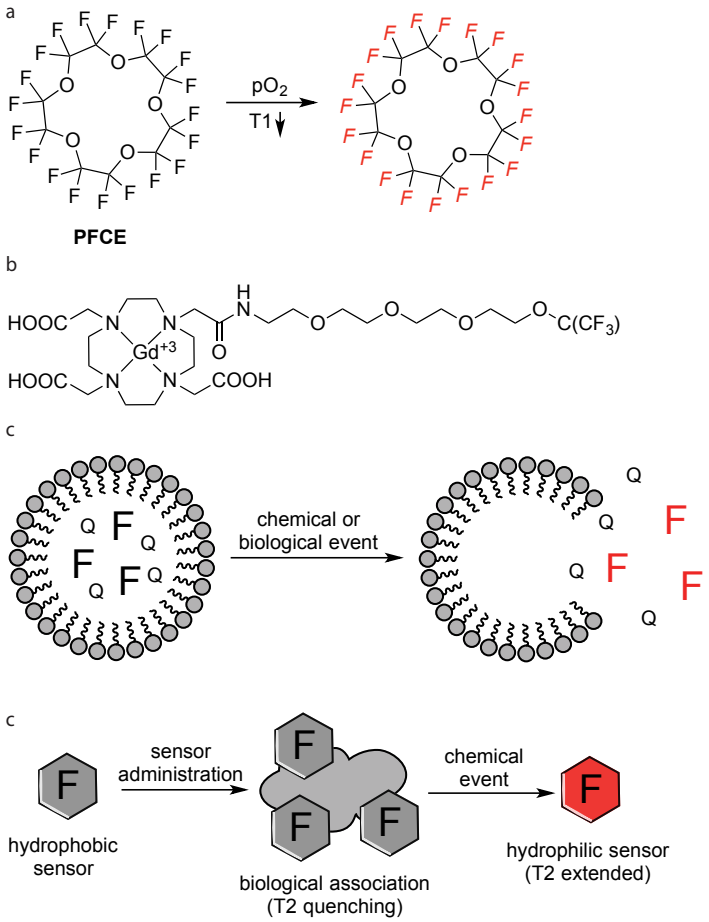

Figure D-01. Established methods of ^{19}F MRI detection[191].
a) One of the more common uses of ^{19}F sensors for MRA is in the use of perfluorinated compounds that undergo oxygen concentration-dependent decreased T1 relaxation times. b) Other paramagnetic elements such as gadolinium and manganese can enhance T1 relaxation times; however, they can also decrease T2 relaxation times, leading to signal broadening. Thus the contrast agents must be carefully designed. c) Colocalization of ^{19}F and a quencher can lead to a decrease in signal, and upon release an increase in S/N is established. d) Coordination of hydrophobic fluoro compounds to blood results in the coordination to hydrophobic sponge of HSA. Upon treatment, the compound becomes more hydrophilic and is released from the serum albumin. This increases the T2 relaxation time, reducing line broadening and increasing S/N.

While being a much less sensitive technique than PET, it allows multidimensional additional modes of study over simply determining spacial position and concentration (bioaccumulation). To demonstrate this, amyloidophilic tracers were used to analyze plaques via ^{19}F and ^{1}H in vivo[187]. Both FSB (Figure 3-Xi) and BSB[275] (Figure 3-Xii) are

structurally similar to the Congo Red (CR), which is known to bind to β-amyloid plaques. Upon administration of these sensors, Higuchi et al recreated the three-dimensional structure of the brain using spin-echo rapid acquisition with relaxation enhancement (RARE) sequence designed for ^{19}F. The ^{19}F images were obtained on a 400 MHz / 9.4 T imaging spectrometer over the course of 90 min looking directly at a peak at about -118.7 ppm[276] (Figure 3-Xa). Because extremely high background of protons in the brain and their similarity to each other in terms of chemical shifts (ppm), the ^{1}H scans utilized T1-weighted gradient-echo coronal ^{1}H magnetic resonance images to differentiate tissues from each other (Figure 3-Xb). Together, the two modes of analysis confer a multidimensional analysis, increasing the confidence of the measurement (Figure 3-Xc). In contrast, BSB has no ^{19}F, but it produces the same T1 enhancement of the amyloid regions, while the vehicle (DMSO) does not have that effect, which is recapitulated by examining FSB and CR side-by-side (Figure 3-Xe-g). Figures 3Xd,e are confirming that the sensor / dye are colocalized with the plaque.

As a reporter group, ^{19}F is possesses single-atom minimalist functionality[186] and, unlike ^{18}F, is indefinitely stable. It has several convenient commercial active methylene compound starting materials (**Scheme B9 & B10**), as well as several powerful and commercially available sources of electrophilic ("F^{+}") and nucleophilic ("F^{-}") fluorine (**Figure B3**), allowing for much greater synthetic reach over ^{18}F, which has no commercial products at all.

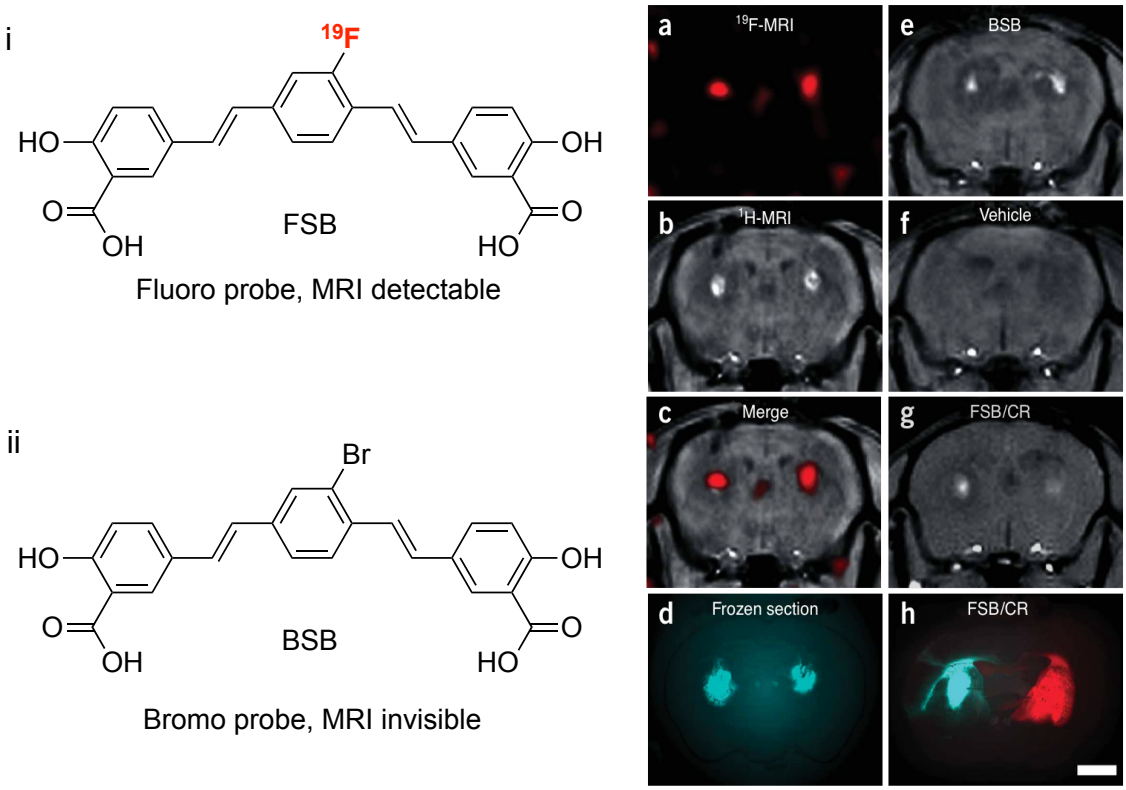

Figure D-02. Illustration of the potential of ^{19}F MRI over/combined with ^{1}H MRI. i) FSB is a Congo Red-like sensor that binds to β-amyloid plaques. ii) BSB is a similar probe, but it lacks the ^{19}F reporter group. a,e) ^{19}F imaging of FSB/BSB. b,f) 1H time resolved imaging with FSB/vehicle. c.g) Merge of $^{19}F/^{1}H$ images, and 1H spectrum of a FSB/CR coinjection. d,h) Fluorescence imaging of brain slices. Images taken from reference[187].

A wide array of effective and clever ^{19}F NMR/MRI contrast and imaging agents have been developed[277]. An early use of ^{19}F sensors are as interrogators of oxygen tension. Upon administration, the sensors biodistribute to the appropriate tissues, and the T1 spin-lattice relaxation time has been found to be linearly dependent on the partial pressure of the paramagnetic molecular oxygen (pO_2) (**Figure 3-2a**)[278]. Other paramagnetic elements and ions can be used, such as gadolinium (**Figure 3-2b**) to reduce T1 and increase S/N; however, these may have the side effect to reduce T2, leading to line broadening and effective signal quenching. Careful design of the sensors

is necessary to ensure optimal signal, however, once this effect is achieved, a number of physical parameters of can be achieved including chemical shift of the fluorine (δ, ppm), T1/T2 relaxation times (ms), and pH and thermal response[279]. General methods for the ^{19}F NMR signal quenching by colocalization either occur by macrostructure containment[280] or by covalent connection, with increase in signal occurring when these structures or connections are disrupted (**Figure 3-2c** and **3-2d**). Fluorine-containing nanoparticles were encased in a disulfide-bridged gadolinium shell[281]. The Gd^{+3} complex in this case enhanced the T2, and not T1, relaxation time, leading to broadening of signal and loss of magnetic coherence. Upon cleavage with TCEP, the signal increased dramatically.

A simple way to linearly increase S/N is to increase the number of fluorines[204], and even better, degenerate fluorines, as is the case with the perfluorinated 15-crown-5[282], which features 20 chemically identical fluorines, resulting in a 20-fold S/N increase.

From a long-term clinical perspective of *in vivo* work, unlike the aforementioned imaging techniques of X-ray and PET, radio waves and magnetic fields are non-ionizing radiation that is easily transmitted through the body, which increases their application for clinical and diagnostic potential, particularly in pregnancies where the fetus is highly susceptible to DNA damage.

References

References

(1) Phelan, S. A. *Antioxidants & Redox Signaling* **1999**, *1*, 571.

(2) Milo, R. P., R. 2016; Vol. 2016.

(3) Berner, R. A. *Proceedings of the National Academy of Sciences* **1999**, *96*, 10955.

(4) Mach, W. J.; Thimmesch, A. R.; Pierce, J. T.; Pierce, J. D. *Nurs Res Pract* **2011**, *2011*, 260482.

(5) Geider, R. J.; Delucia, E. H.; Falkowski, P. G.; Finzi, A. C.; Grime, J. P.; Grace, J.; Kana, T. M.; La Roche, J.; Long, S. P.; Osborne, B. A.; Platt, T.; Prentice, I. C.; Raven, J. A.; Schlesinger, W. H.; Smetacek, V.; Stuart, V.; Sathyendranath, S.; Thomas, R. B.; Vogelmann, T. C.; Williams, P.; Woodward, F. I. *Global Change Biology* **2001**, *7*, 849.

(6) Wood, P. M. *Biochemical Journal* **1988**, *253*, 287.

(7) Widomska, J.; Raguz, M.; Subczynski, W. K. *Biochimica et Biophysica Acta (BBA) - Biomembranes* **2007**, *1768*, 2635.

(8) Collman, J. P.; Brauman, J. I.; Halbert, T. R.; Suslick, K. S. *Proceedings of the National Academy of Sciences of the United States of America* **1976**, *73*, 3333.

(9) Jastroch, M.; Divakaruni, A. S.; Mookerjee, S.; Treberg, J. R.; Brand, M. D. *Essays in biochemistry* **2010**, *47*, 53.

(10) Lambeth, J. D. *Nature reviews. Immunology* **2004**, *4*, 181.

(11) Bielski, B. H. J.; Allen, A. O. *The Journal of Physical Chemistry* **1977**, *81*, 1048.

(12) Rao, P. S.; Hayon, E. *The Journal of Physical Chemistry* **1975**, *79*, 397.

(13) Lemire, J. A.; Harrison, J. J.; Turner, R. J. *Nat Rev Micro* **2013**, *11*, 371.

(14) Requena, J. R.; Chao, C. C.; Levine, R. L.; Stadtman, E. R. *Proceedings of the National Academy of Sciences of the United States of America* **2001**, *98*, 69.

(15) Moller, I. M.; Rogowska-Wrzesinska, A.; Rao, R. S. *Journal of proteomics* **2011**, *74*, 2228.

(16) Thomas, E. L. *Infection and Immunity* **1979**, *23*, 522.

(17) Lau, D.; Mollnau, H.; Eiserich, J. P.; Freeman, B. A.; Daiber, A.; Gehling, U. M.; Brümmer, J.; Rudolph, V.; Münzel, T.; Heitzer, T.; Meinertz, T.; Baldus, S. *Proceedings of the National Academy of Sciences of the United States of America* **2005**, *102*, 431.

(18) Papayannopoulos, V.; Metzler, K. D.; Hakkim, A.; Zychlinsky, A. *The Journal of Cell Biology* **2010**, *191*, 677.

(19) Davies, M. J. *Journal of Clinical Biochemistry and Nutrition* **2011**, *48*, 8.

(20) Cotton, F. A. W., G. *Advanced Inorganic Chemistry*; 5th ed.; Wiley-Interscience: New York, 1988.

(21) Moncada, S.; Palmer, R. M. J.; Higgs, E. A. *Biochemical Pharmacology* **1989**, *38*, 1709.

(22) Vanini, F.; Kashfi, K.; Nath, N. *Redox Biology* **2015**, *6*, 334.

(23) Bradley, S. A.; Steinert, J. R. *Oxidative medicine and cellular longevity* **2016**, *2016*, 5681036.
(24) Chaudhury, A. *Frontiers in medicine* **2014**, *1*, 8.
(25) Courtney, M. J.; Li, L. L.; Lai, Y. Y. *Frontiers in cellular neuroscience* **2014**, *8*, 252.
(26) Zhu, J.; Song, W.; Li, L.; Fan, X. *Molecular brain* **2016**, *9*, 30.
(27) Dempsey, G. T.; Bates, M.; Kowtoniuk, W. E.; Liu, D. R.; Tsien, R. Y.; Zhuang, X. *Journal of the American Chemical Society* **2009**, *131*, 18192.
(28) Zhao, Y.; Vanhoutte, P. M.; Leung, S. W. *Journal of pharmacological sciences* **2015**, *129*, 83.
(29) Hibbs, J. B.; Taintor, R. R.; Vavrin, Z.; Rachlin, E. M. *Biochemical and Biophysical Research Communications* **1988**, *157*, 87.
(30) Green, S. J.; Scheller, L. F.; Marletta, M. A.; Seguin, M. C.; Klotz, F. W.; Slayter, M.; Nelson, B. J.; Nacy, C. A. *Immunology letters* **1994**, *43*, 87.
(31) Angulo, J.; Wright, H. M.; Cuevas, P.; Gonzalez-Corrochano, R.; Fernandez, A.; Cuevas, B.; La Fuente, J. M.; Gupta, S.; Saenz de Tejada, I. *The journal of sexual medicine* **2010**, *7*, 2681.
(32) Hopper, R. A.; Garthwaite, J. *The Journal of neuroscience : the official journal of the Society for Neuroscience* **2006**, *26*, 11513.
(33) Pacher, P.; Beckman, J. S.; Liaudet, L. *Physiological reviews* **2007**, *87*, 315.
(34) Augusto, O.; Bonini, M. G.; Amanso, A. M.; Linares, E.; Santos, C. C. X.; De Menezes, S. l. L. *Free Radical Biology and Medicine* **2002**, *32*, 841.
(35) Jansson, E. A.; Huang, L.; Malkey, R.; Govoni, M.; Nihlen, C.; Olsson, A.; Stensdotter, M.; Petersson, J.; Holm, L.; Weitzberg, E.; Lundberg, J. O. *Nat Chem Biol* **2008**, *4*, 411.
(36) Lindenmann, J.; Matzi, V.; Neuboeck, N.; Ratzenhofer-Komenda, B.; Maier, A.; Smolle-Juettner, F. M. *Diving and hyperbaric medicine* **2010**, *40*, 213.
(37) Chiku, T.; Padovani, D.; Zhu, W.; Singh, S.; Vitvitsky, V.; Banerjee, R. *J Biol Chem* **2009**, *284*, 11601.
(38) Dominy, J. E.; Stipanuk, M. H. *Nutrition reviews* **2004**, *62*, 348.
(39) Furne, J.; Saeed, A.; Levitt, M. D. *American journal of physiology. Regulatory, integrative and comparative physiology* **2008**, *295*, R1479.
(40) Bełtowski, J.; Jamroz-Wiśniewska, A. *Molecules* **2014**, *19*, 21183.
(41) Szabo, C. *Nature reviews. Drug discovery* **2007**, *6*, 917.
(42) Qiu, X.; Villalta, J.; Lin, G.; Lue, T. F. *Journal of andrology* **2012**, *33*, 529.
(43) Tan, B. H.; Wong, P. T.; Bian, J. S. *Neurochemistry international* **2010**, *56*, 3.
(44) Han, Y.; Qin, J.; Chang, X.; Yang, Z.; Tang, X.; Du, J. *Biochem Biophys Res Commun* **2005**, *327*, 431.
(45) Pan, J. G.; Zhang, J.; Zhou, H.; Chen, L.; Tang, Y. H.; Zheng, Y. *Respiratory physiology & neurobiology* **2011**, *178*, 230.
(46) Morikawa, T.; Kajimura, M.; Nakamura, T.; Hishiki, T.; Nakanishi, T.; Yukutake, Y.; Nagahata, Y.; Ishikawa, M.; Hattori, K.; Takenouchi, T.; Takahashi, T.; Ishii, I.; Matsubara, K.; Kabe, Y.; Uchiyama, S.; Nagata, E.; Gadalla, M. M.; Snyder, S. H.; Suematsu, M. *Proceedings of the National Academy of Sciences of the United States of America* **2012**, *109*, 1293.
(47) Wei, X.; Zhang, B.; Cheng, L.; Chi, M.; Deng, L.; Pan, H.; Yao, X.; Wang, G. *Brain Research* **2015**, *1622*, 292.
(48) Qu, K.; Chen, C. P. L. H.; Halliwell, B.; Moore, P. K.; Wong, P. T.-H. *Stroke* **2006**, *37*, 889.
(49) Blackstone, E.; Morrison, M.; Roth, M. B. *Science (New York, N.Y.)* **2005**, *308*, 518.

(50) Morrison, M. L.; Blackwood, J. E.; Lockett, S. L.; Iwata, A.; Winn, R. K.; Roth, M. B. *The Journal of trauma* **2008**, *65*, 183.
(51) Goldstein, M. *Journal of Emergency Nursing* **2008**, *34*, 538.
(52) McGuffie, C.; Wyatt, J.; Kerr, G.; Hislop, W. *Journal of Accident & Emergency Medicine* **2000**, *17*, 38.
(53) Blumenthal, D. C.; Kassner, R. J. *J Biol Chem* **1980**, *255*, 5859.
(54) Wu, L.; Wang, R. *Pharmacological Reviews* **2005**, *57*, 585.
(55) Lamb, D. C.; Lei, L.; Warrilow, A. G.; Lepesheva, G. I.; Mullins, J. G.; Waterman, M. R.; Kelly, S. L. *Journal of virology* **2009**, *83*, 8266.
(56) Hu, S.; Kincaid, J. R. *FEBS Letters* **1992**, *314*, 293.
(57) Estabrook, R. W.; Franklin, M. R.; Hildebrandt, A. G. *Annals of the New York Academy of Sciences* **1970**, *174*, 218.
(58) Forster, R. E. *Annals of the New York Academy of Sciences* **1970**, *174*, 233.
(59) Taillé, C.; El-Benna, J.; Lanone, S.; Dang, M.-C.; Ogier-Denis, E.; Aubier, M.; Boczkowski, J. *Journal of Biological Chemistry* **2004**, *279*, 28681.
(60) Thorup, C.; Jones, C. L.; Gross, S. S.; Moore, L. C.; Goligorsky, M. S. *American Journal of Physiology - Renal Physiology* **1999**, *277*, F882.
(61) Willis, D.; Tomlinson, A.; Frederick, R.; Paulclark, M. J.; Willoughby, D. A. *Biochemical and Biophysical Research Communications* **1995**, *214*, 1152.
(62) Coburn, R. F.; Mayers, L. B. *Am J Physiol* **1971**, *220*, 66.
(63) Stone, J. R.; Marletta, M. A. *Biochemistry* **1994**, *33*, 5636.
(64) Alcaraz, M. J.; Fernandez, P.; Guillen, M. I. *Current Pharmaceutical Design* **2003**, *9*, 2541.
(65) Johnson, R. A.; Kozma, F.; Colombari, E. *Brazilian journal of medical and biological research = Revista brasileira de pesquisas medicas e biologicas / Sociedade Brasileira de Biofisica ... [et al.]* **1999**, *32*, 1.
(66) Brune, B.; Ullrich, V. *Molecular pharmacology* **1987**, *32*, 497.
(67) Glaum, S. R.; Miller, R. J. *Molecular pharmacology* **1993**, *43*, 965.
(68) Stevens, C. F.; Wang, Y. *Nature* **1993**, *364*, 147.
(69) Jacquez, J. *Respiratory Physiology*; McGraw-Hill, 1979.
(70) Zgiczynski, J. M.; Stelmaszynska, T. *Biochimica et biophysica acta* **1979**, *567*, 309.
(71) Chung, J.; Wood, J. L. *Archives of biochemistry and biophysics* **1970**, *141*, 73.
(72) Way, J. L. *Annual review of pharmacology and toxicology* **1984**, *24*, 451.
(73) Pavlakovic, G.; Eyer, C. L.; Isom, G. E. *Brain Res* **1995**, *676*, 205.
(74) Borowitz, J. L.; Gunasekar, P. G.; Isom, G. E. *Brain Research* **1997**, *768*, 294.
(75) Gunasekar, P. G.; Prabhakaran, K.; Li, L.; Zhang, L.; Isom, G. E.; Borowitz, J. L. *Neuroscience Research* **2004**, *49*, 13.
(76) Kirkup, S. E.; Cheng, Z.; Elmes, M.; Wathes, D. C.; Abayasekara, D. R. *Reproduction (Cambridge, England)* **2010**, *140*, 943.
(77) Cadas, H.; di Tomaso, E.; Piomelli, D. *The Journal of neuroscience : the official journal of the Society for Neuroscience* **1997**, *17*, 1226.
(78) Das, U. N.; Fams *Nutrition (Burbank, Los Angeles County, Calif.)* **2003**, *19*, 62.
(79) Spickett, C. M. *Redox Biology* **2013**, *1*, 145.
(80) Kruman, I.; Bruce-Keller, A. J.; Bredesen, D.; Waeg, G.; Mattson, M. P. *The Journal of neuroscience : the official journal of the Society for Neuroscience* **1997**, *17*, 5089.
(81) Reed, T. T.; Pierce, W. M.; Markesbery, W. R.; Butterfield, D. A. *Brain Research* **2009**, *1274*, 66.
(82) Stevens, J. F.; Maier, C. S. *Molecular Nutrition & Food Research* **2008**, *52*, 7.
(83) Baldwin, A. S., Jr. *Annual review of immunology* **1996**, *14*, 649.
(84) Orlowski, R. Z.; Baldwin, A. S., Jr. *Trends Mol Med* **2002**, *8*, 385.

(85) Satoh, T.; Okamoto, S. I.; Cui, J.; Watanabe, Y.; Furuta, K.; Suzuki, M.; Tohyama, K.; Lipton, S. A. *Proc Natl Acad Sci U S A* **2006**, *103*, 768.
(86) Mustafa, A. K.; Gadalla, M. M.; Snyder, S. H. *Science signaling* **2009**, *2*, re2.
(87) Fisher, A. *Antioxidants & Redox Signaling* **2009**, *11*, 7.
(88) Grek, C. L.; Zhang, J.; Manevich, Y.; Townsend, D. M.; Tew, K. D. *J Biol Chem* **2013**, *288*, 26497.
(89) Dawson, R. M. C., p 16.
(90) Spaans, S. K.; Weusthuis, R. A.; van der Oost, J.; Kengen, S. W. *Frontiers in microbiology* **2015**, *6*, 742.
(91) Poole, L. B.; Nelson, K. J. *Molecules and cells* **2016**, *39*, 53.
(92) Amir Aslani, B.; Ghobadi, S. *Life sciences* **2016**, *146*, 163.
(93) Glorieux, C.; Zamocky, M.; Sandoval, J. M.; Verrax, J.; Calderon, P. B. *Free radical biology & medicine* **2015**, *87*, 84.
(94) Nordberg, J.; Arnér, E. S. J. *Free Radical Biology and Medicine* **2001**, *31*, 1287.
(95) Mustacich, D.; Powis, G. *Biochemical Journal* **2000**, *346*, 1.
(96) Gupta, V.; Carroll, K. S. *Biochimica et Biophysica Acta (BBA) - General Subjects* **2014**, *1840*, 847.
(97) Pan, J.; Carroll, K. S. *ACS Chemical Biology* **2013**, *8*, 1110.
(98) Zhang, D.; Macinkovic, I.; Devarie-Baez, N. O.; Pan, J.; Park, C. M.; Carroll, K. S.; Filipovic, M. R.; Xian, M. *Angewandte Chemie (International ed. in English)* **2014**, *53*, 575.
(99) Jeong, J.; Jung, Y.; Na, S.; Jeong, J.; Lee, E.; Kim, M. S.; Choi, S.; Shin, D. H.; Paek, E.; Lee, H. Y.; Lee, K. J. *Molecular & cellular proteomics : MCP* **2011**, *10*, M110.000513.
(100) Dalle-Donne, I.; Carini, M.; Orioli, M.; Vistoli, G.; Regazzoni, L.; Colombo, G.; Rossi, R.; Milzani, A.; Aldini, G. *Free radical biology & medicine* **2009**, *46*, 1411.
(101) Fraenkel-Conrat, H. *Journal of Biological Chemistry* **1955**, *217*, 373.
(102) Eisen, H. N.; Belmam, S. *The Journal of experimental medicine* **1953**, *98*, 533.
(103) Shechter, Y.; Patchornik, A.; Burstein, Y. *Journal of Biological Chemistry* **1974**, *249*, 413.
(104) Armstrong, D. A.; Buchanan, J. D. *Photochemistry and Photobiology* **1978**, *28*, 743.
(105) Parker, D. J.; Allison, W. S. *Journal of Biological Chemistry* **1969**, *244*, 180.
(106) Ehring, R.; Colowick, S. P. *J Biol Chem* **1969**, *244*, 4589.
(107) Allison, W. S.; Benitez, L. V.; Johnson, C. L. *Biochemical and Biophysical Research Communications* **1973**, *52*, 1403.
(108) Allison, W. S. *Accounts of Chemical Research* **1976**, *9*, 293.
(109) Penn, R. E.; Block, E.; Revelle, L. K. *Journal of the American Chemical Society* **1978**, *100*, 3622.
(110) McGrath, A. J.; Garrett, G. E.; Valgimigli, L.; Pratt, D. A. *Journal of the American Chemical Society* **2010**, *132*, 16759.
(111) Wages, P. A.; Lavrich, K. S.; Zhang, Z.; Cheng, W.-Y.; Corteselli, E.; Gold, A.; Bromberg, P.; Simmons, S. O.; Samet, J. M. *Chemical Research in Toxicology* **2015**, *28*, 2411.
(112) Brown, D. I.; Griendling, K. K. *Free radical biology & medicine* **2009**, *47*, 1239.
(113) Baez, N. O. D.; Reisz, J. A.; Furdui, C. M. *Free radical biology & medicine* **2015**, *80*, 191.
(114) Sivaramakrishnan, S.; Cummings, A. H.; Gates, K. S. *Bioorganic & medicinal chemistry letters* **2010**, *20*, 444.
(115) Zhou, H.; Singh, H.; Parsons, Z. D.; Lewis, S. M.; Bhattacharya, S.; Seiner, D. R.; LaButti, J. N.; Reilly, T. J.; Tanner, J. J.; Gates, K. S. *Journal of the American Chemical Society* **2011**, *133*, 15803.
(116) Paulsen, C. E.; Truong, T. H.; Garcia, F. J.; Homann, A.; Gupta, V.; Leonard, S. E.; Carroll, K. S. *Nature Chemical Biology* **2012**, *8*, 57.

(117) Paulsen, C. E.; Truong, T. H.; Garcia, F. J.; Homann, A.; Gupta, V.; Leonard, S. E.; Carroll, K. S. *Nat Chem Biol* **2012**, *8*, 57.

(118) Truong, T. H.; Carroll, K. S. *Biochemistry* **2012**, *51*, 9954.

(119) Tanner, J. J. P., Z. D.; Cummings, A.H.; Zhou, H.; and Gates, K.S. *Antioxidants & Redox Signaling* **2011**, *15*, 21.

(120) Ho, G. P.; Selvakumar, B.; Mukai, J.; Hester, L. D.; Wang, Y.; Gogos, J. A.; Snyder, S. H. *Neuron* **2011**, *71*, 131.

(121) Majmudar, J. D.; Konopko, A. M.; Labby, K. J.; Tom, C. T.; Crellin, J. E.; Prakash, A.; Martin, B. R. *J Am Chem Soc* **2016**, *138*, 1852.

(122) Lavis, L. D.; Raines, R. T. *ACS Chemical Biology* **2008**, *3*, 142.

(123) Lichtman, J. W.; Conchello, J.-A. *Nat Meth* **2005**, *2*, 910.

(124) Huang, B.; Babcock, H.; Zhuang, X. *Cell*, *143*, 1047.

(125) Grimm, J. B.; English, B. P.; Chen, J.; Slaughter, J. P.; Zhang, Z.; Revyakin, A.; Patel, R.; Macklin, J. J.; Normanno, D.; Singer, R. H.; Lionnet, T.; Lavis, L. D. *Nat Meth* **2015**, *12*, 244.

(126) Wardman, P. *Free radical biology & medicine* **2007**, *43*, 995.

(127) Mizukami, S.; Takikawa, R.; Sugihara, F.; Shirakawa, M.; Kikuchi, K. *Angewandte Chemie International Edition* **2009**, *48*, 3641.

(128) Xuan, W.; Pan, R.; Cao, Y.; Liu, K.; Wang, W. *Chemical Communications* **2012**, *48*, 10669.

(129) Montoya, L. A.; Pluth, M. D. *Chemical Communications* **2012**, *48*, 4767.

(130) Zhu, B.; Gao, C.; Zhao, Y.; Liu, C.; Li, Y.; Wei, Q.; Ma, Z.; Du, B.; Zhang, X. *Chemical Communications* **2011**, *47*, 8656.

(131) Liu, C.; Pan, J.; Li, S.; Zhao, Y.; Wu, L. Y.; Berkman, C. E.; Whorton, A. R.; Xian, M. *Angewandte Chemie International Edition* **2011**, *50*, 10327.

(132) Qian, Y.; Karpus, J.; Kabil, O.; Zhang, S.-Y.; Zhu, H.-L.; Banerjee, R.; Zhao, J.; He, C. *Nat Commun* **2011**, *2*, 495.

(133) Cao, X.; Lin, W.; Zheng, K.; He, L. *Chemical Communications* **2012**, *48*, 10529.

(134) Miller, E. W.; Albers, A. E.; Pralle, A.; Isacoff, E. Y.; Chang, C. J. *Journal of the American Chemical Society* **2005**, *127*, 16652.

(135) Kojima, H.; Nakatsubo, N.; Kikuchi, K.; Kawahara, S.; Kirino, Y.; Nagoshi, H.; Hirata, Y.; Nagano, T. *Analytical Chemistry* **1998**, *70*, 2446.

(136) Gabe, Y.; Urano, Y.; Kikuchi, K.; Kojima, H.; Nagano, T. *Journal of the American Chemical Society* **2004**, *126*, 3357.

(137) Sasaki, E.; Kojima, H.; Nishimatsu, H.; Urano, Y.; Kikuchi, K.; Hirata, Y.; Nagano, T. *Journal of the American Chemical Society* **2005**, *127*, 3684.

(138) Hu, J. J.; Wong, N.-K.; Ye, S.; Chen, X.; Lu, M.-Y.; Zhao, A. Q.; Guo, Y.; Ma, A. C.-H.; Leung, A. Y.-H.; Shen, J.; Yang, D. *Journal of the American Chemical Society* **2015**, *137*, 6837.

(139) Chen, Y.; Zhu, C.; Yang, Z.; Chen, J.; He, Y.; Jiao, Y.; He, W.; Qiu, L.; Cen, J.; Guo, Z. *Angewandte Chemie International Edition* **2013**, *52*, 1688.

(140) Montoya, L. A.; Pearce, T. F.; Hansen, R. J.; Zakharov, L. N.; Pluth, M. D. *The Journal of Organic Chemistry* **2013**, *78*, 6550.

(141) Bouffard, J.; Kim, Y.; Swager, T. M.; Weissleder, R.; Hilderbrand, S. A. *Organic Letters* **2008**, *10*, 37.

(142) Albers, A. E.; Dickinson, B. C.; Miller, E. W.; Chang, C. J. *Bioorganic & medicinal chemistry letters* **2008**, *18*, 5948.

(143) Du, L.; Li, M.; Zheng, S.; Wang, B. *Tetrahedron Letters* **2008**, *49*, 3045.

(144) DeLeon, E. R.; Gao, Y.; Huang, E.; Arif, M.; Arora, N.; Divietro, A.; Patel, S.; Olson, K. R. *American Journal of Physiology - Regulatory, Integrative and Comparative Physiology* **2016**.

(145) Heim, R.; Prasher, D. C.; Tsien, R. Y. *Proceedings of the National Academy of Sciences of the United States of America* **1994**, *91*, 12501.
(146) Shaner, N. C.; Patterson, G. H.; Davidson, M. W. *Journal of Cell Science* **2007**, *120*, 4247.
(147) Østergaard, H.; Henriksen, A.; Hansen, F. G.; Winther, J. R. *The EMBO Journal* **2001**, *20*, 5853.
(148) Østergaard, H.; Tachibana, C.; Winther, J. R. *The Journal of Cell Biology* **2004**, *166*, 337.
(149) Hanson, G. T.; Aggeler, R.; Oglesbee, D.; Cannon, M.; Capaldi, R. A.; Tsien, R. Y.; Remington, S. J. *Journal of Biological Chemistry* **2004**, *279*, 13044.
(150) Zhao, Y.; Jin, J.; Hu, Q.; Zhou, H.-M.; Yi, J.; Yu, Z.; Xu, L.; Wang, X.; Yang, Y.; Loscalzo, J. *Cell Metabolism*, *14*, 555.
(151) Enyedi, B.; Zana, M.; Donkó, Á.; Geiszt, M. *Antioxidants & Redox Signaling* **2012**, *19*, 523.
(152) Qian, J.; Klomsiri, C.; Wright, M. W.; King, S. B.; Tsang, A. W.; Poole, L. B.; Furdui, C. M. *Chemical Communications* **2011**, *47*, 9203.
(153) Poole, L. B.; Klomsiri, C.; Knaggs, S. A.; Furdui, C. M.; Nelson, K. J.; Thomas, M. J.; Fetrow, J. S.; Daniel, L. W.; King, S. B. *Bioconjugate chemistry* **2007**, *18*, 2004.
(154) Truong, T. H.; Garcia, F. J.; Seo, Y. H.; Carroll, K. S. *Bioorg Med Chem Lett* **2011**, *21*, 5015.
(155) Liang, L.; Astruc, D. *Coordination Chemistry Reviews* **2011**, *255*, 2933.
(156) Seo, Y. H.; Carroll, K. S. *Proceedings of the National Academy of Sciences of the United States of America* **2009**, *106*, 16163.
(157) Shiau, T. P.; Erlanson, D. A.; Gordon, E. M. *Organic Letters* **2006**, *8*, 5697.
(158) Gupta, V.; Carroll, K. S. *Chemical Science* **2016**, *7*, 400.
(159) Qian, J.; Wani, R.; Klomsiri, C.; Poole, L. B.; Tsang, A. W.; Furdui, C. M. *Chemical communications (Cambridge, England)* **2012**, *48*, 4091.
(160) Gupta, V.; Carroll, K. S. *Biochimica Et Biophysica Acta-General Subjects* **2014**, *1840*, 847.
(161) Poole, T. H.; Reisz, J. A.; Zhao, W.; Poole, L. B.; Furdui, C. M.; King, S. B. *J. Am. Chem. Soc.* **2014**, *136*, 6167.
(162) Ellis, H. R.; Poole, L. B. *Biochemistry* **1997**, *36*, 13349.
(163) Paulsen, C. E.; Carroll, K. S. *Chem. Rev.* **2013**, *113*, 4633.
(164) Devarie-Baez, N. O.; Silva Lopez, E. I.; Furdui, C. M. *Free radical research* **2015**, 1.
(165) Crump, K. E.; Juneau, D. G.; Poole, L. B.; Haas, K. M.; Grayson, J. M. *European Journal of Immunology* **2012**, *42*, 2152.
(166) Poole, L. B.; Zeng, B.-B.; Knaggs, S. A.; Yakubu, M.; King, S. B. *Bioconjugate Chem.* **2005**, *16*, 1624.
(167) Reddie, K. G.; Seo, Y. H.; Muse Iii, W. B.; Leonard, S. E.; Carroll, K. S. *Mol. BioSyst.* **2008**, *4*, 521.
(168) Benitez, L. V.; Allison, W. S. *The Journal of biological chemistry* **1974**, *249*, 6234.
(169) Qian, J.; Klomsiri, C.; Wright, M. W.; King, S. B.; Tsang, A. W.; Poole, L. B.; Furdui, C. M. *Chemical communications* **2011**, *47*, 9203.
(170) Yang, J.; Gupta, V.; Carroll, K. S.; Liebler, D. C. *Nature Communications* **2014**, *5*.
(171) Liu, C. T.; Benkovic, S. J. *J. Am. Chem. Soc.* **2013**, *135*, 14544.
(172) Qian, J.; Klomsiri, C.; Wright, M. W.; King, S. B.; Tsang, A. W.; Poole, L. B.; Furdui, C. M. *Chem. Commun.* **2011**, *47*, 9203.
(173) Stewart, W. W. *Cell* **1978**, *14*, 741.
(174) Gupta, V.; Carroll, K. S. *Biochim. Biophys. Acta, Gen. Subj.* **2014**, *1840*, 847.
(175) Deb, M. L.; Bhuyan, P. J. *Tetrahedron Lett.* **2005**, *46*, 6453.

(176) Kudirka, R.; Barfield, Robyn M.; McFarland, J.; Albers, Aaron E.; de Hart, Gregory W.; Drake, Penelope M.; Holder, Patrick G.; Banas, S.; Jones, Lesley C.; Garofalo, Albert W.; Rabuka, D. *Chem. Biol.* **2015**, *22*, 293.

(177) Requena, J. R.; Chao, C. C.; Levine, R. L.; Stadtman, E. R. *Proc. Natl. Acad. Sci. U. S. A.* **2001**, *98*, 69.

(178) Cairns, R. A.; Harris, I. S.; Mak, T. W. *Nat. Rev. Cancer* **2011**, *11*, 85.

(179) Ye, X.; Weinberg, R. A. *Trends in Cell Biology* **2015**, *25*, 675.

(180) Hernandez, J. H. D., D.; Majumudar, J.D.; Won, S.J.; Martin, B.R. **2016**, *In Revision*.

(181) Frangioni, J. V. *Curr Opin Chem Biol* **2003**, *7*, 626.

(182) Fei, X.; Gu, Y. *Progress in Natural Science* **2009**, *19*, 1.

(183) Hong, G.; Zou, Y.; Antaris, A. L.; Diao, S.; Wu, D.; Cheng, K.; Zhang, X.; Chen, C.; Liu, B.; He, Y.; Wu, J. Z.; Yuan, J.; Zhang, B.; Tao, Z.; Fukunaga, C.; Dai, H. *Nat Commun* **2014**, *5*.

(184) Wu, H.; Zhao, H.; Song, X.; Li, S.; Ma, X.; Tan, M. *Journal of Materials Chemistry B* **2014**, *2*, 5302.

(185) He, X.; Gao, J.; Gambhir, S. S.; Cheng, Z. *Trends in molecular medicine* **2010**, *16*, 574.

(186) Gerig, J. T. *Biophysical Society* **2001**, 35.

(187) Higuchi, M.; Iwata, N.; Matsuba, Y.; Sato, K.; Sasamoto, K.; Saido, T. C. *Nat Neurosci* **2005**, *8*, 527.

(188) Kitamura, N.; Tanaka, K.; Chujo, Y. *Bioorganic & Medicinal Chemistry Letters* **2013**, *23*, 281.

(189) Yamaguchi, K.; Ueki, R.; Nonaka, H.; Sugihara, F.; Matsuda, T.; Sando, S. *Journal of the American Chemical Society* **2011**, *133*, 14208.

(190) Yu, J.-X.; Kodibagkar, V. D.; Liu, L.; Zhang, Z.; Liu, L.; Magnusson, J.; Liu, Y. *Chemical Science* **2013**, *4*, 2132.

(191) Tirotta, I.; Dichiarante, V.; Pigliacelli, C.; Cavallo, G.; Terraneo, G.; Bombelli, F. B.; Metrangolo, P.; Resnati, G. *Chemical Reviews* **2015**, *115*, 1106.

(192) Ye, D.; Shuhendler, A. J.; Pandit, P.; Brewer, K. D.; Tee, S. S.; Cui, L.; Tikhomirov, G.; Rutt, B.; Rao, J. *Chemical Science* **2014**, *5*, 3845.

(193) Saleur, D.; Bouillon, J.-P.; Portella, C. *The Journal of Organic Chemistry* **2001**, *66*, 4543.

(194) Fuchigami, T.; Shimojo, M.; Konno, A. *The Journal of Organic Chemistry* **1995**, *60*, 3459.

(195) Stein, A.; Gregor, H. P.; Spoerri, P. E. *Journal of the American Chemical Society* **1956**, *78*, 6185.

(196) Puig-de-la-Bellacasa, R.; Giménez, L.; Pettersson, S.; Pascual, R.; Gonzalo, E.; Esté, J. A.; Clotet, B.; Borrell, J. I.; Teixidó, J. *European Journal of Medicinal Chemistry* **2012**, *54*, 159.

(197) Al-Turkistani, A. A.; Al-Deeb, O. A.; El-Brollosy, N. R.; El-Emam, A. A. *Molecules* **2011**, *16*, 4764.

(198) Jansa, P.; Holý, A.; Dračínský, M.; Kolman, V.; Janeba, Z.; Kostecká, P.; Kmoníčková, E.; Zídek, Z. *Medicinal Chemistry Research* **2014**, *23*, 4482.

(199) Varano, F.; Catarzi, D.; Squarcialupi, L.; Betti, M.; Vincenzi, F.; Ravani, A.; Varani, K.; Dal Ben, D.; Thomas, A.; Volpini, R.; Colotta, V. *European Journal of Medicinal Chemistry* **2015**, *96*, 105.

(200) Provins, L.; Christophe, B.; Danhaive, P.; Dulieu, J.; Durieu, V.; Gillard, M.; Lebon, F.; Lengelé, S.; Quéré, L.; van Keulen, B. *Bioorganic & Medicinal Chemistry Letters* **2006**, *16*, 1834.

(201) Abdel-Rahman, T. M. *Journal of Heterocyclic Chemistry* **2005**, *42*, 1257.

(202) Moses, W. W. *Nuclear instruments & methods in physics research. Section A, Accelerators, spectrometers, detectors and associated equipment* **2011**, *648 Supplement 1*, S236.
(203) Fruede, D. *Spectroscopy - Ch 4: NMR*, 2006.
(204) Schwarz, R.; Schuurmans, M.; Seelig, J.; Künnecke, B. *Magnetic Resonance in Medicine* **1999**, *41*, 80.
(205) Yamane, T.; Hanaoka, K.; Muramatsu, Y.; Tamura, K.; Adachi, Y.; Miyashita, Y.; Hirata, Y.; Nagano, T. *Bioconjugate chemistry* **2011**, *22*, 2227.
(206) Lee, T.; Zhang, X. A.; Dhar, S.; Faas, H.; Lippard, S. J.; Jasanoff, A. *Chemistry & biology* **2010**, *17*, 665.
(207) Spirk, S.; Madl, T.; Pietschnig, R. *Organometallics* **2008**, *27*, 500.
(208) Gupta, V.; Carroll, K. S. *Chemical Communications* **2016**, *52*, 3414.
(209) Gottlieb, H. E.; Kotlyar, V.; Nudelman, A. *Journal of Organic Chemistry* **1997**, *62*, 7512.
(210) Shao, Y.; Gan, Z.; Epifanovsky, E.; Gilbert, A. T. B.; Wormit, M.; Kussmann, J.; Lange, A. W.; Behn, A.; Deng, J.; Feng, X.; Ghosh, D.; Goldey, M.; Horn, P. R.; Jacobson, L. D.; Kaliman, I.; Khaliullin, R. Z.; Kuś, T.; Landau, A.; Liu, J.; Proynov, E. I.; Rhee, Y. M.; Richard, R. M.; Rohrdanz, M. A.; Steele, R. P.; Sundstrom, E. J.; Woodcock, H. L.; Zimmerman, P. M.; Zuev, D.; Albrecht, B.; Alguire, E.; Austin, B.; Beran, G. J. O.; Bernard, Y. A.; Berquist, E.; Brandhorst, K.; Bravaya, K. B.; Brown, S. T.; Casanova, D.; Chang, C.-M.; Chen, Y.; Chien, S. H.; Closser, K. D.; Crittenden, D. L.; Diedenhofen, M.; DiStasio, R. A.; Do, H.; Dutoi, A. D.; Edgar, R. G.; Fatehi, S.; Fusti-Molnar, L.; Ghysels, A.; Golubeva-Zadorozhnaya, A.; Gomes, J.; Hanson-Heine, M. W. D.; Harbach, P. H. P.; Hauser, A. W.; Hohenstein, E. G.; Holden, Z. C.; Jagau, T.-C.; Ji, H.; Kaduk, B.; Khistyaev, K.; Kim, J.; Kim, J.; King, R. A.; Klunzinger, P.; Kosenkov, D.; Kowalczyk, T.; Krauter, C. M.; Lao, K. U.; Laurent, A. D.; Lawler, K. V.; Levchenko, S. V.; Lin, C. Y.; Liu, F.; Livshits, E.; Lochan, R. C.; Luenser, A.; Manohar, P.; Manzer, S. F.; Mao, S.-P.; Mardirossian, N.; Marenich, A. V.; Maurer, S. A.; Mayhall, N. J.; Neuscamman, E.; Oana, C. M.; Olivares-Amaya, R.; O'Neill, D. P.; Parkhill, J. A.; Perrine, T. M.; Peverati, R.; Prociuk, A.; Rehn, D. R.; Rosta, E.; Russ, N. J.; Sharada, S. M.; Sharma, S.; Small, D. W.; Sodt, A. *Molecular Physics* **2015**, *113*, 184.
(211) Becke, A. D. *The Journal of Chemical Physics* **1993**, *98*, 5648.
(212) Lee, C.; Yang, W.; Parr, R. G. *Physical Review B* **1988**, *37*, 785.
(213) Hay, P. J.; Wadt, W. R. *The Journal of Chemical Physics* **1985**, *82*, 270.
(214) Hay, P. J.; Wadt, W. R. *The Journal of Chemical Physics* **1985**, *82*, 299.
(215) Wadt, W. R.; Hay, P. J. *The Journal of Chemical Physics* **1985**, *82*, 284.
(216) Chai, J.-D.; Head-Gordon, M. *Physical Chemistry Chemical Physics* **2008**, *10*, 6615.
(217) Balabanov, N. B.; Peterson, K. A. *The Journal of Chemical Physics* **2005**, *123*, 064107.
(218) Dunning, T. H. *The Journal of Chemical Physics* **1989**, *90*, 1007.
(219) Woon, D. E.; Dunning, T. H. *The Journal of Chemical Physics* **1993**, *98*, 1358.
(220) Zimmerman, P. *Journal of Chemical Theory and Computation* **2013**, *9*, 3043.
(221) Zimmerman, P. M. *The Journal of Chemical Physics* **2013**, *138*, 184102.
(222) Zimmerman, P. M. *Journal of Computational Chemistry* **2015**, *36*, 601.
(223) E. D. Glendening, J. K. B., A. E. Reed, J. E. Carpenter, J. A. Bohmann, C. M. Morales, and F. Weinhold Theoretical Chemistry Institute, University of Wisconsin, Madison, WI, 2001, 2001.
(224) Fischer, M.; Stadlbauer, W. *Journal of Heterocyclic Chemistry* **1997**, *34*, 993.
(225) Markiewicz, J. T.; Wiest, O.; Helquist, P. *Journal of Organic Chemistry* **2010**, *75*, 4887.

(226) Prakash, G. K. S.; Wang, F.; Shao, N.; Mathew, T.; Rasul, G.; Haiges, R.; Stewart, T.; Olah, G. A. *Angewandte Chemie International Edition* **2009**, *48*, 5358.
(227) Cesario, C.; Miller, M. J. *J Org Chem* **2009**, *74*, 5730.
(228) Sevier, C. S.; Kaiser, C. A. *Biochimica et Biophysica Acta (BBA) - Molecular Cell Research* **2008**, *1783*, 549.
(229) Frand, A. R.; Kaiser, C. A. *Molecular cell* **1999**, *4*, 469.
(230) Sevier, C. S.; Qu, H.; Heldman, N.; Gross, E.; Fass, D.; Kaiser, C. A. *Cell*, *129*, 333.
(231) Tu, B. P.; Weissman, J. S. *J Cell Biol* **2004**, *164*, 341.
(232) Princiotta, M. F.; Finzi, D.; Qian, S.-B.; Gibbs, J.; Schuchmann, S.; Buttgereit, F.; Bennink, J. R.; Yewdell, J. W. *Immunity* **2003**, *18*, 343.
(233) Rehder, D. S.; Borges, C. R. *Biochemistry* **2010**, *49*, 7748.
(234) Lee, Jun H.; Budanov, Andrei V.; Karin, M. *Cell Metabolism*, *18*, 792.
(235) Saveljeva, S.; Cleary, P.; Mnich, K.; Ayo, A.; Pakos-Zebrucka, K.; Patterson, J. B.; Logue, S. E.; Samali, A. *Oncotarget* **2016**.
(236) Garaeva, A. A.; Kovaleva, I. E.; Chumakov, P. M.; Evstafieva, A. G. *Cell cycle (Georgetown, Tex.)* **2016**, *15*, 64.
(237) Tomasovic, A.; Kurrle, N.; Surun, D.; Heidler, J.; Husnjak, K.; Poser, I.; Schnutgen, F.; Scheibe, S.; Seimetz, M.; Jaksch, P.; Hyman, A.; Weissmann, N.; von Melchner, H. *J Biol Chem* **2015**, *290*, 9738.
(238) Jin, S. H.; Yang, J. H.; Shin, B. Y.; Seo, K.; Shin, S. M.; Cho, I. J.; Ki, S. H. *Toxicology and Applied Pharmacology* **2013**, *271*, 95.
(239) Yang, J. H.; Kim, K. M.; Kim, M. G.; Seo, K. H.; Han, J. Y.; Ka, S. O.; Park, B. H.; Shin, S. M.; Ku, S. K.; Cho, I. J.; Ki, S. H. *Free radical biology & medicine* **2015**, *78*, 156.
(240) Ro, S. H.; Nam, M.; Jang, I.; Park, H. W.; Park, H.; Semple, I. A.; Kim, M.; Kim, J. S.; Park, H.; Einat, P.; Damari, G.; Golikov, M.; Feinstein, E.; Lee, J. H. *Proc Natl Acad Sci U S A* **2014**, *111*, 7849.
(241) DeNicola, G. M.; Karreth, F. A.; Humpton, T. J.; Gopinathan, A.; Wei, C.; Frese, K.; Mangal, D.; Yu, K. H.; Yeo, C. J.; Calhoun, E. S.; Scrimieri, F.; Winter, J. M.; Hruban, R. H.; Iacobuzio-Donahue, C.; Kern, S. E.; Blair, I. A.; Tuveson, D. A. *Nature* **2011**, *475*, 106.
(242) Kallenborn-Gerhardt, W.; Lu, R.; Syhr, K. M.; Heidler, J.; von Melchner, H.; Geisslinger, G.; Bangsow, T.; Schmidtko, A. *Antioxid Redox Signal* **2013**, *19*, 2013.
(243) Arrigo, A. P. *Biological chemistry* **1998**, *379*, 19.
(244) Preville, X.; Salvemini, F.; Giraud, S.; Chaufour, S.; Paul, C.; Stepien, G.; Ursini, M. V.; Arrigo, A. P. *Experimental cell research* **1999**, *247*, 61.
(245) Papp, E.; Nardai, G.; Soti, C.; Csermely, P. *BioFactors (Oxford, England)* **2003**, *17*, 249.
(246) Baker, A.; Santos, B. D.; Powis, G. *Biochem Biophys Res Commun* **2000**, *268*, 78.
(247) Zuo, Y.; Xiang, B.; Yang, J.; Sun, X.; Wang, Y.; Cang, H.; Yi, J. *Cell Res* **2009**, *19*, 449.
(248) Rossig, L.; Fichtlscherer, B.; Breitschopf, K.; Haendeler, J.; Zeiher, A. M.; Mulsch, A.; Dimmeler, S. *J Biol Chem* **1999**, *274*, 6823.
(249) Mannick, J. B.; Hausladen, A.; Liu, L.; Hess, D. T.; Zeng, M.; Miao, Q. X.; Kane, L. S.; Gow, A. J.; Stamler, J. S. *Science (New York, N.Y.)* **1999**, *284*, 651.
(250) Torok, N. J.; Higuchi, H.; Bronk, S.; Gores, G. J. *Cancer research* **2002**, *62*, 1648.
(251) Shalini, S.; Kumar, S. *Molecular & Cellular Oncology* **2015**, *2*, e1004956.
(252) Wang, Y. Y., J; and Yi, J *Antioxidants & Redox Signaling* **2012**, *16*, 8.
(253) Sobotta, M. C.; Liou, W.; Stöcker, S.; Talwar, D.; Oehler, M.; Ruppert, T.; Scharf, A. N. D.; Dick, T. P. *Nat Chem Biol* **2015**, *11*, 64.

(254) Gautier, V.; Le, H.-T.; Malki, A.; Messaoudi, N.; Caldas, T.; Kthiri, F.; Landoulsi, A.; Richarme, G. *Journal of Molecular Biology* **2012**, *421*, 662.

(255) Bonifati, V.; Rizzu, P.; van Baren, M. J.; Schaap, O.; Breedveld, G. J.; Krieger, E.; Dekker, M. C.; Squitieri, F.; Ibanez, P.; Joosse, M.; van Dongen, J. W.; Vanacore, N.; van Swieten, J. C.; Brice, A.; Meco, G.; van Duijn, C. M.; Oostra, B. A.; Heutink, P. *Science (New York, N.Y.)* **2003**, *299*, 256.

(256) Messaoudi, N.; Gautier, V.; Kthiri, F.; Lelandais, G.; Mihoub, M.; Joseleau-Petit, D.; Caldas, T.; Bohn, C.; Tolosa, L.; Rao, G.; Tao, K.; Landoulsi, A.; Bouloc, P.; Richarme, G. *Journal of Bacteriology* **2013**, *195*, 1167.

(257) Hwang, N. R.; Yim, S. H.; Kim, Y. M.; Jeong, J.; Song, E. J.; Lee, Y.; Lee, J. H.; Choi, S.; Lee, K. J. *The Biochemical journal* **2009**, *423*, 253.

(258) Humphrey, L. L.; Deffebach, M.; Pappas, M.; Baumann, C.; Artis, K.; Mitchell, J. P.; Zakher, B.; Fu, R.; Slatore, C. G. *Annals of Internal Medicine* **2013**, *159*, 411.

(259) Westwood, M. J., M; Grutters, J; Redekop, K; Armstrong, N; Lee, K; Gloy, V; Raatz, H; Misso, K ; Severens, J; and Kleijnen, J. *Health Technology Assessment* **2013**, *17*, 268.

(260) Hulten, E.; Pickett, C.; Bittencourt, M. S.; Villines, T. C.; Petrillo, S.; Di Carli, M. F.; Blankstein, R. *Journal of the American College of Cardiology* **2013**, *61*, 880.

(261) Seigneurin, A.; Field, J. K.; Gachet, A.; Duffy, S. W. *Annals of Oncology* **2013**.

(262) Lusic, H.; Grinstaff, M. W. *Chemical reviews* **2013**, *113*, 10.1021/cr200358s.

(263) Gambhir, S. S. *Nat Rev Cancer* **2002**, *2*, 683.

(264) Wood, K. A.; Hoskin, P. J.; Saunders, M. I. *Clinical Oncology* **2007**, *19*, 237.

(265) Pennant, M.; Takwoingi, Y.; Pennant, L.; Davenport, C.; Fry-Smith, A.; Eisinga, A.; Andronis, L.; Arvanitis, T.; Deeks, J.; Hyde, C. *Health technology assessment (Winchester, England)* **2010**, *14*, 1.

(266) AGENCY, I. A. E. *Technical Reports Series* **2008**, 230.

(267) McQuade, P.; McCarthy, D. W.; Welch, M. J. In *Positron Emission Tomography: Basic Sciences*; Bailey, D. L., Townsend, D. W., Valk, P. E., Maisey, M. N., Eds.; Springer London: London, 2005, p 237.

(268) SM., Q. *The Quarterly Journal of Nuclear Medicine and Molecular Imaging* **2008**, *52*, 10.

(269) Freudenberg, L. S.; Schueler, A. O.; Beyer, T.; Antoch, G.; Kuhl, H.; Bornfeld, N.; Bockisch, A.; Egelhof, T. *Survey of ophthalmology* **2004**, *49*, 537.

(270) Buijsen, J.; van den Bogaard, J.; Janssen, M. H. M.; Bakers, F. C. H.; Engelsman, S.; Öllers, M.; Beets-Tan, R. G. H.; Nap, M.; Beets, G. L.; Lambin, P.; Lammering, G. *Radiotherapy and Oncology* **2011**, *98*, 270.

(271) Ross, T. L.; Wester, H. J. In *Handbook of Nuclear Chemistry*; Vértes, A., Nagy, S., Klencsár, Z., Lovas, R. G., Rösch, F., Eds.; Springer US: Boston, MA, 2011, p 2021.

(272) Riedi, P. C.; Lord, J. S. In *Interstitial Intermetallic Alloys*; Grandjean, F., Long, G. J., Buschow, K. H. J., Eds.; Springer Netherlands: Dordrecht, 1995, p 267.

(273) Saitô, H.; Ando, I.; Ramamoorthy, A. *Progress in nuclear magnetic resonance spectroscopy* **2010**, *57*, 181.

(274) Dowsett, D. *Radiological Sciences Dictionary: Keywords, names and definitions*; CRC Press 2009.

(275) Skovronsky, D. M.; Zhang, B.; Kung, M. P.; Kung, H. F.; Trojanowski, J. Q.; Lee, V. M. *Proc Natl Acad Sci U S A* **2000**, *97*, 7609.

(276) Sato, K.; Higuchi, M.; Iwata, N.; Saido, T. C.; Sasamoto, K. *European Journal of Medicinal Chemistry* **2004**, *39*, 573.

(277) Knight, J. C.; Edwards, P. G.; Paisey, S. J. *RSC Advances* **2011**, *1*, 1415.

(278) Mason, R. P.; Rodbumrung, W.; Antich, P. P. *NMR in Biomedicine* **1996**, *9*, 125.

(279) Jiang, Z. X.; Feng, Y.; Yu, Y. B. *Chemical communications (Cambridge, England)* **2011**, *47*, 7233.
(280) Peng, H.; Blakey, I.; Dargaville, B.; Rasoul, F.; Rose, S.; Whittaker, A. K. *Biomacromolecules* **2009**, *10*, 374.
(281) Nakamura, T.; Matsushita, H.; Sugihara, F.; Yoshioka, Y.; Mizukami, S.; Kikuchi, K. *Angewandte Chemie International Edition* **2015**, *54*, 1007.
(282) Ahrens, E. T.; Flores, R.; Xu, H.; Morel, P. A. *Nat Biotech* **2005**, *23*, 983.